

**Host Factors Involved in the
Entry of Coronaviruses
into
Mammalian Cells**

Christine Burkard

Cover art: Christine Burkard
Layout and design: Christine Burkard
Print: Ipskamp Drukkers, Enschede

Copyright: Christine Burkard, 2014. All rights reserved.

All figures and published articles have been reprinted with permission of the respective journals. Please refer to the policy of the respective journals.

A good traveler has no fixed plans,
and is not intent on arriving.

Lao Tzu

Nothing can stop the man with the right mental attitude
from achieving his goal; nothing on earth can help the man
with the wrong mental attitude.

Thomas Jefferson

The greater danger for most of us lies not in setting our aim
too high and falling short; but in setting our aim too low,
and achieving our mark.

Michelangelo

Host Factors Involved in the Entry of Coronaviruses into Mammalian Cells

Gastheerfactoren die betrokken zijn bij de
binnenkomst van coronavirussen in zoogdiercellen

(met een samenvatting in het Nederlands)

Proefschrift

ter verkrijging van de graad van doctor aan de Universiteit Utrecht op gezag
van de rector magnificus, prof. dr. G.J. van der Zwaan, ingevolge het besluit
van het college voor promoties in het openbaar te verdedigen op

dinsdag 27 januari 2015 des middags te 12.45 uur

door

Christine Burkard
geboren op 4 april 1986 te Sursee (Zwitserland)

Promotor: Prof. dr. P.J.M. Rottier
Copromotoren: Dr. C.A.M. de Haan
Dr. B.J. Bosch

The research described in this thesis was financially supported by the EU Seventh Framework Programme for Research (FP7) PITN-GA-2009-235649-Virus Entry.

TABLE OF CONTENTS

Chapter 1

General Introduction 9

Chapter 2

Replication-independent analysis of virus binding, internalization, and penetration using minimal complementation of β -galactosidase 37

Chapter 3

Identification and Characterization of a Proteolytically Primed Form of the Murine Coronavirus Spike Proteins after Fusion with the Target Cell 69

Chapter 4

Coronavirus cell entry occurs through the endo-/lysosomal pathway in a proteolysis-dependent manner 95

Chapter 5

ATP1A1-mediated Src signaling inhibits coronavirus entry into host cells 145

Chapter 6

General Discussion 173

Summary - English 189

Samenvatting - Nederlands 195

Acknowledgments 201

Curriculum Vitae 207

List of Publications 209

CHAPTER
ONE

General Introduction

Viral infections constitute one of the major public health threats of our time. Just during the last decade the world was confronted with the emergence of deadly examples such as the severe acute respiratory syndrome coronavirus (SARS-CoV; 2002/2003), the new pandemic influenza H1N1 virus (2009), and, more recently and still spreading, the Middle East respiratory syndrome CoV (MERS-CoV) and the Ebola virus. In all these cases the causative agents could be tracked back to an animal source: horseshoe bats, pigs, camels and monkeys, respectively (1-4), thereby demonstrating the zoonotic potential of these viruses.

Virus particles consist of nothing more than genomic material surrounded by a protein coat (capsid), which is sometimes contained within a lipid membrane (envelope). Viral particles are quite diverse. They differ, among others, in the way genomic information is stored, i.e. single- or double-stranded DNA or RNA, the shape of the capsid, and the absence or presence of a lipid envelope (5). Although viruses can replicate and evolve, they are generally not considered to be organisms, as they do not have a metabolism of themselves. Nevertheless, once a virus gains entrance into a host cell it is able to manipulate this cell and abuse its machinery and metabolism for the production of new infectious virus particles.

The virus life cycle starts by attachment of virus particles to a new target cell. Subsequently the viral genomic material is introduced into the host cell. These first steps, referred to as viral entry, are followed by replication of the genomic material, synthesis of the structural proteins, and the assembly and release of newly formed virus particles. Each of the steps of the virus life cycle is highly coordinated and not only involves the interaction between viral components, but also requires the viral proteins to interact with and to trigger responses from many host cellular factors.

To initiate infection, non-enveloped and enveloped virus particles both have to deliver their genome across the limiting cellular membrane. Yet, since the mechanism of viral entry into cells is largely determined by the structural composition of a virus particle, entry of enveloped virus particles differs fundamentally from that of virus particles that lack an envelope. This thesis deals with the involvement of host factors in the entry of CoVs into cells. As CoVs are enveloped viruses, this introduction is focused on the entry of enveloped viruses in general and CoVs in particular.

1. Entry of enveloped viruses

Virus entry starts with the attachment of viral particles to the outer surface of a target cell. A variety of glycoproteins and lipids can function as attachment factors. The barrier posed by the glycocalyx, a meshwork of glycoproteins, glycolipids, and membrane-bound proteoglycans (6) found on the surface of most target cells is overcome by viruses by using components of the glycocalyx as attachment factors (7). Binding to attachment factors also allows viruses to concentrate at cell surface locations suitable for uptake. Virus particles may furthermore prime the cell for entry and infection by activating signaling systems of the cell via binding of receptors at the cell surface (reviewed in (8-11)).

Enveloped viruses deliver their capsids to the cytosol by fusing their envelope with a membrane of the host cell. Few viruses fuse at the cell surface, whereas most enveloped viruses require to be taken up via endocytosis prior to fusion and therefore trigger endocytic uptake mechanisms. Entering cells via endocytosis allows viruses to catch a free taxi ride into the cell, avoiding a barrier hidden below the plasma membrane, the cortical cytoskeleton (12). Once delivered into the cytoplasm, the capsid needs to be uncoated, resulting in the release of the

genomic material in the cell, to allow initiation of virus replication. The capsids of some viruses, such as influenza A virus (IAV), are transported to an appropriate intracellular location (e.g. the nucleus) before uncoating, after which replication ensues (11).

1.1. Mechanisms of fusion

The key step in the entry of all enveloped viruses is the fusion between viral and host cell membranes. In general, the fusion mechanism of all biological membranes involves the pulling together of membranes by helper proteins to achieve a very close apposition (Figure 1A-3). This is necessary to overcome the repulsion of the two hydrophilic head groups of the lipid bilayers and to initially enable hemifusion to occur, a stage in which only the outer leaflets of the two lipid bilayers have merged (Figure 1A-4, Figure 1B). The subsequent fusion of the inner leaflets, which again requires overcoming an energetic barrier, leads to the formation of the fusion pore and the consequent full collapse, by which the fusion reaction reaches its lowest energy stage (Figure 1A-5 & 6, Figure 1B)(13-16). The energy required for virus-cell membrane fusion is provided by the structural rearrangements of the so-called viral fusion proteins in interaction with the target cell membrane receptor. Viral fusion glycoproteins can be assigned to three different categories of fusion proteins; class I, II or III (17). The three classes are defined by the structural characteristics of the fusion proteins, which in turn define the mechanism by which membrane fusion occurs.

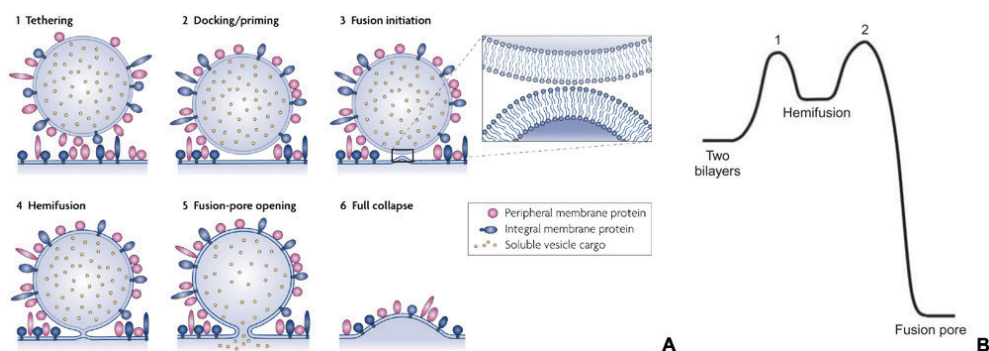


Figure 1: Membrane fusion. A) **General mechanism of membrane fusion.** Step 1; surface proteins on the approaching vesicle interact with the target membrane or proteins displayed and tether the membranes together. Step 2; docking occurs, triggered by environmental cues or protein-interaction. Proteins involved in tethering the membranes together, thereby providing the energy needed for fusion to occur are primed. Step 3; fusion is initiated by bringing the two lipid monolayers in approximate position, most likely via a nipple like extrusion formed in between two tethering complexes. Step 4; the two proximal lipid monolayers merge to form a hemifusion pore. Step 4; also the second lipid monolayers merge to form a fusion pore. Step 6; the fusion pore expands and the incoming, merging membrane collapses to form part of the target membrane. B) **Energy changes during membrane fusion.** The approximation of the two membranes raises the repulsion of the two hydrophilic bilayer surfaces before energy reaches an intermediate low when the hemifusion occurs. Another energy barrier needs to be overcome to form a fusion pore before the ideal low energy state of the fusion pore and subsequent collapse are reached. (Figure reproduced from (15) and (14))

Class I fusion proteins are defined by a central, perpendicular, trimeric coiled-coil of α -helices. There are many well-known members within the class I fusion proteins, such as the influenza virus hemagglutinin (HA) (18), the human immunodeficiency virus Env (19), the Ebola virus glycoprotein (GP) (20) and the CoV spike glycoprotein (S) (21). By structural analysis of rearrangement intermediates of class I fusion proteins, in particular HA, a detailed picture of the membrane fusion mechanism could be drawn. The class I fusion glycoproteins

are synthesized as precursors in a fusion-incompetent state and require proteolytic cleavage for activation, so called priming. Cleaved subunits remain linked, sometimes covalently by disulfide bonds. Triggers are required to induce an ejection of the hydrophobic fusion peptide (Figure 2, stage 2) (22-24). The viral membrane-distal exposure of the peptide allows insertion into the target membrane to form a so-called prehairpin (Figure 2, stage 3). The bridge in the core region of the prefusion intermediate collapses and starts zipping up, thereby pulling the opposing membranes together (Figure 2, stage 4). The formation of a six-helix bundle (6HB) provides the energy needed to distort the membrane and to achieve the hemifusion stage of membrane fusion (Figure 2, stage 5) (23). After hemifusion the other pair of monolayers merges as well to form a fusion pore. The transmembrane domain and fusion loop become juxtaposed generating the final trimer-of-hairpin conformation (Figure 2, stage 6) (25). Several fusion proteins are likely to be required to achieve pore formation (26).

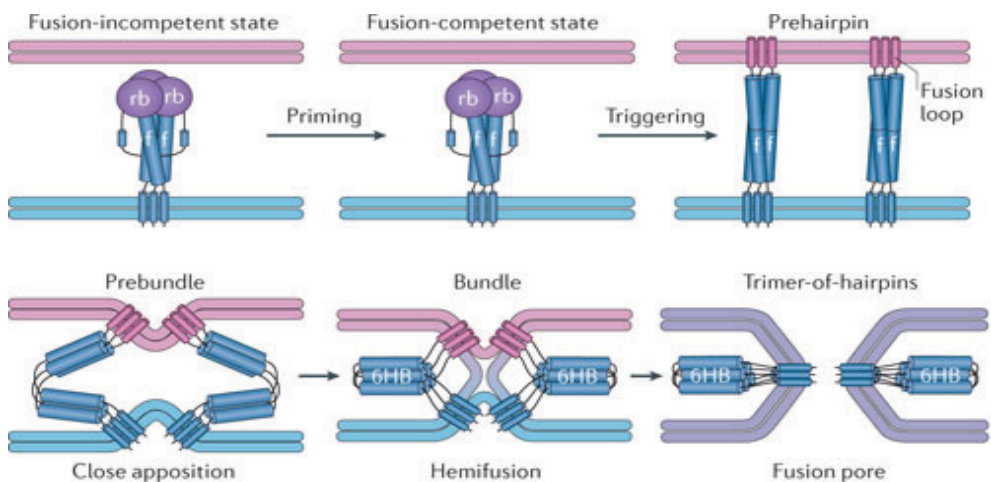


Figure 2: Fusion mechanism of Class I viral fusion proteins. Stage 1, Fusion-incompetent state: viral spike proteins are present in a fusion-incompetent state on the newly formed virion. Common features of the class I fusion glycoproteins in that state are an exposed receptor binding (rb) domain and a coiled-coil of α -helices, which form the fusion (f) domain. Stage 2, Fusion-competent state: Upon priming by proteolytic cleavage the fusion protein reaches a fusion-competent state. Stage 3, Prehairpin: Upon activation by an environmental trigger, such as low pH, receptor binding, or proteolytic cleavage, the fusion loop is exposed at the membrane-distal end of the viral fusion protein. The loop inserts into the target membrane to form the prehairpin structure. Stage 4, Prebundle: The central bridge of the fusion domain collapses and the two helix bundles refold in a zipper-like manner. Stage 5, Bundle: Formation of the so-called six-helix bundles (6HB) upon refolding of the f domain provides enough energy for the two proximal lipid monolayers to fuse and first form the hemifusion state. Stage 6, Trimer-of-hairpins: After hemifusion the second set of monolayers merges as well to form a fusion pore. The transmembrane domain and fusion loop are brought into juxtaposition to form the final trimer-of-hairpin conformation. (Figure reproduced from (22))

Class II fusion proteins are largely composed of β -sheet structures, rather than α -helices. They consist of a central β -barrel and a fusion loop at the membrane-distal end of the ectodomain (Figure 3, orange stars). So far class II type fusion glycoproteins have only been found in virus families, whose virions are characterized by an icosahedral grid of spike proteins, including alphaviruses (27), flaviviruses (28) and bunyaviruses (29). Rather than needing proteolytic priming of the protein itself, as is the case for class I fusion proteins, proteolytic cleavage of a 'protector' protein associated with the class II viral fusion proteins renders the fusion proteins fusion-competent. When triggered by acidic pH, a series of conformational changes

is induced (Fig. 3), which generates enough traction and energy to render the two membranes into the hemifusion stage and to subsequently induce the formation of the fusion pore. (14, 30, 31)

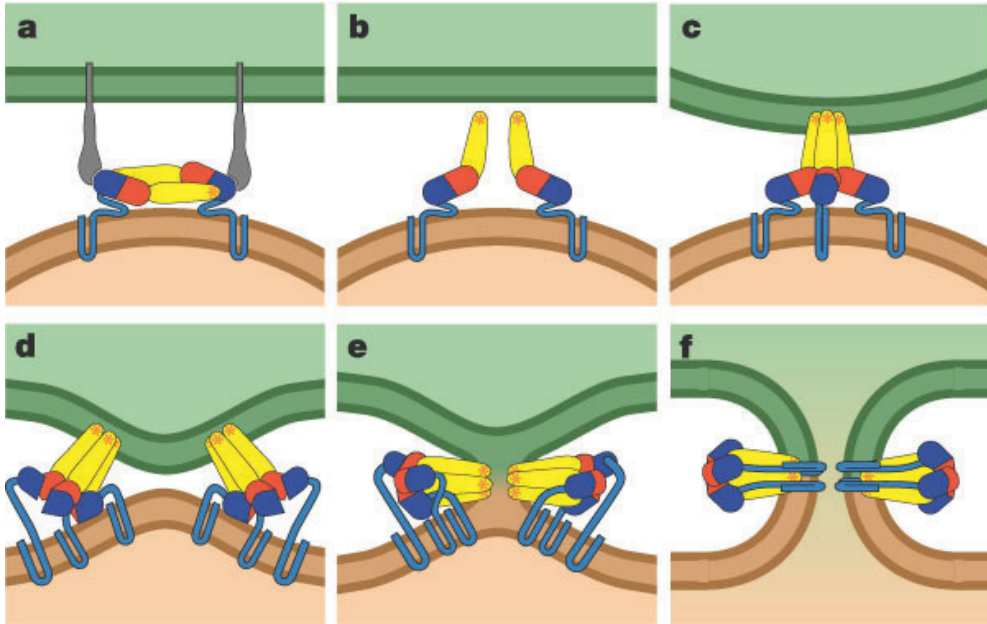


Figure 3: Fusion mechanism of Class II fusion proteins. Stage a: Binding of the viral fusion protein dimers to one or multiple receptors and attachment factors at the cell surface triggers endocytic uptake. Stage b: Environmental cues in the endosomal system, such as low pH render the fusion proteins fusion-competent. This triggers an extrusion of domain II (yellow) towards the target membrane, thereby exposing the viral fusion loops (orange) at the membrane-distal end. Stage c: Insertion of the fusion loops into the target membranes induces the formation of trimers. Stage d: Trimer formation triggers a series of structural rearrangements culminating in domain III (blue) to flip outwards. Now the domain III can zip up towards the central helix inducing a tethering of the two opposing membranes. Stage e: Refolding of the fusion proteins provides sufficient energy for the formation of the hemifusion state. Stage f: The fusion of the first lipid monolayer set is followed by the second set of lipid monolayers to form a fusion pore. Trans-membrane domain and fusion loop juxtapose to form the irreversible post-fusion state of the fusion protein. (Figure reproduced from (30)).

Class III fusion proteins consist of a mixture of α -helices and β -sheet structures. Around a central domain of an elongated coiled coil of α -helices four additional domains are arranged. Two hydrophobic fusion loops are located in the membrane distal, β -sheet rich domain I. Class III fusion proteins have been found in the rhabdovirus (32, 33), baculovirus (34) and herpesvirus (35) families. The fusion proteins do not seem to need proteolytic cleavage, like class I proteins, or a cleavage of a chaperone, like class II proteins, to become fusion-competent. Fusion of the class III fusion glycoproteins can be triggered solely by low pH or receptor binding (36). It is believed that the general fusion mechanism of class III proteins closely resembles the one of class II fusion proteins, even though there is only one pre-fusion structure known yet, that of the vesicular stomatitis virus G protein (32). Upon low pH exposure the protein opens up and elongates such that the fusion loops are displayed at the membrane-distal tip. The fusion loops insert shallowly into the target membrane upon which membrane proximal domains collapse into the cervix formed by the other domains. The post

fusion form is an elongated hairpin-like structure resembling the structure of a class I trimer-of-hairpin fusion protein structure. (37, 38)

The fusion proteins carried by newly assembled viruses occur in a metastable prefusion structure that needs to be triggered for fusion to occur. The environmental cues that initiate fusion differ between viruses. For some viruses that fuse directly at the cell surface, the structural rearrangements of the viral fusion proteins can be triggered solely by receptor interaction. However, many viruses are endocytosed prior to fusion. For these viruses, other environmental cues are generally required for the induction of structural rearrangements in the viral fusion proteins. During the maturation of endocytic vesicles, the microenvironment within these vesicles changes with respect to pH, which decreases, proteolytic activity, and redox environment (39-41). For several viruses, low pH is known as a main environmental cue to trigger viral fusion. Also proteolytic processing of viral fusion proteins in the endosomal system may be required for fusion as has recently been shown for Ebola virus and respiratory syncytial virus (RSV) (42-45). The requirement for specific environmental cues allows a virus to prevent premature fusion activation and to initiate fusion at a specific location in the endosomal pathway.

1.2. Viral entry pathways

While some viruses, such as herpes simplex virus, Sendai virus, and human immunodeficiency virus, appear to be capable of direct fusion at the plasma membrane after initial attachment (46-50), the majority of enveloped viruses use endocytosis for uptake and transport into the cell prior to fusion.

A wide variety of endocytic pathways has been described over the past fifty years. These pathways are used for import of nutrients and other cellular factors, that are involved in communication of the cell with the surrounding environment and neighboring cells. Since viruses are abusing these transport systems for their own uptake they have proven excellent tools in the investigation and characterization of these pathways. Thus, viruses have been very helpful for the discovery and description of several endocytic pathways, including classical clathrin-mediated endocytosis, macropinocytosis, lipid raft-mediated endocytosis as well as several other clathrin-independent pathways (Figure 4). These pathways are classified by their dependence on certain host factors, such as clathrin, lipid rafts, and dynamin but also by their morphology or mode of engulfment of particles or fluids. Several pathways used by viruses for entry are discussed in more detail below.

Clathrin-mediated endocytosis (CME) (Figure 4, C) is the best-studied endocytic uptake mechanism for viral entry. Already in the 1980ies it was identified as the uptake pathway for vesicular stomatitis virus (VSV) (51). CME is a continuous process in host cells and mediates uptake of nutrients and growth factors, as well as being involved in specific processes, such as recycling of synaptic vesicle proteins in neuronal cells (52-54). The first step in the clathrin-mediated endocytosis is the interaction of AP2 complexes with the cytoplasmic domains of receptors (55). Subsequently, clathrin triskelions are recruited, which assemble into a growing cage (Figure 5A, Steps 1 & 2, Figure 5B). Upon recruitment of other factors, such as dynamin and amphiphysin, the clathrin coated pit starts to invaginate (Figure 5A, Step 2). Upon GTP binding dynamin redistributes to the neck of the pit and aids the scission of the vesicle and budding of the coated pit (Figure 5A, Step 3). The coated vesicle gradually loses its protein coat in a regulated manner (Figure 5A, Step 4) (56, 57). The cargo receptors and

other factors are recycled to the plasma membrane, released to the cytosol in a pH-dependent manner, or end up in lysosomes where they are degraded (58, 59). *De novo* clathrin coated pit formation has been shown to be initiated by virus binding, most likely through the activation of signaling systems of the cell (60-62).

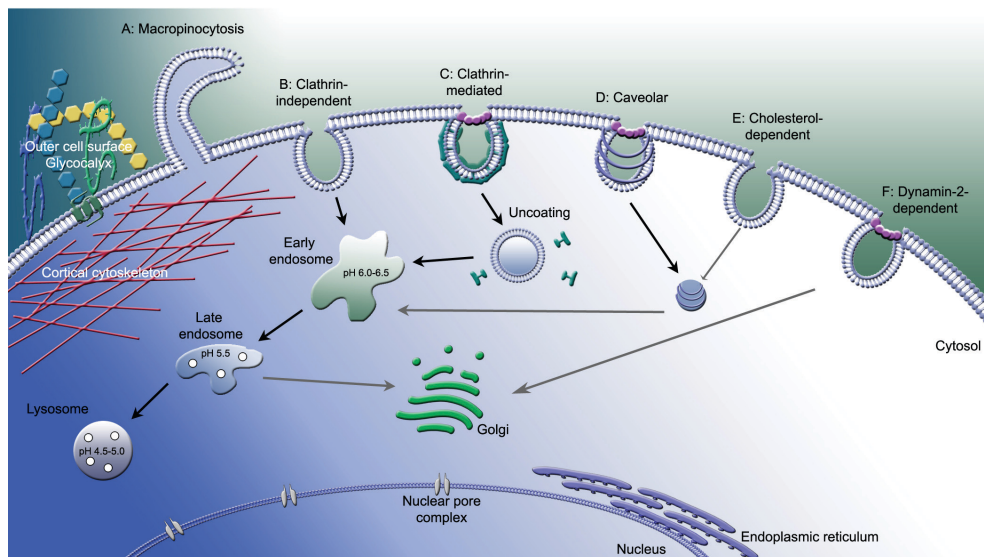


Figure 4: Endocytic entry pathways used by viruses. To avoid intracellular barriers, such as the cortical cytoskeleton, the majority of viruses makes use of endocytosis to enter host cells. The various uptake mechanisms are defined by the cellular host factors required for entry and include but are not limited to macropinocytosis, clathrin-independent, clathrin-mediated, caveolar, cholesterol- or lipid raft-dependent, and dynamin-2-dependent uptake mechanisms.

A large number of clathrin-independent pathways have been reported to be used by viruses for their uptake. These pathways are generally much less characterized than CME. Macropinocytosis involves the uptake of fluid and cargo into relatively large vesicles (Figure 4, A). It was shown to be involved in the entry of vaccinia virus, adenoviruses, and RSV (42, 63, 64). Macropinocytosis is strongly dependent on several signaling cascades and on actin, which is amongst others involved in the formation of membrane ruffles and protrusions that engulf a virion. Both dynamin-dependent and -independent modes of macropinocytosis have been described. It appears that factors involved in this entry pathway are cargo- and cell type specific (42, 63-65).

Other clathrin-independent pathways are classified based on the involvement of cellular host factors, morphology and cargo (Figure 4, B, D-F). Several cholesterol and lipid-raft dependent pathways have been described that require a variety of different host factors (Figure 4, D & E). Some of the lipid-raft mediated pathways are dependent on caveolin. Caveolin is a lipid-raft associated scaffold protein, capable of forming long-lived plasma membrane invaginations, so-called caveolae. Caveolae-mediated pathways have been shown to be involved in facilitating viral entry by formation of caveolin-coated invaginations and vesicles. However, caveolin itself has also been proposed to be involved as a negative regulator of other raft-mediated endocytosis pathways (66-69). Considerably less is known about these other raft-mediated pathways. They can be either dynamin-dependent (Figure 4, F), as shown for ligands like interleukin-2 and cholera toxin B only (70), or -independent (Figure 4, E). Recent

studies on SV40 have shown that in cells devoid of caveolin-1, the virus can employ a lipid raft dependent, but dynamin-2 independent entry pathway (71). Lymphocytic choriomeningitis virus has been shown to use a novel cholesterol-dependent but lipid raft independent entry route to achieve fusion in late endosomes (72, 73).

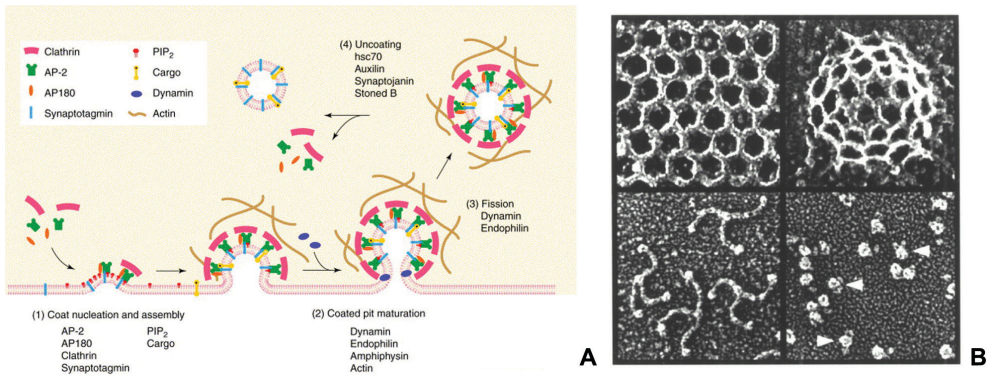


Figure 5: Clathrin-coated vesicle formation. A) Step 1: Recruitment of adaptors is initiated by receptor binding. Step 2: Recruitment of additional factors, such as dynamin, amphiphysin, and/or endophilin induces the curvature of the membrane and an invagination is formed. Step 3: Dynamin relocates from the lattice to the neck of the invagination to induce fission of the membrane by which the coated vesicle buds off. Step 4: In a coordinated process, uncoating of the vesicle occurs, followed by recycling of factors to the plasma membrane or their release into the cytosol. (Figures reproduced and adapted from (56, 57))

Once endocytosed, vesicles merge with early endosomes (EEs) (Figure 4). These compartments are characterized by a mildly acidic (pH 6.6-6.0) environment. Additional factors used to identify early endosomal compartments are Rab5 and the VPS34/p150 effector complex. Rab5 remains associated with the endosomal vesicles until these vesicles have matured to become late endosomes (LEs). Mature LEs are characterized by a pH between 6.0-4.9 and contain numerous intraluminal vesicles. The formation of late endosomes is initiated by the recruitment of Rab7 to the EEs by Rab5-GTP. In a closely coordinated process LEs mature further before they fuse with lysosomes. During this process the environment in the LEs shows an additional drop in pH and the number of ILVs increases further. The vesicles move to the perinuclear area and acquire new (lysosomal) components, particularly tethering complexes and SNAREs required for fusion with lysosomes. The process of LE to lysosome maturation is closely regulated by various protein complexes, including the CORVET and HOPS complexes. (40)

1.3. Study of viral entry pathways

Studying viral entry is a difficult task, since the particles are small and usually present in low numbers under physiologically relevant conditions. Therefore viral entry into host cells is mostly studied by measuring post-entry parameters, such as viral replication and/or the expression of a reporter, rather than by measuring entry *per se* (reviewed in (9, 74, 75)). The use of post-entry parameters does not allow distinguishing between the different stages of the entry process: e.g. binding, internalization, and fusion. The virus replication-dependent assays are, however, quite useful for studying entry in combination with a variety of host cell perturbations by using chemical inhibitors, RNAi-mediated gene silencing, or transfection of

plasmids expressing dominant-negative or constitutively-active regulatory proteins. Replication-dependent assays can give general insights into viral entry and when paired with the right controls may provide a good general picture of host factors and entry pathways employed by a virus. (74, 76-78)

To study different viral entry stages (attachment, uptake, penetration and uncoating) other methods need to be applied. One of the earliest methods used was based on electron microscopy (EM), in particular transmission EM. With this method, virus particles can be visualized during various stages of the entry process. However, it is difficult to identify cellular factors and pathways involved in the uptake process with this technique. In addition, EM is very labor intensive, usually requires high virus concentrations, and is not very suitable for medium or high throughput applications. New developments in the electron microscopy field have extended this method's success and usefulness in virological studies. Thus, focused ion beam-scanning electron microscopy allows for analysis of entire cells without having to continuously thin-sectioning and laborious re-location of the same spot, while correlation of light microscopy with transmission or scanning EM allows for easier localization of organelles and viruses without antibody staining being required. Furthermore, technical developments such as higher resolution cameras and introduction of point-spread functions allow for resolutions down to 5nm.

Another early means of studying virus entry was the use of radioactively-labeled virus particles. Radioactive labeling of viral structural components can be used to detect binding and internalization (51, 79, 80). In addition to requiring the handling of radioactive components and elaborate protocols, this technique does not allow the detection of virus fusion directly.

Virus entry has also been studied by fluorescence microscopy (FM), either by detecting replication-dependent (fluorescent) protein expression or by imaging of fluorescently-labeled virions. Fluorescent virions may be generated by the expression of structural proteins that are genetically fused to fluorescent proteins or by chemical labeling. Investigating virus entry using fluorescent virions allows for the examination of various details of the entry process by using e.g. co-localization, live-cell microscopy, or virus tracking (e.g. (79, 81-84)). Whereas FM studies based on the expression of fluorescent reporter proteins may be used for high-throughput experiments and can be used for a wide variety of viruses, the study of fluorescently-labeled virions is laborious, requires high magnification and resolution, and is rarely suited for non-enveloped viruses.

Different specialized fusion assays have been developed over the last few decades. Early examples involved labeling of virions using self-quenching dyes or the activation of photosensitized labeling on virions by fluorescent lipids on target membranes. Fusion of the viruses leads to a short-lived spark of fluorescence resulting from dequenching or activation of the dyes before the signal dies off due to diffusion (85-87). Unfortunately, these assays solely allow for the investigation of fusion and not of other entry steps, are technically challenging and difficult to adapt to non-enveloped viruses.

More recently, enzymes have been employed as reporters for virus entry by incorporating them into virions thereby allowing the investigation of entry independent of virus replication. Different enzymes, including firefly and gaussia luciferase, and β -lactamase, have been incorporated into virions via genetic fusion of these proteins to structural proteins (88-93). These enzyme-labeled virions may be used to analyze internalization of virus particles, simply

by analyzing the uptake of enzymatic activity, or for the specific analysis of virus-cell fusion events. In these latter assays, only the enzymatic activity of enzymes exposed to the cytosol is measured, as only these enzymes have access to their substrate. However, the integration of an entire enzyme can severely affect virus assembly and/or infectivity.

2. Coronaviruses

Coronaviruses (CoVs) are enveloped, plus-strand, nonsegmented RNA viruses belonging to the subfamily *Coronavirinae* of the family *Coronaviridae* in the order *Nidovirales*. CoVs can infect a wide variety of mammalian and avian species. In mammals, CoVs generally cause respiratory and/or intestinal tract disease. CoVs are widespread in companion and farm animals and may cause large economic losses. For example, porcine epidemic diarrhea virus (PEDV), which causes severe diarrhea and dehydration, is particularly threatening to piglets. PEDV is widespread in East-Asia and has recently transmitted to the USA and Canada (94, 95). Another example is feline enteric coronavirus (FECV), a frequently occurring pathogen, particularly in multipersettle cat households. Infection with FECV may end with a fatal peritonitis when the virus mutates into the much more pathogenic feline infectious peritonitis virus (FIPV) (96, 97). Human coronaviruses (HCoVs) are known as major causes of the common cold (e.g. HCoV-229E and HCoV-OC43). However, the emergence of new HCoVs of zoonotic origin has shown the potential of CoVs to cause life-threatening disease in humans as was demonstrated during the 2002/2003 SARS-CoV epidemics and more recently for MERS-CoV in the Middle East (98, 99). The well-studied murine hepatitis virus (MHV) is often used as a safe model to study CoV infections.

2.4. Coronavirion

CoVs contain a plus-stranded RNA genome of between 26-32 Kb long the first about two-thirds of which encode the replicase polyproteins, while the remaining 3'-part encodes the structural and accessory proteins. The CoV virion contains a canonical set of four structural proteins forming a pleomorphic virion of about 80-120 nm in diameter (Figure 6). Viral genomic RNA is encapsidated by the nucleocapsid protein (N) to form the flexible, helical nucleocapsid. N proteins bind the 5'-capped, polyadenylated RNA genome in a beads-of-string configuration (100). Surrounding the capsid is the viral lipoprotein envelope, which contains the membrane protein (M), the small envelope protein (E), as well as the spike glycoprotein (S). The triple spanning M protein is the most abundant structural protein of the virion that does interact with all other structural virion components (100, 101). The E polypeptide has ion channel activity and plays an important role in virion assembly. Co-expression of M and E allows the formation of virion like particles devoid of RNPs and S proteins (102). Some of the group 2 coronaviruses encode another membrane protein, the haemagglutinin-esterase (HE). Functioning as an interaction partner with the cellular glycolyx HE seems to be vital to viruses *in vivo*, however not *in vitro* (103). Trimers of the S protein, a type I membrane protein belonging to the class I fusion proteins, form the peplomers that protrude from the virion surface (21). S functions as attachment and fusion protein.

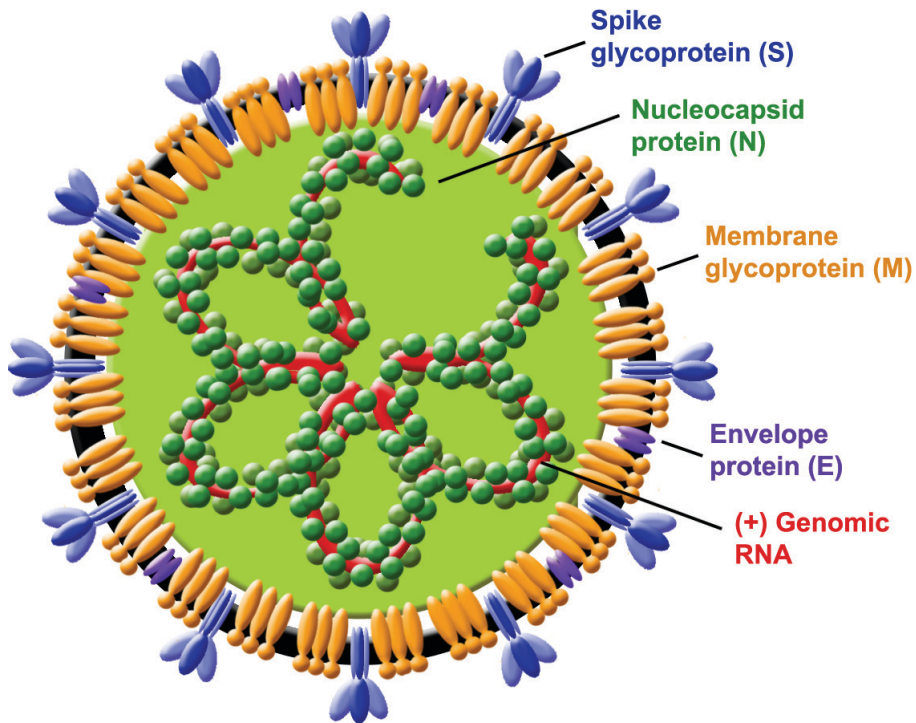


Figure 6: Structure of the coronavirus virion: The schematic depicts the four canonical structural proteins of the coronavirus virion; spike glycoprotein S, nucleocapsid protein N, membrane glycoprotein M, envelope protein E, as well as the encapsidated (+) strand, non-segmented viral genomic RNA.

2.5. Coronavirus life cycle

Binding of S protein to a host-specific receptor initiates the uptake mechanism of CoVs into a host cell (Figure 7). A number of different receptors have been described for different CoVs; examples are angiotensin-converting enzyme 2 (ACE2) acting as receptor for SARS-CoV, dipeptidyl peptidase-4 (DPP4) for MERS-CoV, and carcinoembryonic antigen-related cell adhesion molecule-1 (CEACAM1) for MHV (reviewed in (104)). A few studies suggest that some CoVs may enter via direct fusion at the plasma membrane, mainly based on the observation that these CoVs are able to induce cell-cell fusion at neutral pH (105, 106). However, most studies appear to indicate that CoVs need to enter via endocytic uptake prior to penetration.

Once the virion nucleocapsid, containing the genomic RNA, is released into the cytosol translation of the open reading frames (ORFs) 1a and 1b, the so-called *replicase* genes may begin. Translation of ORF1a and ORF1b generates two large polyproteins, pp1a and pp1ab. The latter is synthesized via a ribosomal frameshift mechanism. Precursors pp1a and pp1ab are autoproteolytically cleaved into nsps 1-10 or nsps 1-15/16, respectively. The nsps induce the formation of a complex three-dimensional replicative structure of membranes, which consists among others of a network of convoluted membranes (CMs) and double-membrane

vesicles (DMVs) (107-109) (Figure 7, bottom). Together with yet unknown host proteins, the nsps form the replication-transcription complexes (RTC), which are associated with the replicative structures. The exact intracellular location of RNA synthesis is not yet known (110, 111).

Once the RTCs are formed, the positive-sense genomic RNA is transcribed into a full-length as well as into subgenomic-length negative strands, the latter via a discontinuous transcription process. The negative strands serve as templates for the synthesis of the nested set of 3'-coterminal plus-sense genomic- and subgenomic(sg)-length mRNAs. While the genome-length mRNAs are translated into the pp1a and pp1ab, the sg mRNAs are translated into the structural and accessory proteins (112, 113).

The virion membrane proteins E, M, S and, in some viruses, HE are inserted into the endoplasmic reticulum (ER) where they are glycosylated and folded. N is translated in the cytosol, where it assembles with the genomic viral RNA to form new viral nucleocapsids. The structural viral proteins are transported from the ER to the endoplasmic reticulum-Golgi intermediate compartment (ERGIC) where new virions are assembled via budding of the nucleocapsids through the membrane of the ERGIC that is modified by M, E and S. Virion assembly may shift later in infection to the ER (114). The M protein appears to be the key player in the assembly, as it interacts with all other virion components. Expression of M with E is sufficient for the assembly of enveloped virus-like particles. (102), However, assembly appears more efficient when the N protein is co-expressed (115). After their formation, virions are exported from the cells by exocytic transport to the plasma membrane. (114, 116, 117)

2.6. Coronavirus spike protein

The CoV S protein binds to host cell receptors. It is therefore the main determinant of the host range of a CoV. The S protein also mediates virus-cell fusion. The S protein belongs to the class I virus fusion glycoproteins and features in addition to a typical, mostly α -helical structure also the other structural elements typical of this class of fusion proteins (Fig. 8). The up to 1450 amino acid long protein is targeted co-translationally to the ER by an N-terminal signal peptide. A transmembrane region close to the C-terminus keeps the protein anchored in the membrane upon removal of the signal peptide. The CoV S protein is heavily glycosylated at up to 35 predicted glycosylation sites. Following synthesis, S proteins assemble into homotrimeric complexes that are directed to the site of virion formation by targeting signals in the S protein's C-terminus as well as by interactions with the M protein. The S protein can be divided into two functional subunits. The amino-terminal S1 subunit contains the receptor-binding domain, while the carboxy-terminal S2 subunit contains domains required for fusion, including the fusion peptide (FP), heptad repeat domains (HR) HR1 and HR2, and the transmembrane (TM) domain (104, 118). (114, 119)

There are two proteolytic cleavage sites within the MHV spike protein that have been indicated to influence virus entry and fusion. One cleavage site is found at the S1/S2 interface and occurs only in a subset of CoVs, including most b- and g-CoVs and a few a-CoVs (feline coronaviruses in particular). The S1/S2 cleavage site consists of a usually suboptimal furin cleavage site with an R-X-(R/K)-R amino acid sequence. Proteolysis is mediated by furin and furin-like serine proteases during exocytosis of the virus. The cleavage is generally incomplete, meaning that only about 30% of all S proteins present on a virion are cleaved at this site (106).

The other cleavage site, the so-called S2' site has been proposed to be located immediately upstream of FP for three coronaviruses; MHV-2, SARS-CoV, and IBV (reviewed in (104)).

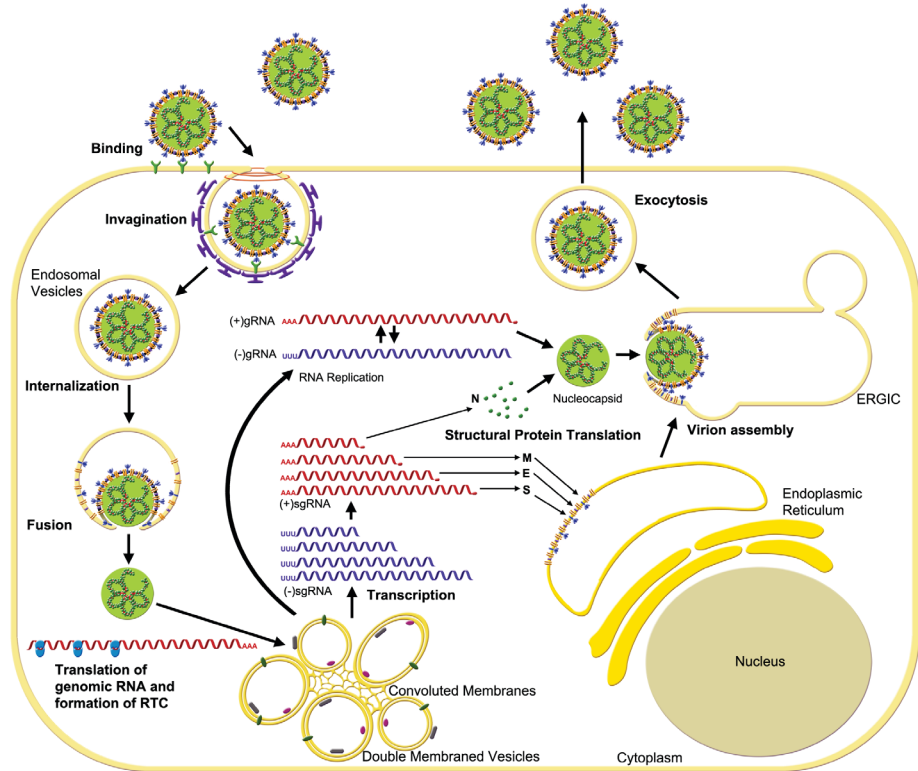


Figure 7: Overview of the coronavirus life cycle. Viruses bind to a cell-specific receptor at the host cell surface. They become internalized by endocytic uptake and their nucleocapsid is delivered to the cytosol. Translation of the *replicase* genes initiates the formation of the replicative structures that consist of CMs and DMVs and that contain the replication-transcription complexes (RTC). Genomic viral RNA is replicated and transcribed into sub-genomic RNA (sgRNA) at the RTCs. Translation of the sgRNA leads to the production of structural proteins in the cytosol and at the ER membrane. In the cytosol, interaction of N with the genomic viral RNA allows formation of nucleocapsids. Virion assembly takes place at the endoplasmic reticulum-Golgi intermediate compartment (ERGIC), by budding of nucleocapsids through membranes of the ERGIC that contain the other structural viral proteins S, M, E and, in some cases, HE. Using an exocytic pathway the virions get exported to the extracellular space.

Class I fusion proteins require proteolytic priming and a subsequent trigger to undergo the rearrangements necessary for membrane fusion. Priming is a process that is only incompletely understood in CoVs. It is not clear to what extent cleavage at the S1/S2 correlates with proteolytic priming as cleavage at this position is not observed for all CoVs, and does not seem to be required for infectivity. The MHV-2 strain has been shown to be uncleaved at the S1/S2 site (120). Consistently, when the S1/S2 cleavage site present in the strain MHV-A59 S protein was removed it had no effect on infectivity; yet, the mutation strongly reduced the cell-cell fusion abilities of the virus (121-123). In contrast to the cleavages observed for other class I fusion proteins, including influenza virus haemagglutinin or HIV-1 Env protein, where

the cleavage site is located immediately upstream of the fusion peptide (18, 19, 23), the S1/S2 site is located far upstream of the putative fusion peptide (Fig. 8). In this respect, a proposed cleavage site at the S2' site seems to correlate better with the cleavage sites observed in other class I fusion proteins. However, while cleavage at this position has been suggested for some CoVs (reviewed in (104)), it has not been formally demonstrated yet.

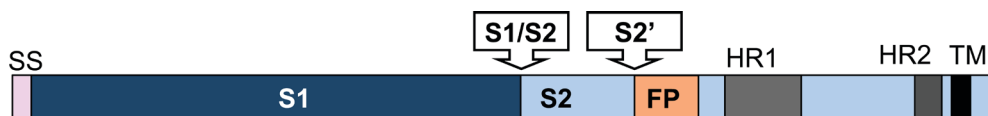


Figure 8: Schematic outline of the structure of a CoV S glycoprotein. The signal sequence (SS) at the N-terminus, which gets removed post-translationally. The S1 domain (dark blue) containing the receptor-binding domain. The S2 domain (light blue) containing the putative fusion peptide (FP), heptad repeat domains (HR) HR1 and HR2, and the transmembrane domain (TM). The two potential proteolytic cleavage sites have been indicated above; S1/S2 and S2'.

2.7. Coronavirus entry pathways

The particular route of entry taken by a virus is likely not only determined by the receptors used for attachment and uptake, but also by the specific environmental cues that trigger fusion. The triggers that induce CoV-cell fusion have, however, not been elucidated. As previously described, the entry of coronaviruses is under debate as to whether the viruses are capable of initiating a successful infection by fusion at the plasma membrane, or whether endocytic uptake is required. This situation is not made any easier by the fact that even different strains of the same coronavirus have been reported to display different S protein proteolytic cleavages and pH sensitivities, and to use different entry routes.

Several CoV S proteins can induce cell-cell fusion when expressed at the surface of receptor-containing cells. For MHV and SARS-CoV, this phenomenon could be linked to the proteolytic processing of their S proteins (106, 120-122, 124, 125). As these processes happen at neutral pH, it was initially thought that the cell-cell fusogenicity of CoVs reflected the ability of these viruses to fuse at the plasma membrane. For instance, the strain MHV-4 (also known as MHV-JHM) is able to cause extensive cell-cell fusion and to spread from infected cells containing the MHV receptor mCEACAM1 to non-receptor-containing cells (126-129).

Despite the ability of several CoVs to induce cell-cell fusion, multiple papers indicate that endocytic uptake is required for successful infection. However, no common endocytic pathway has been shown to be required for infection with different CoVs or even with different strains of the same virus. Three different strains of the well-studied model for CoV infections, MHV, have been described to rely on different factors relating to viral entry. MHV-4 and MHV-2 have been described to rely on endosomal maturation, at least in certain cells as described above (130-132). MHV-2 entry was further characterized to occur by a clathrin-dependent endocytic pathway, independent of the adaptor protein Epsin 15 (132). For the most commonly used MHV strain, MHV-A59, there is some divergence in the findings on entry pathways. While some studies report that MHV-A59 enters via clathrin-mediated endocytosis and is sensitive to lysosomotropic agents that affect endocytosis (133), this is not the case according to others (132). Entry of MHV has also been reported to be dependent on lipid rafts (134). Clathrin-dependent as well as clathrin- and caveolae-independent entry pathways have been reported for SARS-CoV (135, 136). Also feline infectious peritonitis virus (FIPV)

was suggested to enter via a clathrin- and caveolae-independent endocytic route (137, 138). For the avian coronavirus infectious bronchitis virus (IBV) endosomal maturation was shown to be required for infection (139). The human coronavirus HCoV-229E has been described to use a caveolae-dependent endocytic uptake pathway (140).

Interestingly, evaluation of mutant CoVs showed that cell-cell fusion, but not viral infection was inhibited by mutation of the S1/S2 proteolytic cleavage site (121, 122, 125, 141). Treatment of cell-bound virus particles with different proteases was shown to enhance virus entry and/or cell-cell fusion (123, 132, 142-148). For a number of CoVs, the proteolytic activity in the endosomal compartments has been shown to be important for successful infection. Inhibitors of cathepsin proteases were shown to inhibit entry of SARS-CoV and feline CoVs (137, 149, 150). Interestingly, although MHV-2 and -A59 were both reported to enter via clathrin-mediated endocytosis, entry of MHV-2 but not of MHV-A59, was blocked by inhibitors of low-pH activated cathepsin proteases (132, 151). Some studies indicate cathepsin to cleave close to the S1/S2 boundary of CoVs (149, 150, 152). However, from other studies on SARS-CoV and IBV it appears that a proteolytic cleavage of the S protein at a more downstream position than the S1/S2 boundary upon receptor binding is also of importance for cell entry (143, 146, 153-155).

3. Aim and outline of this thesis

As described in the previous sections and subchapters, many aspects to CoV entry are still unclear or under debate by the science community. Many fundamental questions concerning the cleavage requirements of the CoV S proteins, the CoV uptake mechanism and the role of host factors in CoV remain to be elucidated. The aim of this thesis is to get a better understanding of CoV entry processes in general and that of MHV in particular. We aim to shed light on the priming and triggering mechanisms involved in MHV fusion and to link them to the entry pathways employed by CoVs.

Studies of viral entry still mostly depend on the interpretation of post-entry parameters. The lack of assays to study biochemical and cell biological aspects of this important process directly hampers the analysis of this key process in virus infection. In chapters two and three we therefore set out to develop novel techniques to investigate the different steps of viral entry including binding, internalization, penetration and proteolytic processing in a replication-independent manner. In chapter two we describe a novel, highly adaptable viral entry assay making use of minimal complementation of the *E. coli* β -galactosidase in mammalian cells. Enzyme activity is reconstituted when a small intravirion peptide (α -peptide) is complementing the inactive mutant form Δ M15 of β -galactosidase. The method allowed us to dissect and detect binding, internalization, and fusion of viruses during host cell entry. In chapter three we describe a novel biochemical assay to study the biochemical aspects of MHV S protein priming and triggering. Proteolytic priming of the CoV S fusion protein had been proposed, but not yet formally demonstrated to occur in the target cell, rather than the producer cell (reviewed in (104)). Development of a conditional biotinylation assay for the prototypic coronavirus MHV allowed detection of S protein cleavage only of those virus particles that actually fused with the target cells. We demonstrated that MHV S proteins are indeed cleaved upon virus endocytosis and identified a novel processing product.

While MHV had been demonstrated to enter via clathrin-mediated endocytosis (132, 133), no other host factors critical for entry of MHV had previously been identified. Using our

newly developed entry assays, described in chapter 2, in combination with other cell biological and biochemical techniques, we characterized the MHV entry process and the host factor requirements in detail. In chapter four we confirmed the importance of clathrin-mediated endocytosis and demonstrated that trafficking of MHV to lysosomes is required for fusion and productive entry to occur. We furthermore showed that entry of MHV depended on proteolytic processing of its fusion protein S by lysosomal proteases. Manipulation of the S2' cleavage site allowed us to relocate the intracellular site of fusion from lysosomes to early endosomes. Also for other CoVs the identity of the cleavage site directly upstream of the fusion peptide was shown to correlate with fusion in early endosomes or lysosomes, which led us to conclude that this cleavage is an essential determinant of the intracellular site of fusion.

In chapter five, we zoomed in on one critical cellular component in the CoV entry process and elucidated the importance of the α -subunit of the Na^+, K^+ -ATPase, encoded by the ATP1A1 gene. By using gene silencing as well as by applying cardiotonic drugs that bind to the ATP1A1 we could reveal that Src signaling mediated via ATP1A1 plays a crucial role in the inhibition of CoVs. Cardiotonic steroids were shown to inhibit entry of MHV at an early stage resulting in the accumulation of virus particles close to the cell surface.

Chapter six of this thesis provides a summarizing discussion in which our findings on CoV entry are placed in the broader context of the available literature with the aim to integrate the different aspects of CoV entry – including endocytic uptake, proteolytic cleavage of S and the intracellular site of fusion – into a general picture.

REFERENCES

1. Ge XY, Li JL, Yang XL, Chmura AA, Zhu G, Epstein JH, Mazet JK, Hu B, Zhang W, Peng C, Zhang YJ, Luo CM, Tan B, Wang N, Zhu Y, Cramer G, Zhang SY, Wang LF, Daszak P, Shi ZL. 2013. Isolation and characterization of a bat SARS-like coronavirus that uses the ACE2 receptor. *Nature* **503**:535-538.
2. Memish ZA, Cotten M, Meyer B, Watson SJ, Alshahfi AJ, Al Rabeeah AA, Corman VM, Sieberg A, Makhdoom HQ, Assiri A, Al Masri M, Aldabbagh S, Bosch BJ, Beer M, Muller MA, Kellam P, Drosten C. 2014. Human infection with MERS coronavirus after exposure to infected camels, Saudi Arabia, 2013. *Emerging infectious diseases* **20**:1012-1015.
3. Smith GJ, Vijaykrishna D, Bahl J, Lycett SJ, Worobey M, Pybus OG, Ma SK, Cheung CL, Raghvani J, Bhatt S, Peiris JS, Guan Y, Rambaut A. 2009. Origins and evolutionary genomics of the 2009 swine-origin H1N1 influenza A epidemic. *Nature* **459**:1122-1125.
4. Peters CJ, LeDuc JW. 1999. An introduction to Ebola: the virus and the disease. *The Journal of infectious diseases* **179 Suppl 1**:ix-xvi.
5. Knipe DM, Howley PME. 2013. *Fields virology*. Philadelphia: Lippincott Williams & Wilkins **6th ed**.
6. Reitsma S, Slaaf DW, Vink H, van Zandvoort MA, oude Egbrink MG. 2007. The endothelial glycocalyx: composition, functions, and visualization. *Pflügers Archiv : European journal of physiology* **454**:345-359.
7. Bomsel M, Alfsen A. 2003. Entry of viruses through the epithelial barrier: pathogenic trickery. *Nature reviews. Molecular cell biology* **4**:57-68.
8. Marsh M, Helenius A. 1989. Virus entry into animal cells. *Advances in virus research* **36**:107-151.
9. Marsh M, Helenius A. 2006. Virus entry: open sesame. *Cell* **124**:729-740.
10. Mercer J, Schelhaas M, Helenius A. 2010. Virus entry by endocytosis. *Annual review of biochemistry* **79**:803-833.
11. Whittaker GR, Kann M, Helenius A. 2000. Viral entry into the nucleus. *Annual review of cell and developmental biology* **16**:627-651.
12. Radtke K, Dohner K, Sodeik B. 2006. Viral interactions with the cytoskeleton: a hitchhiker's guide to the cell. *Cellular microbiology* **8**:387-400.
13. Chernomordik LV, Kozlov MM. 2003. Protein-lipid interplay in fusion and fission of biological membranes. *Annual review of biochemistry* **72**:175-207.
14. Harrison SC. 2008. Viral membrane fusion. *Nature structural & molecular biology* **15**:690-698.
15. Martens S, McMahon HT. 2008. Mechanisms of membrane fusion: disparate players and common principles. *Nature reviews. Molecular cell biology* **9**:543-556.
16. Chernomordik LV, Zimmerberg J, Kozlov MM. 2006. Membranes of the world unite! *The Journal of cell biology* **175**:201-207.
17. Igonet S, Rey FA. 2012. SnapShot: Viral and eukaryotic protein fusogens. *Cell* **151**:1634-1634 e1631.
18. Wilson IA, Skehel JJ, Wiley DC. 1981. Structure of the haemagglutinin membrane glycoprotein of influenza virus at 3 Å resolution. *Nature* **289**:366-373.

19. **Tran EE, Borgnia MJ, Kuybeda O, Schauder DM, Bartesaghi A, Frank GA, Sapiro G, Milne JL, Subramaniam S.** 2012. Structural mechanism of trimeric HIV-1 envelope glycoprotein activation. *PLoS pathogens* **8**:e1002797.
20. **Weissenhorn W, Carfi A, Lee KH, Skehel JJ, Wiley DC.** 1998. Crystal structure of the Ebola virus membrane fusion subunit, GP2, from the envelope glycoprotein ectodomain. *Molecular cell* **2**:605-616.
21. **Bosch BJ, van der Zee R, de Haan CA, Rottier PJ.** 2003. The coronavirus spike protein is a class I virus fusion protein: structural and functional characterization of the fusion core complex. *Journal of virology* **77**:8801-8811.
22. **White JM, Schornberg KL.** 2012. A new player in the puzzle of filovirus entry. *Nature reviews. Microbiology* **10**:317-322.
23. **Bullough PA, Hughson FM, Skehel JJ, Wiley DC.** 1994. Structure of influenza haemagglutinin at the pH of membrane fusion. *Nature* **371**:37-43.
24. **Skehel JJ, Wiley DC.** 2000. Receptor binding and membrane fusion in virus entry: the influenza hemagglutinin. *Annual review of biochemistry* **69**:531-569.
25. **Chen J, Skehel JJ, Wiley DC.** 1999. N- and C-terminal residues combine in the fusion-pH influenza hemagglutinin HA(2) subunit to form an N cap that terminates the triple-stranded coiled coil. *Proceedings of the National Academy of Sciences of the United States of America* **96**:8967-8972.
26. **Danieli T, Pelletier SL, Henis YI, White JM.** 1996. Membrane fusion mediated by the influenza virus hemagglutinin requires the concerted action of at least three hemagglutinin trimers. *The Journal of cell biology* **133**:559-569.
27. **Lescar J, Roussel A, Wien MW, Navaza J, Fuller SD, Wengler G, Wengler G, Rey FA.** 2001. The Fusion glycoprotein shell of Semliki Forest virus: an icosahedral assembly primed for fusogenic activation at endosomal pH. *Cell* **105**:137-148.
28. **Kuhn RJ, Zhang W, Rossmann MG, Pletnev SV, Corver J, Lenches E, Jones CT, Mukhopadhyay S, Chipman PR, Strauss EG, Baker TS, Strauss JH.** 2002. Structure of dengue virus: implications for flavivirus organization, maturation, and fusion. *Cell* **108**:717-725.
29. **Tischler ND, Gonzalez A, Perez-Acle T, Roseblatt M, Valenzuela PD.** 2005. Hanta-virus Gc glycoprotein: evidence for a class II fusion protein. *The Journal of general virology* **86**:2937-2947.
30. **Modis Y, Ogata S, Clements D, Harrison SC.** 2004. Structure of the dengue virus envelope protein after membrane fusion. *Nature* **427**:313-319.
31. **Vaney MC, Rey FA.** 2011. Class II enveloped viruses. *Cellular microbiology* **13**:1451-1459.
32. **Roche S, Rey FA, Gaudin Y, Bressanelli S.** 2007. Structure of the prefusion form of the vesicular stomatitis virus glycoprotein G. *Science* **315**:843-848.
33. **Roche S, Bressanelli S, Rey FA, Gaudin Y.** 2006. Crystal structure of the low-pH form of the vesicular stomatitis virus glycoprotein G. *Science* **313**:187-191.
34. **Kadlec J, Loureiro S, Abrescia NG, Stuart DI, Jones IM.** 2008. The postfusion structure of baculovirus gp64 supports a unified view of viral fusion machines. *Nature structural & molecular biology* **15**:1024-1030.
35. **Heldwein EE, Lou H, Bender FC, Cohen GH, Eisenberg RJ, Harrison SC.** 2006. Crystal structure of glycoprotein B from herpes simplex virus 1. *Science* **313**:217-220.

36. Eisenberg RJ, Atanasiu D, Cairns TM, Gallagher JR, Krummenacher C, Cohen GH. 2012. Herpes virus fusion and entry: a story with many characters. *Viruses* **4**:800-832.
37. Backovic M, Jardetzky TS. 2009. Class III viral membrane fusion proteins. *Current opinion in structural biology* **19**:189-196.
38. Roche S, Albertini AA, Lepault J, Bressanelli S, Gaudin Y. 2008. Structures of vesicular stomatitis virus glycoprotein: membrane fusion revisited. *Cellular and molecular life sciences* : CMLS **65**:1716-1728.
39. Authier F, Posner BI, Bergeron JJ. 1996. Endosomal proteolysis of internalized proteins. *FEBS letters* **389**:55-60.
40. Huotari J, Helenius A. 2011. Endosome maturation. *The EMBO journal* **30**:3481-3500.
41. Plemper RK. 2011. Cell entry of enveloped viruses. *Current opinion in virology* **1**:92-100.
42. Krzyzaniak MA, Zumstein MT, Gerez JA, Picotti P, Helenius A. 2013. Host cell entry of respiratory syncytial virus involves macropinocytosis followed by proteolytic activation of the F protein. *PLoS pathogens* **9**:e1003309.
43. Wool-Lewis RJ, Bates P. 1999. Endoproteolytic processing of the ebola virus envelope glycoprotein: cleavage is not required for function. *Journal of virology* **73**:1419-1426.
44. Zimmer G, Budz L, Herrler G. 2001. Proteolytic activation of respiratory syncytial virus fusion protein. Cleavage at two furin consensus sequences. *The Journal of biological chemistry* **276**:31642-31650.
45. Chandran K, Sullivan NJ, Felbor U, Whelan SP, Cunningham JM. 2005. Endosomal proteolysis of the Ebola virus glycoprotein is necessary for infection. *Science* **308**:1643-1645.
46. Fuller AO, Spear PG. 1987. Anti-glycoprotein D antibodies that permit adsorption but block infection by herpes simplex virus 1 prevent virion-cell fusion at the cell surface. *Proceedings of the National Academy of Sciences of the United States of America* **84**:5454-5458.
47. Sodeik B, Ebersold MW, Helenius A. 1997. Microtubule-mediated transport of incoming herpes simplex virus 1 capsids to the nucleus. *The Journal of cell biology* **136**:1007-1021.
48. Okada Y. 1969. Factors in fusion of cells by HVJ. *Current topics in microbiology and immunology* **48**:102-128.
49. Permanyer M, Ballana E, Este JA. 2010. Endocytosis of HIV: anything goes. *Trends in microbiology* **18**:543-551.
50. Stein BS, Gowda SD, Lifson JD, Penhallow RC, Bensch KG, Engleman EG. 1987. pH-independent HIV entry into CD4-positive T cells via virus envelope fusion to the plasma membrane. *Cell* **49**:659-668.
51. Matlin KS, Reggio H, Helenius A, Simons K. 1982. Pathway of vesicular stomatitis virus entry leading to infection. *Journal of molecular biology* **156**:609-631.
52. Brodsky FM, Chen CY, Knuehl C, Towler MC, Wakeham DE. 2001. Biological basket weaving: formation and function of clathrin-coated vesicles. *Annual review of cell and developmental biology* **17**:517-568.
53. Conner SD, Schmid SL. 2003. Regulated portals of entry into the cell. *Nature* **422**:37-44.
54. De Camilli P, Takei K. 1996. Molecular mechanisms in synaptic vesicle endocytosis and recycling. *Neuron* **16**:481-486.

-
55. **Kirchhausen T.** 1993. Coated Pits and Coated Vesicles - Sorting It All Out. *Current opinion in structural biology* **3**:182-188.
 56. **Schmid SL.** 1997. Clathrin-coated vesicle formation and protein sorting: an integrated process. *Annual review of biochemistry* **66**:511-548.
 57. **Takei K, Haucke V.** 2001. Clathrin-mediated endocytosis: membrane factors pull the trigger. *Trends in cell biology* **11**:385-391.
 58. **Ungewickell EJ, Hinrichsen L.** 2007. Endocytosis: clathrin-mediated membrane budding. *Current opinion in cell biology* **19**:417-425.
 59. **Young A.** 2007. Structural insights into the clathrin coat. *Seminars in cell & developmental biology* **18**:448-458.
 60. **Rust MJ, Lakadamyali M, Zhang F, Zhuang X.** 2004. Assembly of endocytic machinery around individual influenza viruses during viral entry. *Nature structural & molecular biology* **11**:567-573.
 61. **Johannsdottir HK, Mancini R, Kartenbeck J, Amato L, Helenius A.** 2009. Host cell factors and functions involved in vesicular stomatitis virus entry. *Journal of virology* **83**:440-453.
 62. **Cureton DK, Massol RH, Saffarian S, Kirchhausen TL, Whelan SP.** 2009. Vesicular stomatitis virus enters cells through vesicles incompletely coated with clathrin that depend upon actin for internalization. *PLoS pathogens* **5**:e1000394.
 63. **Mercer J, Helenius A.** 2008. Vaccinia virus uses macropinocytosis and apoptotic mimicry to enter host cells. *Science* **320**:531-535.
 64. **Amstutz B, Gastaldelli M, Kalin S, Imelli N, Boucke K, Wandeler E, Mercer J, Hemmi S, Greber UF.** 2008. Subversion of CtBP1-controlled macropinocytosis by human adenovirus serotype 3. *The EMBO journal* **27**:956-969.
 65. **Grimmer S, van Deurs B, Sandvig K.** 2002. Membrane ruffling and macropinocytosis in A431 cells require cholesterol. *Journal of cell science* **115**:2953-2962.
 66. **Le PU, Guay G, Altschuler Y, Nabi IR.** 2002. Caveolin-1 is a negative regulator of caveolae-mediated endocytosis to the endoplasmic reticulum. *The Journal of biological chemistry* **277**:3371-3379.
 67. **Nabi IR, Le PU.** 2003. Caveolae/raft-dependent endocytosis. *The Journal of cell biology* **161**:673-677.
 68. **Pelkmans L, Kartenbeck J, Helenius A.** 2001. Caveolar endocytosis of simian virus 40 reveals a new two-step vesicular-transport pathway to the ER. *Nature cell biology* **3**:473-483.
 69. **Puri V, Watanabe R, Singh RD, Dominguez M, Brown JC, Wheatley CL, Marks DL, Pagano RE.** 2001. Clathrin-dependent and -independent internalization of plasma membrane sphingolipids initiates two Golgi targeting pathways. *The Journal of cell biology* **154**:535-547.
 70. **Lamaze C, Dujancourt A, Baba T, Lo CG, Benmerah A, Dautry-Varsat A.** 2001. Interleukin 2 receptors and detergent-resistant membrane domains define a clathrin-independent endocytic pathway. *Molecular cell* **7**:661-671.
 71. **Damm EM, Pelkmans L, Kartenbeck J, Mezzacasa A, Kurzchalia T, Helenius A.** 2005. Clathrin- and caveolin-1-independent endocytosis: entry of simian virus 40 into cells devoid of caveolae. *The Journal of cell biology* **168**:477-488.

72. **Quirin K, Eschli B, Scheu I, Poort L, Kartenbeck J, Helenius A.** 2008. Lymphocytic choriomeningitis virus uses a novel endocytic pathway for infectious entry via late endosomes. *Virology* **378**:21-33.
73. **Rojek JM, Perez M, Kunz S.** 2008. Cellular entry of lymphocytic choriomeningitis virus. *Journal of virology* **82**:1505-1517.
74. **Mercer J, Schelhaas M, Helenius A.** 2010. Virus entry by endocytosis. *Annu Rev Biochem* **79**:803-833.
75. **Sieczkarski SB, Whittaker GR.** 2002. Dissecting virus entry via endocytosis. *J Gen Virol* **83**:1535-1545.
76. **Dutta D, Donaldson JG.** 2012. Search for inhibitors of endocytosis: Intended specificity and unintended consequences. *Cellular logistics* **2**:203-208.
77. **Mercer J, Helenius A.** 2009. Virus entry by macropinocytosis. *Nat Cell Biol* **11**:510-520.
78. **Lozach PY, Mancini R, Bitto D, Meier R, Oestereich L, Overby AK, Pettersson RF, Helenius A.** 2010. Entry of bunyaviruses into mammalian cells. *Cell host & microbe* **7**:488-499.
79. **Johannsdottir HK, Mancini R, Kartenbeck J, Amato L, Helenius A.** 2009. Host cell factors and functions involved in vesicular stomatitis virus entry. *J Virol* **83**:440-453.
80. **Matlin KS, Reggio H, Helenius A, Simons K.** 1981. Infectious entry pathway of influenza virus in a canine kidney cell line. *J Cell Biol* **91**:601-613.
81. **Fero M, Pogliano K.** 2010. Automated quantitative live cell fluorescence microscopy. *Cold Spring Harb Perspect Biol* **2**:a000455.
82. **Brandenburg B, Lee LY, Lakadamyali M, Rust MJ, Zhuang X, Hogle JM.** 2007. Imaging poliovirus entry in live cells. *PLoS Biol* **5**:e183.
83. **Engel S, Heger T, Mancini R, Herzog F, Kartenbeck J, Hayer A, Helenius A.** 2011. Role of endosomes in simian virus 40 entry and infection. *J Virol* **85**:4198-4211.
84. **Ewers H, Schelhaas M.** 2012. Analysis of virus entry and cellular membrane dynamics by single particle tracking. *Methods Enzymol* **506**:63-80.
85. **Chen YD, Blumenthal R.** 1989. On the use of self-quenching fluorophores in the study of membrane fusion kinetics. The effect of slow probe redistribution. *Biophysical chemistry* **34**:283-292.
86. **Lowy RJ, Sarkar DP, Chen Y, Blumenthal R.** 1990. Observation of single influenza virus-cell fusion and measurement by fluorescence video microscopy. *Proc Natl Acad Sci U S A* **87**:1850-1854.
87. **Raviv Y, Viard M, Bess J, Jr., Blumenthal R.** 2002. Quantitative measurement of fusion of HIV-1 and SIV with cultured cells using photosensitized labeling. *Virology* **293**:243-251.
88. **Cavrois M, De Noronha C, Greene WC.** 2002. A sensitive and specific enzyme-based assay detecting HIV-1 virion fusion in primary T lymphocytes. *Nature biotechnology* **20**:1151-1154.
89. **Kolokoltsov AA, Davey RA.** 2004. Rapid and sensitive detection of retrovirus entry by using a novel luciferase-based content-mixing assay. *J Virol* **78**:5124-5132.
90. **Saeed MF, Kolokoltsov AA, Davey RA.** 2006. Novel, rapid assay for measuring entry of diverse enveloped viruses, including HIV and rabies. *J Virol Methods* **135**:143-150.

-
91. **Wolf MC, Wang Y, Freiberg AN, Aguilar HC, Holbrook MR, Lee B.** 2009. A catalytically and genetically optimized beta-lactamase-matrix based assay for sensitive, specific, and higher throughput analysis of native henipavirus entry characteristics. *Virology journal* **6**:119.
 92. **Tscherne DM, Manicassamy B, Garcia-Sastre A.** 2010. An enzymatic virus-like particle assay for sensitive detection of virus entry. *J Virol Methods* **163**:336-343.
 93. **Laliberte JP, Weisberg AS, Moss B.** 2011. The membrane fusion step of vaccinia virus entry is cooperatively mediated by multiple viral proteins and host cell components. *PLoS pathogens* **7**:e1002446.
 94. **Huang YW, Dickerman AW, Pineyro P, Li L, Fang L, Kiehne R, Opriessnig T, Meng XJ.** 2013. Origin, evolution, and genotyping of emergent porcine epidemic diarrhea virus strains in the United States. *mBio* **4**:e00737-00713.
 95. **Song D, Park B.** 2012. Porcine epidemic diarrhoea virus: a comprehensive review of molecular epidemiology, diagnosis, and vaccines. *Virus genes* **44**:167-175.
 96. **Pedersen NC.** 2014. An update on feline infectious peritonitis: Diagnostics and therapeutics. *Veterinary journal* **201**:133-141.
 97. **Pedersen NC.** 2014. An update on feline infectious peritonitis: Virology and immunopathogenesis. *Veterinary journal* **201**:123-132.
 98. **Peiris JS, Lai ST, Poon LL, Guan Y, Yam LY, Lim W, Nicholls J, Yee WK, Yan WW, Cheung MT, Cheng VC, Chan KH, Tsang DN, Yung RW, Ng TK, Yuen KY.** 2003. Coronavirus as a possible cause of severe acute respiratory syndrome. *Lancet* **361**:1319-1325.
 99. **Zaki AM, van Boheemen S, Bestebroer TM, Osterhaus AD, Fouchier RA.** 2012. Isolation of a novel coronavirus from a man with pneumonia in Saudi Arabia. *N Engl J Med* **367**:1814-1820.
 100. **McBride R, van Zyl M, Fielding BC.** 2014. The Coronavirus Nucleocapsid Is a Multifunctional Protein. *Viruses* **6**:2991-3018.
 101. **Ruch TR, Machamer CE.** 2012. The coronavirus E protein: assembly and beyond. *Viruses* **4**:363-382.
 102. **Vennema H, Godeke GJ, Rossen JW, Voorhout WF, Horzinek MC, Opstelten DJ, Rottier PJ.** 1996. Nucleocapsid-independent assembly of coronavirus-like particles by co-expression of viral envelope protein genes. *The EMBO journal* **15**:2020-2028.
 103. **Lissenberg A, Vrolijk MM, van Vliet AL, Langereis MA, de Groot-Mijnes JD, Rottier PJ, de Groot RJ.** 2005. Luxury at a cost? Recombinant mouse hepatitis viruses expressing the accessory hemagglutinin esterase protein display reduced fitness in vitro. *Journal of virology* **79**:15054-15063.
 104. **Belouzard S, Millet JK, Licitra BN, Whittaker GR.** 2012. Mechanisms of coronavirus cell entry mediated by the viral spike protein. *Viruses* **4**:1011-1033.
 105. **Stauber R, Pfeleiderera M, Siddell S.** 1993. Proteolytic cleavage of the murine coronavirus surface glycoprotein is not required for fusion activity. *The Journal of general virology* **74** (Pt 2):183-191.
 106. **Sturman LS, Ricard CS, Holmes KV.** 1985. Proteolytic cleavage of the E2 glycoprotein of murine coronavirus: activation of cell-fusing activity of virions by trypsin and separation of two different 90K cleavage fragments. *Journal of virology* **56**:904-911.

107. **Knoops K, Kikkert M, Worm SH, Zevenhoven-Dobbe JC, van der Meer Y, Koster AJ, Mommaas AM, Snijder EJ.** 2008. SARS-coronavirus replication is supported by a reticulovesicular network of modified endoplasmic reticulum. *PLoS biology* **6**:e226.
108. **Ziebuhr J.** 2008. Coronavirus replicative proteins. In: Perlman S, Gallagher T, Snijder EJ (ed.). *Nidoviruses*. **Washington, DC**:65-81.
109. **Ulasli M, Verheije MH, de Haan CA, Reggiori F.** 2010. Qualitative and quantitative ultrastructural analysis of the membrane rearrangements induced by coronavirus. *Cellular microbiology* **12**:844-861.
110. **Snijder EJ, van der Meer Y, Zevenhoven-Dobbe J, Onderwater JJ, van der Meulen J, Koerten HK, Mommaas AM.** 2006. Ultrastructure and origin of membrane vesicles associated with the severe acute respiratory syndrome coronavirus replication complex. *Journal of virology* **80**:5927-5940.
111. **Hagemeijer MC, Vonk AM, Monastyrska I, Rottier PJ, de Haan CA.** 2012. Visualizing coronavirus RNA synthesis in time by using click chemistry. *Journal of virology* **86**:5808-5816.
112. **Sawicki SG, Sawicki DL, Siddell SG.** 2007. A contemporary view of coronavirus transcription. *Journal of virology* **81**:20-29.
113. **Hagemeijer MC, Rottier PJ, de Haan CA.** 2012. Biogenesis and dynamics of the coronavirus replicative structures. *Viruses* **4**:3245-3269.
114. **de Haan CA, Rottier PJ.** 2005. Molecular interactions in the assembly of coronaviruses. *Advances in virus research* **64**:165-230.
115. **Siu YL, Teoh KT, Lo J, Chan CM, Kien F, Escriou N, Tsao SW, Nicholls JM, Altmeyer R, Peiris JS, Bruzzone R, Nal B.** 2008. The M, E, and N structural proteins of the severe acute respiratory syndrome coronavirus are required for efficient assembly, trafficking, and release of virus-like particles. *Journal of virology* **82**:11318-11330.
116. **Hogue BG, Machamer CE.** 2008. Coronavirus structural proteins and virus assembl. In: Perlman S, Gallagher T, Snijder EJ (ed). *Nidoviruses*. **Washington, DC**:179-200.
117. **Masters PS, Perlman S.** 2013. Coronaviridae. In: Knipe DM, Howley PM (ed). *Fields Virology 6th Philadelphia: Lippincott Williams & Wilkins*:825-858.
118. **Heald-Sargent T, Gallagher T.** 2012. Ready, set, fuse! The coronavirus spike protein and acquisition of fusion competence. *Viruses* **4**:557-580.
119. **Perlman S, Netland J.** 2009. Coronaviruses post-SARS: update on replication and pathogenesis. *Nature reviews. Microbiology* **7**:439-450.
120. **Yamada YK, Takimoto K, Yabe M, Taguchi F.** 1998. Requirement of proteolytic cleavage of the murine coronavirus MHV-2 spike protein for fusion activity. *Advances in experimental medicine and biology* **440**:89-93.
121. **Bos EC, Luytjes W, Spaan WJ.** 1997. The function of the spike protein of mouse hepatitis virus strain A59 can be studied on virus-like particles: cleavage is not required for infectivity. *Journal of virology* **71**:9427-9433.
122. **de Haan CA, Stadler K, Godeke GJ, Bosch BJ, Rottier PJ.** 2004. Cleavage inhibition of the murine coronavirus spike protein by a furin-like enzyme affects cell-cell but not virus-cell fusion. *Journal of virology* **78**:6048-6054.
123. **Gombold JL, Hingley ST, Weiss SR.** 1993. Fusion-defective mutants of mouse hepatitis virus A59 contain a mutation in the spike protein cleavage signal. *Journal of virology* **67**:4504-4512.

-
124. **Taguchi F.** 1993. Fusion formation by the uncleaved spike protein of murine coronavirus JHMV variant cl-2. *Journal of virology* **67**:1195-1202.
 125. **Follis KE, York J, Nunberg JH.** 2006. Furin cleavage of the SARS coronavirus spike glycoprotein enhances cell-cell fusion but does not affect virion entry. *Virology* **350**:358-369.
 126. **Gallagher TM.** 1997. A role for naturally occurring variation of the murine coronavirus spike protein in stabilizing association with the cellular receptor. *Journal of virology* **71**:3129-3137.
 127. **Krueger DK, Kelly SM, Lewicki DN, Ruffolo R, Gallagher TM.** 2001. Variations in disparate regions of the murine coronavirus spike protein impact the initiation of membrane fusion. *Journal of virology* **75**:2792-2802.
 128. **Phillips JJ, Chua MM, Lavi E, Weiss SR.** 1999. Pathogenesis of chimeric MHV4/MHV-A59 recombinant viruses: the murine coronavirus spike protein is a major determinant of neurovirulence. *Journal of virology* **73**:7752-7760.
 129. **Taguchi F, Matsuyama S.** 2002. Soluble receptor potentiates receptor-independent infection by murine coronavirus. *Journal of virology* **76**:950-958.
 130. **Gallagher TM, Escarmis C, Buchmeier MJ.** 1991. Alteration of the pH dependence of coronavirus-induced cell fusion: effect of mutations in the spike glycoprotein. *Journal of virology* **65**:1916-1928.
 131. **Nash TC, Buchmeier MJ.** 1997. Entry of mouse hepatitis virus into cells by endosomal and nonendosomal pathways. *Virology* **233**:1-8.
 132. **Qiu Z, Hingley ST, Simmons G, Yu C, Das Sarma J, Bates P, Weiss SR.** 2006. Endosomal proteolysis by cathepsins is necessary for murine coronavirus mouse hepatitis virus type 2 spike-mediated entry. *Journal of virology* **80**:5768-5776.
 133. **Eifart P, Ludwig K, Bottcher C, de Haan CA, Rottier PJ, Korte T, Herrmann A.** 2007. Role of endocytosis and low pH in murine hepatitis virus strain A59 cell entry. *Journal of virology* **81**:10758-10768.
 134. **Choi KS, Aizaki H, Lai MM.** 2005. Murine coronavirus requires lipid rafts for virus entry and cell-cell fusion but not for virus release. *Journal of virology* **79**:9862-9871.
 135. **Inoue Y, Tanaka N, Tanaka Y, Inoue S, Morita K, Zhuang M, Hattori T, Sugamura K.** 2007. Clathrin-dependent entry of severe acute respiratory syndrome coronavirus into target cells expressing ACE2 with the cytoplasmic tail deleted. *Journal of virology* **81**:8722-8729.
 136. **Wang H, Yang P, Liu K, Guo F, Zhang Y, Zhang G, Jiang C.** 2008. SARS coronavirus entry into host cells through a novel clathrin- and caveolae-independent endocytic pathway. *Cell research* **18**:290-301.
 137. **Regan AD, Shraybman R, Cohen RD, Whittaker GR.** 2008. Differential role for low pH and cathepsin-mediated cleavage of the viral spike protein during entry of serotype II feline coronaviruses. *Veterinary microbiology* **132**:235-248.
 138. **Van Hamme E, Dewerchin HL, Cornelissen E, Verhasselt B, Nauwynck HJ.** 2008. Clathrin- and caveolae-independent entry of feline infectious peritonitis virus in monocytes depends on dynamin. *The Journal of general virology* **89**:2147-2156.
 139. **Chu VC, McElroy LJ, Chu V, Bauman BE, Whittaker GR.** 2006. The avian coronavirus infectious bronchitis virus undergoes direct low-pH-dependent fusion activation during entry into host cells. *Journal of virology* **80**:3180-3188.
-

140. **Nomura R, Kiyota A, Suzaki E, Kataoka K, Ohe Y, Miyamoto K, Senda T, Fujimoto T.** 2004. Human coronavirus 229E binds to CD13 in rafts and enters the cell through caveolae. *Journal of virology* **78**:8701-8708.
141. **Hingley ST, Leparç-Goffart I, Seo SH, Tsai JC, Weiss SR.** 2002. The virulence of mouse hepatitis virus strain A59 is not dependent on efficient spike protein cleavage and cell-to-cell fusion. *Journal of neurovirology* **8**:400-410.
142. **Simmons G, Reeves JD, Rennekamp AJ, Amberg SM, Piefer AJ, Bates P.** 2004. Characterization of severe acute respiratory syndrome-associated coronavirus (SARS-CoV) spike glycoprotein-mediated viral entry. *Proceedings of the National Academy of Sciences of the United States of America* **101**:4240-4245.
143. **Belouzard S, Chu VC, Whittaker GR.** 2009. Activation of the SARS coronavirus spike protein via sequential proteolytic cleavage at two distinct sites. *Proceedings of the National Academy of Sciences of the United States of America* **106**:5871-5876.
144. **Matsuyama S, Ujike M, Morikawa S, Tashiro M, Taguchi F.** 2005. Protease-mediated enhancement of severe acute respiratory syndrome coronavirus infection. *Proceedings of the National Academy of Sciences of the United States of America* **102**:12543-12547.
145. **Belouzard S, Madu I, Whittaker GR.** 2010. Elastase-mediated activation of the severe acute respiratory syndrome coronavirus spike protein at discrete sites within the S2 domain. *The Journal of biological chemistry* **285**:22758-22763.
146. **Kam YW, Okumura Y, Kido H, Ng LF, Bruzzone R, Altmeyer R.** 2009. Cleavage of the SARS coronavirus spike glycoprotein by airway proteases enhances virus entry into human bronchial epithelial cells in vitro. *PloS one* **4**:e7870.
147. **Bertram S, Glowacka I, Muller MA, Lavender H, Gnirss K, Nehlmeier I, Niemeyer D, He Y, Simmons G, Drosten C, Soilleux EJ, Jahn O, Steffen I, Pohlmann S.** 2011. Cleavage and activation of the severe acute respiratory syndrome coronavirus spike protein by human airway trypsin-like protease. *Journal of virology* **85**:13363-13372.
148. **Shulla A, Heald-Sargent T, Subramanya G, Zhao J, Perlman S, Gallagher T.** 2011. A transmembrane serine protease is linked to the severe acute respiratory syndrome coronavirus receptor and activates virus entry. *Journal of virology* **85**:873-882.
149. **Simmons G, Gosalia DN, Rennekamp AJ, Reeves JD, Diamond SL, Bates P.** 2005. Inhibitors of cathepsin L prevent severe acute respiratory syndrome coronavirus entry. *Proceedings of the National Academy of Sciences of the United States of America* **102**:11876-11881.
150. **Bosch BJ, Bartelink W, Rottier PJ.** 2008. Cathepsin L functionally cleaves the severe acute respiratory syndrome coronavirus class I fusion protein upstream of rather than adjacent to the fusion peptide. *Journal of virology* **82**:8887-8890.
151. **Matsuyama S, Taguchi F.** 2009. Two-step conformational changes in a coronavirus envelope glycoprotein mediated by receptor binding and proteolysis. *Journal of virology* **83**:11133-11141.
152. **Simmons G, Rennekamp AJ, Chai N, Vandenberghe LH, Riley JL, Bates P.** 2003. Folate receptor alpha and caveolae are not required for Ebola virus glycoprotein-mediated viral infection. *Journal of virology* **77**:13433-13438.

-
153. **Yamada Y, Liu DX.** 2009. Proteolytic activation of the spike protein at a novel RRRR/S motif is implicated in furin-dependent entry, syncytium formation, and infectivity of coronavirus infectious bronchitis virus in cultured cells. *Journal of virology* **83**:8744-8758.
 154. **Matthews SP, Werber I, Deussing J, Peters C, Reinheckel T, Watts C.** 2010. Distinct protease requirements for antigen presentation in vitro and in vivo. *Journal of immunology* **184**:2423-2431.
 155. **Watanabe R, Matsuyama S, Shirato K, Maejima M, Fukushi S, Morikawa S, Taguchi F.** 2008. Entry from the cell surface of severe acute respiratory syndrome coronavirus with cleaved S protein as revealed by pseudotype virus bearing cleaved S protein. *Journal of virology* **82**:11985-11991.

CHAPTER

TWO

*Replication-independent analysis of
virus binding, internalization,
and penetration using
minimal complementation of
 β -galactosidase*

Christine Burkard, Louis-Marie Bloyet, Oliver Wicht,
Frank J. van Kuppeveld, Peter J. M. Rottier,
Cornelis A. M. de Haan, Berend Jan Bosch

ABSTRACT

Studies of viral entry into host cells often rely on the detection of post-entry parameters, such as viral replication or the expression of a reporter gene, rather than on measuring entry *per se*. The lack of assays to easily detect the different steps of entry severely hampers the analysis of this key process in virus infection. Here we describe novel, highly adaptable viral entry assays making use of minimal complementation of the *E. coli* β -galactosidase in mammalian cells. Enzyme activity is reconstituted when a small intravirion peptide (α -peptide) is complementing the inactive mutant form Δ M15 of β -galactosidase. The method allows to dissect and to independently detect binding, internalization, and fusion of viruses during host cell entry. Here we use it to confirm and extend current knowledge on the entry process of two enveloped viruses: vesicular stomatitis virus (VSV) and murine hepatitis coronavirus (MHV).

INTRODUCTION

Viral infections pose one of the major public health threats of our time, as demonstrated by the emergence of the SARS-coronavirus (SARS-CoV) in 2002/2003 and the new pandemic influenza H1N1 virus in 2009. Viruses are obligatory intracellular pathogens, which depend on host cells for their replication. Understanding the viral life cycle and studying the cellular factors involved in viral infection are crucial for the identification of new antiviral targets and the development of antiviral drugs. As virus entry is the first step in the viral life cycle, inhibition of this essential process is an attractive approach to block virus infection [1]. Current methods for studying viral entry into host cells mostly rely on post-entry parameters, such as replication or the expression of a reporter gene, rather than on measuring entry per se [2-4]. Studying virus entry directly, i.e. in a virus replication-independent manner, has proven to be difficult, certainly when using low, physiologically relevant amounts of virus particles.

To study distinct virus entry stages (binding, internalization, penetration/fusion) a variety of methods have been applied. Radioactive labeling of structural viral components and electron microscopy (EM) of infected cells have been used to investigate virus binding and internalization [5-9]. Radioactive labeling of structural viral components, mostly using [35S]methionine-labeling, can be used mainly to observe binding, internalization, and low-pH induced membrane fusion [5,10,11]. In addition to requiring the handling of radioactive components and elaborate protocols, this technique does not allow observing virus fusion directly. The study of virus infections by EM has been used to study infections per se and the viral entry or release process (reviewed in [9], as well as [5,8,10,11]). Even though EM techniques are able to give visual insight into virus entry, including various stages of the entry process, it is still difficult to identify cellular factors and pathways involved in the uptake process with this technique. Also, EM is very labor intensive, usually requires high virus concentrations, and is hardly suitable for medium or high throughput experiments. Virus entry has also been studied by fluorescence microscopy (FM), either by detecting replication-dependent viral protein or reporter-fusion protein expression or by imaging of fluorescently labeled virions. Investigating virus entry by FM of fluorescent reporter protein expression as the name already indicates requires viral replication. This process occurs long after viral entry and fusion has occurred and thus does not allow differentiating between entry and replication (e.g. [12]). The only way to partially differentiate the processes is to add perturbing agents in timely intervals. Investigating entry using fluorescently labeled virions by expression of structural fusion proteins or chemical labeling allows to investigate virus entry in further details, e.g. using co-localization, live-cell microscopy, or tracking studies (e.g. [10,13-16]). Whereas FM reporter protein expression experiments may be used for high-throughput experiments and can be used for a wide variety of viruses, the study of fluorescently labeled virions is laborious, requires high magnification and resolution, and is rarely suited for non-enveloped viruses.

More specialized fusion assays have been developed over the last few decades. Early examples involved labeling of virions using self-quenching dyes or the activation of photosensitized labeling on virions by fluorescent lipids on target membranes [17-19]. However, these assays solely allow for the investigation of fusion and not other entry steps, and are very complex and difficult to adapt to non-enveloped viruses. Recently, enzymes have been employed as reporters for virus entry by incorporating them into virions to allow for investigation of entry independent of replication. Therefore either firefly- or *gaussia* luciferase, or β -lactamase

have been incorporated as structural (luminal) fusion proteins into virions [20-25]. However, the integration of an entire enzyme of several hundred amino acid in size can severely affect virus assembly and/or infectivity. Also only fusion towards the cytosol may be investigated in intact cells. When using the assays by lysing cells it cannot distinguish between internalized and fused virions. The enzymatic assays published so far, with the exception of gaussia-tagged vaccinia virus [25], have been mainly used for fusion measurements only. While all of the above-mentioned methods have their strengths and weaknesses and have proven useful, the lack of assays that distinctly detect the different steps in viral entry hampers the analysis of this important process significantly. There is a clear need for an easy-to-use assay, allowing monitoring of virus penetration, independent of other stages of virus entry or replication in a medium- or high-throughput fashion.

Presented here is a versatile assay usable in different formats to allow distinctive analysis of the viral penetration/ fusion process, as well as binding and internalization of viral particles in a replication-independent manner. They use minimal enzyme complementation of the well-studied *E. coli* enzyme β -galactosidase. Enzyme activity is reconstituted when a small peptide (α -peptide) is paired with an inactive mutant form of β -galactosidase (Δ M15), lacking residues 11-41 of the lacZ β -galactosidase [26]. The 45aa α -peptide, representing aa 5-51 of the lacZ β -galactosidase, is attached to either the C- or the N-terminus of an intravirion viral protein [27]. Δ M15 is expressed transiently or stably in the cytosol of target cells. When the spatial separation of the α -peptide in the virion and Δ M15 is removed, for instance when viral and cellular membrane fuse, complementation can be detected.

We have established and tested the method for two different enveloped viruses: murine hepatitis coronavirus (MHV strain A59, further referred to as MHV), which belongs to the Coronaviridae, and vesicular stomatitis virus (VSV) belonging to the Rhabdoviridae. Coronaviruses (CoVs), plus-stranded RNA viruses, infect a variety of mammals and birds. They include important pathogens, such as SARS-CoV [28] and MERS-CoV [29], which cause severe respiratory tract diseases in humans. VSV is a negative-sense RNA virus with a broad host spectrum, which ranges from mammals to insects. It regularly causes severe epidemics in livestock [30,31]. VSV is a good model virus for this new method as its entry process has been well characterized [10,30]. We generated α -peptide tagged MHV and VSV virions. By using enzymatic amplification the binding, internalization, and fusion of both viruses could be separately and efficiently measured at low multiplicity of infection (MOI).

MATERIALS AND METHODS

Cells, viruses, and antibodies.

Murine LR7 fibroblast [32] (based on murine L cells, orig. ATCC), feline FCWF (ATCC) and human HEK293T (ATCC) cells were used to propagate the viruses (i.e. recombinant MHV, interspecies chimeric coronavirus fMHV [32], and pseudotyped VSV, respectively). Cells were maintained as monolayer cultures in Dulbecco's modified Eagle's medium (DMEM, Lonza), supplemented with 10% fetal calf serum (FCS).

LR7 and HEK293T stably or transiently expressing Δ M15 in the cytosol have been used for infection experiments. Stable cell lines were generated using a Moloney murine leukemia (MLV) retroviral vector. MLV was produced in HEK293T cells by triple plasmid transfection of a transfer vector containing Δ M15 gene as well as a puromycin resistance marker gene, in combination with expression vectors encoding the MLV Gag-Pol, and VSVG spike protein, respectively. Upon MLV transduction, stably transduced cells were selected at 2 μ g/ml puromycin, maintenance at 1 μ g/ml puromycin (Sigma) in DMEM, supplemented with 10% FCS.

The rabbit polyclonal antisera K114 [33] and K135 [34] to VSV and MHV-A59, respectively, have been described before as is the mouse monoclonal antiserum 10G, which is directed against the MHV-A59 S2 domain [35].

Chemicals

The MHV fusion inhibitor HR2 peptide has been described before [36] and was synthesized by GenScript. The peptide was diluted in Tris/HCl 50 mM, pH7.8, 4 μ M EGTA at 1 mM stock solution and used at 10 μ M final concentration. Fluorescein-di- β -D-galactosipyranoside (FDG) (AnaSpec) was diluted in DMSO to a stock solution of 20mM. Purified *E. coli* β -galactosidase (Sigma-Aldrich) was diluted to 1E-7 g/ μ l in 100 mM Sodium Phosphate Buffer, pH 7.3 immediately prior to use.

Stocks of 5-bromo-4-chloro-3-indolyl- β -D-galactopyranoside (X-Gal, Sigma) were prepared at 40mg/ml in dimethyl sulfoxide (DMSO). Stocks of 500 mM potassium ferrocyanide (K₄[Fe(CN)₆], 500 mM potassium ferricyanide (K₃[Fe(CN)₆], and 200 mM magnesium chloride (MgCl, all Sigma) were prepared in water (H₂O).

Stocks of 700 mM cycloheximide (CHX, Sigma), 125 μ M bafilomycin A1 (BafA1, Enzo Life Sciences), 120 mM dynasore (Dyn, Enzo Life Sciences), 1 mM nocodazole (Noc, Sigma), 1mM latrunculin A (LatA, Sigma), 2 mM jasplakinolide (Jasp, Sigma), 1 mM brefeldin A (BrefA, Sigma) were prepared in DMSO and used at 1:1000 final concentration.

Stocks of 2 M ammonium chloride (NH₄Cl, Fluka), 10 mM chlorpromazine (Chlorpro, Sigma) were prepared in H₂O and used at 1:100, 1:1000, and 1:250 final concentration, respectively.

A stock of 6 mM monensin (Mon, Sigma) was prepared in methanol (MeOH) and used at 1:1000 final concentration.

Plasmids

The α -peptide cDNA was isolated from an *E. coli* field isolate by DNA extraction and PCR. The cDNA was subcloned into a pCAGGS vector by restriction / ligation (BamHI/SbfI) and used from there. The Δ M15 gene was isolated from a DH5 α *E. coli* lab strain by DNA extraction and PCR. The gene was cloned into a pCAGGS vector for (transient) expression and

into a MLV-based pQCXIP transfer vector (Clontech) for the generation of stable cell lines, by restriction / ligation (XmaI/NotI in pCAGGS, SmaI/PacI in pQCXIP).

The transcription vectors for the production of donor RNA for targeted interspecies recombination of fMHV were derived from pMH54 [32,37]. Constructs containing S- α , or α -N fusion genes were made by overlap-extension PCR and cloned into the parental pMH54 vector by restriction and ligation (MluI/SbfI for S- α , XbaI/NheI for α -N), resulting in the pMH54-S α and pMH54- α N vectors, respectively. The expression vector pCAGGS-VSVG α for producing pseudotyped VSV Δ G/FLuc-G α^* or VSV Δ G/GFP-G α^* viruses was cloned from a pCAGGS-VSVG vector by overlap extension PCR and cloning (restriction/ligation with SacI/NotI).

Generation of recombinant (pseudo-) viruses

Recombinant MHV- α N and MHV-S α viruses were generated by targeted RNA recombination as described before [32]. Briefly, donor RNA was generated from linearized transfer vectors, described above, and electroporated into FCWF cells infected with interspecies chimeric fMHV coronavirus (an MHV-A59 derivative, in which the ectodomain of spike has been replaced by a spike ectodomain of a feline coronavirus, thereby changing host cell tropism). The electroporated FCWF cells were seeded onto a monolayer of LR7 cells. After 24 h of incubation at 37°C, supernatant medium containing progeny viruses was harvested. Recombinant viruses were subjected to two rounds of plaque purification on either LR7 or LR7 Δ M15, after which passage 1 stocks were grown. Genotypes of the recombinant viruses were confirmed in passage 1 stocks, passage 2 stocks were used in experiments.

Recombinant MHV-EGFPM was generated as described above using the transcription plasmid pXHEGFPM, containing a GFP expression cassette between the E and M genes, while lacking ORFs 2a, HE, 4a, 4b, and 5a.

Recombinant VSV Δ G/GFP or FLuc-G α^* pseudovirus was generated as described before [38]. Briefly, target HEK293T cells were transfected with pCAGGS-VSVG α 24 h prior to infection. VSVG α expressing cells were inoculated at MOI=0.01 with VSV Δ G/GFP or FLuc-G α^* pseudovirus. Cells were washed thoroughly at 4hpi. At 20hpi, or upon visible cytotoxicity of the viral infection in ca. 90% of the cells, virus-containing supernatant was harvested. This procedure was repeated once more in order to get rid of any residual VSV Δ G/GFP or FLuc-G α^* pseudovirus in the new virus stocks.

Viruses were stored in culture medium, supplemented with 25 mM HEPES or upon sucrose cushion purification in TN buffer (10 mM Tris-Cl, pH 7.4, 10 mM NaCl).

Blue/White selection – plaque purification of recombinant viruses

Monolayers of LR7 Δ M15 cells were inoculated with MHV- α N or MHV-S α viruses at appropriate (or increasing) dilutions. After 2 h of incubation at 37°C in infection medium (DMEM, supplied with 2% FCS) the inoculum was removed. Cells were subsequently overlaid with a 1:1 mixture of 3% purified Agar (Sigma) in H₂O (previously prepared and autoclaved, reheated prior to use and kept at 42-50°C until use) and EMEM (Gibco) supplemented with 20% FCS, 200IU/ml penicillin, and 200 μ g/ml streptomycin (both Life Technologies), 5 mM K₃[Fe(CN)₆], 5 mM K₄[Fe(CN)₆], 2 mM MgCl₂, and 400 μ g/ml X-Gal (EMEM solution pre-warmed to 37°C prior to use).

Infected and overlaid cells were incubated for up to two days at 37°C. Recombinant

viruses, containing the α -peptide were selected based on the blue color of the plaques generated by these viruses. Blue cell plaques were excised and taken up in water and subjected to three freeze/thaw cycles, after which passage 1 stock was grown.

Entry kinetics experiments

To determine their entry kinetics, MHV-EGFPM virus or VSV Δ G/GFP-G* pseudovirus were bound to target cells in infection medium at 4°C for 90 min at MOI=1 (after washing ca. 5-10% of cells got infected) to synchronize infection. Unbound virus was washed away with ice-cold PBS. Warm infection medium, containing 2% FCS, was added and cells kept at 37°C. At indicated time points post infection the medium was replaced by pre-warmed NH₄Cl-containing infection medium. Virus infection was allowed to progress until 8hpi upon which cells were harvested by trypsinization and fixed in 4% final concentration formaldehyde solution. Infection was quantified by FACS analysis on a FACS Calibur (Benson Dickson) using FlowJo software, 10⁷000 events of living cells were collected for each sample.

Analysis of β -galactosidase activity in the fusion assay

Virus was bound to target cells in infection medium at MOI=10 (unless indicated otherwise) to synchronize infection for 90 min at 4°C. After synchronization cells were shifted to 37°C to allow infection for a suitable amount of time (allowing fusion to occur but stopping before virus is being degraded; 40 min for VSV, 90 min for MHV). To stop infection and harvest, cells were washed with cold trypsin-EDTA (Gibco), containing 25 mM HEPES and NH₄Cl (to stop infection from progression). NH₄Cl-containing trypsin was added and cells were incubated on ice for 30min. Cells were resuspended with 5%FCS in PBS and transferred into cold 2ml Eppendorf tubes. Cells were collected by centrifugation at 450rcf for 5 min at 4°C and, after removal of supernatant, resuspended in 100 μ l room-temperature 5%FCS/PBS. Immediately 100 μ l room-temperature FDG (at 200 μ M in H₂O) was added. This induced a hypotonic shock enabling the uptake of the FDG substrate. After 3 min cells were rescued by adding an excess of ice-cold 5%FCS/PBS. Cells were again collected by centrifugation at 450rcf for 5 min at 4°C, followed by removal of supernatant after which the cells were resuspended in 100 μ l ice-cold 5%FCS/PBS and transferred into FACS tubes. FDG loaded cells were incubated on ice for 8-16 h (unless otherwise indicated 14h, for details see Fig. S5 in Supplementary Information) and analyzed by FACS. While this was the preferred protocol for our investigations of the effect of endocytosis affecting agents on viral entry, we also developed an alternative method to pre-load cells with FDG prior to treatment, where needed, and then infecting the cells.

Therefore, the supernatant of adherent target cells was removed and replaced by a 1:1 mixture (room temperature) of 5%FCS/PBS : 200 μ M FDG/H₂O. After 3 min incubation at room-temperature an excess of 5%FCS/PBS was added, supernatant removed and replaced by growth medium. Cells were allowed to recover for 30 min at 37°C before further treatment (infection, drug treatment, etc.) was undertaken. Binding and infection were carried out as described above. Cells were harvested after 2 h of infection (allows fluorescein signal to build up) by trypsinization with trypsin-EDTA (containing 25 mM HEPES and NH₄Cl) at 37°C for 10min. Cells were harvested with ice-cold 5%FCS/PBS and transferred to Eppendorf tubes, collected by centrifugation at 450 rcf for 5 min at 4°C, supernatant removed and cells resuspended in 100 μ l ice-cold 5%FCS/PBS, after which they were immediately analyzed by FACS.

This was our protocol of choice for investigations of more long-lasting agents/treatments, such as siRNA and dn/ca construct transfection.

For adherent cell microscopy analysis cells may be infected without pre-loading as described above. After the appropriate infection time supernatant is removed and replaced by a 1:1 mixture (room temperature) of 5%FCS/PBS : 1 mM FDG/H₂O. Upon a 3min incubation at room-temperature an excess of ice-cold 5%FCS/PBS is added to stop the hypotonic shock. The supernatant is removed and the cells overlaid with ice-cold 5%FCS/PBS. The samples are incubated at 4°C for 8-16 h. Cells are allowed to recover and flatten by incubation at 37°C for 30min before they are analyzed by microscopy. Cells were analyzed using an EVOS inverted fluorescence microscope.

Cycloheximide may be added to the cells to prevent viral protein synthesis. Microscopy analysis is also compatible with a pre-loading protocol.

Western blotting

For western blotting of viral structural proteins the viruses were purified and concentrated over a 20% Sucrose (in TN buffer) cushion at 75'000 average rcf. Pelleted virus was resuspended in TN buffer overnight at 4°C, SDS loading buffer added to a final concentration of 100 mM DTT, boiled for 5 min at 95°C and subjected to western blotting in 7% acrylamide (37.5:1, Bio-Rad) gels. Upon transfer to a nitrocellulose membrane (Millipore) the viral proteins were probed with antibodies K135 (rabbit anti-MHV pAb), 10G (mouse anti S2 mAb), and K114 (rabbit anti-VSV pAb) on MHV- α N, MHV-S α , and VSV Δ G/GFP or FLuc-G α^* , respectively (all 1:1000). Blots were developed using Rabbit anti-mouse HRP or Swine anti-rabbit HRP (both 1:5000, DAKO)

To analyze intracellular virus protein, infected cells were harvested as described above for the entry assay. Due to the trypsin treatment cell-bound virus was removed and only intracellular virus remained. Half of the cells were then subjected to FDG treatment and β -galactosidase activity measurement, whereas the other half was mixed with SDS loading buffer and subjected to western blotting as described above. GM130 (rabbit monoclonal, Abcam) antibody was used as loading control detection.

Analysis of β -galactosidase activity in the binding and internalization assay

Virus was bound to the target cells at MOI=10 (unless otherwise indicated) for 90 min at 4°C.

For the binding assay unbound virus was washed away with ice-cold PBS. The cells and viruses were subsequently lysed with NP-40 lysis buffer (50 mM Tris/HCl pH 8.0, 150 mM NaCl, 0.5% NP-40) supplemented with Complete Protease Inhibitor Cocktail (Roche) for 10 min at room-temperature. An appropriate amount of the lysate was transferred into a luminometer plate and supplemented 1:1 with 100 mM Sodium Phosphate Buffer, pH 7.3. After transfer to the Centro LB 960 luminometer (Berthold technologies) 30 μ l/well Beta-Glo reagent (Promega) was added to each well, the sample was mixed and incubated for 30-210 min and light units were measured over 0.1 second.

For the internalization assay unbound virus was washed away with ice-cold PBS after a short heat shock at 37°C for 1min, warm infection medium was added and cells shifted to 37°C for an appropriate amount of time (30 and 80 min for VSV and MHV, respectively). Cells

were trypsinized to remove surface bound but not internalized virus. Cells were resuspended in ice-cold 5% FCS/PBS and immediately collected by centrifugation at 450 rcf for 5 min at 4°C. Supernatant was removed and the cell pellet resuspended in lysis buffer. β -galactosidase activity was measured as described above for the binding assay.

To generate calibration curves we used either purified *E. coli* β -galactosidase diluted in 1:1 NP-40 lysis/100 mM Sodium Phosphate buffer, pH 7.3 or sucrose cushion purified virus resuspended in TN (analyzed for infectivity) and lysed by NP-40 lysis buffer.

Infection assays

For all infection assays target cells were pre-treated with drugs if indicated for 30 min at 37°C prior to virus binding. Subsequent binding, internalization, and fusion (as far as needed for the respective assay) were carried out in presence of the drugs at indicated concentrations (see chemicals section).

Growth curves of recombinant viruses

LR7 cells were infected at MOI=0.5 of the respective virus (MHV-A59 wt, MHV- α N and MHV-S α viruses) in infection medium containing 25 mM HEPES. After 3 h of infection supernatant was replaced by fresh infection medium and infection was allowed to progress over a period of 24h. Every 3 h a small sample of the supernatant was collected and immediately frozen. The supernatant samples were subsequently analyzed in TCID50 assays on LR7 cells.

Electron microscopy

VSV Δ G/GFP-G* or VSV Δ G/GFP-G α * pseudovirus was purified through a sucrose cushion as described before. Virus was prepared as described before [39]. Briefly, pelleted virus was resuspended in 50 mM Tris-HCl, pH7.5 with 100 mM NaCl buffer or in 50 mM MOPS, pH6.6 with 100 mM NaCl buffer. The pH6.6 dissolved virus was incubated for 15 min at 37°C and subsequently dialyzed at room temperature against 50 mM MOPS, pH5.5 with 100 mM NaCl buffer for 30 min. The virus preps (pH 7.5 and pH5.5) were adsorbed onto a discharged carbon film and subjected to negative staining (2% uranyl acetate solution). Probes were analyzed with a Philips CM200 microscope at 100 kV.

RESULTS

Outline of the replication-independent entry assays

Based on minimal complementation of β -galactosidase we devised three assay formats to enable the differential analysis of cell binding, internalization, and fusion of viruses. In the binding assay recombinant viruses containing the α -peptide as an intravirion protein tag (α -viruses) are allowed to bind to the surface of target cells on ice. After removal of unbound virus the amount of bound virus particles is quantified by enzyme complementation upon lysis of cells and their attached virions, Δ M15 being provided either by expression in the target cells or by including it in the lysis buffer. Complementation is detected using a sequential system of substrate conversion by β -galactosidase and luciferase to generate a luminescent signal (Fig. 1, left). In the internalization assay the previously surface-bound α -viruses are allowed to enter cells by warming to 37°C. Surface-bound but not internalized virus particles are removed by protease treatment (e.g. Trypsin or Proteinase K) on ice prior to lysis of cells and internalized virions. This is followed by measurement of complementation as described before (Fig. 1, middle). The fusion assay is based on analysis of intact cells. Thus, α -virus is bound to cells expressing Δ M15 and allowed to enter at 37°C. The spatial separation of the α -peptide and Δ M15 is not lifted by lysis but by fusion or penetration of the α -virus. Subsequently, the activity of the complemented β -galactosidase is quantitated by measuring its degradation of the non-fluorescent substrate fluorescein-di- β -D-Galactopyranoside (FDG) into green fluorescent fluorophores fluorescein (Fig. 1, right).

Attachment of the α -peptide to viral proteins and validation of complementation

To investigate the possibilities and consequences of the integration of α -peptide into virions we generated MHV and VSV derivatives carrying α -peptide-tagged structural proteins. Thus, recombinant MHV were obtained with the α -peptide fused either to the C-terminus of the spike protein (α S) or to the N-terminus of the nucleocapsid protein (α N) (Fig. S1 in Supplementary Information). We pre-tested the complementation assay by transient co-expression of the tagged proteins with the Δ M15 protein in HEK293T cells, which confirmed that both fusion proteins efficiently complemented the defective galactosidase Δ M15 as shown for the α N protein in Figure S2a in Supplementary Information. The recombinant viruses were generated by homologous targeted RNA recombination [37]. Their growth properties were affected slightly by the addition of the α -peptide tag to the N or S protein. The impact on growth of MHV- α N seems to be merely a delay in growth. The decrease of viral yield for MHV- α S is significantly lower but within comparable margins for other recombinant MHV viruses with modified spike proteins (Fig. S3 in Supplementary Information). Analysis of their structural proteins by western blot showed the predicted weight shift of 5kDa for the α -peptide tagged N protein. Due to its larger size and heterogeneous glycosylation, a shift in electrophoretic mobility was not clearly visible for the MHV- α S protein (Fig. 2a and b). The genetic identity of the recombinant coronaviruses was confirmed by sequence analysis.

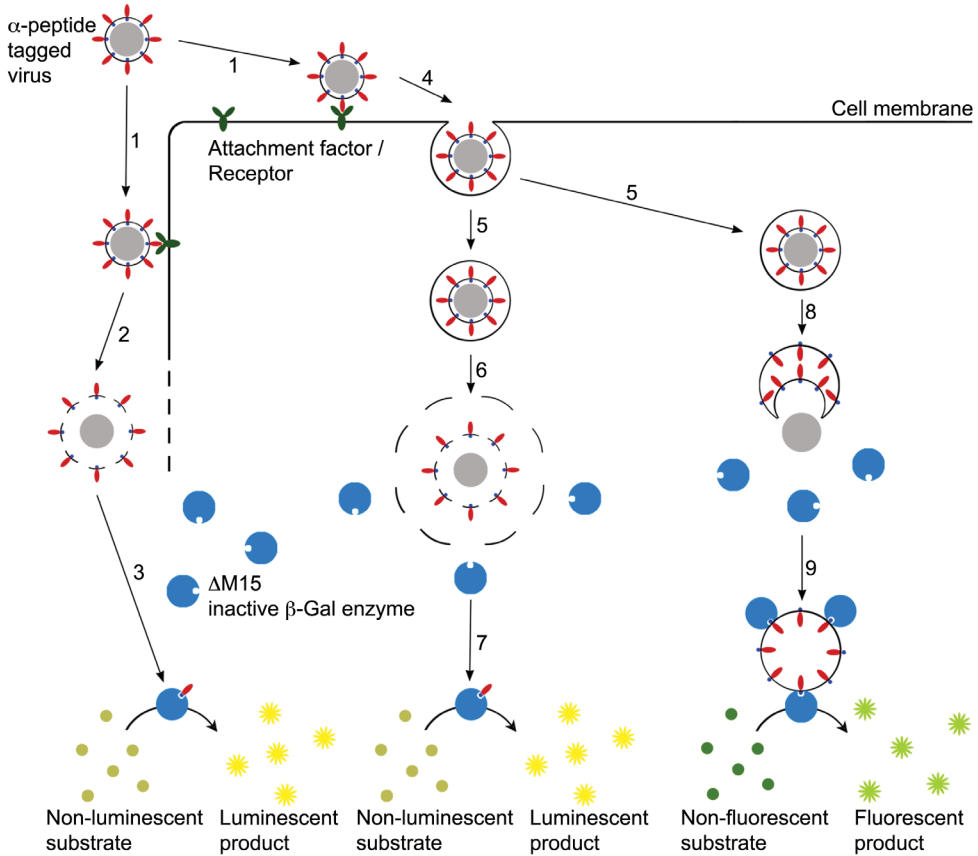


Figure 1: Design of the virus entry assays. Schematic overview of binding- (left), internalization- (middle), and fusion assay (right). 1 - Binding of virus to cell membrane; 2 - Lysis of cells and surface-bound virus; 3 - Complementation of $\Delta M15$ by intravirion α -peptide, substrate conversion yielding luminescent readout; 4 - Invagination and 5 - Budding of endosomal vesicles containing virus particles; 6 - Lysis of cell, intracellular compartment, and virion (after removal of cell surface-bound virions by protease treatment); 7 - Complementation of $\Delta M15$ by intravirion α -peptide, substrate conversion yielding luminescent readout; 8 - Fusion of virion with endosomal membrane, exposure of intravirion α -peptide to the cytosol; 9 - Complementation of intracellular $\Delta M15$ by virion α -peptide in intact cells, substrate conversion yielding fluorescent readout.

To demonstrate complementation in infected cells and to devise a potential new way of selecting recombinant (MHV) viruses we adapted the blue/ white screening method generally used for the selection of transformed bacterial colonies [40]. $\Delta M15$ -expressing cells infected with recombinant virus were overlaid with an agar-medium mixture containing 5-bromo-4-chloro-indolyl- β -D-galactopyranoside (X-Gal). Degradation of X-Gal by β -galactosidase yields a blue colored precipitate (5,5'-dibromo-4,4'-dichloro-indigo). Indeed, recombinant viruses containing the α -peptide fusion protein generated blue plaques. Performing blue/ white screening provided a convenient way to score plaque assays by eye and simplified the selection and purification of recombinant viruses (Fig. 2d). X-Gal did not appear to harm the target cells, even when treated for several days, which allowed us to monitor plaque growth and viral spread in live cells (Fig. 2e).

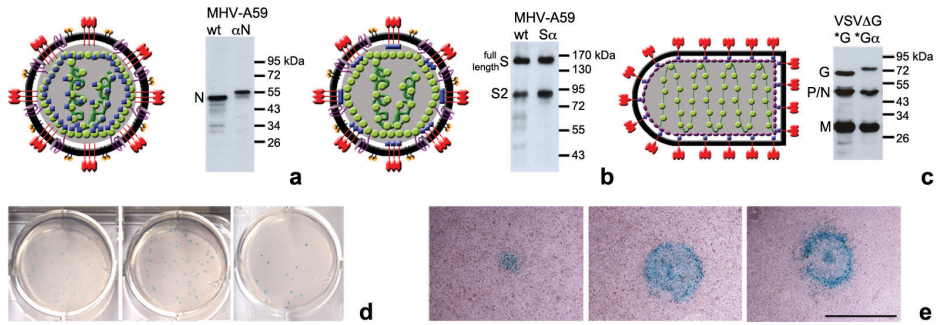


Figure 2: Model of viruses carrying α -peptide tagged proteins and plaque growth by α -complementation. (a-c) α -peptide is shown as blue squares. (a) Model of MHV- α N and western blot analysis of N protein in purified virus stock. (b) Model of MHV-S α and western blot analysis of S protein in purified virus stock. (c) Model of VSV Δ G-G α^* pseudovirus and western blot analysis of VSV structural proteins in purified virus stock. (d) Serial dilution plaque assay of recombinant MHV- α N on LR7 Δ M15 cell monolayers. After inoculation cells were covered for 2 days with a X-Gal containing agar-medium overlay. (e) Visualization of plaque growth of MHV- α N in LR7 Δ M15 cell monolayers after 16, 30 or 48 h incubation (from left to right). Size bar corresponds to 1 mm.

As a second model system, we chose pseudotyped VSV (described by Tani et al. [38]). VSV lacking the G-gene in its genome was complemented with a C-terminally tagged VSV-G α protein expressed in cells used to produce the pseudotyped VSV (Fig. S1 in Supplementary Information). In the genome of the pseudovirus the G gene was substituted by the gene for firefly luciferase or green fluorescent protein (GFP). Western blot analysis of structural virus proteins demonstrated the characteristic 5kDa shift in electrophoretic mobility of G α protein due to the addition of α -peptide (Fig 2c). VSV pseudotyped with the G α (VSV Δ G-G α^*) amplified to similar titers as its wild type counterpart (VSV Δ G-G α^* ; data not shown). Incorporation of VSV-G α was confirmed by EM. Functionality of these proteins was confirmed by low pH treatment of pseudotyped particles, which resulted in the previously observed structural rearrangement of the spikes on the virion surface (Fig. S4 in Supplementary Information) [39].

Virus-cell fusion assay

Our initial aim was the establishment of the virus-cell fusion assay. Fusion of the viruses containing α -peptide-tagged structural proteins with host cells was assessed by inoculation of Δ M15 expressing cells with increasing concentrations of purified, concentrated α -virus. To synchronize infection MHV- α N, MHV-S α , and VSV Δ G-G α^* were allowed to bind to LR7 or HEK293T cells expressing Δ M15 for 90 min on ice. Unbound virus was then removed and cultures were shifted to 37°C and incubated for 100 (MHV) or 40 min (VSV), based on earlier studies of virus entry kinetics (Fig. S5 in Supplementary Information). Incubation was stopped by cooling the cells to 4°C. Cells were detached on ice and FDG substrate was added in combination with a short hypotonic shock, which results in pinocytotic uptake of FDG [41]. Similar results were obtained when cells were pre-loaded with substrate (data not shown, see methods for procedure). To prevent protein degradation and further progression of the infection, resulting in expression of new viral proteins, cells were continuously kept on ice. As low temperatures slow down the enzymatic activity of β -galactosidase, prolonged incubation was required to obtain a strong fluorescein signal. After MHV- α N inoculation at MOI=10, a maximum fluorescein signal was reached after 10h incubation on ice, which remained stable

for 24h (Fig. S6 in Supplementary Information). Inoculation at increasing MOI resulted in increased β -galactosidase activity, as measured by flow cytometry. The cell density plots show that the maximum fluorescence is equal in low and high MOI infections (Fig. 3a). The median fluorescence shifts to higher values at higher MOI. With this fusion assay significant increases in fluorescein signals were obtained already at MOIs around 2-4 for MHV- α N and at MOIs of 5-10 for MHV-S α and VSV Δ G-G α^* (Fig. 3b). In all subsequent fusion assays an MOI of 10 was used and, because of its stronger signal, MHV- α N rather than MHV-S α was the tagged MHV of choice.

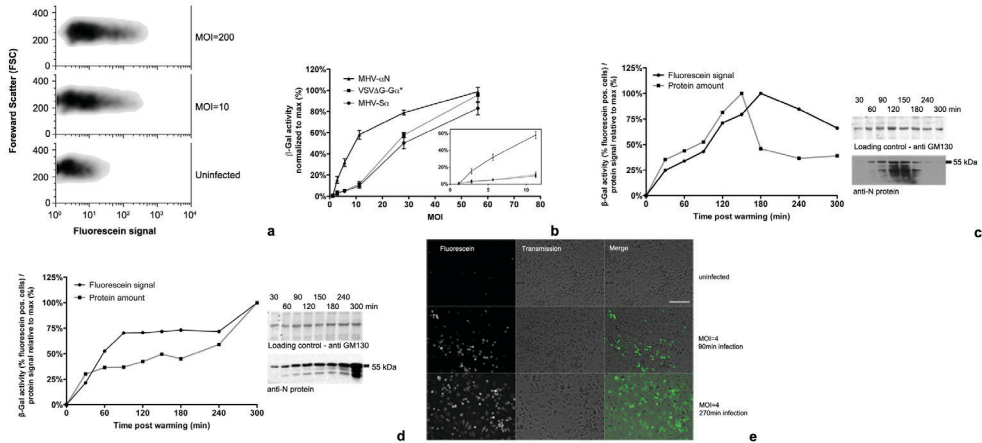


Figure 3: Fusion assay. (a) Virus-cell fusion measured by flow cytometry. Sorting of MHV- α N infected cells by flow cytometry showed increasing fluorescence at increasing MOI. Cells were treated as described in b. (b) Increase of fusion signal relative to MOI. Increasing amounts of MHV- α N, MHV-S α , and VSV Δ G-G α^* were bound to Δ M15 expressing cells on ice. 40 min (VSV) or 100 min (MHV) post warming to 37°C fusion was assayed by measuring β -galactosidase activity using FDG substrate and flow cytometry. Inlay highlights β -galactosidase activity at low MOI. Error bars represent 1 SEM, n=3. (c, d) Kinetics of internalized α -peptide tagged protein in comparison to β -galactosidase activity. MHV- α N (MOI=100) was bound to cells on ice. Unbound virus was removed, and samples shifted to 37°C with (c) or without addition of cycloheximide (d). At the indicated time points, cells were washed and trypsinized on ice, removing surface bound virus. Virus-cell fusion was measured by β -galactosidase activity using flow cytometry or cells were lysed and immunoblotted against N for quantification of the internalized α -peptide proteins. (e) Fluorescence microscopy image of β -galactosidase activity in infected cells. MHV- α N was bound to LR7 Δ M15 cells on ice. Inoculum was washed off and cultures shifted to 37°C for the indicated time periods. β -galactosidase activity was visualized by fluorescein production using fluorescence microscopy. Size bar corresponds to 250 μ m.

In order to confirm that β -galactosidase activity depends on the presence of the α -peptide in the cells we assessed the correlation between the intracellular presence of tagged protein and fluorescein signal. Therefore, LR7 Δ M15 cells were inoculated with MHV- α N as described above. Cells were detached by trypsinization, which also removed cell surface-bound viruses. Cells were analyzed by the fusion assay as described above. In parallel samples, cells were lysed and the intracellular viral α N protein content was determined by immunoblotting against N. The presence of intracellular α N protein correlated with the fluorescein signal generated by β -galactosidase activity. In the presence of the protein synthesis inhibitor cycloheximide (CHX), the signals peaked at 150 or 180 min (Fig. 3c). In absence of CHX the signals leveled off after 90 min and increased strongly after 300 min of infection, consistent with viral gene expression (Fig. 3d). Similar results were obtained for VSV Δ G-G α^* (Fig. S7 in Supplementary Information).

The β -galactosidase activity in infected cells was also visualized by fluorescence microscopy. LR7 Δ M15 cells were inoculated with MHV- α N as described above. At 90 or 240 min post infection FDG was added to the cells. Samples were incubated for 14h on ice and analyzed by fluorescence microscopy. Infection for 90 min generated fluorescent signals in the target cells. Prolonged infection, allowing replication-dependent increase of α N levels, resulted in increased fluorescent signals (Fig. 3e). Similar results were obtained for VSV Δ G-G α^* (Fig. S8 in Supplementary Information).

Virus binding and internalization assays

Binding and internalization of the α -peptide carrying viruses were assessed in assays, in which cells expressing Δ M15 were lysed after virus binding or internalization to allow complementation. For an initial characterization of virus binding, LR7 Δ M15 cells were inoculated with increasing concentrations of purified, concentrated MHV- α N. Cells were overlaid with virus inoculum for 90 min on ice before removing unbound virus. Cells and viruses were lysed and incubated with Beta-Glo substrate, which allows a luminescent read-out of the β -galactosidase activity. Incubation for 50 min with the substrate at room temperature was optimal for measuring low β -galactosidase activities (data not shown). Lysis buffer did not interfere with the activity of the β -galactosidase (data not shown). Binding at very low MOI already increased the luciferase signal significantly. The half maximum value was reached approximately at MOI=2 and a plateau was reached above MOI=10 (Fig. 4a).

For the internalization assay LR7 Δ M15 cells were inoculated with different concentrations of purified, concentrated MHV- α N. Cells were overlaid with virus inoculum for 90 min on ice before removing unbound virus. Virus was allowed to internalize by incubation at 37°C for 60 min. Cell surface bound virus was removed by trypsinization before cells and viruses were lysed. Samples were incubated with Beta-Glo substrate and β -galactosidase activity was measured as described above. The half maximum value was reached at MOI~80 (Fig. 4b). A β -galactosidase standard allows the quantification of complemented enzymes corresponding to virus particles that fused or were present upon lysis, an example of which is shown in Figure S9 in Supplementary Information.

To assess the specificity of the binding and internalization assays MHV- α N was bound to LR7 Δ M15 cells in the absence or presence of anti-murine Ceacam1a (CC1a) antibody, which blocks the CC1a entry receptor used by MHV [42] and treated as described above for the binding assay. As a control, cell surface-bound virus was removed using trypsin before lysis. Trypsinization and blockage of the receptor dramatically decreased virus binding. Also virus internalization was inhibited by CC1a-antibody-dependent receptor blockage (Fig. 4c).

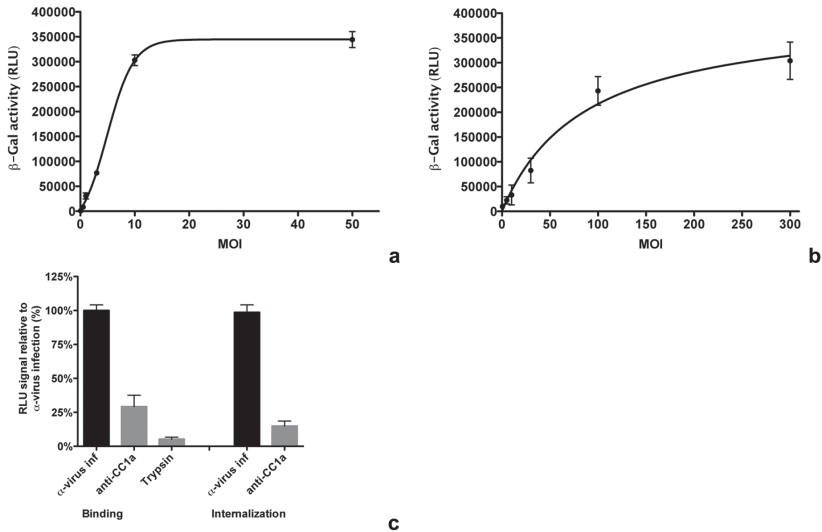


Figure 4: Binding and internalization assay. (a) Luminescent signal after virus binding at various MOI. Increasing amounts of MHV- α N were bound to LR7 Δ M15 cells on ice for 90 min before removing the inoculum and washing-off of unbound virus with ice-cold PBS. Cells and bound viruses were lysed and binding was determined by measuring the β -galactosidase activity using Beta-Glo substrate conversion to a luminescent product. (b) Internalization signal relative to MOI. Increasing amounts of MHV- α N were bound to LR7 Δ M15 cells on ice for 90min. Inoculum was removed and samples transferred to 37°C for 40min. Cell-surface bound virus was removed by trypsinization. Cells and intracellular viruses were lysed and internalization determined by measuring β -galactosidase activity using Beta-Glo substrate conversion to a luminescent product. (c) Controls of binding and internalization assay. Samples were treated as described in a (binding) and b (internalization). After binding, attached virus was removed by trypsin treatment (trypsin). Binding and internalization were inhibited by incubation of cells with MHV receptor CC1a blocking anti-CC1a antibody (anti-CC1a) 30min prior to and during inoculation. Error bars in a - c represent 1 SEM, n=3.

Effect of inhibitors on distinct phases of VSV and MHV entry

To functionally assess the applicability of the entry assays we determined the effect of inhibitors on different entry stages of MHV and VSV. Prior to inoculation, Δ M15 expressing target cells were treated with inhibitory agents for 30 min at 37°C, and the same inhibitors were kept present throughout the experiment. The different stages of virus entry were assessed as described above.

Infection with non- α -peptide containing (wt) virus and solvents dimethyl sulfoxide (DMSO) and methanol (MeOH) were included as controls. Treatment of cells with CHX did not affect binding, internalization or fusion of MHV or VSV. Inhibition of endosome maturation with ammonium chloride (NH₄Cl) or bafilomycin A1 (BafA1) strongly reduced fusion of MHV and VSV, but did not have a significant effect on binding or internalization. Treatment with dynasore (Dyn), an inhibitor of vesicle scission factor dynamin-2 prevented fusion for both viruses, only partially affected internalization, and had no influence on binding. Interference with the assembly of clathrin-coated vesicles using chlorpromazine (Chlopro) strongly decreased internalization and fusion of both viruses, as did the ionophore monensin (Mon), a known inhibitor of VSV entry [43]. Actin destabilizing agent latrunculin A (LatA) lead to reduced fusion for VSV and MHV and also affected internalization of both viruses (Fig. 5a-f).

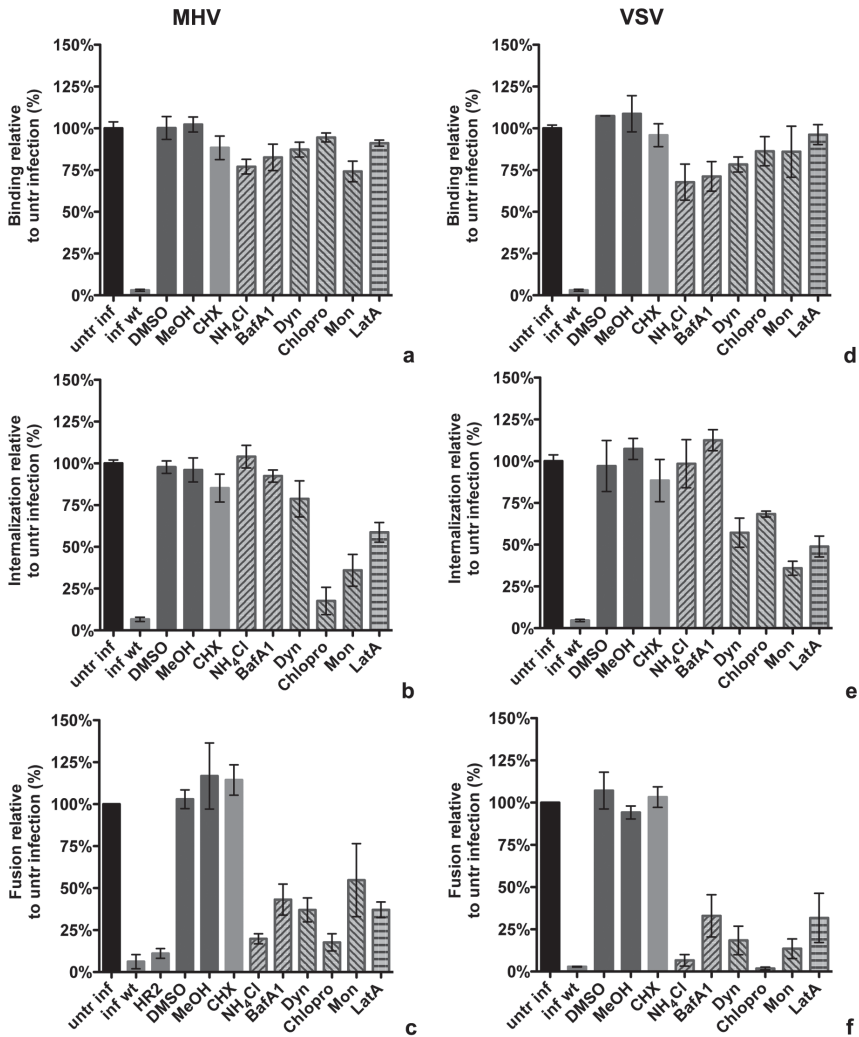


Figure 5: Effects of drugs on binding, internalization, and fusion of MHV and VSV. (a-f) Cells were pretreated with cycloheximide (CHX), ammonium chloride (NH₄Cl), bafilomycin A1 (BafA1), dynasore (Dyn), chlorpromazine (Chlopro), monensin (Mon), or latrunculin A (LatA), as well as with solvents dimethyl sulfoxide (DMSO) and methanol (MeOH) for 30 min. MHV and VSV viruses without α -peptide were included as background controls (untr inf). Error bars represent 1SEM, n=3. (a, d) MHV- α N or VSV-G α^* were bound to Δ M15 expressing cells in presence of compounds on ice for 90min. Cells were washed, lysed and assayed with Beta-Glo substrate as described in 4a. Binding was determined relative to the complementation luminescence signal generated by virus bound to Δ M15 cells, treated without compound added (untr inf). (b,e) After binding as described in a, MHV- α N and VSV-G α^* were allowed to internalize at 37°C in presence of compounds for 40 and 30min, respectively. Internalization was determined relative to the complementation luminescence signal of virus internalized into Δ M15 cells, treated without compound added (untr inf). (c,f) After binding as described in a, MHV- α N or VSV-G α^* were allowed to internalize and fuse at 37°C in presence of compounds for 100 and 40 min, respectively. MHV fusion inhibitor HR2 peptide (HR2) was included as control. Fusion was determined relative to the number of positive cells showing complementation fluorescein signal of virus fused in Δ M15 cells, treated without compound added (untr inf).

DISCUSSION

In this article we present a novel method to dissect viral entry. Using minimal complementation of the β -galactosidase enzyme we were able to detect low numbers of virus particles at any stage of the entry process independent of replication. The assay discriminates between virus binding and internalization and makes it possible to specifically detect and quantify those virus particles that underwent fusion with a host cell. Measuring virus fusion in live cells not only allows for quantitative analysis but also for sorting infected from non-infected cells thereby enabling re-culture these cells. This also allows for combination of the entry assays with replication-dependent reporter assays to investigate later stages of the viral life cycle. Integration of α -peptide into both model viruses was feasible and had limited influence on their viability, suggesting that this novel method can be applicable to other viruses, including non-enveloped viruses. Particularly for the latter viruses it has proven difficult to integrate bulky tags, while labeling of a surrounding lipid layer is not possible. Generally, every virus for which it has been shown possible to attach tags to intravirion structural proteins will be a good candidate for this assay. Using cytosolic expression of Δ M15 in target cells does limit the applicability of the assay to viruses fusing towards the cytosol. However, this could be changed by expressing Δ M15 as a fusion protein in a fusion protein target compartment. Unfortunately, the need to express Δ M15 in the target cells hampers the investigation of fusion in e.g. primary cells. For “native” cells, not expressing Δ M15, the assay can be used to investigate binding and internalization by supplying Δ M15 during or after lysis.

The entry assays confirm and extend current knowledge on virus entry of MHV and VSV. Using the fusion assay we confirmed clathrin-mediated endocytosis of VSV to depend on the actin cytoskeleton [10,30]. Interestingly, the effect of inhibitory agents on MHV entry was very similar to VSV, indicating a comparable uptake mechanism for both viruses. Treatment of cells with chlorpromazine, which causes clathrin lattices to redistribute, affected virus internalization and fusion of both VSV and MHV. Dynasore severely reduced fusion of MHV, but hardly affected internalization of this virus. While dynasore inhibits endocytosis by inhibition of the vesicle scission factor dynamin-2, it does not prevent the formation of invaginations. Viral particles, especially MHV, which in comparison to VSV can be engulfed completely by endocytic vesicles of approximately 100nm diameter, trapped in such invaginations are likely much less accessible for removal by trypsin.

The novel entry assays provide several advantages over conventional assays. Using enzymatic amplification of a tagged viral protein allows looking at viral entry events independent of gene expression. Drugs affecting replication in general, such as translation inhibitors, which will inadvertently affect viral gene expression, can be tested independently for their effect on virus entry. The enzymatically-amplified readout allows performing infections at physiologically relevant conditions. With complementation happening timely proximal to the membrane fusion event, the assay allows for more precise kinetic measurements on virus entry. Also it should become easier to dissect effects of mutations in virions on entry and/or replication. Furthermore, the enzymatic activity can be quantified by a variety of different methods, opening up opportunities for high-throughput analysis by FACS or by automated fluorescence microscopy. The fusion assay might be improved by using yet to be developed alternatives to the FDG substrate, the fluorescein product of which is photolabile. Importantly, as we demonstrated the entry assays can be used in combination with various methods to

perturb cellular processes involved in viral entry, including the use of inhibitors, RNA interference, knock-out cells, and by expression of dominant-negative or constitutive-active proteins. Hence we expect them to facilitate research on virus entry significantly.

ACKNOWLEDGMENTS

We thank W. Bartelink for help with the electron microscopic analysis. We thank Prof. Y.Matsuura, National Institute of Infectious Diseases, Tokyo, for providing the pCAGGS-VS-VG plasmid and pseudotype VSV Δ G-G* virus.

REFERENCES

1. Caffrey M (2011) HIV envelope: challenges and opportunities for development of entry inhibitors. *Trends in microbiology* 19: 191-197.
2. Mercer J, Schelhaas M, Helenius A (2010) Virus entry by endocytosis. *Annual review of biochemistry* 79: 803-833.
3. Sieczkarski SB, Whittaker GR (2002) Dissecting virus entry via endocytosis. *The Journal of general virology* 83: 1535-1545.
4. Marsh M, Helenius A (2006) Virus entry: open sesame. *Cell* 124: 729-740.
5. Matlin KS, Reggio H, Helenius A, Simons K (1981) Infectious entry pathway of influenza virus in a canine kidney cell line. *The Journal of cell biology* 91: 601-613.
6. Summers MD (1971) Electron microscopic observations on granulosis virus entry, uncoating and replication processes during infection of the midgut cells of *Trichoplusia ni*. *Journal of ultrastructure research* 35: 606-625.
7. Dunnebacke TH, Levinthal JD, Williams RC (1969) Entry and release of poliovirus as observed by electron microscopy of cultured cells. *Journal of virology* 4: 505-513.
8. Mercer J, Helenius A (2009) Virus entry by macropinocytosis. *Nature cell biology* 11: 510-520.
9. Roingard P (2008) Viral detection by electron microscopy: past, present and future. *Biology of the cell / under the auspices of the European Cell Biology Organization* 100: 491-501.
10. Johannsdottir HK, Mancini R, Kartenbeck J, Amato L, Helenius A (2009) Host cell factors and functions involved in vesicular stomatitis virus entry. *Journal of virology* 83: 440-453.
11. Matlin KS, Reggio H, Helenius A, Simons K (1982) Pathway of vesicular stomatitis virus entry leading to infection. *J Mol Biol* 156: 609-631.
12. Matula P, Kumar A, Worz I, Erfle H, Bartenschlager R, et al. (2009) Single-cell-based image analysis of high-throughput cell array screens for quantification of viral infection. *Cytometry Part A : the journal of the International Society for Analytical Cytology* 75: 309-318.
13. Fero M, Pogliano K (2010) Automated quantitative live cell fluorescence microscopy. *Cold Spring Harbor perspectives in biology* 2: a000455.
14. Brandenburg B, Lee LY, Lakadamyali M, Rust MJ, Zhuang X, et al. (2007) Imaging poliovirus entry in live cells. *PLoS biology* 5: e183.
15. Engel S, Heger T, Mancini R, Herzog F, Kartenbeck J, et al. (2011) Role of endosomes in simian virus 40 entry and infection. *Journal of virology* 85: 4198-4211.
16. Ewers H, Schelhaas M (2012) Analysis of virus entry and cellular membrane dynamics by single particle tracking. *Methods in enzymology* 506: 63-80.
17. Chen YD, Blumenthal R (1989) On the use of self-quenching fluorophores in the study of membrane fusion kinetics. The effect of slow probe redistribution. *Biophys Chem* 34: 283-292.
18. Lowy RJ, Sarkar DP, Chen Y, Blumenthal R (1990) Observation of single influenza virus-cell fusion and measurement by fluorescence video microscopy. *Proc Natl Acad Sci U S A* 87: 1850-1854.

19. Raviv Y, Viard M, Bess J, Jr., Blumenthal R (2002) Quantitative measurement of fusion of HIV-1 and SIV with cultured cells using photosensitized labeling. *Virology* 293: 243-251.
20. Cavrois M, De Noronha C, Greene WC (2002) A sensitive and specific enzyme-based assay detecting HIV-1 virion fusion in primary T lymphocytes. *Nat Biotechnol* 20: 1151-1154.
21. Kolokoltsov AA, Davey RA (2004) Rapid and sensitive detection of retrovirus entry by using a novel luciferase-based content-mixing assay. *J Virol* 78: 5124-5132.
22. Saeed MF, Kolokoltsov AA, Davey RA (2006) Novel, rapid assay for measuring entry of diverse enveloped viruses, including HIV and rabies. *J Virol Methods* 135: 143-150.
23. Wolf MC, Wang Y, Freiberg AN, Aguilar HC, Holbrook MR, et al. (2009) A catalytically and genetically optimized beta-lactamase-matrix based assay for sensitive, specific, and higher throughput analysis of native henipavirus entry characteristics. *Virology* 6: 119.
24. Tscherne DM, Manicassamy B, Garcia-Sastre A (2010) An enzymatic virus-like particle assay for sensitive detection of virus entry. *Journal of virological methods* 163: 336-343.
25. Laliberte JP, Weisberg AS, Moss B (2011) The membrane fusion step of vaccinia virus entry is cooperatively mediated by multiple viral proteins and host cell components. *PLoS Pathog* 7: e1002446.
26. Langley KE, Villarejo MR, Fowler AV, Zamenhof PJ, Zabin I (1975) Molecular basis of beta-galactosidase alpha-complementation. *Proceedings of the National Academy of Sciences of the United States of America* 72: 1254-1257.
27. Wehrman TS, Casipit CL, Gewertz NM, Blau HM (2005) Enzymatic detection of protein translocation. *Nature methods* 2: 521-527.
28. Peiris JS, Lai ST, Poon LL, Guan Y, Yam LY, et al. (2003) Coronavirus as a possible cause of severe acute respiratory syndrome. *Lancet* 361: 1319-1325.
29. Zaki AM, van Boheemen S, Bestebroer TM, Osterhaus AD, Fouchier RA (2012) Isolation of a novel coronavirus from a man with pneumonia in Saudi Arabia. *The New England journal of medicine* 367: 1814-1820.
30. Matlin KS, Reggio H, Helenius A, Simons K (1982) Pathway of vesicular stomatitis virus entry leading to infection. *Journal of molecular biology* 156: 609-631.
31. Rodriguez LL (2002) Emergence and re-emergence of vesicular stomatitis in the United States. *Virus research* 85: 211-219.
32. Kuo L, Godeke GJ, Raamsman MJ, Masters PS, Rottier PJ (2000) Retargeting of coronavirus by substitution of the spike glycoprotein ectodomain: crossing the host cell species barrier. *Journal of virology* 74: 1393-1406.
33. Vennema H, Heijnen L, Zijderveld A, Horzinek MC, Spaan WJ (1990) Intracellular transport of recombinant coronavirus spike proteins: implications for virus assembly. *J Virol* 64: 339-346.
34. Rottier PJ, Horzinek MC, van der Zeijst BA (1981) Viral protein synthesis in mouse hepatitis virus strain A59-infected cells: effect of tunicamycin. *J Virol* 40: 350-357.
35. Schulze H, Kolter T, Sandhoff K (2009) Principles of lysosomal membrane degradation: Cellular topology and biochemistry of lysosomal lipid degradation. *Biochim Biophys Acta* 1793: 674-683.

36. Bosch BJ, van der Zee R, de Haan CA, Rottier PJ (2003) The coronavirus spike protein is a class I virus fusion protein: structural and functional characterization of the fusion core complex. *Journal of virology* 77: 8801-8811.
37. de Haan CA, Haijema BJ, Masters PS, Rottier PJ (2008) Manipulation of the coronavirus genome using targeted RNA recombination with interspecies chimeric coronaviruses. *Methods in molecular biology* 454: 229-236.
38. Tani H, Komoda Y, Matsuo E, Suzuki K, Hamamoto I, et al. (2007) Replication-competent recombinant vesicular stomatitis virus encoding hepatitis C virus envelope proteins. *Journal of virology* 81: 8601-8612.
39. Libersou S, Albertini AA, Ouldali M, Maury V, Maheu C, et al. (2010) Distinct structural rearrangements of the VSV glycoprotein drive membrane fusion. *The Journal of cell biology* 191: 199-210.
40. Messing J, Gronenborn B, Muller-Hill B, Hans Hopschneider P (1977) Filamentous coliphage M13 as a cloning vehicle: insertion of a HindII fragment of the lac regulatory region in M13 replicative form in vitro. *Proceedings of the National Academy of Sciences of the United States of America* 74: 3642-3646.
41. Madshus IH, Sandvig K, Olsnes S, van Deurs B (1987) Effect of reduced endocytosis induced by hypotonic shock and potassium depletion on the infection of Hep 2 cells by picornaviruses. *Journal of cellular physiology* 131: 14-22.
42. Schickli JH, Zelus BD, Wentworth DE, Sawicki SG, Holmes KV (1997) The murine coronavirus mouse hepatitis virus strain A59 from persistently infected murine cells exhibits an extended host range. *J Virol* 71: 9499-9507.
43. Schlegel R, Willingham M, Pastan I (1981) Monensin blocks endocytosis of vesicular stomatitis virus. *Biochem Biophys Res Commun* 102: 992-998.
44. Beniac DR, Andonov A, Grudeski E, Booth TF (2006) Architecture of the SARS coronavirus prefusion spike. *Nature structural & molecular biology* 13: 751-752.
45. Escors D, Camafeita E, Ortego J, Laude H, Enjuanes L (2001) Organization of two transmissible gastroenteritis coronavirus membrane protein topologies within the virion and core. *Journal of virology* 75: 12228-12240.
46. Neuman BW, Kiss G, Kunding AH, Bhella D, Baksh MF, et al. (2011) A structural analysis of M protein in coronavirus assembly and morphology. *Journal of structural biology* 174: 11-22.

SUPPLEMENTARY INFORMATION

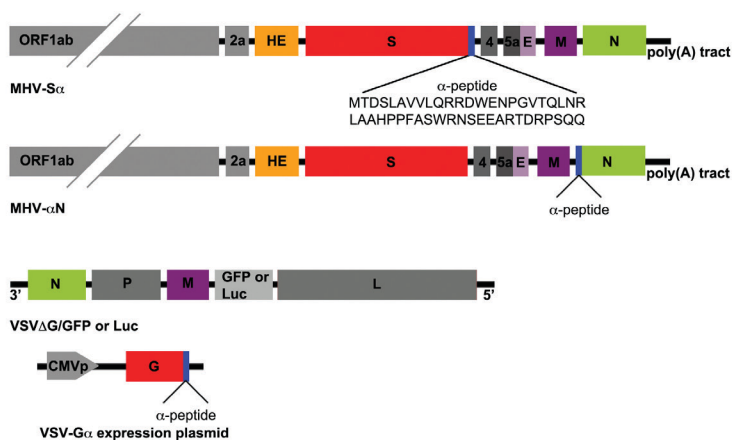


Figure S1. Schematic layout of the genome of recombinant viruses. MHV-S α , encoding C-terminally α -peptide-tagged spike protein (top). MHV- α N, encoding the N-terminally α -peptide-tagged nucleocapsid protein (middle) and pseudotyped VSV Δ G/GFP or -Luc virus coding a GFP or firefly luciferase expression cassette substituting the gene encoding the G protein. C-terminally tagged VSV-G α is provided by the producer cells stably expressing VSV-G α under the control of a CMV promoter.

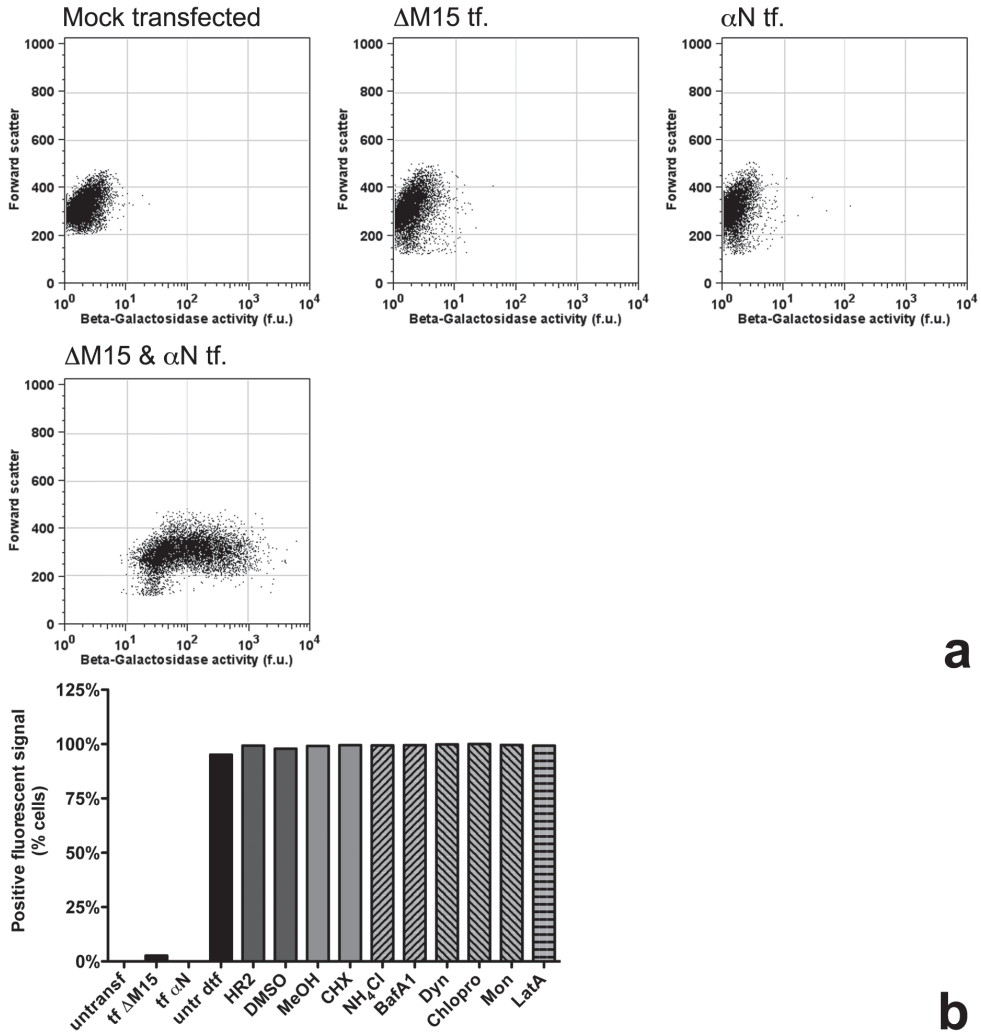


Figure S2. Effect of drug treatment on FDG uptake. (a) HEK293T cells were transfected singly or co-transfected with plasmids encoding ΔM15 or αN. Cells were trypsinized and FDG was added by hypotonic shock. Cells were incubated on ice for 1h and β-galactosidase activity measured by determining the production of fluorescein using FACS. (b) HEK293T cells co-transfected with ΔM15 and αN encoding plasmids were pretreated with the drugs used in the fusion assay (described in 5c and f). Following pretreatment cells were trypsinized and FDG added by hypotonic shock. Cells were incubated on ice for 1h and β-galactosidase activity measured by determining the production of fluorescein using FACS.

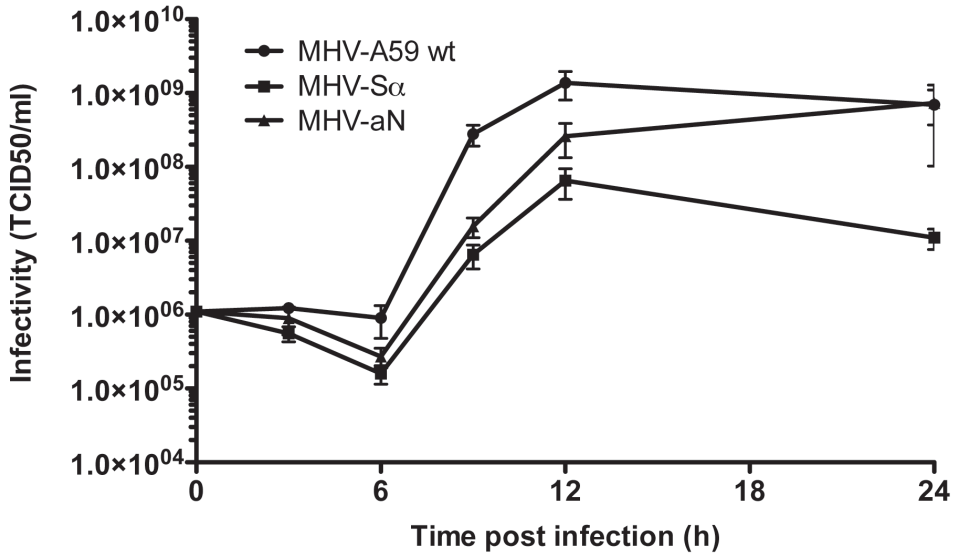
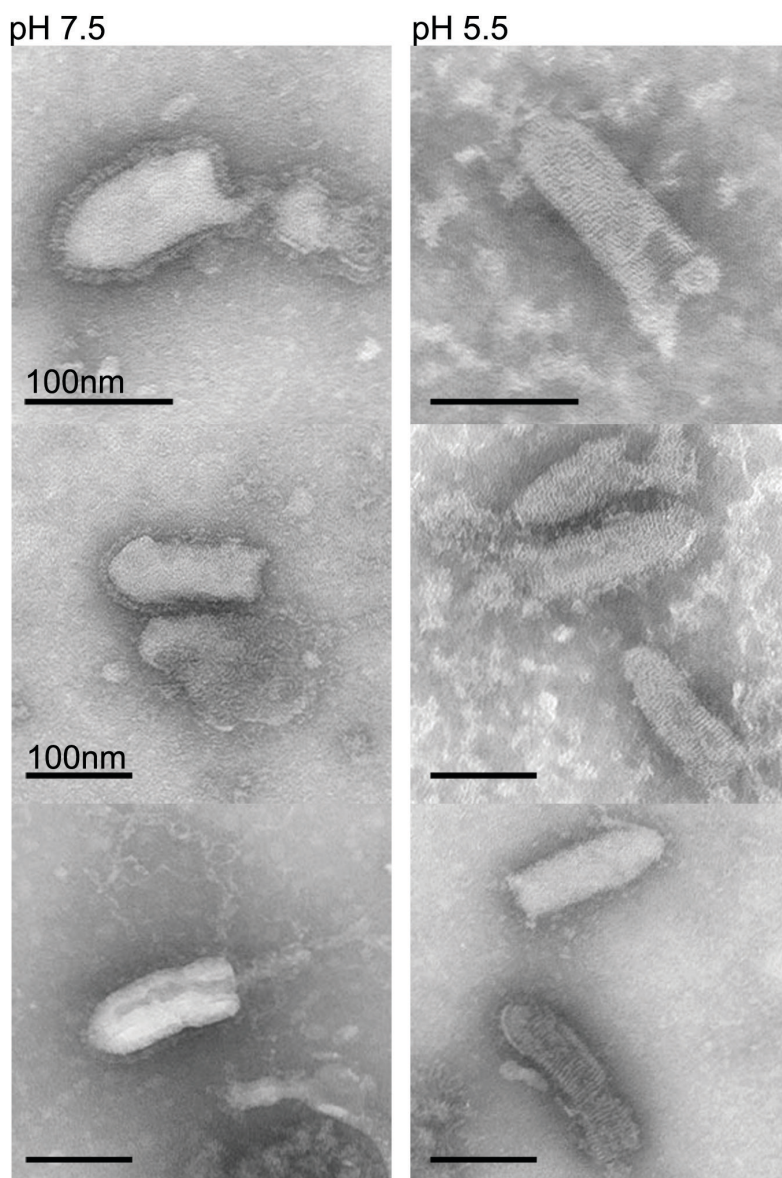


Figure S3. Growth curves of recombinant MHV- α viruses. Murine LR7 cells were inoculated at MOI=1 with the recombinant and wild-type A59 strain viruses, respectively. At the indicated times post infection, infectivity in the culture supernatants was assayed by TCID50 analysis. Error bars represent 1 SEM, n=4.



2

Figure S4. Morphology of negatively stained VSV Δ G/GFP-G α virus at neutral and low pH. 20% sucrose cushion purified stocks of VSV Δ G/GFP-G α , resuspended in TD buffer were sequentially brought to pH 6.5 and to the final pH of 5.5. Samples were negatively stained and imaged by electron microscopy. Three representative images for pH 6.5 and pH 5.5 are shown in the left or right panel, respectively.

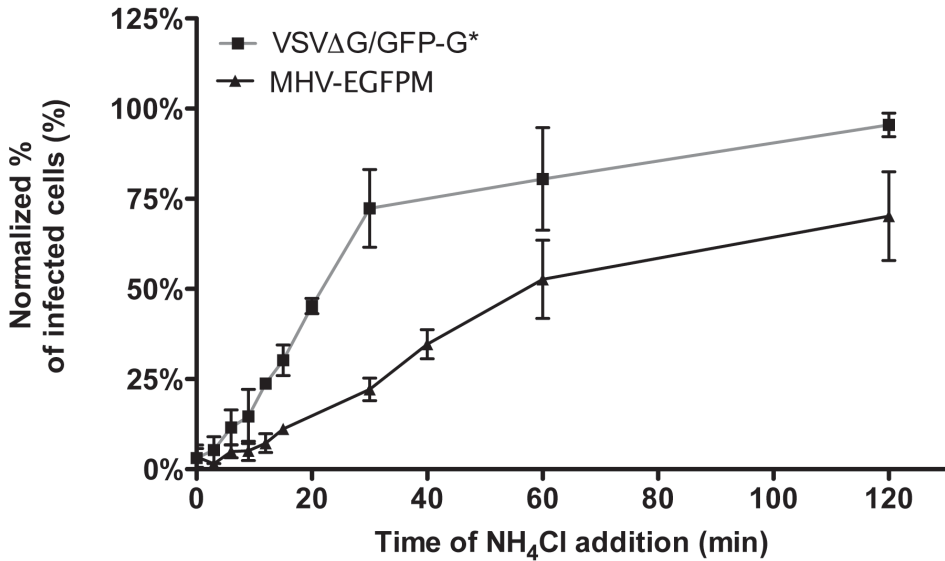


Figure S5. Virus entry kinetics of MHV and VSV as measured by their sensitivity to lysosomal tropic agent NH₄Cl. VSVΔG/GFP-G* and MHV-EGFPM were bound to cells on ice for 90 min at MOI=1. Unbound virus was removed with ice-cold PBS, and cultures were shifted to 37°C by adding warm medium. NH₄Cl was added at the indicated time points to stop endosome maturation and thus virus entry. At 8h post warming, infection was scored by FACS analysis of GFP expression. Half maximum infection of VSV was obtained within 20 min, after 40 min approximately 80% of the maximal number of infected cells was obtained. MHV appeared to enter cells much slower and less synchronized. After about 50 min of warming only half maximum infection was obtained, after 100 min approximately 60% of the maximal number of infected cells was observed. Error bars in **a** & **b** represent 1SEM, n=3.

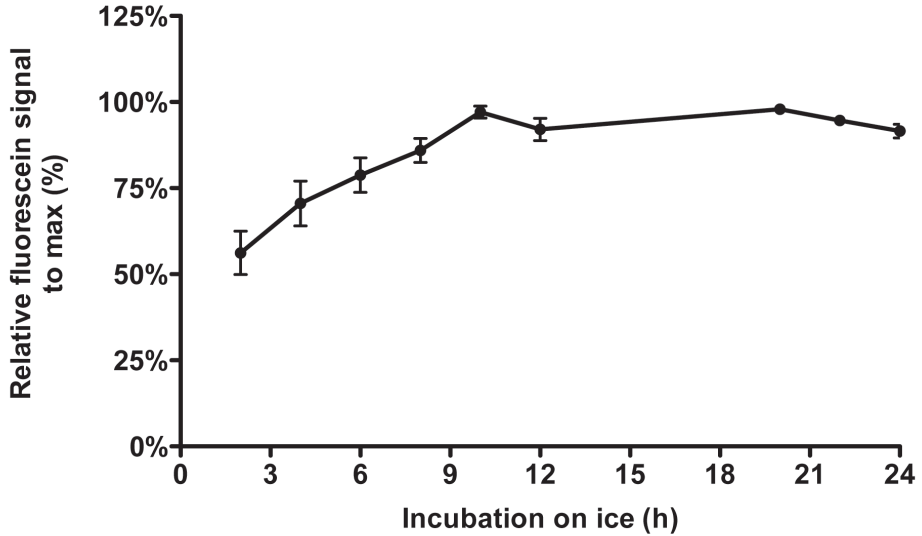


Figure S6. Fluorescein signal dependence on the incubation on ice. LR7 Δ M15 cells were inoculated at an MOI of 10 with MHV- α N by binding the virus to the cells for 90 min on ice, removal of unbound virus, and shifting of the cultures to 37°C for 100min. FDG was administered by hypotonic shock and subsequently the samples were incubated on ice for the indicated amount of time. β -galactosidase activity was measured by determining fluorescein production using FACS.

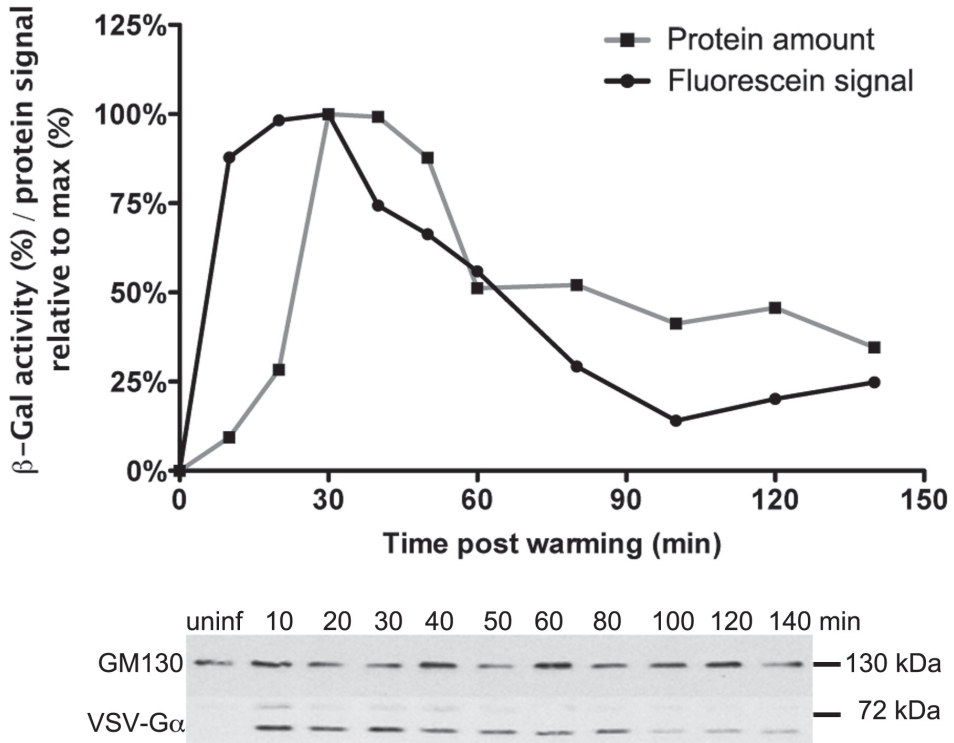


Figure S7. Intracellular α -tagged protein level in relation to β -galactosidase activity. VSV Δ G/Luc-G α^* (MOI=100) was bound to cells on ice. Unbound virus was washed off, and culture temperature shifted to 37°C in the presence of CHX. At the indicated time points cells were washed and trypsinized on ice. Fusion was assessed by β -galactosidase activity-driven fluorescein production using FACS. In parallel samples cells were lysed and G-protein content was measured by western blot analysis.

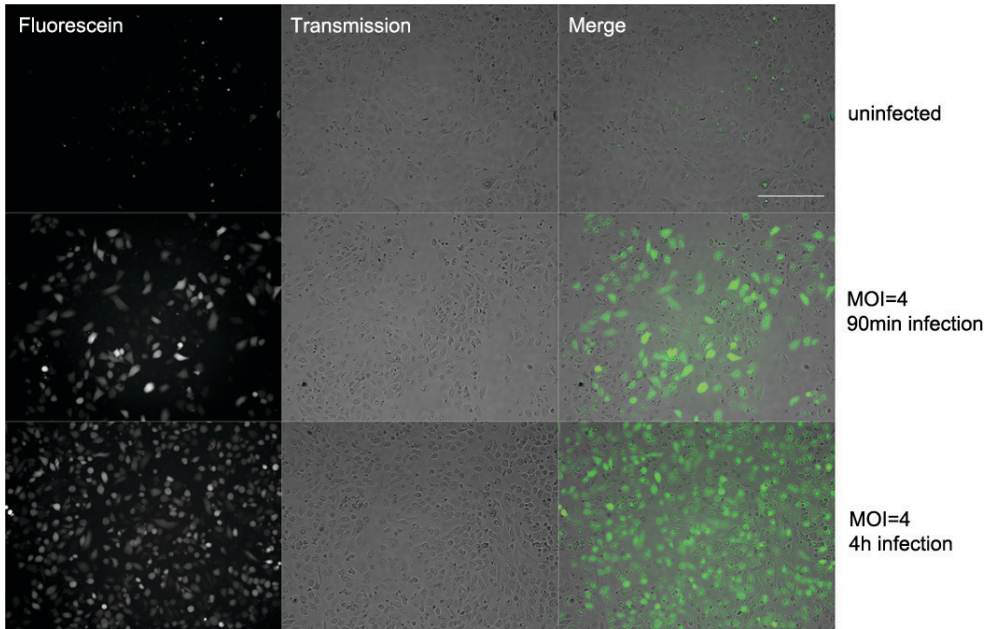
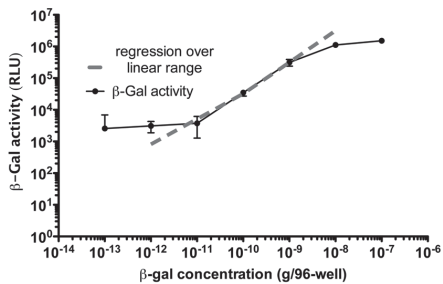


Figure S8. Fluorescence microscopy of β -galactosidase activity in α -virus infected cells. VSV Δ G/Luc-G α^* virus was bound to Δ M15 transfected HEK293T cells on ice. Unbound virus was washed off and culture temperature shifted to 37°C for the indicated time periods. Fusion-dependent β -galactosidase activity-driven fluorescein production in cells was visualized by wide-field fluorescence microscopy. Size bar corresponds to 250 μ m.

Using linear regression to calculate No. of Virions binding / internalizing

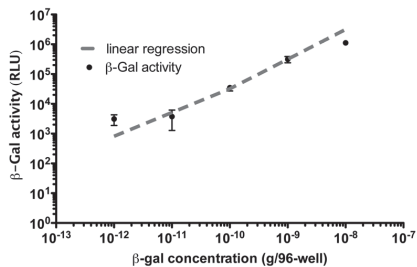


Calculating back from grams / well to molecules / well

Mw β -Galactosidase = 116519.7 (Da)

N_A = 6.022 E23 (1/mol)

Mw/ N_A = 1.93 E-19 (g) per β -Galactosidase molecule



Regression over the linear range of the standard curve

$$y \text{ [RLU]} = 6.014E-5 \times [\beta\text{-Gal/well}] + 505.3$$

$$x = (y-505.3)/6.014E-5$$

Comparing measurement results with estimated virion numbers

Calculating the No. of active enzymes / well from RLU measurements

- Using the linear regression from the standard curve

Calculation No. of N proteins / well

No. of cells/24-well = 4.0E5

No. of N-proteins / MHV virion = 730-2200 [Ref. 31-33]

Assumption for calculations

No. N/virion = 1000

Calc. No. N/well = No. cells * MOI * No. N/virion

Calc. MOI = Calc No. act. enzymes / No. cells / (No. N/virion)

BINDING

MOI	β -Gal activity (RLU)	Calc. No. of active enzymes / well	Calc. No. of N proteins / well	Calc. MOI
1	30748	5.03E+08	4.00E+08	1.26
3	76870	1.27E+09	1.20E+09	3.17
10	303005	5.03E+09	4.00E+09	12.57

INTERNALIZATION

MOI	β -Gal activity (RLU)	Calc. No. of active enzymes / well	Calc. No. of N proteins / well	Calc. MOI
10	33004	5.40E+08	4.00E+09	1.35
30	82510	1.36E+09	1.20E+10	3.41
100	243213	4.04E+09	4.00E+10	10.09

Figure S9. Calculating virus binding and internalization using a standard curve. (a) Correlation between β -galactosidase activity and amount of β -galactosidase protein with indicated linear range. Increasing amounts of purified wild-type *E. coli* β -galactosidase were added to cell lysates of LR7 Δ M15 cells. Samples were probed with Beta-Glo[®] substrate and incubated for 40 min at RT in the dark before measuring the β -galactosidase activity using a luminescence read-out. **(b)** Linear range of the β -galactosidase activity of the standard curve. **(c)** Calculation of number of active enzymes per well from the standard curve and correlation thereof with the estimated number of N proteins present in the binding assay based on literature.[44-46] **(d)** Calculation of the number of active enzymes per well from the standard curve and correlation thereof with the estimated number N proteins per well in the internalization assay.

CHAPTER

THREE

Identification and Characterization of a Proteolytically Primed Form of the Murine Coronavirus Spike Proteins after Fusion with the Target Cell

Oliver Wicht, Christine Burkard, Cornelis A.M. de Haan, Frank
J.M. van Kuppeveld, Peter J.M. Rottier, Berend Jan Bosch

J Virol. 2014 May;88(9):4943-52. doi: 10.1128/JVI.03451-13.
Epub 2014 Feb 19.

ABSTRACT

Enveloped viruses carry highly specialized glycoproteins that catalyze membrane fusion under strict spatial and temporal control. To prevent premature activation after biosynthesis, viral class I fusion proteins adopt a locked conformation and require proteolytic cleavage to render them fusion-ready. This priming step may occur during virus exit from the infected cell, in the extracellular milieu or during entry at or in the next target cell. Proteolytic processing of coronavirus spike (S) fusion proteins during virus entry has been suggested but not yet formally demonstrated, while the nature and functionality of the resulting subunit is still unclear. We used the prototype coronavirus - mouse hepatitis virus (MHV) - to develop a conditional biotinylation assay that enables the specific identification and biochemical characterization of viral S proteins on virions that mediated membrane fusion with the target cell. We demonstrate that MHV S proteins are indeed cleaved upon virus endocytosis and we identified a novel processing product S2* with characteristics of a fusion-active subunit. The precise cleavage site and the enzymes involved remain to be elucidated.

3

IMPORTANCE

Virus entry determines the tropism and is a crucial step in the virus life cycle. We developed an approach to characterize structural components of virus particles after entering new target cells. A prototype coronavirus was used to illustrate how the virus fusion machinery can be controlled.

INTRODUCTION

Enveloped viruses must fuse their envelope with a target cell membrane to get access to host cells and deliver their genetic information. They carry specialized surface glycoproteins that mediate attachment to and fusion with the host membrane. Viral fusion proteins can generally be divided into three distinct classes according to their molecular organization and fusion mechanism (1). Class I fusion proteins like the influenza virus hemagglutinin and the human immunodeficiency virus *env* occur as homotrimeric glycoproteins that are oriented perpendicular to the viral membrane and contain typical structural elements, including a receptor binding domain, heptad repeat regions (HR), an amphipathic fusion peptide (FP), and a C-terminal transmembrane domain (2). These fusion proteins also feature a common fusion mechanism (3). Initial conformational rearrangements triggered by cues like receptor binding or low pH lead to the exposure and insertion of the FP into the target membrane. Subsequent structural reorganization pulls the two membranes together to achieve fusion. The free energy is provided by the S proteins and released by zipping up of the heptad repeat regions into an energetically favorable, stable six-helix bundle (1). To prevent premature activation, class I fusion proteins are produced in a locked conformation that needs proteolytic cleavage to acquire fusion competence. Cleavage typically occurs just upstream of the FP and causes N-terminal liberation thereof (4). Furin or furin-like proteases often prime the fusion proteins in the producer cell before virions are released. Alternatively, the cleavage event can take place after the release of virions from the infected cell, i.e. in the extracellular space or upon entry into new host cells (5-7). Prevention of fusion protein cleavage by mutagenesis of the cleavage site as well as by inhibition of cellular proteases often renders viruses non-infectious (8-10).

Coronavirus (CoV) entry is mediated by the spike (S) protein, an exceptionally large glycoprotein of approximately 1200-1450 amino acid residues in length that comprises the canonical structural features of class I fusion proteins and shares the typical fusion mechanism (11). The trimeric S proteins characteristically decorate the extracellular virus particles and two subunits of similar size can be distinguished. The Nterminal S1 subunit contains the receptor binding domain while the Cterminal S2 subunit comprises the fusion machinery including a putative FP, HR regions and transmembrane domain.

Some CoV S proteins are cleaved at the S1/S2 junction during biogenesis by furin(-like) proteases, but many CoV lack a furin cleavage site at the S1/S2 junction and hence carry uncleaved S protein in their virions (12). Other cellular proteases have been reported to cleave CoV S proteins, but those are only available upon attachment or during uptake of virions by the next target cells (13). The infection of some CoV can be blocked by protease inhibitors, thereby underlining the importance of proteolytic activation that should render class I fusion proteins into their fusion-competent form (6, 14-16). Remarkably, a cleavage at the S1/S2 junction does not liberate a putative FP at the Nterminus of S2 (17). Rather than at the S1/S2 junction, cleavage can occur at alternative positions within the S2 domain of the protein to promote the fusion competence. Such alternative cleavage sites have been described within the S2 subunit for the S proteins of severe acute respiratory syndrome coronavirus (SARS)-CoV, mouse hepatitis virus (MHV), and infectious bronchitis virus (IBV) (16, 18, 19). In general, a variety of putative, alternative cleavage sites and cleavage timings have been reported or suggested for CoV, yet the role of S protein cleavage remains largely undefined.

Despite extensive research on the proteolytic requirements for entry, the exact cleavage position within the CoV S protein generating the fusogenic subunit has been difficult to predict and the formal demonstration of S protein cleavage upon entry is currently lacking. In this study, we developed a novel unbiased approach to selectively identify and characterize the S proteins of incoming viruses that accomplish fusion. The assay employs a combination of a protein biotin ligase (BirA) and a biotin acceptor peptide added as an extension to the cytoplasmic tail of the S protein. When incoming viral proteins gain access to the cytoplasm of cells expressing BirA ligase, they are specifically labeled with biotin which then enables isolation, enrichment and detection. With this assay, we investigated the S glycoprotein of the prototype coronavirus MHV (strain A59). The MHV S proteins are partially cleaved into the non-covalently linked subunits at the S1/S2 junction by furin or furin-like proteases (20). Intriguingly, preventing furin cleavage by mutation or the use of furin inhibitors has no effect on virus infectivity of MHV (21-23). With our new approach we demonstrate that the MHV S proteins participating in fusion are proteolytically processed in the target cells at a different position in the S2 subunit. The newly identified S2* subunit has characteristics of the functional fusion machinery.

MATERIAL AND METHODS

Cells, viruses, antibodies and HR2 peptide.

HEK-293T, HeLa, Vero-CCL81 and LR7 (24) cells were maintained in Dulbecco modified Eagle medium supplemented with 10 % fetal bovine serum. Generally, murine hepatitis viruses (MHV, strain A59) were propagated and titrated in LR7 cells in culture medium supplemented with 20 mM HEPES. For the immune detection of S protein in virus supernatants, MHV was grown to high titers in Dulbecco modified Eagle medium supplemented with 0.3 % tryptose phosphate broth (Sigma, T9157). For immunoprecipitation (IP) and immune detection, MHV S protein was reacted with polyclonal rabbit anti-BAP antibody (Genscript, Avi-Tag A00674) or mouse monoclonal anti-S2 (10G) antibody and subsequently with anti-mouse or anti-rabbit immunoglobulin G conjugated horseradish peroxidase (Dako, P0217) (25, 26). A polyclonal rabbit antiMHV serum (K135) was used to detect infected cells by reacting with anti-rabbit immunoglobulin G conjugated horseradish peroxidase. Biotin was detected by streptavidin-HRP conjugate (Thermo Scientific, 21126). The MHV fusion inhibitor HR2 peptide (DLSLDFEKLNVTLDLTYEMNRIQDAIKKLNESYINLKE) was synthesized by GenScript (11).

Construction of recombinant viruses.

Recombinant MHVs were generated by targeted recombination as described earlier (27). A transfer vector based on pXHERLM was generated to create the recombinant MHV-BAP virus encoding a tandem repeat of the 15 amino acid long biotin acceptor peptide including linkers DLPGGLNDIFEAQKIEWHEPPGGLNDIFEAQKIEWHE (BAP sequence is underlined) as a Cterminal extension of the S protein (28). The recombinant viruses MHV^{FC}BAP and MHV^{S2}BAP were generated by introducing additional point mutations into the transfer vector using site directed mutagenesis. MHV^{FC}BAP S protein carries three point mutations R713S, R7174, and R717S that substitute all arginines at the furin cleavage site by serines. MHV^{S2}BAP S protein carries two point mutations R867S and R869S that substitute the arginines at the putative S2' cleavage site by serines.

Generation of stable cell lines.

The pQCXIN-CCM plasmid encoding the MHV receptor - murine carcinoembryonic antigen-related cell adhesion molecule 1a (CCM) - was generated by cloning the CCM gene into the pQCXIN Moloney murine leukemia virus (MLV) packaging vector (Clontech) (29). Likewise, the human codon optimized gene encoding Biotin Protein Ligase (BirA) with an N-terminal HA- and FLAG-tag (the pUM376-BirA PCR template was kindly provided by V. Ogryzko) was cloned into the pQCXIP vector (Clontech), generating the pQCXIP-BirA packaging vector (30). HEK-293T, HeLa and Vero-CCL81 cell lines expressing the CCM receptor were made after transduction with vesicular stomatitis virus G protein pseudotyped MLV using the pQCXIN-CCM packaging vector. The polyclonal HEKCCM, HeLaCCM, VeroCCM cell lines stably expressing CCM, as well as murine LR7 cells were selected and maintained with G418 (PAA). CCM expression was confirmed by immune detection using mouse monoclonal anti-CCM (mAb CC1 provided by K. Holmes (31)). Polyclonal LR7 cells stably expressing biotin protein ligase (LR7-BirA) were similarly made with the MLV-pseudotyped virus using the pQCXIP-BirA packaging vector. LR7-BirA cells were selected at

15 µg/ml and maintained at 10 µg/ml puromycin (Sigma, P8833). BirA expression was confirmed by immune detection using Cy3 conjugated mouse monoclonal anti-FLAG (Sigma, A9594). No BirA enzyme was detected in the cell culture supernatants of LR7-BirA cells after 72 hours incubation as analyzed by western blot using a mouse monoclonal anti-FLAG antibody conjugated horseradish peroxidase.

Conditional biotinylation assay.

LR7 or LR7-BirA cells were cultured to confluence in 6 well clusters. Cells were inoculated with virus-containing cell culture supernatant supplemented with 50 µg/ml DEAE-dextran (Sigma, D9885) and 10 µM biotin (Sigma, B4639) with a multiplicity of infection (MOI) of 10. After 30 min, protein biosynthesis was inhibited by addition of 50 µg/ml cycloheximide (Sigma C7698) to prevent S protein synthesis from virus infections. At 90 min post infection (p.i.), cells were chilled on ice, washed twice with ice-cold phosphate buffered saline (PBS) and lysed in ice-cold radio immunoprecipitation assay buffer (RIPA, 150 mM NaCl, 1 % Nonidet P-40, 0.5 % *Sodium deoxycholate*, 0.1 % *Sodium dodecyl sulfate (SDS)*, 50 mM Tris-HCl pH 8) supplemented with Complete Protease Inhibitor Cocktail Tablets (Roche 11836153001) to prevent further proteolysis and with or without 6 mM Napyrophosphate (PP, Sigma, 71516) to quench the activity of BirA in cell lysates (32). The cell lysates were cleared by centrifugation at 10,000 x g for 10 min at 4°C. The supernatants were combined with 20 µl 50:50 slurry of protein G sepharose (Biovision, 6511) supplemented with 0.5 mg polyclonal anti-BAP antibody (Genscript, Avi-Tag A00674) and incubated under rotation for 2 h at 8°C to immunoprecipitate the S proteins. Next, sepharose beads were pelleted at 6,000 x g for 5 min at 4°C and washed trice with an excess of ice-cold RIPA buffer. Excess supernatant was carefully removed and, finally, samples were denatured by addition of sample buffer and subjected to western blotting.

If inhibitory compounds were used during the infection, cells were pretreated for 30 min at 37°C followed by infection in the presence of the respective compounds. The following protease inhibitors were used at their highest recommended working range concentration according to Sigma's protease inhibitor technical bulletin INHIB1 (final concentration): Pepstatin A (1.5 µM, Sigma, P5318), Leupeptin (100 µM, Sigma, L2023), E64d (10 µM, Sigma, E8640), phosphoramidon (10 µM, Sigma, R7385) AEBSF (100 µM, Sigma, A8456). HR2 peptide was used at 25 µM concentration. The following lysosomotropic agents were used (final concentration): ammonium chloride (25 mM NH₄Cl, Merck, Darmstadt), Bafilomycin A1 (125 µM, Enzo Life sciences).

Time course biotinylation assay.

LR7 or LR7-BirA cells were cultured to confluence on 10 cm dishes and the inoculum was prepared similar to the conditional biotinylation assay. First, cells were washed twice with ice-cold PBS and ice-cold inoculum was added for 45 min to allow attachment of the virus to the target cells at 8°C. Next, inoculum was removed and cell layer washed once with ice-cold PBS, followed by the addition of 37°C culture medium supplemented with 10 µM biotin. Differential periods of infection were achieved by successively delaying the start of attachment and infection, while maintaining an equal duration. All samples were harvested at the same time to even out the time between lysis and immunoprecipitation. 50 µg/ml cycloheximide was added 30 min after warming up the infection to 37°C for all samples with an infection

period longer than 30 min or at the end of the infection. The sample for 0 min was prepared for lysis after 1 minute at 37°C. Lysis and immunoprecipitation was performed as described in the conditional biotinylation assay and IP-samples were analyzed by western blotting.

HR2 inhibition of MHV infection.

Multiple wells containing LR7 cells were infected with wild-type MHV for 1.5 min to synchronize infection. Inoculum was replaced by culture medium at the start of infection. At increasing time points supernatants of individual wells were replenished with culture medium supplemented with 20 μ M HR2 peptide to block MHV entry. 4 h p.i., supernatant was replaced with culture medium containing 1 μ M HR2 peptide to inhibit syncytia formation. 7 h p.i., cells were fixed with 3.7 % formalin and immunoperoxidase staining was performed using K135 serum and visualized with AEC substrate kit (Vector Laboratories). The extent of infection relative to non-inhibited virus infection was calculated from the number of plaques observed.

Deglycosylation.

LR7 or LR7-BirA cells were cultured to confluence in 10 cm dishes, the inoculum was prepared and the infection performed similar to the conditional biotinylation assay. After immunoprecipitation, samples on the sepharose beads were denatured and deglycosylated with PNGase F (New England Biolabs, P0704) according to the manufacturer's protocol. Finally, samples were denatured by addition of sample buffer and subsequently analyzed by western blotting.

Western blot analysis.

For the detection of S protein in virus containing cell culture supernatants, aliquots were directly lysed and denatured in sample buffer containing 50 mM Tris-HCl pH 6.8, 50 % glycerol, 5 % 2-mercaptoethanol, 1 % SDS and bromophenol blue and boiled at 95°C for 10 min. Samples after immunoprecipitation were eluted from beads by boiling at 95°C for 10 min in sample buffer. Supernatant was subjected to SDSpolyacrylamide gel electrophoresis (SDS-PAGE) in a discontinuous gel with 8 % acryl amide in the separating gel (33). Next, samples were transferred to a polyvinylidene fluoride membrane (BioRad, 1620176). Membranes were blocked with bovine serum and reacted with antibodies or streptavidin-HRP in PBS with bovine serum and 0.5 % Tween20. For detection we used Amersham ECL Western Blotting Analysis System (GE healthcare, RPN2109) with X-Omat LS films (Kodak, Sigma F1149).

Computational analysis.

The transmembrane domain of MHV S protein was predicted by TMHMM 2.0 and the signal peptide by SignalP 4.1. HR1 and HR2 regions were defined according to Bosch et al. (11). Glycosylation sites were predicted with NetNGlyc 1.0 (Technical University of Denmark). Western blot signals were quantified using ImageJ. Amino acid sequence alignment was performed by ClustalW2 using S sequences of infectious bronchitis virus (IBV strain Beaudette, NP_040831.1), Middle East respiratory syndrome coronavirus (MERS-CoV strain HCoV-EMC, AFS88936.1), mouse hepatitis virus (MHV strain 2, AAF19386.1 and strain MHV-A59, NP_045300.1), severe acute respiratory syndrome coronavirus (SARS-CoV strain Tor2, NP_828851.1) and transmissible gastroenteritis virus (TGEV strain TO14, AF302263_1).

RESULTS

A biotinylation assay to label S protein after virus-cell fusion.

During inoculation, not all virions successfully fuse with the target cell and deliver their genome into the cytoplasm. According to the current model of class I protein fusion, the Cterminal tail of the CoV S protein is hidden internally in the intact virion. It will be introduced into the cytoplasm after virus and cell membrane have fused. In order to be able to discriminate S proteins coming from virions that successfully achieved fusion from those that failed, we designed a biotinylation assay that uses selective intracellular biotin labeling of the protein's Cterminus. To that end, we generated a recombinant MHV-A59 derivative carrying an S protein with a Cterminally appended 37 amino acid biotin acceptor peptide (MHVBAP; Fig. 1A) and a recombinant murine cell line that constitutively expresses BirA in its cytoplasm (LR7BirA). BirA recognizes the biotin acceptor peptide (BAP) as substrate for biotin ligation in the presence of ATP and free biotin. In intact virions, the BAP faces the luminal side and is protected from modification by BirA, but upon virus-cell fusion it becomes exposed to the enzyme (Fig. 1B). Consequently, BirA can biotinylate the BAP-tag of S proteins of virions that underwent fusion, enabling the selection and characterization of post-fusion S proteins via the biotin label. MHVBAP displayed similar growth kinetics but yielded 10-fold reduced titers compared to wild-type MHV (data not shown).

To characterize the S protein of MHV-BAP and to demonstrate biotinylation of the BAP-tag, we propagated wildtype MHV and the recombinant MHVBAP in LR7 cells and LR7-BirA cells. The cell culture supernatants were analyzed by western blotting with antibodies recognizing the S2 subunit or the BAP-tag, or with the biotin-binding streptavidin (Fig. 1C). The monoclonal antibody recognizing the S2 subunit detected the full-length S protein (S_0) and the S2 subunit of all virus preparations. A polyclonal antibody directed against the BAP specifically detected (S_0) and the S2 subunit of MHVBAP, but not those of wild-type MHV. Importantly, biotinylation of BAP-tagged S protein was only detected for MHV-BAP viruses produced in LR7-BirA cells, demonstrating the BirA dependent biotinylation of the BAP. Recognition of the BAP-tag by the anti-BAP polyclonal antibody was not influenced by its biotinylation status; tagged and non-tagged S proteins were detected equally efficient.

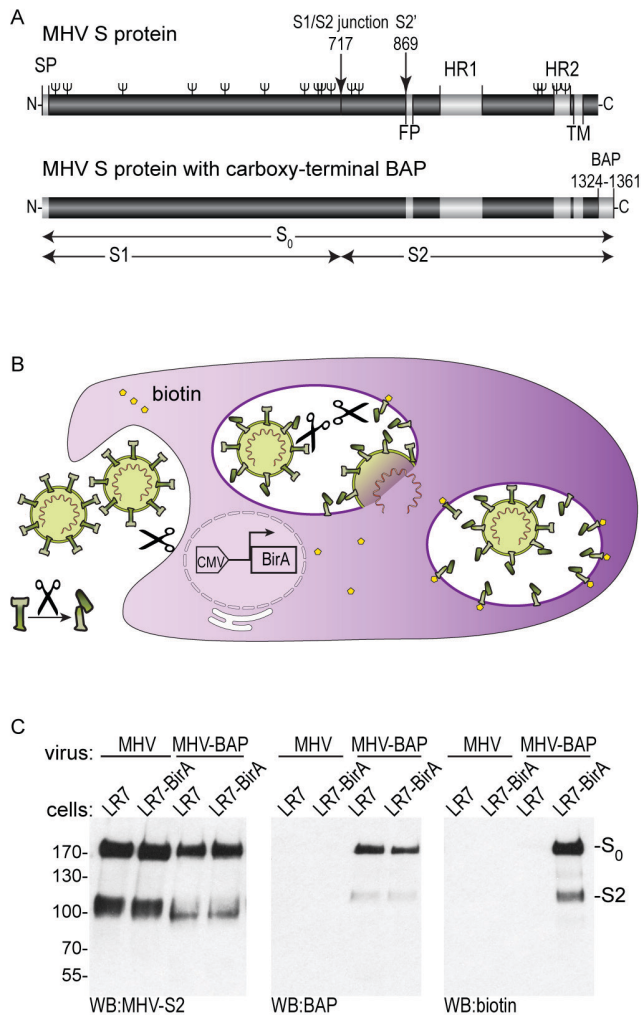


Figure 1: Recombinant MHV-BAP for the detection of biotinylated S proteins. (A) Schematic organization of wild-type (1324 aa) and BAP-tagged MHV (strain A59) S protein (1361 aa) drawn to scale. The S protein has an N-terminal S1 domain, responsible for receptor binding, and a C-terminal S2 domain that holds the fusion machinery. Positions of the signal peptide (SP), predicted N-glycosylation sites (Ψ), the putative fusion peptide (FP), two heptad repeat (HR) regions, the transmembrane domain (TM) and the biotinylation acceptor peptide (BAP) are indicated. MHV S protein contains two predicted protease cleavage sites: a furin cleavage site at the S1/S2 junction and a putative second cleavage site (S2') just upstream of the fusion peptide. (B) A biotinylation assay was designed to selectively identify and characterize S protein of MHV virions that underwent membrane fusion with the cellular target membrane. The biotinylation acceptor peptide was fused to the C-terminus of the S protein. Target cells stably express cytoplasmic protein biotin ligase (BirA) from a CMV promoter. Upon membrane fusion, the C-terminal BAP of S protein will be introduced into the cytoplasm and can be accessed and biotinylated by BirA. (C) Characterization of recombinant MHV-BAP. Virus stocks of MHV-A59 with wild-type S protein (MHV) or with BAP-tagged S protein (MHV-BAP) were produced in LR7 cells or LR7 cells expressing BirA (LRT-BirA) and subjected to western blotting (WB) using a MHV-S2 monoclonal antibody, an anti-BAP polyclonal antibody and streptavidin-HRP for detection of proteins. Full length S protein (S₀) and S2 subunit resulting from cleavage at the S1/S2 junction were detected with antibodies directed against the S2 domain or BAP, and with streptavidin for detection of biotinylation. Size and position of marker proteins (in kilodalton) are indicated at the left.

Biotinylated S proteins after virus-cell fusion: detection of S2*.

Next, we assessed the biotinylation of S proteins after membrane fusion of virions with BirA expressing target cells. The LR7-BirA cells were inoculated with MHV-BAP (MOI = 10) for 90 min to enable binding and fusion. To detect the biotinylated S proteins, anti-BAP antibody was used to immunoprecipitate the BAP-tagged S proteins from whole cell lysates. This purification and concentration step was essential for detection. The BirA enzyme maintains its activity in the lysis buffer, even at low temperatures. Consequently, all S protein present in the cell lysate became biotinylated post lysis and could be detected using streptavidin-HRP conjugate (Fig. 2A lane 1). In addition to the S₀ and S2 forms, which could already be observed in the virus stock (Fig. 1C), an additional product of ~80 kDa was detected which we named S2*. To prevent post lysis biotinylation and analyze the S proteins as they occur in the intact cell, BirA activity was quenched by product feedback inhibition by addition of PP to the lysis buffer and during the IP procedure (Fig. 2A lane 2) (32). Now, the S2* was the most abundant S protein product detected and only limited amounts of S₀ and S2 were observed.

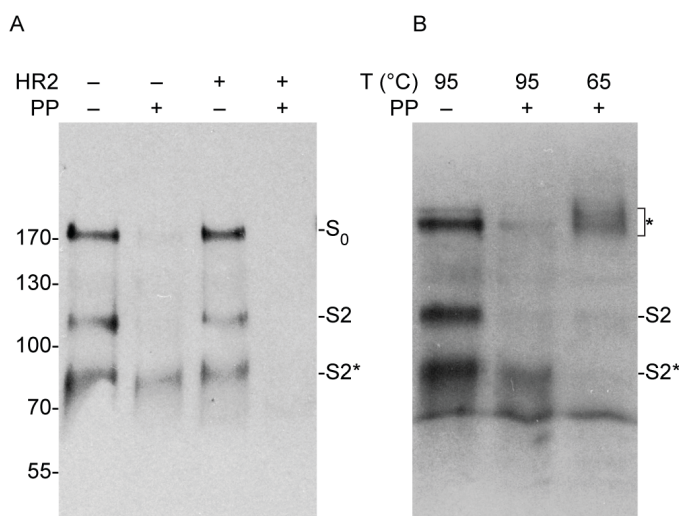


Figure 2: Detection of S protein after membrane fusion with target cells. (A) LR7-BirA cells were inoculated with MHV-BAP for 90 min in the absence or presence of peptidic fusion inhibitor (HR2) and lysed in the absence or presence of the BirA inhibitor PP. Immunoprecipitated S proteins were analyzed by western blotting. Only biotinylated S protein was detected by streptavidin-HRP conjugate. Upon cell lysis in the absence of PP, all S protein was allowed to be biotinylated by BirA; thus full-length (S₀), S protein cleaved at the S1/S2 junction (S2), and a novel product of lower molecular weight designated S2* was detected. The presence of PP during lysis allowed the exclusive detection of S protein that was biotinylated during infection and mainly shows the S2* fragment. (B) IP samples were denatured at 95°C or 65°C before western blot. In the presence of PP, the S2* fragment constitutes the majority of biotinylated S proteins migrating at approximately 80 kDa position. After heating IP samples at 65°C - instead of 95°C - a larger product was present around the ~200 kDa position (indicated by the asterisk).

To test whether the appearance of the S2* protein indeed correlates with successful infection, we exploited the HR2 peptide, a synthetic peptide fusion inhibitor, which effectively blocks the membrane fusion activity of the S protein (11). Addition of the HR2 peptide efficiently abrogated biotinylation of the S protein in the presence of PP (Fig. 2A lane 4). The experiment confirmed that biotinylation of S proteins only occurs after virus-cell fusion, and further demonstrated that the proteolytic processing of S protein is not affected by addition of

HR2 peptide (Fig. 2A lane 3). We hypothesized that the S2* subunit represents the proteolytically primed subunit of MHV S protein.

The S2* subunit occurs in stable multimers.

We examined the novel S2* subunit for characteristic features of the fusion machinery. To drive membrane fusion, the membrane-anchored domains of class I fusion proteins fold into a highly SDS-stable and temperature-resistant post-fusion trimer, facilitated by the zipping up of the two HR domains into six-helix bundles (11, 34). To test whether S2* forms such stable trimers, we analyzed the SDS-PAGE migration of the biotinylated S protein variants after heat treatment of the samples at 65°C, rather than 95°C. The S2* subunit that was biotinylated upon infection of target cells migrated at ~ 80 kDa if denatured at 95°C. This species was, however, absent after denaturation at 65°C; instead, a larger band was observed at ~ 200 kDa, in line with the S2* subunit actually occurring as a stable, multimeric post-fusion complex (Fig. 2B).

Kinetics of S2* appearance, virus cell fusion and MHV infection coincide.

If the novel S2* subunit represents the proteolytically primed form, the kinetics of S protein cleavage should be equal to or faster than productive MHV infection. We monitored the kinetics of S protein cleavage and fusion by performing a time course of infection with MHV-BAP on LR7-BirA cells. To synchronize infections, virus was allowed to bind to cells at 8°C for 1 h, followed by removal of the inoculum after which infection was continued at 37°C. Omitting PP during IP procedure revealed the overall biochemical fate of all (i.e. fused and non-fused) S proteins over a 90 minute time period (Fig. 3A). Western blot analysis of IP samples indicated that the relative amount of the S2* cleavage product increased over time, while the S₀ and S2 signal slowly vanished. To prevent the maturation of endosomes and the acidification of endo-lysosomal compartments, 25 mM NH₄Cl was added to the cells throughout infection (35). This treatment resulted in a net increase of S protein, suggesting that the time dependent overall decrease of S protein in the absence of NH₄Cl was due to lysosomal degradation. In contrast, the proteolytic process leading to S2* formation was not blocked by NH₄Cl. Quantification of the density of the S protein bands over 90 min of infection showed that the fraction of the S2* subunit increased from 3 % to 50 % (Fig. 3A, bar chart). Yet, not all S proteins had undergone proteolytic processing after 90 min. By performing the analysis in the presence of PP during the sample preparation, only S protein from virus-cell fusion events was monitored (Fig. 3B). The appearance of the S2* subunit started early and continued increasingly for at least 90 min.

To confirm the kinetics of virus-cell fusion by an independent approach, we examined the inhibition of MHV infection by HR2 peptide fusion inhibitor. LR7 cells were pulse-inoculated for 1.5 min with wild-type MHV to synchronize binding. Inocula were replaced by culture medium after which HR2 peptide was added to individual samples at successive time points. The relative amount of infection was determined at 7 h p.i. by immune staining of the cells against MHV. The presence of HR2 peptide from the start completely abolished infection, but showed no effect when added 120 min after inoculation (Fig. 3B, line chart). The MHV infection deduced from the HR2 peptide time-of-addition experiment showed similar kinetics to proteolysis of S protein yielding the S2* product but was slower. MHV infection coincided

with the accumulation of the S2* subunit as monitored by intracellular biotinylation. In comparison, the intensities of the biotinylated S2* protein bands observed in the virus-cell fusion experiment were quantified and included in the same graph as a bar chart. (Fig. 3B, bar chart)

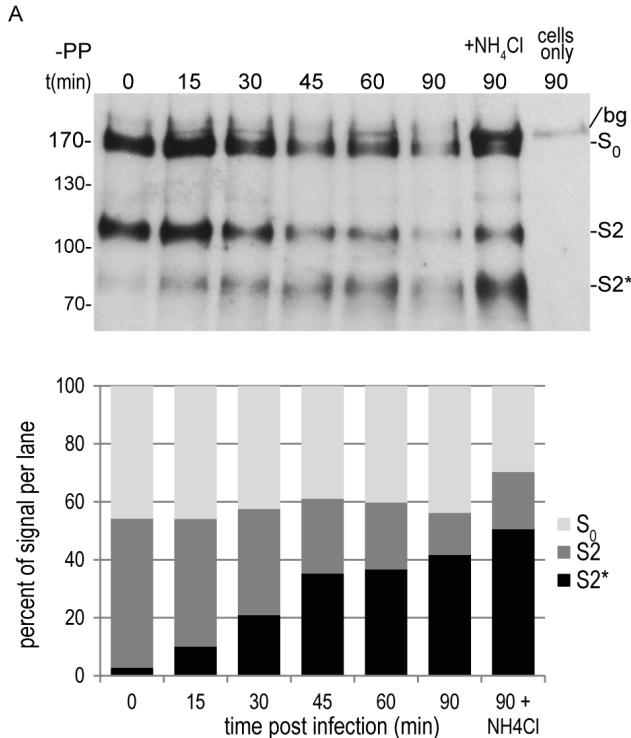


Figure 3: S2* fragment is generated during virus entry. (A) MHV-BAP was bound to LR7-BirA cells and excess virus was removed to synchronize the infection. The infection was stopped at the indicated times post infection by cell lysis in the absence of the BirA inhibitor PP. Immunoprecipitated S proteins were analyzed by western blot and biotinylated protein detected by a streptavidin-HRP conjugate. To assess lysosomal degradation, ammonium chloride (NH₄Cl) was added during infection. A background band (bg) is indicated. The relative amounts of S₀, S₂ and S₂* protein per lane were quantified to illustrate the proteolytic processing over time (lower panel). (B) Same as 3A, except that by addition of PP during lysis, only S protein that has been biotinylated during infection was detected. As controls, MHV-BAP in the absence of cells, infection with wild-type MHV and MHV-BAP infection performed in the presence of the HR2 fusion inhibitor was taken along. The intensity of the S2* fragment, was quantified and displayed as a bar diagram below. In addition, to determine the kinetics of virus entry independently, MHV infections were supplemented in time with the HR2 fusion inhibitor after a synchronized infection (line diagram). At 7 h post infection, infected cells were detected by immunostaining and relative amount of infection was determined.

Conserved arginine is not the cleavage site that yields the S2* subunit.

The identification of the proteolytic cleavage site that yields the fusion active S2* subunit, could provide further information about the requirements for gaining fusion competence. Judged from the molecular weight of the S2* protein, the cleavage site is located within the N-terminal half of the S2 subunit. This region comprises a conserved arginine, previously described as a potential protease target site and termed S2' in the S proteins of SARS-CoV and IBV (18, 36) (Fig. 4A). Cleavage at this arginine would truncate the S2 domain by

approximately 15 kDa and remove two glycosylation sites which is in agreement with the observed difference between the S2 and S2* band. We used a reverse genetic approach to determine whether the MHV S2* subunit indeed results from proteolysis at the putative S2' cleavage site. To that end, mutant MHV-BAP was generated containing two serine substitutions of arginines occurring at or close to the S2' cleavage (MHV^{S2'}-BAP, Fig. 4A, table). Another MHV variant with a mutated furin cleavage site at the S1/S2 junction was generated by replacing the arginines by serines (MHV^{FCS}-BAP). Mutant viruses were viable and used to infect LR7BirA cells for 90 min at equal MOI after which IP samples were prepared in the absence or presence of PP. Western blot analysis of IP samples showed that the knock-out of the furin cleavage site at the S1/S2 junction in MHV^{FCS}-BAP prevented the appearance of the S2 form (22) (Fig. 4A lower panel). In contrast, serine substitution of the two arginines at the presumed S2' cleavage site in MHV^{S2'}-BAP did not prevent the formation of the S2* subunit. When IP was performed in the presence of PP, only allowing the detection of the S proteins involved in fusion, the S2* subunit was clearly detected for all three viruses. The S2* product of the mutant viruses migrated with similar mobility and represented the major form of S protein that underwent fusion. Arginine substitutions at the S1/S2 or S2' site had no detectable effect on virus titers, which remained comparable to MHV-BAP (Figure 4A). As reported earlier, the deletion of the S1/S2 arginine motif resulted in reduced syncytia formation capacity of the virus (22).

Prediction of the S2' cleavage site from the molecular weight of the S2* subunit after deglycosylation.

As we could not predict other protease cleavage sites from the S protein amino acid sequence, we tried to identify the S2' cleavage site by alternative approaches. The biotinylation assay did not yield sufficient amount and purity of the S2* subunit to allow Nterminal amino acid sequencing. Instead, we deglycosylated the S protein to more precisely determine the molecular weight of S2*, from which the approximate location of the cleavage site might then be deduced. To that end, LR7-BirA cells were inoculated with MHV-BAP for 90 min and samples prepared in the absence or presence of PP. After the IP, S protein bound to protein G sepharose beads was denatured and samples were deglycosylated by PNGase F to remove all N-linked glycans. Successful deglycosylation was revealed by the S proteins migrating with higher electrophoretic mobility (Fig. 4B, top and middle panel). Deglycosylation of all S proteins (- PP) and of S proteins from virions that had fused (+ PP) showed a similar effect. The theoretical molecular weight was predicted to be 70 kDa for the S2 domain and 54 kDa for S2* if the cleavage occurs close to the putative FP. The deglycosylated S2 subunit shifted from the 105 kDa position to 80 kDa – slightly higher than predicted – and migrated as a welldefined band. In contrast, the S2* protein also shifted to a lower molecular weight, yet it remained heterogeneous after deglycosylation ranging in size from 60-65 kDa. Similar to S2, the S2* subunit appears larger than its predicted molecular weight of 54 kDa, hence cleavage may occur at the putative S2' cleavage site or further upstream. The blot was restained with antiserum against the BAP in order to visualize the S proteins from infections of LR7 cell without BirA (Fig. 4B, lower panel) and independent of biotinylation. Of note, the prior streptavidin-biotin interaction reduces the anti-BAP antibody reactivity, particularly in fully biotinylated samples prepared in the absence of PP (Fig. 4B, lane 2 & 3).

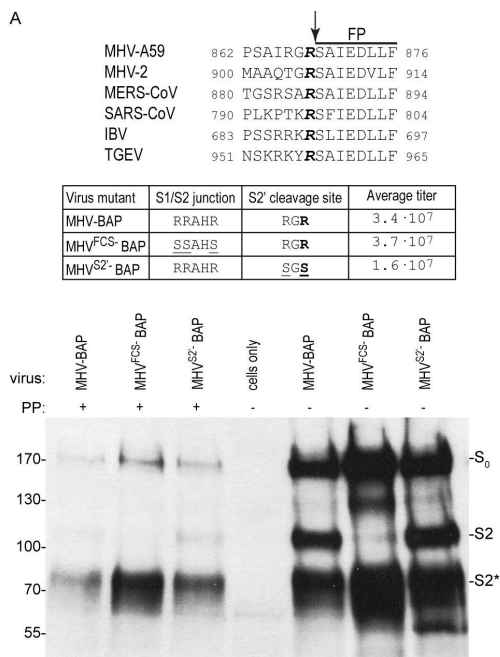


Figure 4: Characterization of the S2* fragment. (A) Sequence alignment of an S protein segment of representative coronaviruses containing the putative S2' cleavage site (arrow) and part of the fusion peptide (FP). The conserved arginine residue adjacent to the putative fusion peptide (FP, (37)) is shown in bold. Table indicates the mutations of generated recombinant MHV viruses, carrying serine substitutions of arginines (underlined) at the furin cleavage site at the S1/S2 junction (MHV^{FCS}-BAP) and the putative S2' site (MHV^{S2'}-BAP). The average titer of three independent virus preparations was determined by end point dilution and reported as TCID50/ml. BirA-cells, infected with the recombinant viruses for 90 minutes, were lysed in the absence and presence of pyrophosphate (PP). Biotinylation of immunoprecipitated S proteins was detected by western blotting, as described above. (B) Deglycosylation of biotinylated S proteins. The biotinylation assay was performed with MHV-BAP as described under A. Prior to western blot analysis, all samples were denatured and selected samples subsequently deglycosylated using PNGaseF. Biotinylated S protein was detected with streptavidin (two exposure times shown) and the same blot was restained with anti-BAP antibody to detect (non-biotinylated) S proteins (of note: streptavidin binding to biotinylated BAP limits detection with the anti-BAP antibody). Full length S protein is indicated by open triangles, S protein cleaved at the S1/S2 junction by solid triangles and S2* fragment by asterisks. All S proteins show faster migration after deglycosylation; S₀ and S₂ are reduced to a defined band upon deglycosylation, whereas the S2* fragment band remains diffuse. A cellular background band is indicated (bg).

Inhibition of cellular proteases that generate the S2* subunit.

To obtain information on the S protein cleavage site and the functional aspect of proteolysis during virus infection we attempted to identify the responsible host cell proteases. SARS-CoV S protein can be cleaved by multiple proteases and availability of those proteases has been linked to the tissue tropism of the virus (7). Yet, expression of the MHV receptor can render cell lines of different species susceptible to MHV infection (31) and if the S2* subunit represents the fusion active form, the priming protease(s) should occur in various cell lines. To test this, we monitored S protein cleavage in non-murine cell lines stably expressing the MHV receptor. Virus preparations containing pre-biotinylated S protein were produced after a single passage on LR7-BirA (MHV-BAP*^{bio}) and typically contained about 70 % of S₀, 30 % of S₂ and a marginal fraction of S2* (Fig. 5A, lane1). After 90 min of inoculation of two

human and one simian cell line (i.e. HEK 293T, HeLa and Vero cells, respectively), the pattern of S₀, S2 and S2* was similar compared to that in the murine LR7-BirA cell line (Fig. 5A). Broad spectrum protease inhibitors can affect various classes of proteases. In order to characterize the proteases involved in S protein cleavage, a virus entry assay was performed in the presence of various protease inhibitors, suppressing the activity of the main classes of proteases. MHV-BAP infection was performed on LR7-BirA cells for 90 min in the presence of the cysteine protease inhibitor E64d, the metalloprotease inhibitor phosphoramidon, the aspartyl protease inhibitor pepstatin A, the serine and thiol protease inhibitor leupeptin, the serine protease inhibitor AEBSF (Fig. 5B) as well as the serine protease inhibitor camostat or 1x concentrated Roche mini cocktail inhibitor (data not shown). In addition, the involvement of low-pH dependent proteases was probed using the lysosomotropic agents NH₄Cl and bafilomycin A1 (Fig. 5C). None of the applied agents could prevent the S protein cleavage that results in the formation of the S2* subunit. The lysosomotropic agents NH₄Cl and bafilomycin A1 abolished fusion similar to HR2 peptide peptide fusion inhibitor as indicated by the lack of biotinylated S when IP was performed in the presence of PP (Fig. 5C).

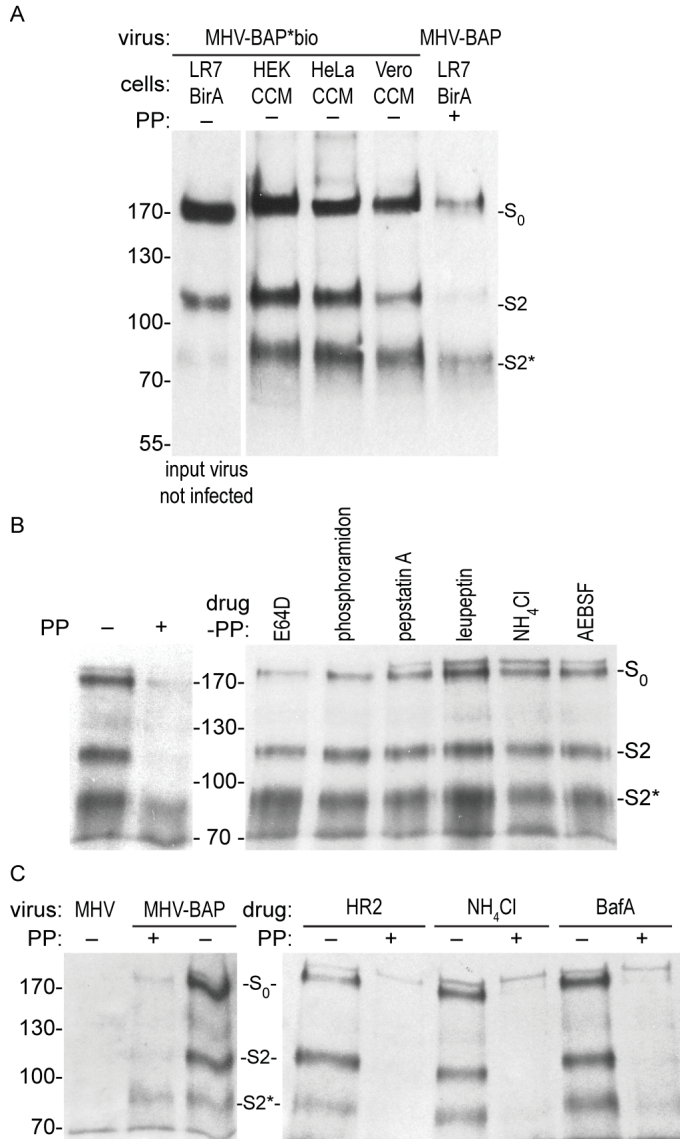


Figure 5: Protease inhibitors or lysosomotropic agents do not prevent S2* formation. (A) Biotinylated MHV-BAP (MHV-BAP**bio*) progeny viruses were produced in LR7-BirA cells. Cells overexpressing the MHV receptor Ceacam1a (CCM) were infected with MHVBAP**bio* for 90 min. Immunoprecipitated S proteins were analyzed by western blot and biotinylation detected by the streptavidin-HRP conjugate. Cleavage status of MHV-BAP**bio* prior to infection was visualized by inoculating LR7-BirA with virus-containing cell culture supernatant for 2 h 15 min at 4°C and direct lysis without warming (first lane). (B) LR7-BirA target cells were pretreated with various broad spectrum protease inhibitors for 30 min. Infection with MHV-BAP was allowed in the presence of protease inhibitors for 90 min and subsequently sample preparation was performed in the absence of PP as described in A. (C) Same as B, infection with MHV or MHV-BAP, infections were performed in the presence of HR2 fusion inhibitor, ammonium chloride (NH₄Cl), or bafilomycin A1 (BafA). Lysates were prepared in the absence or presence of PP.

DISCUSSION

We studied cleavage of the MHV S glycoprotein during virus entry by an unbiased approach that allowed us to isolate fusion proteins of virions that accomplished virus-cell fusion and we newly identified an S2* subunit. It displayed features of the fusion machinery, suggesting that the S2* subunit represents the fusion-active part of the S protein. In support of this, the majority of the post-fusion S proteins were cleaved into the S2* protein and formed heat- and SDS-stable multimers that resemble the post-fusion six-helix bundle. Furthermore, the kinetics of appearance of the biotinylated S2* protein coincided with the kinetics of virus entry as determined by monitoring sensitivity of infection to the HR2 peptide fusion inhibitor. The size of the S2* protein indicates cleavage to occur in the S2' region just upstream of the putative FP. We could not determine the exact cleavage site by reverse genetics, and the low mass amounts of the S2* protein did not allow its identification by mass spectrometry. Deglycosylation of the S2* protein resulted in a heterogeneous product suggesting that cleavage can occur at alternative sites in proximity to the S2' site. Protease inhibitors used to identify the protease responsible for S protein cleavage could not prevent the formation of the S2* subunit. Although the precise details of the cleavage process remain enigmatic, the appearance and characteristics of the S2* subunit support the idea that it represents the fusion-ready subunit.

Previous investigations of CoV fusion protein cleavage have monitored the infectivity of viruses or virus like particles in the presence of protease inhibitors or after genetically modifying the fusion protein. (14, 16, 21, 23, 36, 37). Many studies demonstrate cleavage of S proteins displayed on the cell surface by recombinant proteases, but only few verify proteolysis in virus preparations upon exposure to recombinant proteases and soluble receptor (38, 39). These studies convincingly correlated cleavage of S protein with its membrane fusion capacity, but failed to demonstrate cleavage during virus entry or identifying the fusion competent subunit. In fact, the biochemical fate of viral glycoproteins on virions that are entering host cells at physiological MOIs is difficult to study. Given the limited amount of virus even at high MOI, the significant fraction of non-infectious particles in each virus preparation, and the relatively low number of S proteins per virion, the specific detection of S proteins on successfully fusing virions is a great challenge. In this study we established a novel biochemical assay based on the conditional biotinylation of proteins to concentrate and purify MHV S proteins involved in functional virus-cell fusion events. This enables the identification and characterization of fused S proteins in combination with more classical experiments using site-directed mutagenesis and protease inhibitors. Our approach excludes contributions of non-fused virions hence focuses on functional fusion events. As the infecting virions take a physiological entry route, we do not rely on mimicking the fusion process by addition of soluble receptor, exogenous protease treatment or pH shock. The assay can be adapted to monitor the biochemical fate of structural virion components of any enveloped or non-enveloped virus upon entry.

The entry of various CoV is supported by distinct proteases that can act at the plasma membrane of the target cell or in the endosomal compartments (10, 13). For MHV-A59, proteolytic processing at the S1/S2 junction enables efficient cell-cell fusion resulting in syncytia formation (40) and mutagenesis of the cleavage site limits the syncytia size (23, 41). However, as we showed earlier (22) and confirmed here by substituting all arginines at the S1/S2 junction, the S1/S2 cleavage is dispensable for fusion activity and virus infectivity. This is supported by observations with a natural isolate, MHV-2 (42), or with a cell passaged isolate

MHV/BHK (43), which both lack a genuine furin cleavage site and hence carry uncleaved S proteins on their virions. In our study, only small amounts of the S2 subunit were present on virions that had fused, suggesting that S2 is not the fusion-active form. Nevertheless, cleavage of MHV S protein at the S1/S2 junction may provide additional structural flexibility to increase the accessibility of a cleavage site for priming, as suggested earlier for SARSCoV (36). It is possible that S proteins are processed into S2*, perhaps via a short-lived intermediate S2 form that is not detected. With less priming proteases on the cell surface than in the endolysosomal compartments, this may explain the cell-cell fusion inability of the MHV spikes lacking a functional furin cleavage site.

We observed that S protein cleavage upon MHV infection occurred downstream of the S1/S2 junction and released an S2* fragment of approximately 80 kDa, about 25 kDa smaller than the S2 subunit. Assuming this membrane-bound subunit to carry the membrane fusion function we probed the S2* subunit for criteria of the fusion machinery. First of all, the S2* subunit was the most abundant S protein species observed after virus-cell fusion and hence likely to be involved in membrane fusion. We assume that S₀ and S2 protein decorate virions which failed to reach the cellular compartment where the appropriate stimuli and proteolytic activity occur for S protein activation. However, a limited number of virions reaches the fusion compartment, where a majority of S proteins are proteolytically processed and triggered for fusion. Second, S2* occurred in heat- and detergent-resistant multimers indicative of the characteristic class I post-fusion sixhelix bundle. Similarly, treatment of MHV-2 virions with soluble receptor followed by protease treatment revealed an equivalent pattern of S₀, S2 and S2* (38). Cathepsin L and trypsin cleaved the S protein yielding a 71 kDa fragment which appeared as a stable, post-fusion form, similar to S2* (38). Proteolytic priming of the MHV-2 S proteins upon virus entry was earlier implicated by studies with inhibitors of endolysosomal proteases and lysosomotropic agents, and by trypsin bypass experiments, but the actual processing in cells was not confirmed (6). In our study, proteolytic processing of the S protein and virus-cell fusion, as measured by intracellular biotinylation of the S protein and by an independent virus infection assay, occurred with similar kinetics. The HR2 peptide fusion inhibitor prevents virus from fusion by inhibiting 6-helix bundle formation (11). Consistently, it also prevented S proteins of incoming virions from becoming biotinylated, hence allowing us to discriminate the sequential order of cleavage and fusion. If cleavage is a prerequisite for the S protein to mediate fusion, then HR2 must take effect after the proteolytic event and HR2 peptide indeed did not affect the cleavage of S protein. Taken together, we argue that the S2* fragment fulfills the criteria of the functional fusion protein.

The difference in molecular weight between the S2 and S2* subunits predicts the suspected cleavage site to map approximately 230 amino acids downstream of the S1/S2 junction. Furthermore, priming of the class I fusion proteins often occurs directly N-terminal of the FP which has been described as a conserved sequence of apolar amino acids in the CoV S protein (16, 36, 37). Both predictions point towards two critical arginine residues in the MHV S2 domain and intriguingly, cleavage at the same position (S2') has been implicated to induce SARS-CoV S protein mediated fusion (8, 10). By analogy, we suspected the S2' cleavage site to be used in MHV-A59 S protein, but after mutagenesis of both arginines the infectivity of MHV remained unaffected and the S protein cleavage pattern upon fusion unaltered.

In an attempt to deduce the cleavage site from its molecular weight we enzymatically removed the N-linked glycans of the S2* glycoprotein and analyzed its size. While the

deglycosylated S₀ and S2 proteins were reduced to sharply defined products, S2* remained ill-defined, migrating as a heterogeneous band ranging from 60–65 kDa. Assuming that the S2 and S2* product underwent similar post-translational modifications, the variable size of the S2* fragment can be best explained by promiscuous proteolytic cleavages, while S2 is formed by cleavage precisely at the S1/S2 junction. Heterogeneity of cleavage products might result from a certain degree of plasticity of S2' cleavage either by the existence of alternative cleavage sites or by involvement of multiple or alternative proteolytic enzymes, analogous to the fusion activation of the SARS-CoV S protein (13). The plasticity of the cleavage site also suggests that cleavage directly adjacent to the FP may not be an absolute requirement for fusion.

In search for the cleavage site, we applied broad spectrum protease inhibitors to identify corresponding (classes of) proteases. Testing protease inhibitors in SARS-CoV entry highlighted involvement of cathepsin L and eventually led to the identification of the cathepsin L cleavage site in the S protein (15, 17). In contrast to SARS-CoV, the protease inhibitors leupeptin, E64D and specific cathepsin L/B inhibitors failed to block MHV-A59 infection (6, 14). We observed no effect on the proteolytic processing of MHV S proteins for broad range protease inhibitors targeting cysteine, aspartyl, serine, thiol and metallo proteases. We conclude that heterogeneity of the S2* subunit, our failure to knock-out the S2' cleavage site by mutation and the insensitivity of MHV towards individual protease inhibitors are all consequences of redundant proteases and/or multiple cleavage sites that mediate MHV S protein priming. However, a given protease inhibitor may not block all individual proteases of a specific class and our inhibitor panel was lacking threonine protease inhibitors and aminopeptidases inhibitors that potentially prime the S protein (44). Plasticity in cleavage is further supported by the similarity of S protein processing in various cell lines and may confer flexibility to the virus in infecting different tissues (45). Alternatively, heterogeneous S2* fragment could be explained in analogy to filovirus fusion protein processing which requires gradual trimming by low pH activated endosomal proteases to reach fusion competence (46). However, we do not observe an enrichment of a particular S2* species over time and lysosomotropic agents did not prevent cleavage. Nevertheless, MHV S protein priming is a distinct event that is timed after virus attachment and before lysosomal degradation. Binding to cells alone (Fig. 3A, time course) or incubation of virus preparations with cell lysates (data not shown) was not sufficient to trigger the cleavage event. On the other hand, the application of lysosomotropic agents, which can prevent endosome maturation at higher concentrations, prevented the S protein signal from declining over time. The quantification of the different S forms after 90 min of inoculation in the absence or presence of NH₄Cl indicated that this lysosomal degradation equally affects all forms of S, but did not block cleavage into the S2* subunit. Hence, the S2* fragment is not the product of an unspecific lysosomal degradation processes, but is cleaved by cellular proteases that are active prior to fusion and before degradation in the lysosomal system.

All class I viral fusion proteins have to minimally meet two requirements to accomplish fusion: proteolytic priming and triggering of membrane fusion. Priming by cleavage is a common maturation step to bring fusion proteins into the fusion-ready, metastable form (1, 2). Our data suggest that the S2* subunit represents primed MHV-A59 S protein and indicate, in combination with other observations, that many - if not all - CoV fusion proteins need cleavage to achieve the fusion-ready form (6, 8, 20, 39). In contrast to many typical class I fusion proteins, priming of S proteins does not occur in the producer cell; cleavage in the target cell provides an extra level of spatial and temporal control of virus fusion. Thus, MHV

receptor-induced conformational changes are initiated at the target cell exposing a proteolytic cleavage site (19, 38, 47). SARS CoV S proteins require a first cleavage to facilitate a consecutive cleavage that then renders the S protein fusion competent (36). Nevertheless, an additional trigger of unknown nature is probably necessary to initiate the membrane fusion, since we could block virus-cell fusion - using lysosomotropic agents - but not S protein cleavage. Low pH in the endolysosomal compartment may itself be a trigger but may as well be necessary for priming by low pH-activated proteases (14, 48, 49). Triggers of an alternative nature seem, however, more likely because infection of some CoV can be bypassed using recombinant proteases without pH drop while syncytia formation typically occurs at neutral pH (6, 20, 22, 39, 40). In summary, the priming of S proteins plays a pivotal role in the temporal and spatial regulation of CoV entry. With the conditional biotinylation assay described in this study, the priming events that occur after receptor binding and depend on cellular proteases can be characterized in detail.

3

ACKNOWLEDGEMENTS

We acknowledge Zou Yong for kindly providing Vero CCL-81 cells. This work was supported by EU Framework 7 program PITN-GA-2009-235649-Virus Entry.

REFERENCES

1. **Harrison SC.** 2008. Viral membrane fusion. *Nature structural & molecular biology* **15**:690-698.
2. **White JM, Delos SE, Brecher M, Schornberg K.** 2008. Structures and mechanisms of viral membrane fusion proteins: multiple variations on a common theme. *Critical reviews in biochemistry and molecular biology* **43**:189-219.
3. **Melikyan GB, Smith EC, Dutch RE.** 2012. 5.15 Mechanisms of Enveloped Virus Entry by Membrane Fusion, p. 290-311. *In* Editor-in-Chief: Edward HE (ed.), *Comprehensive Biophysics*. Elsevier, Amsterdam.
4. **Epanand RM.** 2003. Fusion peptides and the mechanism of viral fusion. *Biochimica et biophysica acta* **1614**:116-121.
5. **Chandran K, Sullivan NJ, Felbor U, Whelan SP, Cunningham JM.** 2005. Endosomal proteolysis of the Ebola virus glycoprotein is necessary for infection. *Science* **308**:1643-1645.
6. **Qiu Z, Hingley ST, Simmons G, Yu C, Das Sarma J, Bates P, Weiss SR.** 2006. Endosomal proteolysis by cathepsins is necessary for murine coronavirus mouse hepatitis virus type 2 spike-mediated entry. *Journal of virology* **80**:5768-5776.
7. **Bertram S, Heurich A, Lavender H, Gierer S, Danisch S, Perin P, Lucas JM, Nelson PS, Pohlmann S, Soilleux EJ.** 2012. Influenza and SARS-coronavirus activating proteases TMPRSS2 and HAT are expressed at multiple sites in human respiratory and gastrointestinal tracts. *PloS one* **7**:e35876.
8. **Kawase M, Shirato K, van der Hoek L, Taguchi F, Matsuyama S.** 2012. Simultaneous treatment of human bronchial epithelial cells with serine and cysteine protease inhibitors prevents severe acute respiratory syndrome coronavirus entry. *Journal of virology* **86**:6537-6545.
9. **Burri DJ, da Palma JR, Kunz S, Pasquato A.** 2012. Envelope glycoprotein of arenaviruses. *Viruses* **4**:2162-2181.
10. **Heald-Sargent T, Gallagher T.** 2012. Ready, set, fuse! The coronavirus spike protein and acquisition of fusion competence. *Viruses* **4**:557-580.
11. **Bosch BJ, van der Zee R, de Haan CA, Rottier PJ.** 2003. The coronavirus spike protein is a class I virus fusion protein: structural and functional characterization of the fusion core complex. *Journal of virology* **77**:8801-8811.
12. **de Haan CA, Haijema BJ, Schellen P, Wichgers Schreur P, te Lintelo E, Vennema H, Rottier PJ.** 2008. Cleavage of group 1 coronavirus spike proteins: how furin cleavage is traded off against heparan sulfate binding upon cell culture adaptation. *Journal of virology* **82**:6078-6083.
13. **Belouzard S, Millet JK, Licitra BN, Whittaker GR.** 2012. Mechanisms of coronavirus cell entry mediated by the viral spike protein. *Viruses* **4**:1011-1033.
14. **Eifart P, Ludwig K, Bottcher C, de Haan CA, Rottier PJ, Korte T, Herrmann A.** 2007. Role of endocytosis and low pH in murine hepatitis virus strain A59 cell entry. *Journal of virology* **81**:10758-10768.

15. **Simmons G, Gosalia DN, Rennekamp AJ, Reeves JD, Diamond SL, Bates P.** 2005. Inhibitors of cathepsin L prevent severe acute respiratory syndrome coronavirus entry. *Proceedings of the National Academy of Sciences of the United States of America* **102**:11876-11881.
16. **Watanabe R, Matsuyama S, Shirato K, Maejima M, Fukushi S, Morikawa S, Taguchi F.** 2008. Entry from the cell surface of severe acute respiratory syndrome coronavirus with cleaved S protein as revealed by pseudotype virus bearing cleaved S protein. *Journal of virology* **82**:11985-11991.
17. **Bosch BJ, Bartelink W, Rottier PJ.** 2008. Cathepsin L functionally cleaves the severe acute respiratory syndrome coronavirus class I fusion protein upstream of rather than adjacent to the fusion peptide. *Journal of virology* **82**:8887-8890.
18. **Yamada Y, Liu DX.** 2009. Proteolytic activation of the spike protein at a novel RRRR/S motif is implicated in furin-dependent entry, syncytium formation, and infectivity of coronavirus infectious bronchitis virus in cultured cells. *Journal of virology* **83**:8744-8758.
19. **Matsuyama S, Taguchi F.** 2002. Receptor-induced conformational changes of murine coronavirus spike protein. *Journal of virology* **76**:11819-11826.
20. **Sturman LS, Ricard CS, Holmes KV.** 1985. Proteolytic cleavage of the E2 glycoprotein of murine coronavirus: activation of cell-fusing activity of virions by trypsin and separation of two different 90K cleavage fragments. *Journal of virology* **56**:904-911.
21. **Bos EC, Luytjes W, Spaan WJ.** 1997. The function of the spike protein of mouse hepatitis virus strain A59 can be studied on virus-like particles: cleavage is not required for infectivity. *Journal of virology* **71**:9427-9433.
22. **de Haan CA, Stadler K, Godeke GJ, Bosch BJ, Rottier PJ.** 2004. Cleavage inhibition of the murine coronavirus spike protein by a furin-like enzyme affects cell-cell but not virus-cell fusion. *Journal of virology* **78**:6048-6054.
23. **Gombold JL, Hingley ST, Weiss SR.** 1993. Fusion-defective mutants of mouse hepatitis virus A59 contain a mutation in the spike protein cleavage signal. *Journal of virology* **67**:4504-4512.
24. **Kuo L, Godeke GJ, Raamsman MJ, Masters PS, Rottier PJ.** 2000. Retargeting of coronavirus by substitution of the spike glycoprotein ectodomain: crossing the host cell species barrier. *Journal of virology* **74**:1393-1406.
25. **Janes PW, Griesshaber B, Atapattu L, Nievergall E, Hii LL, Mensinga A, Chheang C, Day BW, Boyd AW, Bastiaens PI, Jorgensen C, Pawson T, Lackmann M.** 2011. Eph receptor function is modulated by heterooligomerization of A and B type Eph receptors. *The Journal of cell biology* **195**:1033-1045.
26. **Taguchi F, Shimazaki YK.** 2000. Functional analysis of an epitope in the S2 subunit of the murine coronavirus spike protein: involvement in fusion activity. *The Journal of general virology* **81**:2867-2871.
27. **de Haan CA, Haijema BJ, Masters PS, Rottier PJ.** 2008. Manipulation of the coronavirus genome using targeted RNA recombination with interspecies chimeric coronaviruses. *Methods in molecular biology* **454**:229-236.
28. **Beckett D, Kovaleva E, Schatz PJ.** 1999. A minimal peptide substrate in biotin holoenzyme synthetase-catalyzed biotinylation. *Protein science : a publication of the Protein Society* **8**:921-929.

29. **Rossen JW, Bekker CP, Strous GJ, Horzinek MC, Dveksler GS, Holmes KV, Rottier PJ.** 1996. A murine and a porcine coronavirus are released from opposite surfaces of the same epithelial cells. *Virology* **224**:345-351.
30. **Mechold U, Gilbert C, Ogrzyzko V.** 2005. Codon optimization of the BirA enzyme gene leads to higher expression and an improved efficiency of biotinylation of target proteins in mammalian cells. *Journal of biotechnology* **116**:245-249.
31. **Dveksler GS, Pensiero MN, Cardellichio CB, Williams RK, Jiang GS, Holmes KV, Dieffenbach CW.** 1991. Cloning of the mouse hepatitis virus (MHV) receptor: expression in human and hamster cell lines confers susceptibility to MHV. *Journal of virology* **65**:6881-6891.
32. **Ng B, Polyak SW, Bird D, Bailey L, Wallace JC, Booker GW.** 2008. Escherichia coli biotin protein ligase: characterization and development of a high-throughput assay. *Analytical biochemistry* **376**:131-136.
33. **Laemmli UK.** 1970. Cleavage of structural proteins during the assembly of the head of bacteriophage T4. *Nature* **227**:680-685.
34. **Miura HS, Nakagaki K, Taguchi F.** 2004. N-terminal domain of the murine coronavirus receptor CEACAM1 is responsible for fusogenic activation and conformational changes of the spike protein. *Journal of virology* **78**:216-223.
35. **Ohkuma S, Chudzik J, Poole B.** 1986. The effects of basic substances and acidic ionophores on the digestion of exogenous and endogenous proteins in mouse peritoneal macrophages. *The Journal of cell biology* **102**:959-966.
36. **Belouzard S, Chu VC, Whittaker GR.** 2009. Activation of the SARS coronavirus spike protein via sequential proteolytic cleavage at two distinct sites. *Proceedings of the National Academy of Sciences of the United States of America* **106**:5871-5876.
37. **Madu IG, Roth SL, Belouzard S, Whittaker GR.** 2009. Characterization of a highly conserved domain within the severe acute respiratory syndrome coronavirus spike protein S2 domain with characteristics of a viral fusion peptide. *Journal of virology* **83**:7411-7421.
38. **Matsuyama S, Taguchi F.** 2009. Two-step conformational changes in a coronavirus envelope glycoprotein mediated by receptor binding and proteolysis. *Journal of virology* **83**:11133-11141.
39. **Matsuyama S, Ujike M, Morikawa S, Tashiro M, Taguchi F.** 2005. Protease-mediated enhancement of severe acute respiratory syndrome coronavirus infection. *Proceedings of the National Academy of Sciences of the United States of America* **102**:12543-12547.
40. **Frana MF, Behnke JN, Sturman LS, Holmes KV.** 1985. Proteolytic cleavage of the E2 glycoprotein of murine coronavirus: host-dependent differences in proteolytic cleavage and cell fusion. *Journal of virology* **56**:912-920.
41. **Bos EC, Heijnen L, Luytjes W, Spaan WJ.** 1995. Mutational analysis of the murine coronavirus spike protein: effect on cell-to-cell fusion. *Virology* **214**:453-463.
42. **Yamada YK, Takimoto K, Yabe M, Taguchi F.** 1997. Acquired fusion activity of a murine coronavirus MHV-2 variant with mutations in the proteolytic cleavage site and the signal sequence of the S protein. *Virology* **227**:215-219.
43. **de Haan CA, Li Z, te Lintelo E, Bosch BJ, Haijema BJ, Rottier PJ.** 2005. Murine coronavirus with an extended host range uses heparan sulfate as an entry receptor. *Journal of virology* **79**:14451-14456.

-
44. **Lopez-Otin C, Bond JS.** 2008. Proteases: multifunctional enzymes in life and disease. *The Journal of biological chemistry* **283**:30433-30437.
 45. **Slobodskaya O, Snijder EJ, Spaan WJ.** 2012. Organ tropism of murine coronavirus does not correlate with the expression levels of the membrane-anchored or secreted isoforms of the carcinoembryonic antigen-related cell adhesion molecule 1 receptor. *The Journal of general virology* **93**:1918-1923.
 46. **Hunt CL, Lennemann NJ, Maury W.** 2012. Filovirus entry: a novelty in the viral fusion world. *Viruses* **4**:258-275.
 47. **Holmes KV, Zelus BD, Schickli JH, Weiss SR.** 2001. Receptor specificity and receptor-induced conformational changes in mouse hepatitis virus spike glycoprotein. *Advances in experimental medicine and biology* **494**:173-181.
 48. **Sturman LS, Ricard CS, Holmes KV.** 1990. Conformational change of the coronavirus peplomer glycoprotein at pH 8.0 and 37 degrees C correlates with virus aggregation and virus-induced cell fusion. *Journal of virology* **64**:3042-3050. **Zelus BD, Schickli JH, Blau DM, Weiss SR, Holmes KV.** 2003. Conformational changes in the spike glycoprotein of murine coronavirus are induced at 37 degrees C either by soluble murine CEACAM1 receptors or by pH 8. *Journal of virology* **77**:830-840.

CHAPTER

FOUR

*Coronavirus cell entry occurs through
the endo-/lysosomal pathway in a
proteolysis-dependent manner*

Christine Burkard, Monique H Verheije, Oliver Wicht,
Sander I van Kasteren, Frank J van Kuppeveld, Bart L Haagmans,
Lucas Pelkmans, Peter J M Rottier, Berend Jan Bosch,
Cornelis A M de Haan

ABSTRACT

Enveloped viruses need to fuse with a host cell membrane in order to deliver their genome into the host cell. While some viruses fuse with the plasma membrane, many viruses are endocytosed prior to fusion. Specific cues in the endosomal microenvironment induce conformational changes in the viral fusion proteins leading to viral and host membrane fusion. In the present study we investigated the entry of coronaviruses (CoVs). Using siRNA gene silencing, we found that proteins known to be important for late endosomal maturation and endosome-lysosome fusion profoundly promote infection of cells with mouse hepatitis coronavirus (MHV). Using recombinant MHVs expressing reporter genes as well as a novel, replication-independent fusion assay we confirmed the importance of clathrin-mediated endocytosis and demonstrated that trafficking of MHV to lysosomes is required for fusion and productive entry to occur. Nevertheless, MHV was shown to be less sensitive to perturbation of endosomal pH than vesicular stomatitis virus and influenza A virus, which fuse in early and late endosomes, respectively. Our results indicate that entry of MHV depends on proteolytic processing of its fusion protein S by lysosomal proteases. Fusion of MHV was severely inhibited by a pan-lysosomal protease inhibitor, while trafficking of MHV to lysosomes and processing by lysosomal proteases was no longer required when a furin cleavage site was introduced in the S protein immediately upstream of the fusion peptide. Also entry of feline CoV was shown to depend on trafficking to lysosomes and processing by lysosomal proteases. In contrast, MERS-CoV, which contains a minimal furin cleavage site just upstream of the fusion peptide, was negatively affected by inhibition of furin, but not of lysosomal proteases. We conclude that a proteolytic cleavage site in the CoV S protein directly upstream of the fusion peptide is an essential determinant of the intracellular site of fusion.

4

AUTHOR SUMMARY

Enveloped viruses need to fuse with a host cell membrane in order to deliver their genome into the host cell. In the present study we investigated the entry of coronaviruses (CoVs). CoVs are important pathogens of animals and man with high zoonotic potential as demonstrated by the emergence of SARS- and MERS-CoVs. Previous studies resulted in apparently conflicting results with respect to CoV cell entry, particularly regarding the fusion-activating requirements of the CoV S protein. By combining cell-biological, infection, and fusion assays we demonstrated that murine hepatitis virus (MHV), a prototypic member of the CoV family, enters cells via clathrin-mediated endocytosis. Moreover, although MHV does not depend on a low pH for fusion, the virus was shown to rely on trafficking to lysosomes for proteolytic cleavage of its spike (S) protein and membrane fusion to occur. Based on these results we predicted and subsequently demonstrated that MERS- and feline CoV require cleavage by different proteases and escape the endo/lysosomal system from different compartments. In conclusion, we elucidated the MHV entry pathway in detail and demonstrate that a proteolytic cleavage site in the S protein of different CoVs is an essential determinant of the intracellular site of fusion.

INTRODUCTION

To achieve successful infection enveloped viruses need to fuse with a host cell membrane to deliver the viral genome into the host cell. Some viruses, such as herpes simplex virus, Sendai virus, and human immunodeficiency virus, appear to be capable of direct fusion at the plasma membrane after initial attachment [1-5]. However, the majority of enveloped viruses use endocytosis for uptake and transport prior to fusion. Since endocytic cargo may eventually end up in the destructive environment of the lysosome, environmental cues are crucial to trigger viral fusion at the right stage of trafficking. These triggers, which may include a decrease in pH, changes in redox environment, and proteolytic activity [6-8], induce conformational changes in the viral fusion proteins leading to the merger of viral and host membranes. Two well-studied viruses; influenza A virus (IAV) and vesicular stomatitis virus (VSV), are known to undergo fusion upon exposure to low pH [9-12]. Other enveloped viruses, such as respiratory syncytial virus (RSV) and Ebola virus, require proteolytic processing of their viral fusion proteins in the endosomal system for fusion to occur [13-16].

Coronaviruses (CoVs) are enveloped, plus-strand RNA viruses belonging to the family *Coronaviridae* in the order *Nidovirales*. They are capable of infecting a wide variety of mammalian and avian species. In most cases they cause respiratory and/or intestinal tract disease. Human coronaviruses (HCoVs) are known as major causes of the common cold (e.g. HCoV-229E and HCoV-OC43). However, the emergence of new HCoVs of zoonotic origin has shown the potential of CoVs to cause life-threatening disease in humans as was demonstrated during the 2002/2003 SARS-CoV epidemics and more recently for MERS-CoV in the Middle East [17,18]. The well-studied mouse hepatitis virus (MHV) is often used as a safe model to study CoV infections.

All CoV virions contain a canonical set of four structural proteins. The viral genomic RNA is encapsidated by the nucleocapsid protein (N) to form the helical nucleocapsid, which is surrounded by the lipoprotein envelope, containing membrane glycoprotein (M), the small envelope protein (E), as well as the spike glycoprotein (S) (reviewed in [19]). Trimers of the CoV S protein, a type I membrane protein belonging to the class I fusion proteins, form the peplomers that protrude from the virion surface [20]. The S protein can be divided into two functional subunits. The amino-terminal S1 subunit contains the receptor-binding domain; while the carboxy-terminal S2 subunit contains domains required for fusion, including the fusion peptide (FP), heptad repeat domains (HR) HR1 and HR2, and the transmembrane (TM) domain.

Various entry routes have been described as being used by different CoVs for infection of cells. Clathrin-dependent as well as clathrin- and caveolae-independent entry pathways have been reported for SARS-CoV [21,22]. Also feline infectious peritonitis virus (FIPV) was suggested to enter via a clathrin- and caveolae-independent endocytic route [23,24]. For the HCoV-229E a caveolae-dependent endocytic uptake has been suggested [25]. Although the ability of MHV S proteins to cause cell-cell fusion at a neutral pH was initially interpreted as an indication for fusion of virions at the cell surface, more recent studies indicate the requirement for clathrin-mediated endocytosis for entry of MHV [26-29]. However, while some studies report that MHV strain A59 is sensitive to lysosomotropic agents that affect endocytosis [26], this is not the case according to others [27].

Proteolytic cleavage of the CoV S proteins appears to be important for the induction of cell-cell fusion and/or virus entry into host cells. Different cleavage sites have been identified for different CoVs, the importance of which seems to differ for cell-cell and virus-cell fusion. Some CoV S proteins, including that of MHV strain A59, are cleaved at the S1/S2 boundary by furin(-like) proteases during transport of the newly assembled virions through the secretory pathway of the producer cell [30-33]. Inhibition of this S protein cleavage was shown to inhibit cell-cell fusion, but not to affect entry of MHV strain A59 into host cells [30,34,35]. MHV strain 2 contains an S protein that is not cleaved at the S1/S2 boundary. Interestingly, although MHV strains 2 and A59 were both reported to enter via clathrin-mediated endocytosis, entry of MHV 2 but not of MHV A59, was blocked by inhibitors of low-pH activated cathepsin proteases [27,36]. Inhibitors of cathepsin proteases have also been shown to inhibit entry of SARS-CoV and feline CoVs [23,37,38], while treatment of cell-bound virus particles with different proteases was shown to enhance virus entry and/or cell-cell fusion [27,34,39-45]. For SARS-CoV and infectious bronchitis virus (IBV), it appears that a proteolytic cleavage of the S protein at a more downstream position than the S1/S2 boundary upon receptor binding is of importance for cell entry [40,43,46-49].

4

In the present study we performed a detailed investigation of the entry of different CoVs. Using siRNA gene silencing, we found that the prototypic coronavirus MHV strain A59 (further referred to as MHV) requires proteins known to be important for late endosomal maturation and endosome-lysosome fusion for efficient infection of cells. By using recombinant MHVs expressing reporter genes as well as by applying a novel, replication-independent fusion assay we confirmed the importance of clathrin-mediated endocytosis and demonstrated that trafficking of MHV virions to lysosomal compartments and processing of the S protein by lysosomal proteases was required for productive entry to occur. Our results indicate that a cleavage site in the S protein of CoVs immediately upstream of the FP determines the site of fusion. In agreement herewith FIPV, which requires processing by lysosomal proteases, was also shown to depend on trafficking to lysosomes. In contrast, MERS-CoV, which contains a minimal furin-cleavage site consensus sequence in the S protein immediately upstream of the FP, was negatively affected by inhibition of furin, but not of lysosomal proteases.

RESULTS

RNAi mediated gene silencing identifies endocytosis-associated proteins to be important in MHV infection

In an automated, high-throughput RNAi screen [50] targeting the druggable genome (approximately 7000 genes) a number of proteins associated with endocytosis were found to be required for efficient infection of HeLa cells with GFP-expressing MHV. To validate these findings these proteins were subjected to a follow-up analysis using siRNA-mediated gene silencing with oligonucleotides from a different supplier than the one used for the initial RNAi screen (Fig. 1A). The follow-up analysis included ACTR2 and ACTR3, two major constituents of the Arp2/3 complex which are important for the formation of actin branches and cell surface protrusions, as well as for the motility of several pathogens inside host cells (reviewed in [51,52]). Also selected were the RAS-related GTP-binding protein family members, RAB7A and RAB7B, which have been shown to be involved in endosomal maturation (reviewed in [53]). RAB7 interacts amongst others with members of the homotypic fusion and vacuole protein sorting (HOPS) tethering complex, involved in late endosome to lysosome maturation. The HOPS subunit VPS39 (reviewed in [54]) was also found to be a strong hit in the siRNA screen and therefore selected. Other proteins included SNX1, involved in retrograde transport of cargo between endosomes and the *trans*-Golgi network (reviewed in [55]), VCL, *inter alia* involved in connecting the Arp2/3 complex with integrins during actin polymerization (reviewed in [56]), and the Ser/Thr-protein kinase PAK1, which is activated by the Rho/Rac/Cdc42 family and is implicated in a variety of downstream effects including modulation of the actin cytoskeleton (reviewed in [57]).

Transfection of HeLa cells carrying the receptor for MHV (HeLa-mCC1a cells) with different siRNAs was followed by an infection with GFP-expressing MHV (MHV-EGFPM) at low multiplicity of infection (MOI), resulting in approximately 10-15% infected cells under control conditions. After 8h of infection cells were collected and GFP expression by the replication of MHV was analyzed by fluorescence-activated cell sorting (FACS). As controls siRNAs silencing GFP and negative-control siRNAs were used. A hit from the screen was considered as confirmed when transfection with at least two out three independent siRNAs resulted in significant reduction in MHV-driven GFP expression relative to the negative-control siRNAs. siRNA-mediated gene silencing of ACTR2 and ACTR3 resulted in reduced infections for all three siRNAs, indicating that actin branching is important for MHV infection (Figure 1A, dark orange). Also the importance of the RAB7A, RAB7B and VPS39 proteins, involved in late-endosome and late-endosome to lysosome maturation, for MHV infection could be confirmed (Figure 1A, turquoise and light green). The importance of SNX1, VCL and PAK1 for infection of HeLa cells with MHV could not be confirmed (Figure 1A, grey). The latter three genes were not studied any further. To validate our transfection protocol and confirm the efficacies of the siRNAs at the mRNA level, quantitative RT-PCR analysis was performed. All siRNAs used reduced the corresponding mRNA levels with 75-95% (Figure 1B). siRNAs targeting RAB7A were shown to inhibit the expression of a RAB7a-fusion protein (Figure S1 in Text S1).

To confirm and extend our understanding of the role of endocytosis in MHV entry we subsequently selected a number of proteins known to be involved in either caveolae-

or clathrin-mediated endocytosis, actin- or microtubule-mediated transport, as well as proteins associated with endosomal vesicles and endosomal maturation, to be screened using the siRNA silencing-approach described above. Again, proteins were considered important for infection with MHV when transfection with at least two out three independent siRNAs resulted in significant reduction in MHV-driven GFP expression relative to the negative-control siRNAs. siRNA-mediated downregulation of proteins involved in caveolae-mediated endocytosis revealed that CAV2, but not the other proteins analyzed are important for infection with MHV (Figure 1C, light blue). Downregulation of most proteins associated with clathrin-mediated endocytosis inhibited MHV infection, including DNM1, DNM2, CLTC, and DAB2. siRNA-mediated silencing of EPS15 or AAK1, accessory factors of clathrin-mediated endocytosis, did not affect MHV replication (Figure 1C, dark blue). Silencing of early endosome-associated genes (EEA1, RAB5A, RAB5B, and RAB5C; Figure 1C, cerulean) each decreased replication-mediated GFP expression. While downregulation of MYO6, involved in actin-based motility, did not influence MHV infection (Figure 1C, dark orange), our results indicate that the microtubule-associated motility proteins DYNC1H1 and DYNC2H1 are important for infection with MHV (Figure 1C, orange). Silencing of NSF, required for transport from early to late endosomes [58], or of the HOPS subunits VPS11 and VPS41, which are involved in late endosome to lysosome maturation (Reviewed in [54]), all resulted in severely reduced MHV infection (Figure 1C, turquoise and light green, respectively).

Endocytosis-affecting agents indicate clathrin-mediated endocytosis and endosome maturation to be important in MHV infection

To further explore the endocytic route and factors involved in MHV infection we determined the effect of inhibitors on MHV infection. HeLa-mCC1a cells were treated with endocytosis-affecting agents for 30min and then infected with luciferase-expressing MHV (MHV-EFLM;[59]) in presence of the inhibitors, after which the inhibitors were kept present until cell lysis. When cells were inoculated with MHV-EFLM in the absence of inhibitors, the inhibitors were added to the cells at 2 h post infection (hpi) to assess effects of inhibitors on post-entry steps. At 7hpi cells were lysed and firefly luciferase expression levels were determined.

Infection in the presence of the solvents dimethyl sulfoxide (DMSO) and methanol (MeOH), as well as the known inhibitors of MHV RNA synthesis Brefeldin A (BrefA, inhibitor of GBF1) [60] and MG132 (proteasome inhibitor, probably also affects MHV entry; [61]) were included as controls. MHV infection was not affected by addition of the solvents, whereas both MG132 and BrefA severely decreased luciferase expression regardless of the time of addition. Inhibition of endosome maturation with ammonium chloride (NH_4Cl), Bafilomycin A1 (BafA1), or Chloroquine (Chloq) severely diminished luciferase expression when the inhibitors were added prior to infection. Much smaller effects were observed when these drugs were added at 2hpi, indicating that the inhibitors mainly affect MHV entry (Figure 2, deep sky blue). Similar effects were observed with known inhibitors of clathrin-mediated endocytosis; Chlorpromazine (Chlopro), Monensin (Mon), Dynasore, and Dyngo-4A (Dyngo). All these compounds strongly decreased MHV replication-mediated luciferase expression when added early but not when added at 2 hpi (Figure 2, dark blue). The actin- and macropinocytosis-affecting drug EIPA, which inhibits the Na^+/H^+ exchanger NHE1, led to reduced luciferase expression both when added prior to and after entry of MHV at 2hpi. Actin cytoskeleton altering

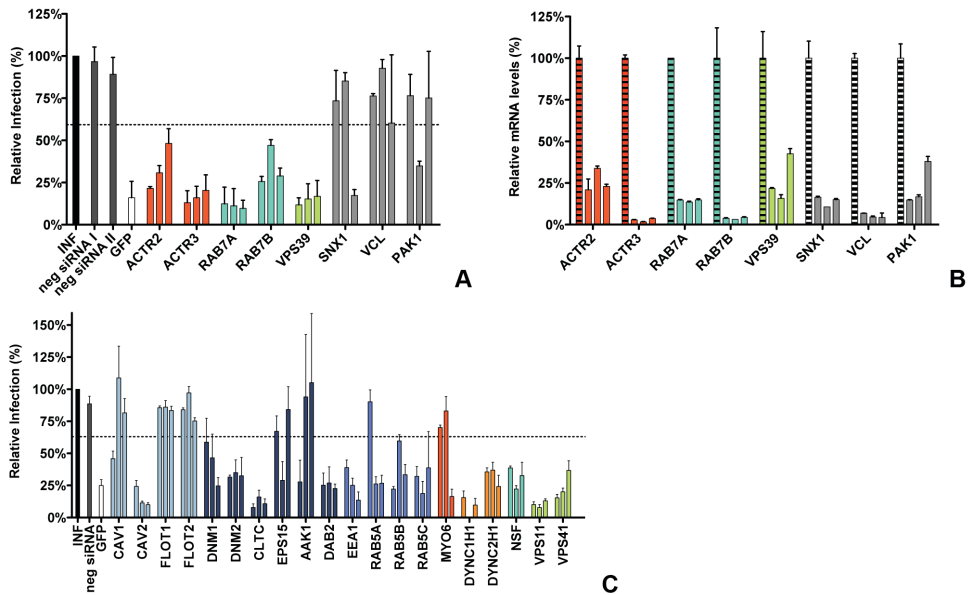


Figure 1: RNAi-mediated downregulation of endocytosis-associated proteins affects MHV infection. A) Confirmation of endocytosis-associated hits from druggable genome-wide siRNA screen. Gene silencing was performed using individual transfection of three different siRNAs per gene in HeLa-mCC1a cells. Cells were infected with MHV-EGFP at MOI=0.5 for 8h and analyzed by FACS for cell viability and virus replication. The effect of downregulation of expression of on MHV infection was studied for the actin cytoskeleton-associated proteins ACTR2 and ACTR3 (orange), late endosomal proteins RAB7A and RAB7B (turquoise), HOPS complex subunit VPS39 (light green), ER/Golgi secretion-associated protein SNX1, Integrin/Actin-associated protein VCL, and Serine/Threonine-protein kinase PAK1 (grey). Error bars represent SEM, n=4. B) Confirmation of siRNA-mediated reduction in mRNA levels. mRNA levels at 72h post transfection were measured by qRT-PCR in comparison to non-transfected cells. Error bars represent SEM, n=3*3. C) The effect of the RNAi-mediated downregulation of an extended set of endocytosis-associated proteins on MHV infection. Infection of MHV-EGFP was analyzed after downregulation of proteins associated with caveolae-mediated endocytosis (light blue), clathrin-mediated endocytosis (dark blue), early endosomes (cerulean), actin cytoskeleton (dark orange), microtubule cytoskeleton (orange), late endosomes (turquoise), and late endosome-to-lysosome trafficking (light green) as described above. Error bars represent SEM, n=3. A, C) Dotted lines show the lower 95% confidence interval of the negative siRNA controls.

drugs Latrunculin A (LatA), Jasp, Cytochalasin B (CytoB), and Cytochalasin D (CytoD), or the inducer of microtubule depolymerization Nocodazole (Noc) only decreased MHV infection when added early, indicating a role for the actin and microtubule cytoskeleton in entry but not RNA replication (Figure 2, dark orange and orange). Likewise U18666A, a cholesterol transport-affecting agent, which also prevents maturation of late endosomes [62], had a strong inhibitory effect on MHV infection when added early (Figure 2, turquoise). Collectively, these results indicate an important role for clathrin-mediated uptake and for endosome- and endosome-to-lysosome maturation for MHV infection.

Clathrin-mediated endocytosis and late endosomal factors are required for MHV fusion

The time-of-addition experiments with the different inhibitors indicated that particularly the entry step of the MHV infection cycle is negatively affected by perturbation of clathrin-mediated endocytosis or of endosome maturation. However, assays based on reporter

gene expression driven by virus replication do not allow discrimination between virus entry and RNA replication when analyzing siRNAs or agents that also affect RNA synthesis. To unequivocally demonstrate the importance of clathrin-mediated endocytosis and endosome maturation for MHV entry, we therefore made use of a fusion assay we recently developed [63]. The assay is based on minimal complementation of defective β -galactosidase (β -galactosidase Δ M15) with the short α -peptide [64]. MHV- α N, a recombinant MHV containing an N protein tagged with the α -peptide (α N), is used to infect Δ M15 fragment expressing target cells. Upon fusion of the virion with a host cell membrane α N is released into the cytoplasm resulting in complementation of the defective β -galactosidase thereby reconstituting a functional enzyme. Conversion of the non-fluorescent substrate fluorescein-di- β -D-galactopyranoside (FDG) by β -galactosidase into green fluorophores fluorescein (FIC) can be measured by FACS or fluorescence microscopy (Figure S2 in Text S1).

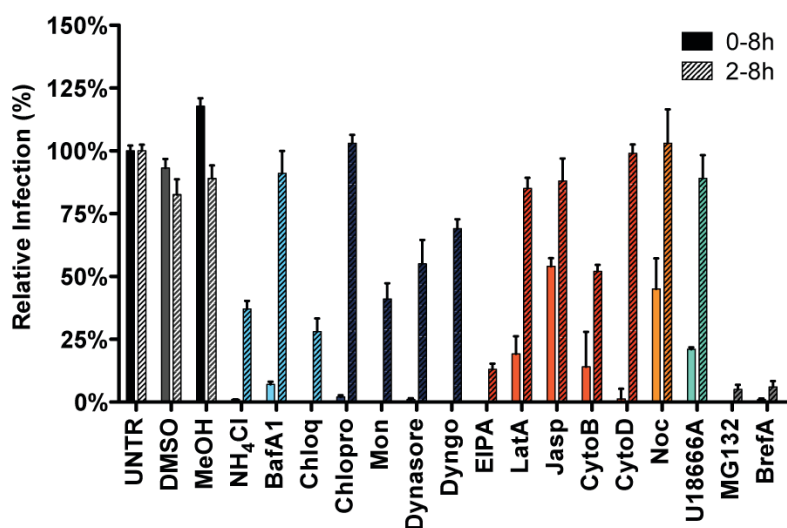


Figure 2: Endocytosis affecting agents indicate clathrin-mediated endocytosis and endosome maturation to be important in MHV infection. HeLa-mCC1a cells, inoculated with MHV-EGFP at MOI=0.5, were treated with the different inhibitors from 30 min prior to 8h post inoculation (0-8h) or from 2-8 h post inoculation (2-8h; hatched bars): ammonium chloride (NH₄Cl), Bafilomycin A1 (BafA1), Chloroquine (Chloq), Chlorpromazine (Chlopro), Monensin (Mon), Dynasore, Dyngo-4A, EIPA, Latrunculin A (LatA), Jasplakinolide (Jasp), Cytochalasin B (CytoB), Cytochalasin D (DytoD), Nocodazole (Noc), MG132, Brefeldin A (BrefA), as well as solvents dimethyl sulfoxide (DMSO) and methanol (MeOH). Infection was determined by FACS and displayed relative to the infection level observed in mock-treated cells (UNTR). Error bars represent SEM, n=3.

To analyze the effect of RNAi-mediated gene silencing on fusion, HeLa cells expressing the MHV receptor and the Δ M15 fragment (HeLa-mCC1a- Δ M15 cells) were transfected with individual siRNAs and inoculated with MHV- α N at 72h post transfection. Before infection cells were pre-loaded with FDG by hypotonic shock. After 100min incubation of cells with virus at 37°C, cells were collected and the amount of FIC generated as a results of enzyme complementation analyzed by FACS. The fusion assay showed that silencing of neither CAV1 nor CAV2 affected MHV fusion (Figure 3A, light blue), even though reduction of CAV2 was shown to affect MHV infection (Figure 1C). However, downregulation of clathrin-mediated endocytosis associated proteins DNM2 and CLTC lead to strongly decreased fusion, as did

the lack of early endosome-associated factors RAB5B and RAB5C (Figure 3A, dark blue and cerulean, respectively). Fusion was also affected by RNAi-mediated reduction of actin cytoskeleton-associated proteins ACTR2 and ACTR3 (Figure 3A, dark orange), proteins known to be involved in late endosome (RAB7A, RAB7B) and late endosome-to-lysosome maturation (VPS11, VPS39, and VPS41) (Figure 3A, turquoise and light green).

The importance of clathrin-mediated endocytosis and endosome maturation for MHV fusion was confirmed by analysis of endocytosis-affecting agents using the fusion assay. After pre-loading with FDG, cells were pre-treated with the inhibitors for 30min at 37°C, after which cells were inoculated with MHV- α N in the presence of the agents, and analyzed by FACS as described above. As controls we included protein synthesis inhibitor cycloheximide (CHX), MHV fusion inhibitor peptide HR2 (HR2, [20]), MG132 and BrefA. Fusion of MHV was not affected by the solvents or CHX, the latter confirming that this assay is independent of RNA replication and protein synthesis. MHV fusion was barely affected by replication inhibitor BrefA, whereas MG132 had a clear negative effect, in agreement with the conclusion drawn previously that MG132 inhibits entry of MHV as well as RNA synthesis [61]. Inhibition of endosomal maturation by NH_4Cl , BafA1 and Chloq (Figure 3B, deep sky blue) or of clathrin-mediated endocytosis by Chlopro, Mon, and Dynasore (Figure 3B, dark blue) severely inhibited MHV fusion. Disturbance of the actin cytoskeleton by EIPA or by Lata, CytoB, or CytoD reduced fusion by 75-80% (Figure 3B, dark orange), while interference with microtubule polymerization by Noc had a smaller effect (Figure 3B, orange). Late endosomal maturation arrest caused by U18666A reduced fusion to approximately 10% (Figure 3B, turquoise). In conclusion, the replication-independent fusion assay confirmed the importance of clathrin-mediated endocytosis and of endosome maturation for entry of MHV. The data indicate that late endosome-to-lysosome maturation is required for efficient entry and fusion.

Live-cell microscopy confirms co-localization, co-tracking and fusion of MHV in endosomal compartments

To confirm the importance of endocytic uptake and the association of MHV with endosomal compartments we performed live-cell confocal microscopy. To this end, sucrose density gradient-purified MHV virus was covalently labeled with the low-pH resistant dye DyLight 488 (MHV-DL488). HeLa-mCC1a cells were transfected with plasmids to express monomeric RFP (mRFP) fusion proteins of RAB5, RAB7, or LAMP1. At 24h post transfection, MHV-DL488 was bound to cells at 4°C for 90 min. Inoculation medium was replaced by warm medium containing trypan blue, which immediately shifts the emission spectrum of surface bound particles rendering them undetectable in the 505-530nm channel unless they get endocytosed [65]. Cells were imaged using a spinning-disc confocal microscope acquiring z-stacks in 30s intervals over 10min time frames from 10-70min post warming. Only low-level RFP fusion protein expressing cells were selected for analysis. Interestingly, MHV particles newly appeared even 60min post warming, in agreement with the notion that MHV enters in an unsynchronized manner (unpublished results). Co-localization and co-trafficking of viruses with endosomal compartments was assessed by detecting virus particles based on size and intensity (green channel) and by measuring the underlying intensity in the red channel (endosomal vesicles). MHV virions were found to co-localize with all three endosomal compartments (Fig. 4A). Whereas newly entering/appearing particles were always co-localizing with RAB5 molecules, they only associated with RAB7 and LAMP1 containing vesicles

at later time points.

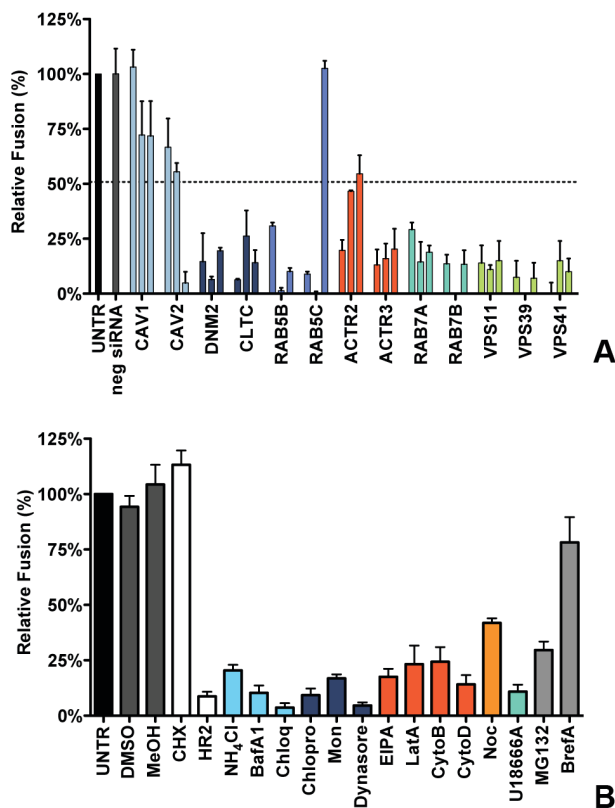


Figure 3: Clathrin-mediated endocytosis and late endosome-to-lysosome trafficking is required for MHV fusion. A) Fusion assay upon siRNA-mediated gene silencing. Three different siRNAs per gene were transfected individually into HeLa-mCC1a-ΔM15. 72h post transfection, cells were pre-loaded with FDG by hypotonic shock. MHV-αN was allowed to bind to the cells on ice at MOI=20 for 90min. 100min post warming to 37°C, cells were collected and analyzed by FACS. Fusion was determined relative to the number of FIC-positive cells observed upon mock treatment of infected cells (UNTR). Error bars represent SEM, n=3. B) Fusion of MHV upon treatment of cells with different inhibitors was studied as in A. Cells were pretreated with ammonium chloride (NH₄Cl), Bafilomycin A1 (BafA1), Chloroquine (Chloq), Chlorpromazine (Chlopro), Monensin (Mon), Dynasore, Dyngo-4A, EIPA, Latrunculin A, (LatA), Jasplakinolide (Jasp), Cytochalasin B (CytoB), Cytochalasin D (DytoD), Nocodazole (Noc), U18666A, MG132, Brefelding A (BrefA), as well as the solvents dimethyl sulfoxide (DMSO) and methanol (MeOH), protein synthesis inhibitor cyclohexamide (CHX), and MHV fusion inhibitor HR2 peptide (HR2) for 30min at 37°C. The inhibitors were kept present during binding of MHV-αN to cells and during warming to 37°C cells for 100 min. Fusion was determined relative to the number of FIC-positive cells after mock treatment (UNTR). Error bars represent SEM, n=3.

To assess the association of MHV with endosomal vesicles during the entry process more extensively, we manually tracked the virus particles in the green channel and independently tracked the endosomal vesicles in the red channel in x/y and z-direction. A virion was categorized as associating with a certain endosomal marker only if this co-localization was observed over at least four sequential 30s interval images. When the initial co-localization was lost, but the virion did not disappear, this virion was classified as associating/dissociating. Complete disappearance of a virus particle (including in other z-stacks) while immediately

previously co-localizing with an endosomal marker was categorized as a fusion event (Figures S3 and S4 in Text S1). When a viral particle co-localized with endosomal compartments but did neither dissociate nor fade during the 10min acquisition period it was classified as non-fusing. With this quantification method we analyzed 75-100 virions in total for each of the endosomal compartment types studied. The fraction of virions not fusing during the acquisition period was consistently found to be at around 10-15%. We observed that all of the entering MHV particles initially co-localized with RAB5-positive early endosomal vesicles and that most virions dissociated (were no longer co-localized) after 4-6min. Notably, it appeared that in these events the RAB5 marker faded rather than moved away. Only a very small percentage of virions were categorized as fusing while in early endosomes. The number of fusion events was much higher for virions co-localizing with RAB7 or LAMP1 (Figure 4B), indicating that most virions fuse in late endosomes or lysosomes.

MHV infection depends on endosomal maturation

Our results so far indicate that most virions enter cells after having accessed late endosomes/lysosomes. We hypothesized that these compartments provide the environmental cues required for productive virus-cell fusion. In order to analyze to what extent the low pH in the endosomal system is required for entry of MHV, we analyzed the inhibition of MHV entry at different concentrations of BafA1. While high concentrations of BafA1 (as used for the results shown in Fig. 2 and 3) affect endosomal maturation, at low concentrations this inhibitor of vacuolar-type H⁺-ATPase only elevates the pH of endosomal compartments but does not affect endosomal trafficking per se [66]. We made use of that property and tested the sensitivity of MHV to BafA1 side by side with the control viruses VSV and IAV. VSV has been described to fuse at pH 6.2 in early and/or late endosomes [9,11,12,67-69], while IAV has been shown to fuse in late endosomes at an even lower pH [9,10,70]. HeLa or HeLa-mCC1a cells were pretreated with increasing concentrations of BafA1 for 30min prior to infection with reporter gene expressing viruses: VSV (VSVΔG/FLuc-G⁺;[71,72]), IAV (IAV-RLuc; [73]), or MHV (MHV-EFLM). Luciferase expression levels indicated that infection of cells with VSV and IAV is much more affected by BafA1, with an IC₅₀ values of 0.80 and 0.63 nM, respectively, compared to MHV, which displays a three to four fold higher IC₅₀ of 2.34 nM (Figure 5A).

Our results thus indicate that MHV is much less affected by perturbation of the endosomal pH than VSV and IAV. Nevertheless RNAi-mediated silencing of HOPS subunits and treatment of cells with U1866A indicates that late endosome-to-lysosome maturation is required for efficient entry. To confirm and extend these observations, we made use of haploid HAP1 cells lacking a functional HOPS complex resulting from lentiviral-mediated knockout of the VPS33A subunit (H1-ΔV33 cells; [74]). Both HAP1 cells and H1-ΔV33 cells were modified to stably express the MHV receptor. As a control, the H1-ΔV33 cells were in addition stably transfected with FLAG-tagged VPS33A (H1-ΔV33-*fV33*). The different cells expressed similar levels of the MHV receptor as determined by FACS analysis (Figure S5 in Text S1). Expression of FLAG-VPS33A was confirmed by Western blot (Figure S6 in Text S1). Functional reconstitution was confirmed by confocal fluorescence imaging of lysosome localization (Figure S7 in Text S1). While in the knockout cells the lysosomes were clustered, the lysosomes were dispersed again throughout the cytoplasm in the FLAG-VPS33A re-transfected cells, as observed in the HAP1 parental cells. The haploid cells were infected with luciferase reporter gene-expressing MHV, VSV, or IAV at low MOI. Cells were lysed at 7 (MHV and VSV) or

16 (IAV) hpi and luciferase expression levels were determined. The lack of a functional HOPS complex had no effect on VSV and IAV infection; however, MHV infection was strongly reduced in the knockout, but not in the re-transfected cells (Figure 5B). These observations confirm the conclusion that late endosome-to-lysosome maturation is required for efficient entry of MHV, a characteristic that is not shared with the pH-sensitive VSV and IAV.

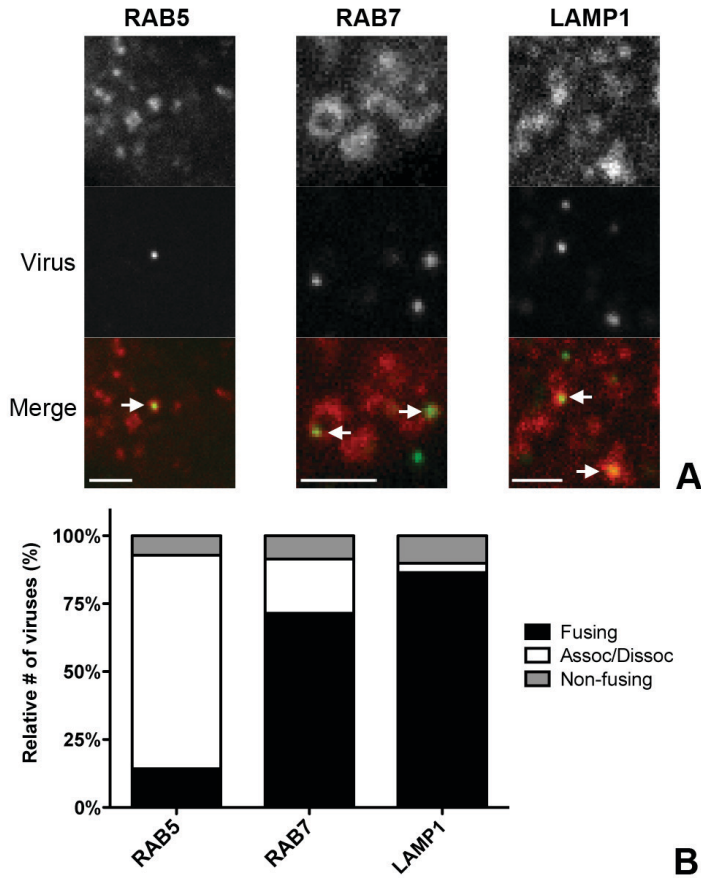


Figure 4: Live-cell microscopy demonstrates co-localization and co-tracking of MHV with endosomal vesicles and fusion of MHV in these vesicles. HeLa-mCC1a cells transfected with plasmids encoding RAB5-mRFP, RAB7-mRFP, or dsRed-LAMP1 were inoculated with DyLight 488-labeled MHV. Live cell imaging was performed to track internalized particles. A) Examples of MHV particles co-localizing with RAB5-, RAB7-, and LAMP1-positive endosomal vesicles. Size bars indicate 0.2 μ m B) Virus particles that could be tracked were classified as 106fusing (Fusing) 106as-associating/dissociating (Assoc/Dissoc), or 106non-fusing (Non-fusing) as described in the Materials and Methods section.

Inhibition of lysosomal proteases prevents MHV fusion

Considering that MHV was much less affected by perturbation of the endosomal pH than IAV and VSV while it requires trafficking to lysosomes for efficient entry, we hypothesized that entry might depend on cleavage of a viral protein by lysosomal proteases. Hence we analyzed the extent to which different protease inhibitors could inhibit MHV entry. Thus,

HeLa-mCC1a- Δ M15 cells were pretreated for 30min with the different inhibitors, after which the cells were inoculated with MHV- α N in inhibitor-containing medium. Cells were collected, loaded with FDG, and FDG conversion to FIC by complementation of β -galactosidase upon viral fusion was assessed by FACS. Our results indicate that most protease inhibitors tested (Fig. 6) hardly inhibited fusion of MHV, if at all. Exceptions were AEBSE, which has been shown to cause aggregation of early endosomal vesicles [75], and a pan-lysosomal protease inhibitor (CPI; cystatin-pepstatin inhibitor) capable of inhibiting the three major protease family members found in lysosomes. Thus, by using CPI we measured the combined effects of an endosomal papain-like cysteine protease inhibitor (PLCP), an aspartyl protease inhibitor, and an asparagine endopeptidase inhibitor (AEP) [76]. From these results we conclude that inhibition of a broad range of endosomal proteases efficiently blocks fusion of MHV, indicating that efficient entry requires the activity of lysosomal proteases.

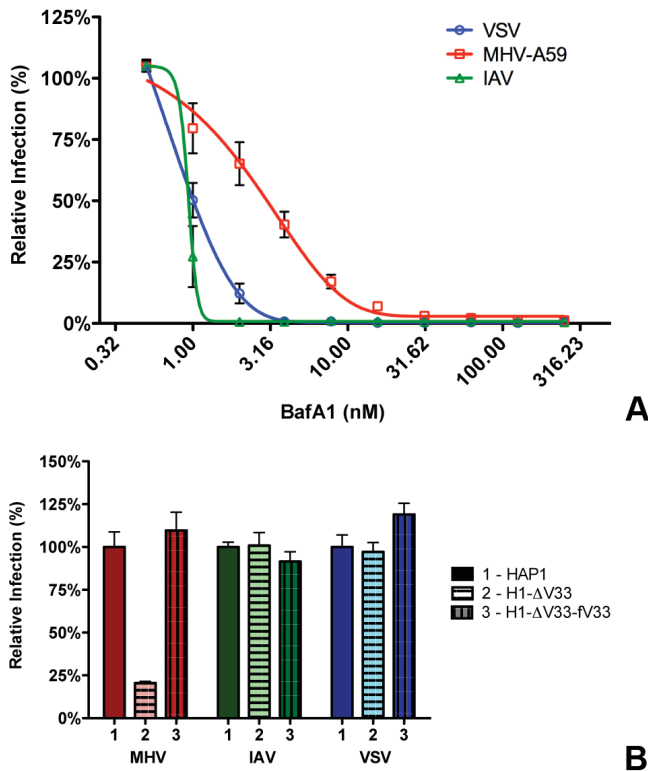


Figure 5: MHV infection depends on endosomal maturation. A) HeLa-mCC1a cells were pretreated with increasing concentrations of Bafilomycin A1 (BafA1) for 30min and subsequently infected with luciferase expressing MHV, VSV, or IAV in the presence of BafA1. Infection levels were determined by assaying the luciferase activity in cell lysates relative to lysates of infected cells that had been mock treated. Error bars represent SEM, $n=3*3$. B) Haploid cells (HAP1), haploid cells lacking VPS33A (H1- Δ V33) or VPS33A-lacking haploid cells retransfected with FLAG-tagged VPS33A (H1- Δ V33-fV33) were infected with luciferase expressing MHV, VSV, or IAV. Cells were lysed at 7h (MHV and VSV) or 16h post infection. Infection is displayed relative to virus-driven luciferase expression levels in HAP1 cells. Error bars represent SEM, $n=3*3$.

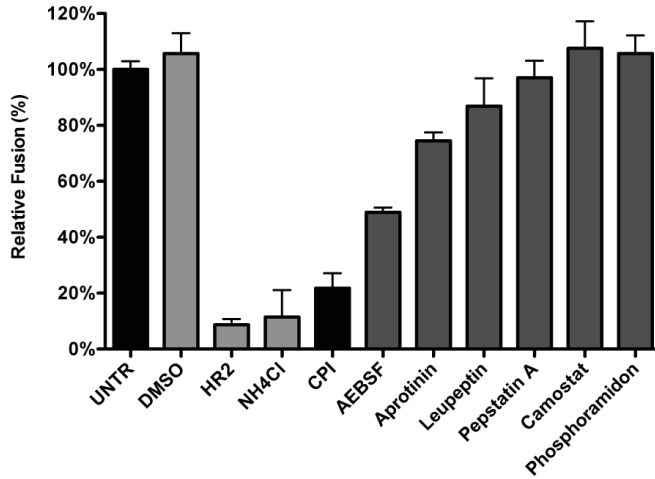


Figure 6: Inhibition of lysosomal proteases prevents MHV fusion. The MHV fusion assay was performed on HeLa-mCC1a-ΔM15 cells as described in the legend to Figure 3, in the presence of the protease inhibitors CPI, AEBSEF, Aprotinin, Leupeptin, Pepstatin A, Camostat, and Phosphoramidon. As controls, cells were treated with solvent DMSO, MHV fusion inhibitor HR2 peptide (HR2), and lysosomotropic agent ammonium chloride (NH₄Cl). Fusion was determined relative to the number of FIC-positive cells after mock treatment (UNTR). Error bars represent SEM, n=3.

Introduction of a furin cleavage site immediately upstream of the fusion peptide renders MHV independent of lysosomal proteases

In general, class I fusion proteins require cleavage just upstream of the FP to render them fusion competent [20,38,77]. However, while the S protein of MHV is cleaved at the S1/S2 boundary (Fig. 7A), no protease cleavage site has been identified close to the fusion peptide. In view of the inhibition of MHV entry by the pan-lysosomal protease inhibitor CPI and in analogy to other class I fusion proteins, we hypothesized that an additional cleavage in the S protein, immediately upstream of the FP, is necessary to induce fusion. To test this hypothesis, we introduced an optimal furin cleavage site (FCS) by substituting three amino acids by Arg (AIRGR → RRRRR) immediately upstream of a highly conserved Arg (indicated in bold) that occurs just N-terminal of the FP. Recombinant MHV carrying this FCS in its S2 subunit was designated MHV-S2'FCS. (Figure 7A). Western blot analysis of the S protein of a purified stock of this virus using an antibody recognizing the S2 subunit showed no evidence of cleavage at the newly introduced FCS (S2' site). Apparently, cleavage at this position does not occur during virus production (Figure S8 in Text S1). MHV carrying wild type or mutant S proteins displayed similar growth kinetics (Figure S9 A and B in Text S1). Next we analyzed whether the introduced FCS affected the sensitivity of the recombinant MHV to CPI, which does not exhibit inhibitory activity towards furin. Thus, HeLa-mCC1a cells were pretreated with CPI for 30min and subsequently infected with wild type S (MHV-EFLM) or mutant S (MHV-S2'FCS) containing viruses expressing luciferase reporter genes in the presence of the protease inhibitor. At 7 hpi the cells were lysed and viral-replication dependent luciferase expression levels were determined. Introduction of the FCS resulted in the recombinant virus being no longer sensitive to inhibition by lysosomal proteases (Figure 7B), probably because

the S protein is now cleaved by furin in an endocytic compartment.

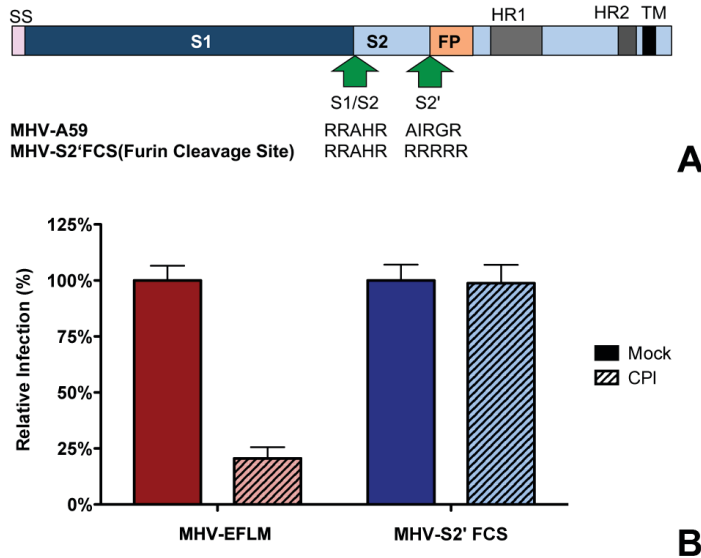


Figure 7: Introduction of a furin cleavage site just upstream of the fusion peptide renders MHV independent of lysosomal proteases. A) Schematic representation of the MHV spike protein. The MHV S proteins are partially processed by furin at the S1/S2 boundary (S1/S2) as indicated by the arrow. The furin cleavage site sequence at this position (RRAHR) is shown. The signal sequence (SS) at the amino-terminal end of the S1 subunit and the approximate positions of the fusion peptide (FP), heptad repeat regions 1 and 2 (HR1 and HR2) and the transmembrane domain (TM) in the S2 subunit are indicated. MHV-S2'FCS virus contains an optimal furin cleavage site (RRRRR) immediately upstream of the FP (S2', indicated by the arrow). B) Effect of pan-lysosomal protease inhibitor (CPI) on MHV and MHV-S2'FCS infection. HeLa-mCC1a cells were pretreated with CPI for 30min and inoculated at MOI=0.2 with luciferase expression cassette containing MHV-EFLM or MHV-S2'FCS in the presence of CPI, after which incubations were continued in the presence of CPI until 7hpi. Infection levels were determined by measuring the luciferase activity in cell lysates relative to mock-treated cells. Error bars represent SEM, n=3*3.

Furin inhibitor renders MHV-S2'FCS sensitive to endosomal maturation and decreases infection

To confirm that MHV-S2'FCS is no longer dependent on cleavage by lysosomal proteases, and to study its presumed dependence on furin cleavage for entry, we analyzed the ability of MHV-S2'FCS to infect the haploid cells that lack VPS33A - and thus the functional HOPS complex required for late endosome-to-lysosome maturation - in the absence or presence of furin inhibitor (FI). After pretreatment of MHV receptor-expressing HAP1, H1-ΔV33, and H1-ΔV33-fV33A cells with furin inhibitor (FI) or mock treatment, cells were inoculated with MHV-EFLM or mutant virus MHV-S2'FCS in presence or absence of FI. At 7 hpi the cells were lysed and viral-replication dependent luciferase expression levels were determined. In agreement with previous results (Fig. 5), infection with MHV carrying a wild type S was severely reduced in cells lacking a functional HOPS complex and addition of the FI did not alter this effect (Figure 8, red bars). In contrast, infection with MHV-S2'FCS was not decreased by the lack of a functional HOPS complex. However, FI treatment had a clearly negative effect on this virus, which was much more dramatic in the absence of a functional HOPS complex in H1-ΔV33 cells (Figure 8, blue). In conclusion, MHV-S2'FCS lost the requirement for a

functional HOPS complex in parallel with this virus becoming insensitive to the pan-lysosomal protease inhibitor CPI. In contrast to the virus with the wild type S, the mutant virus became sensitive to inhibition of furin cleavage.

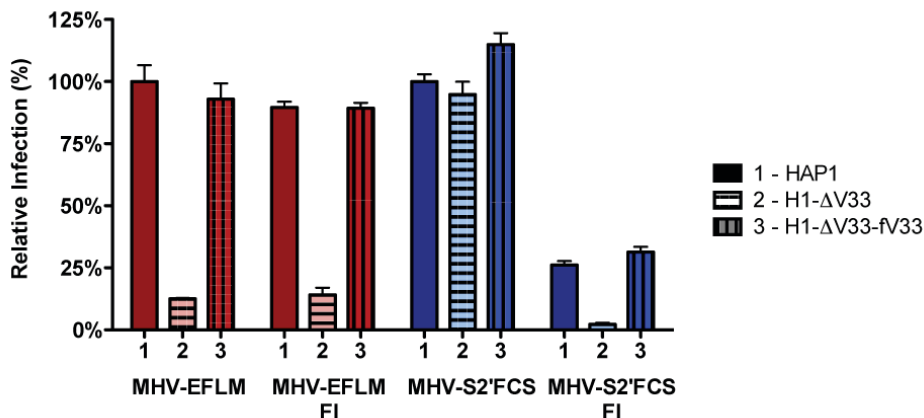


Figure 8: Furin inhibitor reduces infection with MHV-S2'FCS and renders the virus sensitive to endosomal maturation. Haploid HAP1 cells (HAP1), haploid cells lacking VPS33A (H1-ΔV33) or VPS33A-lacking haploid cells retransfected with FLAG-tagged VLP33A (H1-ΔV33-fv33) were infected (MOI=0.2) with MHV-EFLM (MHV-wt) or MHV-S2'FCS for 7h. Where indicated, cells were treated with furin inhibitor (FI). Infection levels were determined by measuring the luciferase activity in cell lysates relative to mock-treated cells. Error bars represent SEM, n=3*3.

MHV-S2'FCS fuses in early endosomes

To explore MHV-S2'FCS entry requirements further we assessed the effect of RNAi-mediated downregulation of early and late endosome and HOPS complex associated genes. Therefore, HeLa-mCC1a-DM15 cells were transfected with each of three different siRNAs per gene for 72h, after which they were infected with wild type (MHV-EFLM) or mutant (MHV-S2'FCS) S protein containing MHV. At 7 hpi the cells were lysed and viral-replication dependent luciferase expression levels were determined. As found previously (Fig. 1), infection with wild type S protein carrying MHV was reduced after gene silencing of RAB5, RAB7, VPS11, and VPS41 (Figure 9, red bars). On the other hand, infection with MHV-S2'FCS was significantly diminished by downregulation of the early endosomal proteins RAB5B and RAB5C, but not of the late endosomal proteins RAB7A and RAB7B or the HOPS complex components VPS11 and VPS41 (Figure 9, blue bars). Consistently, infections with MHV carrying wild type or mutant S protein were equally blocked by inhibitors of clathrin-mediated endocytosis whereas the virus with the mutant S (MHV-S2'FCS) was much less sensitive to inhibitors of endosomal maturation, including BafA1, or to perturbants of the actin cytoskeleton (Figure S10 in Text S1). From these results we conclude that introduction of a FCS immediately upstream of the FP abolishes the requirement for trafficking of virions to lysosomes and for processing by lysosomal proteases. The resulting virus, which still depends on clathrin-mediated endocytosis, now requires furin cleavage for efficient entry, the enzymes for which occur earlier in the endocytic pathway [78].

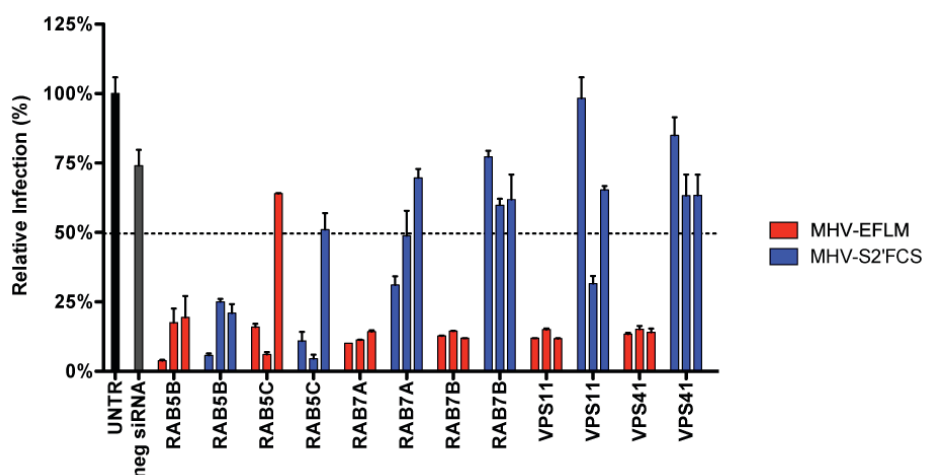


Figure 9: MHV-S2'FCS fuses in early endosomes. siRNA-mediated gene silencing was performed as described in the legend to Figure 1. At 72h post transfection, HeLa-mCC1a were inoculated with MHV-EFLM or MHV-S2'FCS at MOI=0.2 and incubated until 7hpi. Infection levels were determined by measuring the luciferase activity in cell lysates relative to mock-treated cells. Dotted line shows the lower 95% confidence interval of the negative siRNA controls. Error bars represent SEM, $n=3*3$.

Entry of other CoVs

Our results indicate that the protease cleavage site upstream of the spike protein FP is an important determinant of the intracellular site of fusion. To gain more insight into the putative protease cleavage sites in the corresponding region of the S proteins of other CoVs, we analyzed the sequence of this region in several alpha, beta and gamma coronaviruses by performing ClustalW sequence alignment. The fusion peptide sequence was found to be highly conserved amongst the different coronaviruses. Also an Arginine residue immediately upstream of the predicted fusion peptide is highly conserved with the exception of FIPV (serotype II). Interestingly, MERS-CoV and IBV-Beaudette contain a minimal furin cleavage site Arg-X-X-Arg just upstream of the fusion peptide (Figure 10A). In analogy with the results obtained with FCS-mutant MHV, we predicted that FIPV and MERS-CoV would differ in their protease inhibitor sensitivity and lysosomal trafficking requirements. To corroborate these findings, we decided to analyze the entry of these two other coronaviruses.

To this end, HeLa cells expressing the FIPV receptor (HeLa-fAPN cells) were subjected to siRNA-mediated downregulation of late endosomal proteins RAB7A and RAB7B or of HOPS complex subunits VPS11, VPS41, and VPS39, followed by inoculation with luciferase expressing FIPV (FIPV- Δ 3abcRL; [79]). Infection with FIPV was significantly affected by siRNA-mediated downregulation of proteins required for late endosome-to-lysosome fusion (Figure 10B). Since the requirement for a functional HOPS complex is indicative of fusion in lysosomes, as we observed for MHV, we analyzed whether FIPV requires processing by lysosomal proteases for efficient entry as well. The results indicate that this is indeed the case as FIPV-driven luciferase expression was diminished in the presence of the pan-lysosomal protease inhibitor CPI (Fig. 10C). On the other hand, infection with FIPV was not affected by FI.

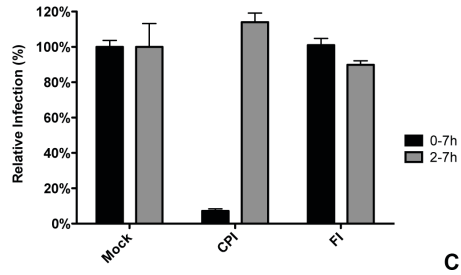
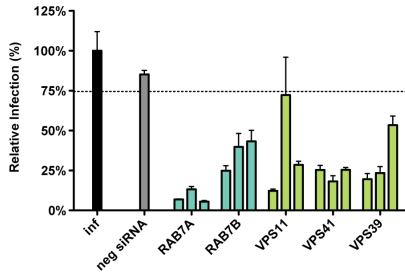
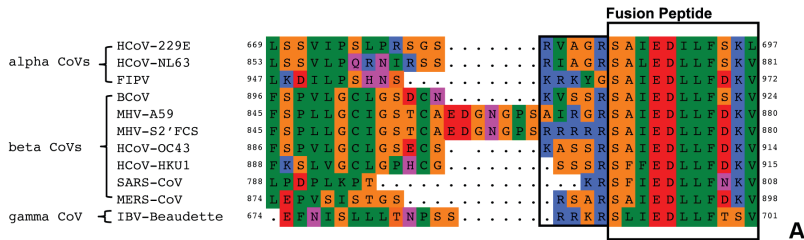


Figure 10: Entry of FIPV. A) Clustal W alignment of spike proteins from several coronaviruses. Displayed is the fusion peptide (boxed) and the area upstream thereof. The area immediately upstream of the fusion peptide that contains the optimal FCS site (RRRRR) in MHV-S2'FCS is also boxed. B) siRNA-mediated gene silencing was performed as described in the legend to Figure 1. At 72h post transfection, HeLa-fAPN cells were inoculated at MOI=0.2 with luciferase expressing FIPV-RLuc. At 7hpi infection was determined by measuring the luciferase activity in cell lysates and displayed relative to mock treated infection (inf). Error bars represent SEM, $n=3 \times 3$. Dotted line shows the lower 95% confidence interval of the negative siRNA controls. C) HeLa-fAPN cells inoculated with FIPV-RLuc at MOI=0.1 were treated with pan-lysosomal protease inhibitor (CPI) or furin inhibitor (FI) from 30 min prior to 7h post inoculation (0-7h) or from 2-7h post inoculation (2-7h; hatched bars). Infection levels were determined by measuring the luciferase activity in cell lysates relative to mock-treated cells. Error bars represent SEM, $n=3 \times 3$.

As MERS-CoV carries a FCS in its S protein immediately upstream of the FP, we hypothesized this virus not to require trafficking to lysosomes and processing by lysosomal proteases for efficient entry. To test this prediction, Huh-7 cells were pretreated with FI or the pan-lysosomal protease inhibitor CPI for 30min. Cells were subsequently inoculated with MERS-CoV at a MOI of 0.1 in the presence of these inhibitors. At 8 hpi the cells were fixed and the number of infected cells determined using immunocytochemistry and wide-field microscopy. The results indicate that, in contrast to wild type MHV and FIPV, but similarly to recombinant MHV carrying a FCS immediately upstream of the FP, infection with MERS-CoV is strongly inhibited by the FI but not by CPI (Figure 11), indicating that MERS-CoV does not require trafficking to lysosomes for efficient entry. Based on these results we conclude that the cleavage site in the CoV S protein immediately upstream of the FP is a key determinant of the intracellular site of fusion.

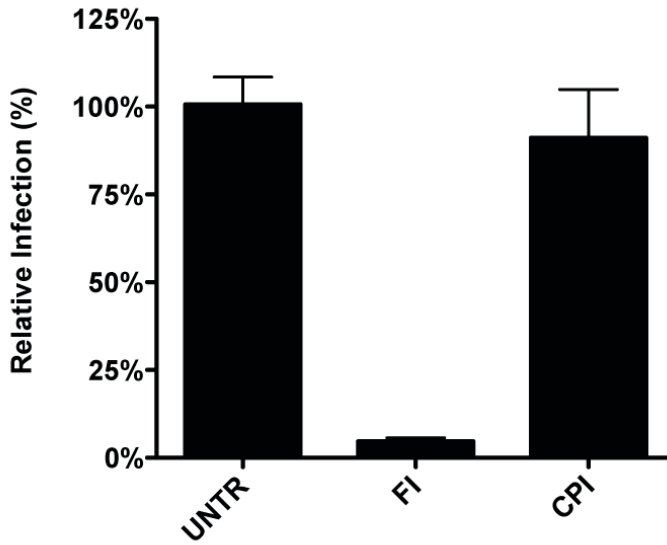


Figure 11: MERS-CoV requires cleavage by furin but not by lysosomal proteases for infection. Huh-7 cells inoculated with MERS-CoV were treated with furin inhibitor (FI) or pan-lysosomal protease inhibitor (CPI) starting from 30min prior to inoculation. Numbers of infected cells was determined by immunocytochemical staining. Error bars represent SEM, n=3.

DISCUSSION

4

The results of this study provide an explanation for several, apparently conflicting results from earlier studies with respect to the process of MHV cell entry, particularly also regarding the necessity of proteolytic cleavage of the CoV S protein. By using a replication-independent fusion assay, we confirmed that MHV entry requires clathrin-mediated endocytosis despite the well-known ability of the MHV S protein to cause cell-cell fusion at neutral pH. We demonstrate that MHV particles traffic to and fuse in lysosomes. Yet, MHV is much less sensitive to perturbation of the low pH in the endo-/lysosomal system than low pH-dependent control viruses VSV and IAV. Our results additionally indicate that, for fusion to occur, the S protein of MHV requires proteolytic cleavage immediately upstream of the FP, like other class I fusion proteins. Efficient inhibition of MHV entry was only observed using a pan-lysosomal protease inhibitor, and could not be achieved using more specific protease inhibitors. Introduction of an optimal furin cleavage site in the S protein immediately upstream of the FP abolished the requirement for trafficking of virions to lysosomes for fusion. However, this virus still required clathrin-mediated uptake for efficient entry. Consistent with a common mechanism for the entry of CoVs, FIPV, but not MERS-CoV, the latter of which contains a furin cleavage site immediately upstream of the FP, was shown to require trafficking to lysosomes and processing by lysosomal proteases for efficient entry. Based on these results we propose a model in which the cleavage site immediately upstream of the FP is an essential determinant of the intracellular site of CoV fusion (Figure 12).

The importance of clathrin-mediated endocytosis and endosomal trafficking in the entry of MHV was revealed by several complementary approaches. One of these was siRNA-mediated gene silencing. Although - with the exception of RAB7A - knockdown was not monitored at the protein level, we believe this approach firmly demonstrates the importance of novel host factors for several reasons. Validated siRNAs were used and the experimental conditions were confirmed by analyzing the mRNA expression levels of several genes by quantitative RT-PCR. Furthermore, we made use of three independent siRNAs per target gene, and a target was only classified as a hit when at least two out three siRNAs showed the same phenotype. Importantly, our findings were strengthened by targeting multiple proteins per host cell pathway/complex, each time with very similar results. Moreover, hits obtained with the replication-dependent reporter assays were confirmed with our novel replication-independent enzyme complementation entry assay. Also the use of recombinant viruses differing only in their spike proteins enabled us to show that inhibition of virus infection upon siRNA transfection resulted from differences in virus entry and not virus replication. Finally, the results obtained were corroborated by using a large panel of inhibitors and by making use of haploid knockout cells, in which late endosome-to-lysosome trafficking was inhibited.

Our results demonstrate that MHV requires endocytic uptake for virus entry despite the S protein's ability to induce cell-cell fusion at neutral pH. Endocytic uptake is also required for a mutant virus carrying a S protein with a FCS immediately upstream of its FP, despite the relative insensitivity to high concentrations of BafA1. Therefore, the ability of a virus to infect cells in the presence of BafA1 does not necessarily imply virus entry to occur at the cell surface. Also a recombinant MHV carrying the spike protein of MHV-4 (MHV-JHM) was found to enter via clathrin-mediated endocytosis (MHV-S4; Figure S10 in Text S1) despite its ability to cause extensive cell-cell fusion [80-82]. The ability of MHV to cause cell-cell fusion at

neutral pH while requiring endocytic uptake for virus-cell fusion suggests different requirements and triggers for these two fusion processes. Similarly, RSV was recently shown to enter cells after endocytic uptake despite the ability of this virus to cause cell-cell fusion [13].

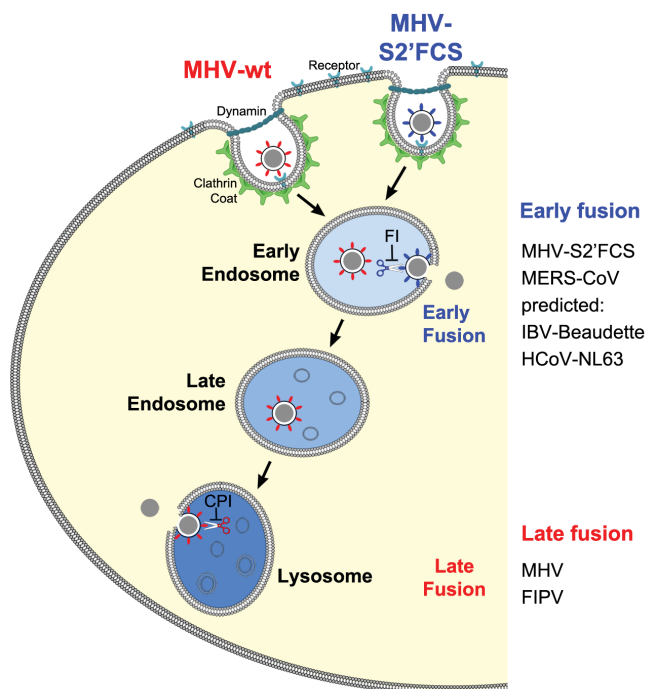


Figure 12: Model of early and late coronavirus fusion. MHV and MHV-S2'FCS are taken up by DAB2-dependent clathrin-mediated endocytosis to end up in RAB5-containing early endosomes. The FCS of MHV-S2'FCS is cleaved by furin or furin-like enzymes to allow fusion of the virus in early endosomes. Trafficking of MHV from late endosomes to lysosomes (RAB7/LAMP1-positive compartments) is required for processing of MHV by lysosomal proteases and viral fusion to occur. We propose that the sequence immediately upstream of the FP is a key determinant of the intracellular site of fusion. MERS-CoV and FIPV enter cells via fusion in early endosomes or lysosomes, respectively. MERS-CoV, which contains a minimal FCS, is inhibited by furin inhibitor (FI) but not by the pan-lysosomal protease inhibitor (CPI). The opposite holds true for FIPV. Based on this model, we predict that IBV strain Beaudette and HCoV-NL63, which contain FCSs (Fig. 10), to fuse in early endosomes in a furin-dependent manner. Other CoVs that do not contain a FCS at this position are predicted to fuse in lysosomes.

The present study confirms and extends previous publications on MHV entry via clathrin-mediated endocytosis [26,83]. Both siRNAs downregulating clathrin-mediated endocytosis-associated proteins, such as clathrin heavy chain (CLTC) and Dynamin 2 (DNM2), and agents affecting this uptake pathway (Chlopro, Dynasore, Dyngo-4a) were capable of inhibiting infection with MHV. Importantly, these findings could be confirmed in our novel replication-independent virus-cell fusion assay, thereby directly showing an involvement of clathrin-mediated endocytosis in entry of MHV. Analysis of several accessory factors of clathrin-mediated endocytosis showed that clathrin-mediated entry of MHV strain A59 depends on clathrin-adaptor DAB2, but not on EPS15 or AAK1. Previously, clathrin-mediated entry of MHV strain 2 was also shown to be independent of EPS15 [83]. Based on the use of inhibitors,

it was earlier concluded that MHV entry depends on cholesterol and lipid-rafts, which may be indicative of caveolae-mediated endocytosis [84,85]. Although our replication-dependent assays indicate a requirement for caveolin 2 (CAV2) for infection, this protein was shown not to be involved in virus entry using our fusion assay. Also depletion of other proteins involved in caveolae-mediated endocytosis, including caveolin 1 (CAV1) and flotillins 1 and 2 (FLOT1 and FLOT2) did not affect MHV infection or fusion. Interestingly, fusion of MHV was severely inhibited by EIPA, an inhibitor of the Na^+/H^+ exchanger NHE1, which is regarded as a hallmark inhibitor of macropinocytosis. Apparently, inhibition of virus entry by EIPA does not prove by itself that a virus enters via this particular pathway. EIPA has been reported to affect several other cellular processes, including actin remodeling, internalization of lipid rafts, distribution of endosomes, and even clathrin-mediated endocytosis [86-90]. Similar to the results obtained with the HeLa cells, also infection of murine LR7 cells was inhibited by compounds interfering with clathrin-mediated endocytosis (Figure S11A in Text S1).

MHV virions require trafficking through the endocytic pathway to lysosomes for efficient entry. Upon clathrin-mediated uptake these virions are temporarily associated with early endosomes as demonstrated by co-localization with RAB5 during live cell imaging. Furthermore, the importance of early endosomes for entry was indicated by siRNA-mediated downregulation of various proteins associated with early endosomes (EEA1, RAB5A, RAB5B, and RAB5C), which inhibited MHV infection, as well as virus-cell fusion. However, only very few MHV particles appeared to fuse in the early endosomes. Live cell imaging indicated fusion largely to occur in late endosomes and/or lysosomes. Consistently, depletion of host proteins associated with late endosome and late endosome-to-lysosome maturation (RAB7A, RAB7B, and the HOPS complex subunits VPS11, VPS33A, VPS39 and VPS41) or addition of U18666A, which blocks late endosome-to-lysosome trafficking, were shown to inhibit both infection and virus-cell fusion. The importance of lysosomes for entry was confirmed by using knockout cells lacking a functional HOPS complex (For a review on the HOPS complex see [54]). Interestingly, in these cells lysosomes are clustered in a perinuclear region of the cell rather than dispersed throughout the cytoplasm. Complementation of the missing HOPS subunit restored the normal lysosome distribution and entry of MHV (Figure S7 in Text S1). The importance of late endosome-to-lysosome trafficking for efficient entry was also observed in murine cells (Figure S11C in Text S1) and for MHV-S4 carrying the S protein of MHV-4 (JHM; Figures S10 and S12 in Text S1).

Corroborating the importance of trafficking of MHV virions through the endocytic pathway, perturbation of endosome maturation by the addition of inhibitory agents, such as ammonium chloride, BafA1, Chloroquine, and Monensin inhibited infection and fusion of MHV. Also the importance of the actin and microtubule cytoskeleton - as demonstrated by the inhibition of MHV entry by downregulation of the Arp2/3 complex factors (ACTR2 and ACTR3), of the microtubule-associated transporter dynein (DYNC1H1 and DYNC2H1), or by addition of actin- or microtubule-affecting drugs - may be explained by the documented involvement of the cytoskeleton in endosome maturation (reviewed in [7]). Indeed, entry of MHV-S2'FCS, which presumably fuses in early endosomes, was much less affected by actin-affecting drugs than that of MHV carrying wild type spike proteins (Figure S10 in Text S1). However, we cannot exclude that actin also plays a role in the clathrin-mediated uptake of MHV particles, as has been observed for VSV and other pathogens that depend on clathrin-mediated endocytosis (reviewed in [91]).

MHV particles require trafficking to the low pH environment of lysosomes to achieve membrane fusion. Nevertheless, MHV was much less sensitive to elevation of pH in the endo-/lysosomal system by the addition of BafA1 than viruses known to fuse in early or late endosomes (VSV and IAV). BafA1, an inhibitor of vacuolar-type H⁺-ATPase was effective in blocking MHV entry only at high concentrations, which are known to prevent endosomal maturation in addition to the elevation of the pH [66]. The absence of a functional HOPS complex, which is required for late endosome-to-lysosome maturation, did not affect infection of cells with VSV or IAV, while entry of MHV was severely reduced. Thus, the low pH trigger that mediates entry of VSV and IAV in the endosomal system of these cells, is not sufficient to induce fusion of MHV. Other environmental cues, present in lysosomes only, are apparently required to activate conformational changes in the S protein leading to fusion. Indeed, inhibition of the three major classes of proteases present in the lysosome by CPI effectively prevented MHV fusion. Infection of murine LR7 cells with MHV was also inhibited by CPI (Figure S11B in Text S1). Strikingly, other inhibitors that affect members of a single protease family had none or only little impact on MHV fusion. These results are in consistence with a functional redundancy of protease family members [47,76] and may explain why previous studies using specific lysosome protease inhibitors [27,92] failed to detect entry inhibition. Also, the inhibition of MHV entry by MG132 may be explained by the known ability of the proteasome inhibitor to negatively affect lysosomal proteases [93-95], although we cannot exclude that MG132 affects entry by its interference with lysosomal trafficking [96].

Our results indicate that cleavage of the S protein immediately upstream of the FP is essential for CoV entry and determines the intracellular site of fusion. Although we did not demonstrate cleavage of MHV S at the FP proximal position directly, a recent study found a cleaved form of the MHV S2 subunit to correspond with the fusion-active form [49]. Furthermore, introduction of an optimal FCS at the FP proximal position abolished the entry inhibition by the pan-lysosomal protease inhibitor whilst introducing a dependency on furin-related enzymes. Consistent with the known presence of active furin in early endosomes (reviewed in [78]) the mutant virus no longer required trafficking to late endosomes/lysosomes for entry to occur. However, in the presence of furin inhibitor, entry of this mutant MHV was much more efficient in wild type cells than in cells lacking a functional HOPS complex (Fig. 8), indicating that under certain circumstances lysosomal proteases may play a role in entry of this virus as well. Trafficking of virions to lysosomes was shown to be also important for entry of FIPV, but not of MERS-CoV, in agreement with the latter virus containing a putative FCS immediately upstream of the FP. Correspondingly, entry of FIPV was inhibited by the pan-lysosomal protease inhibitor CPI but not by furin inhibitor, while the reciprocal held true for MERS-CoV. The importance of S protein cleavage downstream of the S1/S2 boundary and upstream of the FP for infection has so far only been demonstrated for SARS-CoV and IBV [40,43,46-48].

Based on the present study and on the work of others, we conclude that cleavage at the FP proximal position is likely to be a general requirement for CoV entry. With the exception of possibly IBV, cleavage at this position does not appear to occur in the virion-producing cell as it is not observed in released virions, but in the target cell (this study; [40,43,47,48]). This suggests that receptor binding or other environmental cues are necessary to render the cleavage site accessible for proteolysis in the intact virion. Also for several other viruses, including RSV [13] and Ebola virus [16], cleavage of the fusion protein upon endocytosis has been

shown to be required for entry. Our results furthermore show that cleavage at a FP-proximal position is an important determinant of the intracellular site of fusion. The question remains, however, why some CoVs evolved to fuse in early endosomal vesicles while others require trafficking to lysosomes. In view of the growing number of proteases that have been shown to cleave CoV spike proteins [97], this question should probably be studied in relation to the proteolytic enzymes available in the CoV target tissues and cells *in vivo*.

MATERIALS AND METHODS

Cells and viruses.

Murine LR7 fibroblast [98] and feline FCWF cells (ATCC) were used to propagate the recombinant MHV and FIPV viruses, respectively. HEK293T, MDCK and Vero cells were used to propagate pseudotyped VSV Δ G/Luc-G*, Renilla luciferase expressing influenza A pseudovirus, or MERS-CoV, respectively, as described previously [71,73,99]. Cells were maintained as monolayer cultures in Dulbecco's modified Eagle's medium (DMEM, Lonza), supplemented with 10% fetal bovine serum (FBS). HeLa-ATCC cells stably expressing murine CEACAM1a (HeLa-mCC1a) and LR7 cells were used for infection experiments with MHV. HeLa-mCC1a cells stably expressing the deficient β -galactosidase Δ M15 (HeLa-mCC1a- Δ M15) were used in the fusion assay. Stable cell lines were generated using a Moloney murine leukemia (MLV) retroviral vector. MLV was produced in HEK293T cells by triple plasmid transfection of a transfer vector containing the Δ M15 or mCC1a gene as well as a puromycin or neomycin resistance marker gene, respectively, in combination with expression vectors encoding the MLV Gag-Pol, and the VSV spike protein G. Upon MLV transduction, stably transduced cells were selected at 2 μ g/ml puromycin and/or 0.5mg/ml G418 (both Sigma), maintenance at 1 μ g/ml puromycin and/or 0.5 mg/ml G418 in DMEM, supplemented with 10% FBS. HAP1 cells and the VPS33A knock-out derivative thereof (H1- Δ V33) have been described previously [73]. H1- Δ V33 cells were stably transfected with FLAG-tagged VPS33A (H1- Δ V33-fV33) using MLV transduction as described above using a blasticidin resistance marker gene in the transfer vector. Stably transduced cells were selected and maintained at 5 μ g/ml blasticidin. HAP1 cells and its derivatives were also provided with mCC1 as described above to allow infection of these cells with MHV.

Chemicals

The MHV fusion inhibitor HR2 peptide has been described before [100] and was synthesized by GenScript. The peptide was diluted in Tris/HCl 50 mM, pH7.8, 4 μ M EGTA at 1 mM stock solution and used at 10 μ M final concentration. Fluorescein-di- β -D-galactopyranoside (FDG) (AnaSpec) was dissolved in DMSO resulting in a 20mM stock solution. Stocks of 700 μ M cycloheximide (CHX, Sigma), 125 μ M Bafilomycin A1 (BafA1, Enzo Life Sciences), 140mM Chloroquine (Chloq, Sigma), 120 mM Dynasore (Dyn, Enzo Life Sciences), 15mM Dyngo-4a (Dyngo, Abcam), 100mM Ethylisopropyl amiloride (EIPA, Enzo Life Sciences), 1 mM Nocodazole (Noc, Sigma), 1mM Latrunculin A (LatA, Enzo Life Sciences), 2 mM Jaspalakinolide (Jasp, Sigma), 20mM Cytochalasin B (CytoB, Sigma), 20mM Cytochalasin D (CytoD, Sigma), 25mM MG132 (Sigma), 1 mM Brefeldin A (BrefA, Sigma), and 10mM Furin Inhibitor I (FI, Calbiochem) were prepared in DMSO and diluted 1:1000 in the experiments, except when indicated otherwise. Stocks of 2 M ammonium chloride (NH₄Cl, Fluka), 5mM AEBSE, 5mM Leupeptin, 1mM Camostat, 1mg/ml Aprotinin (all obtained from Sigma) were prepared in H₂O and used at 1:100 final concentrations. 10 mM chlorpromazine (Chlopro, Sigma), and 20mM U18666A (Enzo Life Sciences) were prepared in H₂O and used at 1:1000 final concentrations. Stocks of 6 mM Monensin (Mon, Sigma) and 5mM Phosphoramidon (Sigma) were prepared in methanol (MeOH) and used at 1:1000 and 1:100 final concentrations, respectively. 25mg/ml cycloheximide (CHX, Sigma) and 5mM Pepstatin A (Sigma)

were prepared in methanol (EtOH) and used at 1:1000 and 1:100 final concentrations, respectively. Solvents EtOH, MeOH, and DMSO were obtained from Sigma-Aldrich. A stock of 125mM CPI in PBS was made [76] and used at 5mM final concentration.

Plasmids

All plasmids were constructed using conventional cloning techniques. The Δ M15 gene was isolated from a DH5 *E. coli* strain by DNA extraction and PCR. The gene was cloned into a pCAGGS vector for (transient) expression and into a MLV-based pQCXIP transfer vector (Clontech), resulting pQCXIP- Δ M15, for the generation of stable cell lines. The gene encoding the MHV receptor mCC1a [101] was cloned into pQCXIN, resulting in pQCXIN-mCC1a. The RNA transcription vectors used for the generation of recombinant MHV using targeted recombination were generated using pMH54 derivatives [98,102]. pMH54 containing a GFP expression cassette between the E and M gene was generated as described previously for firefly luciferase [59]. The transcription vector used to generate MHV-S2'FCS (pXHERLM-S2'FCS+) was generated by site-directed mutagenesis, thereby changing the sequence encoding AIRGR immediately upstream of the FP into a RRRRR-encoding sequence in vector pXHERLM [59] (GCAATC'CGA'GGG'CGT to AGACGC'CGA'AGG'CGT). The transcription vector used to generate MHV-S4 expressing firefly luciferase, was generated by introducing the firefly luciferase expression cassette between the E and M genes similarly as described previously [59] in a pMH54-derived transcription vector that contains the gene encoding the S protein of MHV-4 (MHV-JHM) [82]. This latter vector was kindly provided by Susan Weiss.

Generation of recombinant / pseudo viruses

Recombinant MHV-EGFPM virus, containing a GFP expression cassette between the E and the M gene, MHV-S2'FCS, containing a *Renilla* luciferase expression cassette between the E and the M gene and a FCS at the FP-proximal position, and MHV-S4 containing the spike gene of MHV-4 (JHM) and a luciferase expression cassette were generated by targeted RNA recombination as described before [98]. Briefly, donor RNA was generated from linearized pMH54-derived transfer vectors described above, and electroporated into FCWF cells infected with interspecies chimeric fMHV coronavirus (an MHV-A59 derivative, in which the ectodomain of the spike protein has been replaced by that of a feline coronavirus, thereby changing host cell tropism). The electroporated FCWF cells were seeded onto a monolayer of LR7 cells. After 24 h of incubation at 37°C, culture supernatant containing progeny viruses was harvested. Genotypes of the recombinant viruses were confirmed after two rounds of plaque purifications. Passage 3 stocks were used in experiments. Generation of MHV-EFLM and MHV-ERLM, containing a firefly or *Renilla* luciferase expression cassette between the E and the M gene, and MHV- α N, containing a N protein tagged with the α -peptide, has been described before [63,103]. Construction of FIPV expressing *Renilla* luciferase was reported previously [79]. Recombinant VSV Δ G/FLuc-G* pseudovirus was generated as described before [71]. Construction of IAV-WSN pseudovirus expressing *Renilla* luciferase has also been described previously [73]. Viruses were stored in culture medium, supplemented with 25 mM HEPES or upon sucrose cushion purification in TN buffer (10 mM Tris-Cl, pH 7.4, 10 mM NaCl).

siRNA transfections

30,000 HeLa-mCC1a-(Δ M15) cells were seeded one day prior to transfection in a 24-well dish. Using Oligofectamine (Life Technologies) reagent three independent, non-overlapping siRNAs (pre-designed Silencer Select siRNAs from Ambion) per gene were individually transfected into target cells according to the manufacturer's instructions. Transfection mix for one well contained 2.5ml of 1mM siRNA and 0.5ml Oligofectamine in 50ml OptiMEM (Gibco). Transfection was done in 250ml final volume of OptiMEM. 4 hours post transfection 125ml of DMEM, 30% FBS were added. Cells were infected 72 hours post transfection.

qRT-PCR of siRNA-mediated gene knockdowns

HeLa-mCC1a cells were subjected to siRNA-mediated gene knockdown as described above. At 72hpi cells were harvested by trypsinization, single-cell suspension counted, and collected by centrifugation. Cellular RNA was extracted using the RNeasy Mini Kit (Qiagen). mRNA levels of genes were analyzed by qRT-PCR using a custom designed pair of specific primers to the gene resulting in about 150bp products. RNA levels were measured using the GoTaq 1-Step RT-qPCR system (Promega) according to the manufacturers' instructions on a LightCycler 480 (Roche). Expression levels were corrected for cell number and viability as determined by the Wst-1 assay (Roche).

Virus infections

Cells were inoculated with MHV-EGFPM at MOI=0.5 (15-20% infected cells) in DMEM, 2% FBS, for 2h at 37°C. The inoculum was replaced by warm DMEM, 10% FBS. At 8hpi, cells infected with MHV-EGFPM were trypsinized and fixed in 4% formaldehyde solution in PBS. Cells were washed and taken up in FACS buffer (2% FBS, 0.05M EDTA, 0.2% NaN₃ in PBS) and GFP expression was quantified by FACS analysis on a FACS Calibur (Benson Dickson) using FlowJo software. Of each sample at least 10,000 cells were analyzed. HeLa, LR7, or HAP1 cells were inoculated with luciferase expressing (pseudo)viruses (MHV-EFLM, VSVAG/FLuc-G*, IAV-RLuc, MHV-S2FCS, or FIPV-RLuc, MHV-EFLM-S4 (JHM)) at MOI=0.2, unless indicated otherwise, in DMEM or IMDM (HAP1), supplemented with 2% FBS at 37°C. At 2hpi the inoculum was replaced by warm culture medium containing 10% FBS. Cells were lysed at 7hpi (MHV, VSV, and FIPV) or 16hpi (IAV) in passive lysis buffer (Promega). Firefly luciferase expression was assessed using the firefly luciferase assay system from Promega or using a homemade system (50mM tricine, 100mM EDTA, 2.5mM MgSO₄, 10mM DTT, 1.25mM ATP, 12.5 mM D-Luciferin). *Renilla* luciferase expression was assessed using the *Renilla* luciferase assay system (Promega). Light emission was measured on a Centro LB 960 luminometer. When indicated cells were transfected with siRNAs prior to inoculation as described above. Luciferase expression levels (in relative light units, RLU) were corrected for cell number and viability as determined by the Wst-1 assay (Roche). When indicated cells were treated with pharmacological inhibitors starting at 30 min prior to or 2 h post inoculation. Huh-7 cells were inoculated with MERS-CoV at a MOI of 0.1 in FBS-containing DMEM. 8h post infection, cells were fixed in 4% formaldehyde in PBS. Cells were stained using rabbit anti-SARS-CoV nsp4 antibodies that are cross-reactive for MERS-CoV, according to a standard protocol using a FITC-conjugated swine-anti-rabbit antibody. Number of infected cells was determined by cell counts on a wide-field fluorescent microscope.

Fusion assay using β -galactosidase complementation

The β -galactosidase complementation fusion assay was performed as described previously [63]. Briefly, cells were preloaded with FDG substrate by incubation of adherent target cells with 2.5% FBS, 100 mM FDG, 50% PBS at room temperature. After 3 min incubation an excess of 5% FBS in PBS was added, supernatant removed and replaced by growth medium. After a recovery period of 30 min at 37°C, cells were (mock) treated with the different inhibitors for 30 min. MHV- α N virus was bound to cells in DMEM with 2%FCS (in the absence or presence of inhibitors) at a MOI=20 for 90 min at 4°C to synchronize infection, after which cells were shifted to 37°C for 2 h. Cells were trypsinized and transferred to Eppendorf tubes, washed and immediately analyzed by FACS. For experiments with protease inhibitors the cells were loaded with FDG by hypotonic shock after trypsination and collection of the cells. In this case, FDG loaded cells were incubated on ice for 14 h before being analyzed by FACS.

Fluorescent labeling of MHV

MHV wt virus was grown on LR7 cells and purified over a 20% sucrose cushion in TN buffer by centrifugation at 110,000 rcf for 2.5h. Supernatant was removed and pellet resuspended in 200ml TN buffer overnight on ice. Concentrated virus solution was subjected to further purification on a Pfefferkorn gradient (10-20%, 25-50%, 50% cushion). After spinning for 1h at 150,000 rcf a clear virus band was visible. The virus band was collected and diluted in TN buffer. The virus was pelleted by centrifugation at 110,000 rcf for 1h and resuspended in 200ml 0.1M sodium phosphate, 0.15M NaCl buffer pH 7.2 overnight on ice. The purified virus solution was labeled using DyLight NHS 488 (Thermo Scientific) according to the manufacturer's instructions. Infectivity of the labeled virus was confirmed by TCID50 analysis and qRT-PCR.

Live-cell microscopy

HeLa-mCC1a cells were seeded into 8-well glass-bottom chambers to reach 60% confluency the next day. Plasmids encoding mRFP-tagged RAB5A or RAB7A, or dsRed-LAMP1 [104] were transfected into the cells one day after seeding using Lipofectamine 2000 (Life Technologies) according to the manufacturer's instructions. 24h after transfection MHV-DyLight488 was bound to cells on ice at MOI=20 for 1.5h in DMEM, 2% FBS. The inoculum was removed and cells washed with cold PBS to remove unbound virus. Warm imaging medium (DMEM without phenol red, 10% FCS) containing 0.008% trypan blue (Invitrogen) was added to the cell chambers. The cell membrane impermeable trypan blue shifts the expression spectrum of cell surface bound particles rendering them undetectable in the 505-530nm channel (described in [65]). Different low to medium RFP expressing cells were imaged live at 37°C, 5% CO₂ in 10min time frames from 10min post warming up to 70min in 30s intervals thereby acquiring z-stack images. Each slice was 0.30 mm in thickness, averaging 12-14 slices per stack. For recording a Zeiss Axio Observer Z1 inverse spinning-disk confocal microscope, equipped with full box stage incubation, including CO₂ (Pecon), argon-krypton and helium-neon laser, two Photometrics Evolve 512 back-illuminated electron-multiplying charge-coupled-device (EM-CCD) cameras, and 100x 1.46NA Oil alpha Plan Aplan objective was used. Fluorescence images were exported as .czi files (Zeiss) and subsequently imported into Fiji (ImageJ, NIH).

Upon import into Fiji, color channels were split and saved as 8-bit tagged image file format. Virus movements were manually tracked in x/y or z direction in the green channel using the MTrackJ plugin. Tracks were saved and subsequently loaded onto the red channel. For each virus spot the area underlying a circle of $0.213 \mu\text{m}^2$ was measured for its gray mean value. Viruses were considered colocalizing if the gray mean value reached 50% of the maximum. Subsequently red and blue color channels were merged, tracks imported and viruses classified using the viral track. If the virus co-localized with the endosomal vesicle over at least four sequential 30s frames the virus was categorized as associating. Viruses that, after initial co-localization, separated from the vesicle were classified as ‘associating/dissociating’. If a virus particle faded and disappeared (and could not be found in other z-stacks) whilst co-localizing in previous intervals with an endosomal vesicle it was categorized as ‘fusing’ (Figure S2 and S3 in Text S1). When a viral particle co-localized with endosomal compartments but did neither dissociate nor fade during the 10min acquisition period it was classified as ‘non-fusing’. With this quantification method we analyzed 12 cells for RAB5 with 75 virions in total, 12 cells for RAB7 with 105 virions in total, and 16 cells for LAMP1 with 115 virions in total, acquired over three independent experiments.

Sequence Alignment

The sequences of MHV-A59 and MHV-S2’FCS were based on pMH54 sequencing results. Sequences for BCoV (GI: 18033975), FIPV (GI: 556925469), HCoV-OC43 (GI: 530802591), HCoV-HKU1 (GI: 306569687), SARS-CoV (GI: 89474484), MERS-CoV (GI: 510937295), HCoV-229E (GI: 82780499), HCoV-NL63 (GI: 530802144), IBV-Beaudette (GI: 138186) were obtained from NCBI. Alignments were performed over the entire length of the spike proteins using MegAlign (Lasergene DNASTAR) using a ClustalW alignment, gap penalty 10, gap length penalty 0.2, delay divergent sequences 30%, DNA translation weight 0.5, protein weight matrix: PAM series, DNA weight matrix: ClustalW.

Confirmation of siRNA-mediated knockdown of RAB7A

HeLa cells were co-transfected with mRFP-tagged RAB7A similarly as described previously [60]. Briefly, 7’500 HeLa cells were seeded one day prior to transfection in a 96-well plate. Using Oligofectamine (Life Technologies) reagent three independent, non-overlapping RAB7A siRNAs (pre-designed Silencer Select siRNAs from Ambion) per gene were individually transfected into target cells with the mRFP-RAB7A plasmid. Transfection mix for one well contained 2.5ml of 1mM siRNA, 10ng plasmid, and 0.5ml Oligofectamine in 12.5ml OptiMEM (Gibco). Transfection was done in 62.5ml final volume of OptiMEM. 4 hours post transfection 125ml of DMEM, 30% FBS were added. RFP expression was analyzed 24h post transfection using an EVOS Cell Imaging System.

Immunostaining of HAP1 cells

Confluent HAP1, H1- Δ V33, and H1- Δ V33-fV33 cells and their stably mCeacam1a expressing counterparts were detached using a cell scraper, homogenized, and fixed. After 30min incubation in blocking buffer (3% BSA (Sigma), in PBS) for 1h cells were incubated in 1:100 N-CEACAM-Fc [80] antibody, washed, and stained with 2ry AF488 goat-anti-rabbit antibody (Life Technologies). After washing cells were analyzed by FACS at 10,000 gated single cells per sample.

Western blotting

HAP1 cells were trypsinized and collected by centrifugation at 350 rcf for 10min. The pellet was resuspended in Laemmli sample buffer containing 100 mM DTT, boiled for 5 min at 95°C and subjected to electrophoresis in 10% acrylamide (Bio-Rad) gels. Viruses were purified and concentrated over a 20% sucrose cushion (in TN buffer) at 110,000 rcf. Pelleted virus was resuspended in TN buffer overnight on ice. After addition of Laemmli sample buffer (1x final concentration, 100 mM DTT), samples were boiled for 5 min at 95°C and subjected to electrophoresis in 7% acrylamide (Bio-Rad) gels. Upon transfer to a nitrocellulose membrane (Millipore), the presence of cellular and viral proteins was probed with antibodies against GM130 (rabbit pAb, Abcam), FLAG (HRP-labeled mouse anti-FLAG mAb, Sigma) or the S2 subunit of MHV A59 [105] (mouse anti-S2 mAb) diluted 1:1000. When necessary, the blots were subsequently incubated with HRP-labeled rabbit anti-mouse or swine anti-rabbit antibodies (both diluted 1:5000; DAKO). Binding of HRP-labeled antibodies was visualized using Amersham ECL Western blotting substrate (GE Healthcare Life Sciences) according to the manufacturer's instructions.

4

Immunofluorescence analysis of HAP1 cells

To image the localization of LAMP1 in HAP1, H1-ΔV33, and H1-ΔV33A-fV33, cells the cells were seeded onto coverslips one day prior to staining. Cells were fixed in 4% formaldehyde in PBS for 15min at RT, washed with PBS, and subsequently permeabilized in PBS containing 0.1% Triton-X-100 for 10min. Cells were incubated with antibody against LAMP1 (rabbit anti-LAMP1 pAb, 1:100 dilution; Abcam) in 3% BSA in PBS followed by incubation with secondary antibodies coupled to AF488, AF-568 phalloidin, and DAPI (all Life Technologies). The samples were analyzed using a confocal laser-scanning microscope (Leica SPE-II).

Growth curves of recombinant viruses

LR7 cells were infected at MOI=0.1 or MOI=4.0 with MHV-ERLM or MHV-S2^{FC}S in DMEM containing 2% FBS and 25 mM HEPES (infection medium). After 3 h of infection supernatant was replaced by fresh infection medium and infection was allowed to progress over a period of 24h. Every 3 h a small sample of the culture supernatant was collected and immediately frozen. The samples were subsequently analyzed in TCID₅₀ assays on LR7 cells and subjected to qRT-PCR analysis to quantify virion production. Therefore viral RNA was extracted from the samples using the QIAamp Viral RNA Mini Kit (Qiagen). The relative amount of viral RNA present was determined with a LightCycler 480 using LightCycler 480 RNA Master Hydrolysis kit (Roche Applied Biosciences) and specific primers and probe targeted against the MHV 1b gene by comparison with a standard curve.

Gene identification numbers

Gene	SwissProt ID
AAK1	Q2M2I8
ACTR2	P61160
ACTR3	P61158
CAV1	Q03135
CAV2	P51636
CLTC	Q00610
DAB2	P98082
DNM1	Q05193
DNM2	P50570
DYNC1H1	Q14204
DYNC2H1	Q8NCM8
EPS15	P42566
FLOT1	O75955
FLOT2	Q14254
LAMP1	P11279
MYO6	Q9UM54
NSF	P46459
PAK1	Q13153
RAB5A	P20339
RAB5B	P61020
RAB5C	P51148
RAB7A	P51149
RAB7B	Q96AH8
SNX1	Q13596
VCL	P18206
VPS11	Q9H270
VPS33A	Q96AX1
VPS39	Q96JC1
VPS41	P49754

Acknowledgments

We would like to thank Dr. Thijn Brummelkamp, Biochemistry Division, Netherlands Cancer Institute, Amsterdam, The Netherlands, for providing us with HAP1 and HAP1-ΔVP-S33A cells, as well as pMX-FLAG-VPS33A plasmid, Dr. Susan Weiss, University of Pennsylvania, Philadelphia PA, USA, for providing us with the pMH54 derived transcription vector that contains the spike gene of MHV-4, and Dr. Tom Gallagher, Department for Microbiology and Immunobiology, Stritch School of Medicine, Loyola University, Chicago IL, USA for providing us with N-CEACAM-Fc antibody. We also would like to thank Prof. Dr. Ari Helenius and the Light Microscopy and Screening Center, Institute of Biochemistry, Swiss Federal Institute of Technology Zurich, Zurich, Switzerland, for providing us with the possibility to carry out light microscopy experiments in their facilities and providing us with scientific input.

REFERENCES

1. Fuller AO, Spear PG (1987) Anti-glycoprotein D antibodies that permit adsorption but block infection by herpes simplex virus 1 prevent virion-cell fusion at the cell surface. *Proceedings of the National Academy of Sciences of the United States of America* 84: 5454-5458.
2. Sodeik B, Ebersold MW, Helenius A (1997) Microtubule-mediated transport of incoming herpes simplex virus 1 capsids to the nucleus. *The Journal of cell biology* 136: 1007-1021.
3. Okada Y (1969) Factors in fusion of cells by HVJ. *Current topics in microbiology and immunology* 48: 102-128.
4. Permanyer M, Ballana E, Este JA (2010) Endocytosis of HIV: anything goes. *Trends in microbiology* 18: 543-551.
5. Stein BS, Gowda SD, Lifson JD, Penhallow RC, Bensch KG, et al. (1987) pH-independent HIV entry into CD4-positive T cells via virus envelope fusion to the plasma membrane. *Cell* 49: 659-668.
6. Authier F, Posner BI, Bergeron JJ (1996) Endosomal proteolysis of internalized proteins. *FEBS letters* 389: 55-60.
7. Huotari J, Helenius A (2011) Endosome maturation. *The EMBO journal* 30: 3481-3500.
8. Plemper RK (2011) Cell entry of enveloped viruses. *Current opinion in virology* 1: 92-100.
9. Sieczkarski SB, Whittaker GR (2003) Differential requirements of Rab5 and Rab7 for endocytosis of influenza and other enveloped viruses. *Traffic* 4: 333-343.
10. Skehel JJ, Bayley PM, Brown EB, Martin SR, Waterfield MD, et al. (1982) Changes in the conformation of influenza virus hemagglutinin at the pH optimum of virus-mediated membrane fusion. *Proceedings of the National Academy of Sciences of the United States of America* 79: 968-972.
11. Carneiro FA, Ferradosa AS, Da Poian AT (2001) Low pH-induced conformational changes in vesicular stomatitis virus glycoprotein involve dramatic structure reorganization. *The Journal of biological chemistry* 276: 62-67.
12. White J, Matlin K, Helenius A (1981) Cell fusion by Semliki Forest, influenza, and vesicular stomatitis viruses. *The Journal of cell biology* 89: 674-679.
13. Krzyzaniak MA, Zumstein MT, Gerez JA, Picotti P, Helenius A (2013) Host cell entry of respiratory syncytial virus involves macropinocytosis followed by proteolytic activation of the F protein. *PLoS pathogens* 9: e1003309.
14. Wool-Lewis RJ, Bates P (1999) Endoproteolytic processing of the ebola virus envelope glycoprotein: cleavage is not required for function. *Journal of virology* 73: 1419-1426.
15. Zimmer G, Budz L, Herrler G (2001) Proteolytic activation of respiratory syncytial virus fusion protein. Cleavage at two furin consensus sequences. *The Journal of biological chemistry* 276: 31642-31650.
16. Chandran K, Sullivan NJ, Felbor U, Whelan SP, Cunningham JM (2005) Endosomal proteolysis of the Ebola virus glycoprotein is necessary for infection. *Science* 308: 1643-1645.

17. Peiris JS, Lai ST, Poon LL, Guan Y, Yam LY, et al. (2003) Coronavirus as a possible cause of severe acute respiratory syndrome. *Lancet* 361: 1319-1325.
18. Zaki AM, van Boheemen S, Bestebroer TM, Osterhaus AD, Fouchier RA (2012) Isolation of a novel coronavirus from a man with pneumonia in Saudi Arabia. *N Engl J Med* 367: 1814-1820.
19. de Haan CA, Rottier PJ (2005) Molecular interactions in the assembly of coronaviruses. *Advances in virus research* 64: 165-230.
20. Bosch BJ, van der Zee R, de Haan CA, Rottier PJ (2003) The coronavirus spike protein is a class I virus fusion protein: structural and functional characterization of the fusion core complex. *Journal of virology* 77: 8801-8811.
21. Inoue Y, Tanaka N, Tanaka Y, Inoue S, Morita K, et al. (2007) Clathrin-dependent entry of severe acute respiratory syndrome coronavirus into target cells expressing ACE2 with the cytoplasmic tail deleted. *Journal of virology* 81: 8722-8729.
22. Wang H, Yang P, Liu K, Guo F, Zhang Y, et al. (2008) SARS coronavirus entry into host cells through a novel clathrin- and caveolae-independent endocytic pathway. *Cell research* 18: 290-301.
23. Regan AD, Shraybman R, Cohen RD, Whittaker GR (2008) Differential role for low pH and cathepsin-mediated cleavage of the viral spike protein during entry of serotype II feline coronaviruses. *Veterinary microbiology* 132: 235-248.
24. Van Hamme E, Dewerchin HL, Cornelissen E, Verhasselt B, Nauwynck HJ (2008) Clathrin- and caveolae-independent entry of feline infectious peritonitis virus in monocytes depends on dynamin. *The Journal of general virology* 89: 2147-2156.
25. Nomura R, Kiyota A, Suzaki E, Kataoka K, Ohe Y, et al. (2004) Human coronavirus 229E binds to CD13 in rafts and enters the cell through caveolae. *Journal of virology* 78: 8701-8708.
26. Eifart P, Ludwig K, Bottcher C, de Haan CA, Rottier PJ, et al. (2007) Role of endocytosis and low pH in murine hepatitis virus strain A59 cell entry. *Journal of virology* 81: 10758-10768.
27. Qiu Z, Hingley ST, Simmons G, Yu C, Das Sarma J, et al. (2006) Endosomal proteolysis by cathepsins is necessary for murine coronavirus mouse hepatitis virus type 2 spike-mediated entry. *Journal of virology* 80: 5768-5776.
28. Stauber R, Pfeleiderera M, Siddell S (1993) Proteolytic cleavage of the murine coronavirus surface glycoprotein is not required for fusion activity. *The Journal of general virology* 74 (Pt 2): 183-191.
29. Sturman LS, Ricard CS, Holmes KV (1985) Proteolytic cleavage of the E2 glycoprotein of murine coronavirus: activation of cell-fusing activity of virions by trypsin and separation of two different 90K cleavage fragments. *Journal of virology* 56: 904-911.
30. de Haan CA, Stadler K, Godeke GJ, Bosch BJ, Rottier PJ (2004) Cleavage inhibition of the murine coronavirus spike protein by a furin-like enzyme affects cell-cell but not virus-cell fusion. *Journal of virology* 78: 6048-6054.
31. Frana MF, Behnke JN, Sturman LS, Holmes KV (1985) Proteolytic cleavage of the E2 glycoprotein of murine coronavirus: host-dependent differences in proteolytic cleavage and cell fusion. *Journal of virology* 56: 912-920.

-
32. Luytjes W, Sturman LS, Bredenbeek PJ, Charite J, van der Zeijst BA, et al. (1987) Primary structure of the glycoprotein E2 of coronavirus MHV-A59 and identification of the trypsin cleavage site. *Virology* 161: 479-487.
 33. Ricard CS, Sturman LS (1985) Isolation of the subunits of the coronavirus envelope glycoprotein E2 by hydroxyapatite high-performance liquid chromatography. *Journal of chromatography* 326: 191-197.
 34. Gombold JL, Hingley ST, Weiss SR (1993) Fusion-defective mutants of mouse hepatitis virus A59 contain a mutation in the spike protein cleavage signal. *Journal of virology* 67: 4504-4512.
 35. Leparac-Goffart I, Hingley ST, Chua MM, Jiang X, Lavi E, et al. (1997) Altered pathogenesis of a mutant of the murine coronavirus MHV-A59 is associated with a Q159L amino acid substitution in the spike protein. *Virology* 239: 1-10.
 36. Matsuyama S, Taguchi F (2009) Two-step conformational changes in a coronavirus envelope glycoprotein mediated by receptor binding and proteolysis. *Journal of virology* 83: 11133-11141.
 37. Simmons G, Gosalia DN, Rennekamp AJ, Reeves JD, Diamond SL, et al. (2005) Inhibitors of cathepsin L prevent severe acute respiratory syndrome coronavirus entry. *Proceedings of the National Academy of Sciences of the United States of America* 102: 11876-11881.
 38. Bosch BJ, Bartelink W, Rottier PJ (2008) Cathepsin L functionally cleaves the severe acute respiratory syndrome coronavirus class I fusion protein upstream of rather than adjacent to the fusion peptide. *Journal of virology* 82: 8887-8890.
 39. Simmons G, Reeves JD, Rennekamp AJ, Amberg SM, Piefer AJ, et al. (2004) Characterization of severe acute respiratory syndrome-associated coronavirus (SARS-CoV) spike glycoprotein-mediated viral entry. *Proceedings of the National Academy of Sciences of the United States of America* 101: 4240-4245.
 40. Belouzard S, Chu VC, Whittaker GR (2009) Activation of the SARS coronavirus spike protein via sequential proteolytic cleavage at two distinct sites. *Proceedings of the National Academy of Sciences of the United States of America* 106: 5871-5876.
 41. Matsuyama S, Ujike M, Morikawa S, Tashiro M, Taguchi F (2005) Protease-mediated enhancement of severe acute respiratory syndrome coronavirus infection. *Proceedings of the National Academy of Sciences of the United States of America* 102: 12543-12547.
 42. Belouzard S, Madu I, Whittaker GR (2010) Elastase-mediated activation of the severe acute respiratory syndrome coronavirus spike protein at discrete sites within the S2 domain. *The Journal of biological chemistry* 285: 22758-22763.
 43. Kam YW, Okumura Y, Kido H, Ng LF, Bruzzone R, et al. (2009) Cleavage of the SARS coronavirus spike glycoprotein by airway proteases enhances virus entry into human bronchial epithelial cells in vitro. *PLoS one* 4: e7870.
 44. Bertram S, Glowacka I, Muller MA, Lavender H, Gnirss K, et al. (2011) Cleavage and activation of the severe acute respiratory syndrome coronavirus spike protein by human airway trypsin-like protease. *Journal of virology* 85: 13363-13372.
 45. Shulla A, Heald-Sargent T, Subramanya G, Zhao J, Perlman S, et al. (2011) A transmembrane serine protease is linked to the severe acute respiratory syndrome coronavirus receptor and activates virus entry. *Journal of virology* 85: 873-882.

46. Yamada Y, Liu DX (2009) Proteolytic activation of the spike protein at a novel RRRR/S motif is implicated in furin-dependent entry, syncytium formation, and infectivity of coronavirus infectious bronchitis virus in cultured cells. *Journal of virology* 83: 8744-8758.
47. Matthews SP, Werber I, Deussing J, Peters C, Reinheckel T, et al. (2010) Distinct protease requirements for antigen presentation in vitro and in vivo. *Journal of immunology* 184: 2423-2431.
48. Watanabe R, Matsuyama S, Shirato K, Maejima M, Fukushi S, et al. (2008) Entry from the cell surface of severe acute respiratory syndrome coronavirus with cleaved S protein as revealed by pseudotype virus bearing cleaved S protein. *Journal of virology* 82: 11985-11991.
49. Wicht O, Burkard C, de Haan CA, van Kuppeveld FJ, Rottier PJ, et al. (2014) Identification and characterization of a proteolytically primed form of the murine coronavirus spike proteins after fusion with the target cell. *Journal of virology* 88: 4943-4952.
50. Snijder B, Sacher R, Ramo P, Liberali P, Mench K, et al. (2012) Single-cell analysis of population context advances RNAi screening at multiple levels. *Molecular systems biology* 8: 579.
51. Gouin E, Welch MD, Cossart P (2005) Actin-based motility of intracellular pathogens. *Current opinion in microbiology* 8: 35-45.
52. May RC (2001) The Arp2/3 complex: a central regulator of the actin cytoskeleton. *Cellular and molecular life sciences : CMLS* 58: 1607-1626.
53. Pfeffer SR (2013) Rab GTPase regulation of membrane identity. *Current opinion in cell biology* 25: 414-419.
54. Balderhaar HJ, Ungermann C (2013) CORVET and HOPS tethering complexes - coordinators of endosome and lysosome fusion. *Journal of cell science* 126: 1307-1316.
55. Bonifacino JS, Hurlley JH (2008) Retromer. *Current opinion in cell biology* 20: 427-436.
56. DeMali KA, Burrridge K (2003) Coupling membrane protrusion and cell adhesion. *Journal of cell science* 116: 2389-2397.
57. Bagrodia S, Cerione RA (1999) Pak to the future. *Trends in cell biology* 9: 350-355.
58. Robinson LJ, Aniento F, Gruenberg J (1997) NSF is required for transport from early to late endosomes. *Journal of cell science* 110 (Pt 17): 2079-2087.
59. de Haan CA, van Genne L, Stoop JN, Volders H, Rottier PJ (2003) Coronaviruses as vectors: position dependence of foreign gene expression. *Journal of virology* 77: 11312-11323.
60. Verheije MH, Raaben M, Mari M, Te Lintelo EG, Reggiori F, et al. (2008) Mouse hepatitis coronavirus RNA replication depends on GBF1-mediated ARF1 activation. *PLoS pathogens* 4: e1000088.
61. Raaben M, Posthuma CC, Verheije MH, te Lintelo EG, Kikkert M, et al. (2010) The ubiquitin-proteasome system plays an important role during various stages of the coronavirus infection cycle. *Journal of virology* 84: 7869-7879.
62. Huynh KK, Gershenson E, Grinstein S (2008) Cholesterol accumulation by macrophages impairs phagosome maturation. *The Journal of biological chemistry* 283: 35745-35755.
63. Burkard C, Bloyet LM, Wicht O, van Kuppeveld FJ, Rottier PJ, et al. (2014) Dissecting Virus Entry: Replication-Independent Analysis of Virus Binding, Internalization, and Penetration Using Minimal Complementation of beta-Galactosidase. *PloS one* 9: e101762.

-
64. Langley KE, Villarejo MR, Fowler AV, Zamenhof PJ, Zabin I (1975) Molecular basis of beta-galactosidase alpha-complementation. *Proceedings of the National Academy of Sciences of the United States of America* 72: 1254-1257.
 65. Engel S, Heger T, Mancini R, Herzog F, Kartenbeck J, et al. (2011) Role of endosomes in simian virus 40 entry and infection. *Journal of virology* 85: 4198-4211.
 66. Bayer N, Schober D, Prchla E, Murphy RF, Blaas D, et al. (1998) Effect of bafilomycin A1 and nocodazole on endocytic transport in HeLa cells: implications for viral uncoating and infection. *Journal of virology* 72: 9645-9655.
 67. Johannsdottir HK, Mancini R, Kartenbeck J, Amato L, Helenius A (2009) Host cell factors and functions involved in vesicular stomatitis virus entry. *Journal of virology* 83: 440-453.
 68. Le Blanc I, Luyet PP, Pons V, Ferguson C, Emans N, et al. (2005) Endosome-to-cytosol transport of viral nucleocapsids. *Nature cell biology* 7: 653-664.
 69. Matos PM, Marin M, Ahn B, Lam W, Santos NC, et al. (2013) Anionic lipids are required for vesicular stomatitis virus G protein-mediated single particle fusion with supported lipid bilayers. *The Journal of biological chemistry* 288: 12416-12425.
 70. Skehel JJ, Wiley DC (2000) Receptor binding and membrane fusion in virus entry: the influenza hemagglutinin. *Annual review of biochemistry* 69: 531-569.
 71. Tani H, Komoda Y, Matsuo E, Suzuki K, Hamamoto I, et al. (2007) Replication-competent recombinant vesicular stomatitis virus encoding hepatitis C virus envelope proteins. *Journal of virology* 81: 8601-8612.
 72. Whitt MA (2010) Generation of VSV pseudotypes using recombinant DeltaG-VSV for studies on virus entry, identification of entry inhibitors, and immune responses to vaccines. *Journal of virological methods* 169: 365-374.
 73. Konig R, Stertz S, Zhou Y, Inoue A, Hoffmann HH, et al. (2010) Human host factors required for influenza virus replication. *Nature* 463: 813-817.
 74. Carette JE, Raaben M, Wong AC, Herbert AS, Obernosterer G, et al. (2011) Ebola virus entry requires the cholesterol transporter Niemann-Pick C1. *Nature* 477: 340-343.
 75. Tveten K, Ranheim T, Berge KE, Leren TP, Kulseth MA (2009) The effect of bafilomycin A1 and protease inhibitors on the degradation and recycling of a Class 5-mutant LDLR. *Acta biochimica et biophysica Sinica* 41: 246-255.
 76. van Kasteren SI, Berlin I, Colbert JD, Keane D, Ovaa H, et al. (2011) A multifunctional protease inhibitor to regulate endolysosomal function. *ACS chemical biology* 6: 1198-1204.
 77. White JM, Delos SE, Brecher M, Schornberg K (2008) Structures and mechanisms of viral membrane fusion proteins: multiple variations on a common theme. *Critical reviews in biochemistry and molecular biology* 43: 189-219.
 78. Thomas G (2002) Furin at the cutting edge: from protein traffic to embryogenesis and disease. *Nature reviews Molecular cell biology* 3: 753-766.
 79. de Haan CA, Haijema BJ, Boss D, Heuts FW, Rottier PJ (2005) Coronaviruses as vectors: stability of foreign gene expression. *Journal of virology* 79: 12742-12751.
 80. Gallagher TM (1997) A role for naturally occurring variation of the murine coronavirus spike protein in stabilizing association with the cellular receptor. *Journal of virology* 71: 3129-3137.

81. Krueger DK, Kelly SM, Lewicki DN, Ruffolo R, Gallagher TM (2001) Variations in disparate regions of the murine coronavirus spike protein impact the initiation of membrane fusion. *Journal of virology* 75: 2792-2802.
82. Phillips JJ, Chua MM, Lavi E, Weiss SR (1999) Pathogenesis of chimeric MHV4/MHV-A59 recombinant viruses: the murine coronavirus spike protein is a major determinant of neurovirulence. *Journal of virology* 73: 7752-7760.
83. Pu Y, Zhang X (2008) Mouse hepatitis virus type 2 enters cells through a clathrin-mediated endocytic pathway independent of Eps15. *Journal of virology* 82: 8112-8123.
84. Choi KS, Aizaki H, Lai MM (2005) Murine coronavirus requires lipid rafts for virus entry and cell-cell fusion but not for virus release. *Journal of virology* 79: 9862-9871.
85. Thorp EB, Gallagher TM (2004) Requirements for CEACAMs and cholesterol during murine coronavirus cell entry. *Journal of virology* 78: 2682-2692.
86. Fretz M, Jin J, Conibere R, Penning NA, Al-Taei S, et al. (2006) Effects of Na⁺/H⁺ exchanger inhibitors on subcellular localisation of endocytic organelles and intracellular dynamics of protein transduction domains HIV-TAT peptide and octaarginine. *Journal of controlled release : official journal of the Controlled Release Society* 116: 247-254.
87. Lagana A, Vadnais J, Le PU, Nguyen TN, Laprade R, et al. (2000) Regulation of the formation of tumor cell pseudopodia by the Na(+)/H(+) exchanger NHE1. *Journal of cell science* 113 (Pt 20): 3649-3662.
88. Meier O, Boucke K, Hammer SV, Keller S, Stidwill RP, et al. (2002) Adenovirus triggers macropinocytosis and endosomal leakage together with its clathrin-mediated uptake. *The Journal of cell biology* 158: 1119-1131.
89. Wadia JS, Stan RV, Dowdy SF (2004) Transducible TAT-HA fusogenic peptide enhances escape of TAT-fusion proteins after lipid raft macropinocytosis. *Nature medicine* 10: 310-315.
90. Ivanov AI, Nusrat A, Parkos CA (2004) Endocytosis of epithelial apical junctional proteins by a clathrin-mediated pathway into a unique storage compartment. *Molecular biology of the cell* 15: 176-188.
91. Kaksonen M, Toret CP, Drubin DG (2006) Harnessing actin dynamics for clathrin-mediated endocytosis. *Nature reviews Molecular cell biology* 7: 404-414.
92. Huang IC, Bosch BJ, Li F, Li W, Lee KH, et al. (2006) SARS coronavirus, but not human coronavirus NL63, utilizes cathepsin L to infect ACE2-expressing cells. *The Journal of biological chemistry* 281: 3198-3203.
93. Lee DH, Goldberg AL (1998) Proteasome inhibitors: valuable new tools for cell biologists. *Trends in cell biology* 8: 397-403.
94. Tawa NE, Jr., Odessey R, Goldberg AL (1997) Inhibitors of the proteasome reduce the accelerated proteolysis in atrophying rat skeletal muscles. *The Journal of clinical investigation* 100: 197-203.
95. van Kerkhof P, Alves dos Santos CM, Sachse M, Klumperman J, Bu G, et al. (2001) Proteasome inhibitors block a late step in lysosomal transport of selected membrane but not soluble proteins. *Molecular biology of the cell* 12: 2556-2566.
96. Zaarur N, Meriin AB, Bejarano E, Xu X, Gabai VL, et al. (2014) Proteasome failure promotes positioning of lysosomes around the aggresome via local block of microtubule-dependent transport. *Molecular and cellular biology* 34: 1336-1348.

-
97. Belouzard S, Millet JK, Licitra BN, Whittaker GR (2012) Mechanisms of coronavirus cell entry mediated by the viral spike protein. *Viruses* 4: 1011-1033.
 98. Kuo L, Godeke GJ, Raamsman MJ, Masters PS, Rottier PJ (2000) Retargeting of coronavirus by substitution of the spike glycoprotein ectodomain: crossing the host cell species barrier. *J Virol* 74: 1393-1406.
 99. van Boheemen S, de Graaf M, Lauber C, Bestebroer TM, Raj VS, et al. (2012) Genomic characterization of a newly discovered coronavirus associated with acute respiratory distress syndrome in humans. *mBio* 3.
 100. Bosch BJ, van der Zee R, de Haan CA, Rottier PJ (2003) The coronavirus spike protein is a class I virus fusion protein: structural and functional characterization of the fusion core complex. *J Virol* 77: 8801-8811.
 101. Dveksler GS, Pensiero MN, Cardellichio CB, Williams RK, Jiang GS, et al. (1991) Cloning of the mouse hepatitis virus (MHV) receptor: expression in human and hamster cell lines confers susceptibility to MHV. *Journal of virology* 65: 6881-6891.
 102. de Haan CA, Haijema BJ, Masters PS, Rottier PJ (2008) Manipulation of the coronavirus genome using targeted RNA recombination with interspecies chimeric coronaviruses. *Methods Mol Biol* 454: 229-236.
 103. Kuo L, Godeke GJ, Raamsman MJ, Masters PS, Rottier PJ (2000) Retargeting of coronavirus by substitution of the spike glycoprotein ectodomain: crossing the host cell species barrier. *Journal of virology* 74: 1393-1406.
 104. Vonderheit A, Helenius A (2005) Rab7 associates with early endosomes to mediate sorting and transport of Semliki forest virus to late endosomes. *PLoS biology* 3: e233.
 105. Schulze H, Kolter T, Sandhoff K (2009) Principles of lysosomal membrane degradation: Cellular topology and biochemistry of lysosomal lipid degradation. *Biochimica et biophysica acta* 1793: 674-683.

SUPPORTING INFORMATION

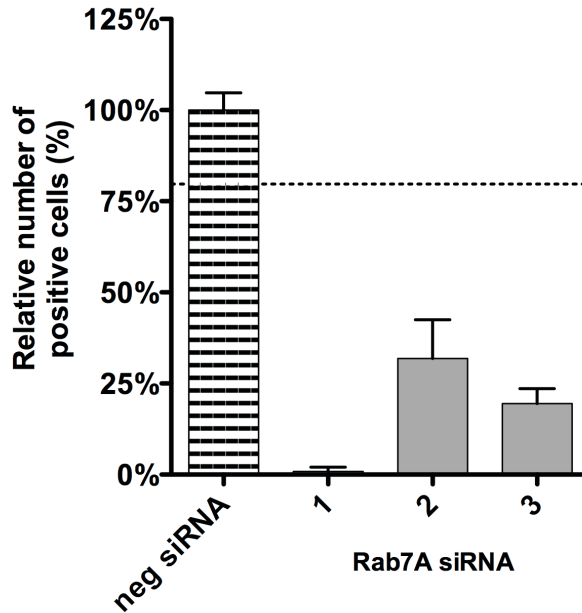


Figure S1. Confirmation of protein knockdown upon Rab7A siRNA transfection. Cells were simultaneously transfected with mRFP-Rab7A plasmid and siRNAs against Rab7A. 24h post transfection cells were fixed and the number of positive cells assessed. Dotted line shows the lower 95% confidence interval of the negative siRNA control. Error bars represent SEM, n=3.

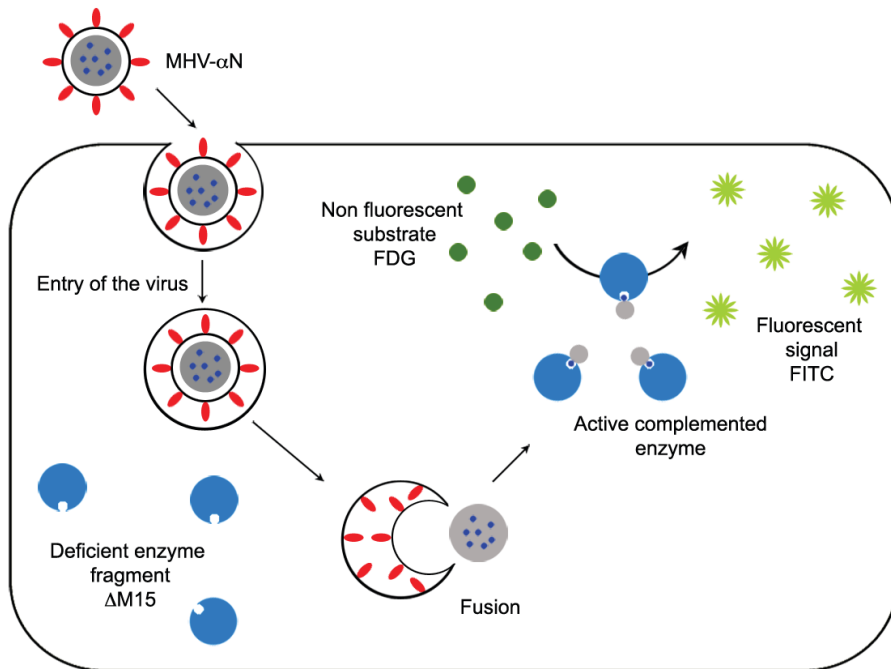


Figure S2. Replication-independent fusion assay. Recombinant MHV containing a nucleocapsid protein with a 45-aa α -peptide extension (α N) are bound and internalized into the target cells. Upon fusion the nucleocapsid proteins are released into the cytosol where the deficient, inactive β -galactosidase enzyme Δ M15 is present. The Δ M15 is subsequently complemented by the α -peptide exposed by the N protein, thereby reconstituting an active enzyme. This enzyme can now convert the FDG substrate fluorescein, the production of which can be measured by FACS or fluorescence microscopy.

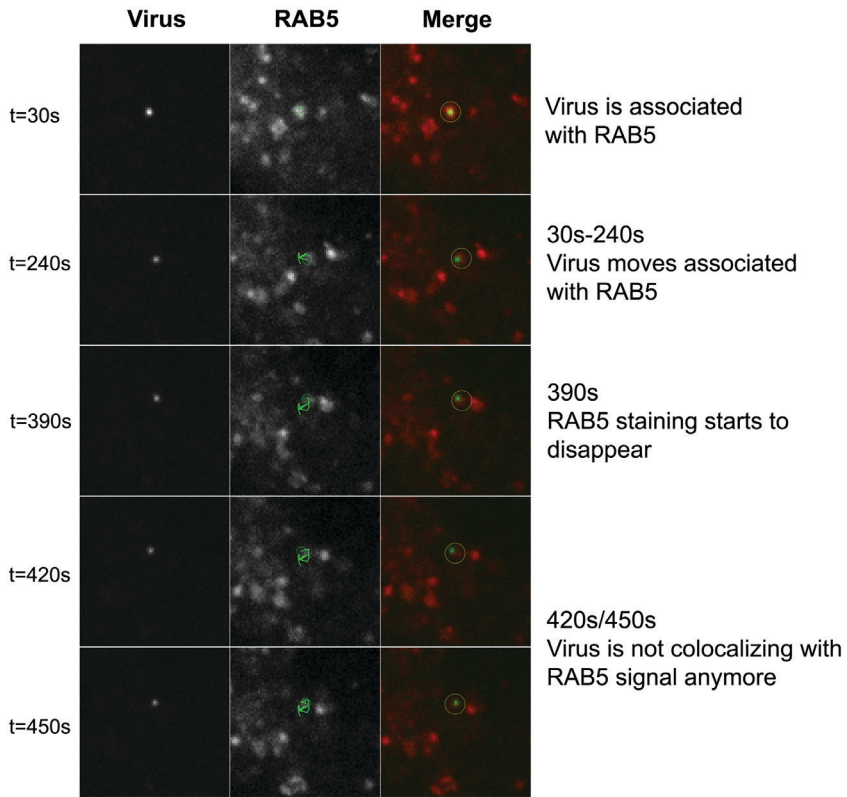


Figure S3. Stills from live-cell co-localization studies of MHV-DL488 with RAB5. Green fluorescently-labeled MHV-DL488 virus was bound to RAB5-mRFP expressing HeLa-mC-C1a cells at 4°C at MOI=20 for 90min. Inoculation medium was replaced by warm, trypan blue-containing medium, which shifts the emission spectrum of surface bound particles and thereby renders them undetectable in the 505-530nm channel [65]. Cells were imaged using a spinning-disc confocal microscope acquiring z-stacks in 30s intervals over 10min time intervals from 10-70min post warming. Virus particles were automatically detected and circled in the green channel. Upon overlay of the selected virion areas with the red channel co-localization was assessed by measurement of the underlying pixel density. Virion and endosomal vesicle movement were manually tracked separately in x/y- and z-direction. Co-localization over time was analyzed and scored (Fig. 4). A virion is shown, which is initially co-localizing/ associating with RAB5. The virus moves together with the vesicle in x/y- and z-direction. 390s after the start of the recording the RAB5 staining surrounding the virion starts to disappear, indicating that the virus is now dissociated from the RAB5-positive vesicle (classified as ‘As-soc/Dissoc’ in Fig. 4B).

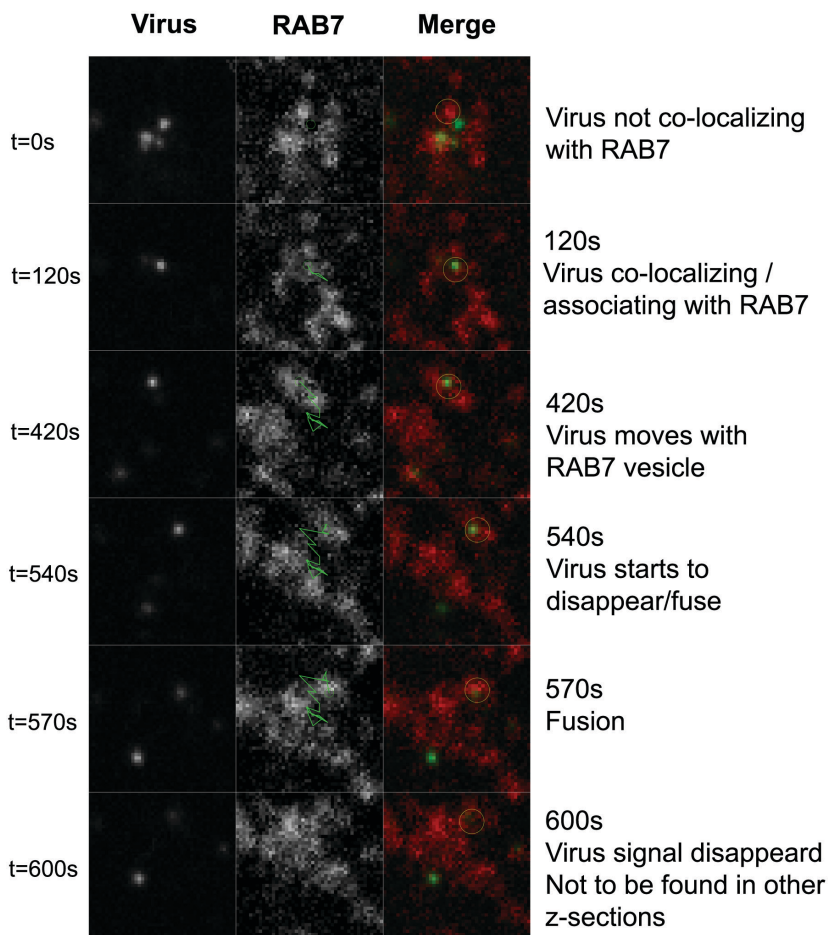


Figure S4. Stills from live-cell co-localization studies of MHV-DL488 with RAB7. Live cell imaging was performed as described in the legend to supplementary Fig. S2, using cells expressing RAB7-mRFP instead of RAB5-mRFP. A virion is shown, which is initially not co-localizing with a RAB7 vesicle. 120s after the start of the recording the virus associates with the RAB7-positive late endosomal/lysosomal (LE/LY) vesicle. The virus moves together with the vesicle in x/y- and z direction until about t=540s, after which the green fluorescence of the virus starts to disappear. At t=600 sec, the green fluorescence has disappeared completely indicating that the virus has fused with the late endosomal/lysosomal compartment (classified as ‘Fusing’ in Fig. 4B).

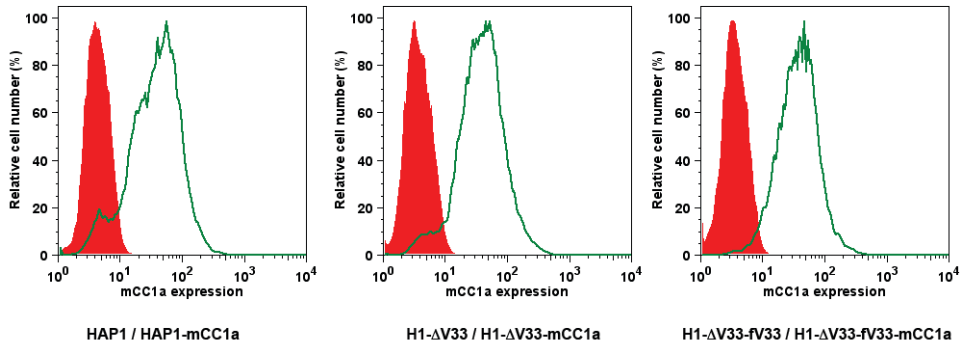


Figure S5. Confirmation of even expression of mCeacam in haploid cells. HAP1, H1-ΔV33, and H1-ΔV33-fV33 cells and their stably mCeacam1a expressing counterparts were immunostained using N-CEACAM-Fc [80] primary and secondary AF488 goat anti-rabbit antibody and analyzed by FACS. Left panel shows HAP1 (red) and HAP1-mCC1a cells (green), middle H1-ΔV33 (red) and H1-ΔV33-mCC1a (green), right H1-ΔV33-fV33 (red) and H1-ΔV33-fV33-mCC1a (green).

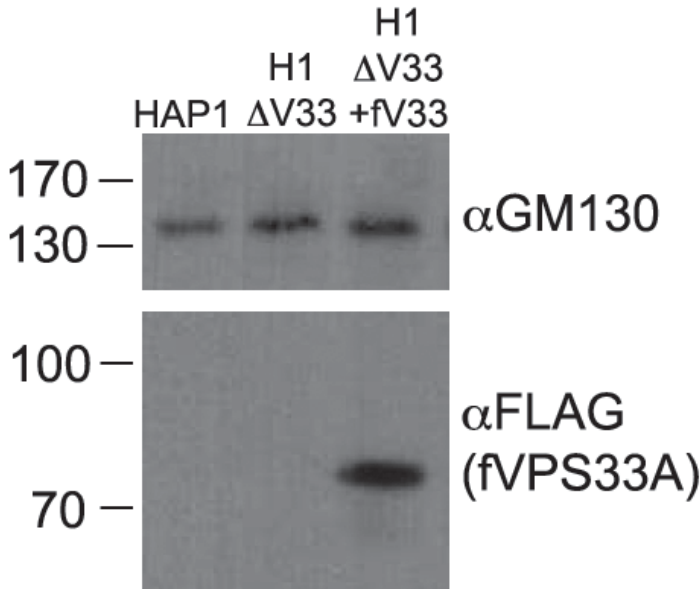


Figure S6. Confirmation of re-transfection of FLAG-VPS33A. Lysates of HAP1, H1-ΔV33, and H1-ΔV33-fV33 cells, the latter stably re-transfected with FLAG-VPS33A, were subjected to immunoblotting after gel electrophoresis. Antibodies used were against FLAG and GM130, the latter to control the loading, were used.

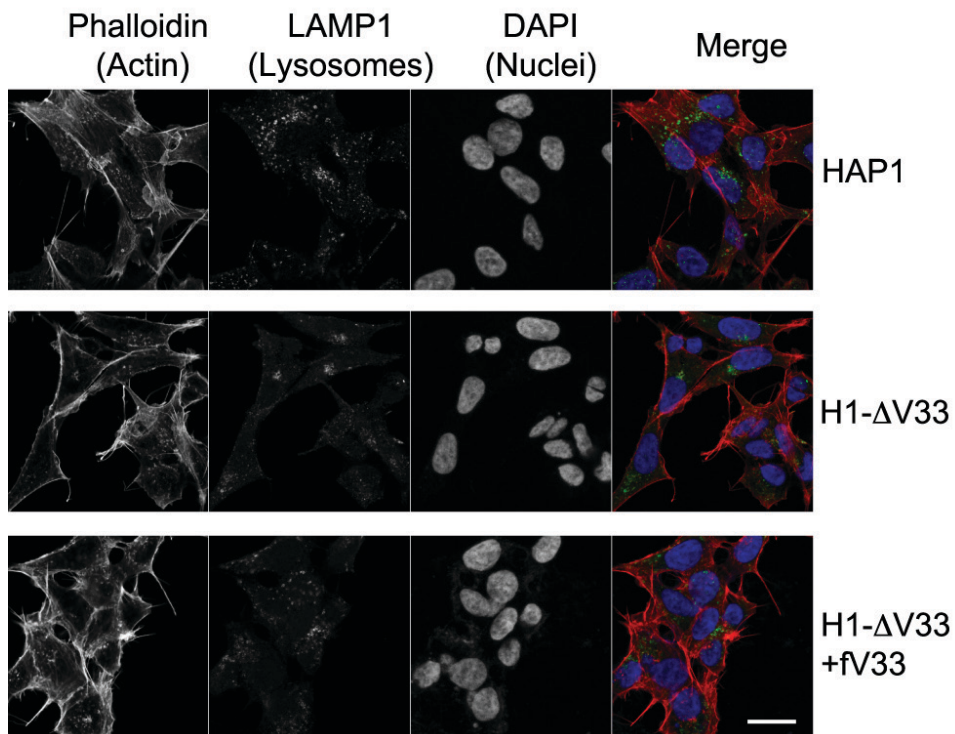


Figure S7: Localization of lysosomes is affected in haploid cells lacking VPS33A. HAP1, H1-ΔV33, and H1-ΔV33-fV33 cells were fixed and stained with rabbit anti-LAMP1 and AF488-conjugated anti-rabbit, AF568-conjugated Phalloidin, and DAPI. Cells were analyzed by confocal microscopy. Scale bar indicates 20mm.

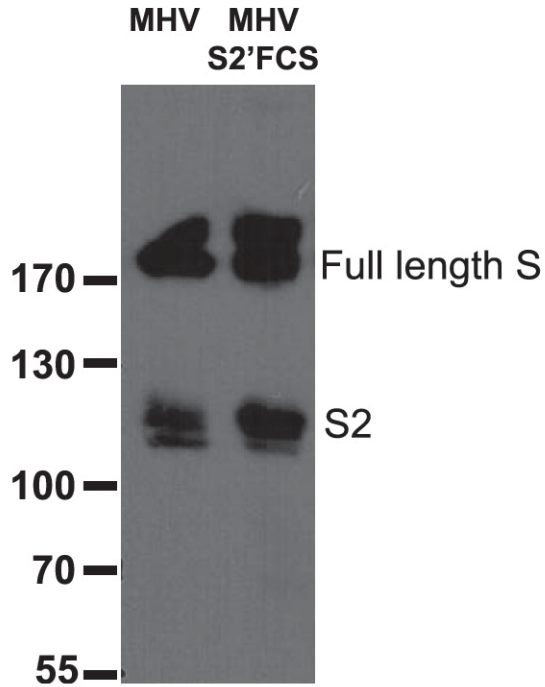


Figure S8. Western blot analysis of spike proteins of purified MHV and MHV-S2'FCS. 20% sucrose cushion purified MHV (MHV) and MHV-S2'FCS were subjected to gel electrophoresis and immunoblotting using antibodies recognizing the carboxy-terminal part of the spike protein. Regardless of the virus preparations used, either the full length S protein or the full length S2 subunit is detected with this antibody. There is no indication that the S protein carrying the FCS is cleaved during biogenesis of the virus ore thereafter.

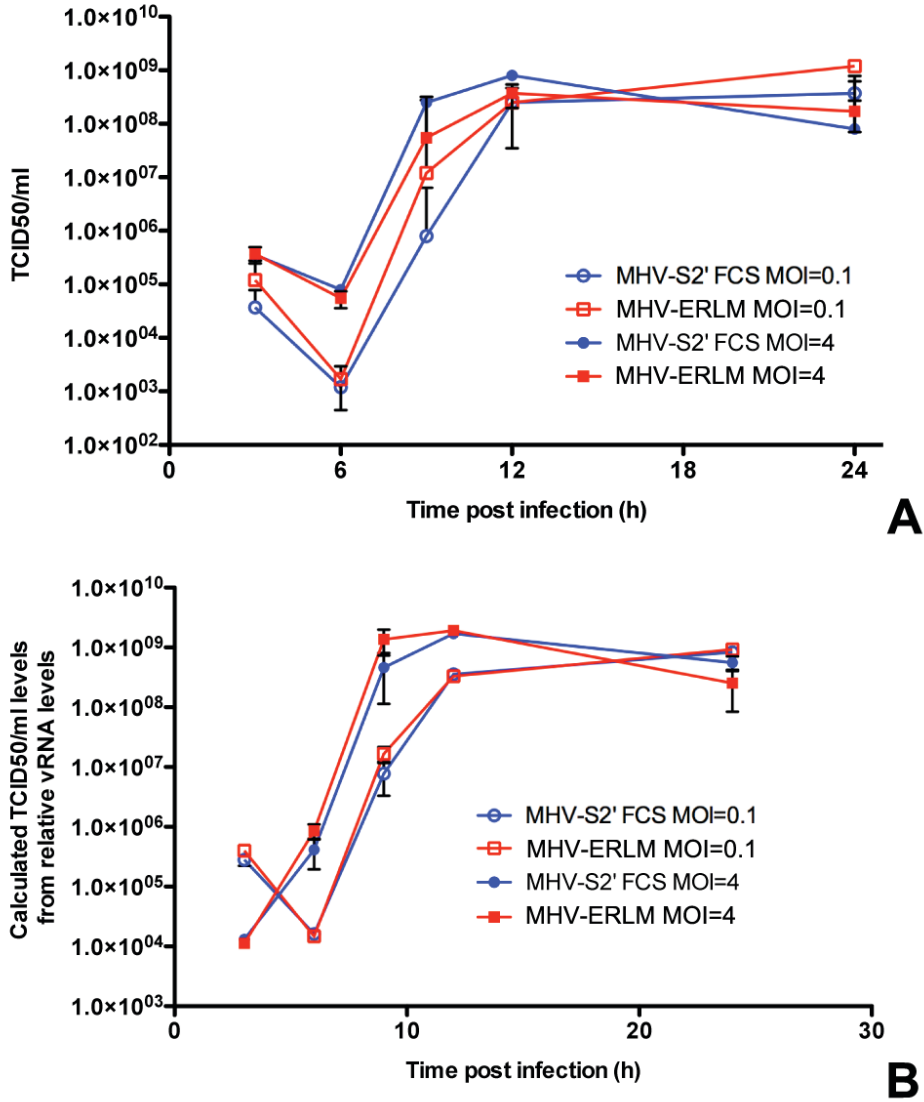
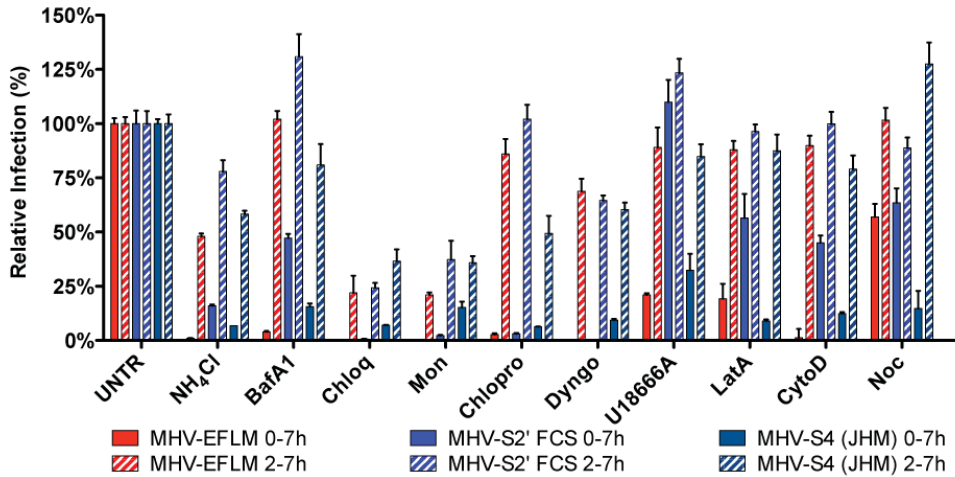


Figure S9. Growth curve of MHV and MHV-S2'FCS. LR7 cells were inoculated with the wild type S containing MHV (MHV-ERLM) or MHV-S2'FCS. At the indicated times thereafter, cell culture supernatants were collected for **A**) TCID50 analysis or **B**) measurement of the amount of released viral RNA by qRT-PCR. Error bars represent SEM, n=3.



Figures S10. Effects of endocytosis-affecting agents on MHV-S2'FCS and MHV-S4 (JHM) infection. HeLa-mCC1a cells were inoculated with MHV-EFLM, MHV-S2'FCS, or MHV-S4 (JHM) at MOI=0.2 or MOI=0.1 (MHV-S4) for 2h. Cells were (pre-)treated with ammonium chloride (NH₄Cl), Bafilomycin A1 (BafA1), Chloroquine (Chloq), Monensin (Mon), Chlorpromazine (Chlopro), Dyngo-4A, U18666A, Latrunculin A, (LatA), Cytochalasin D (DytoD), and Nocodazole (Noc), from 30 min prior to 7h post infection (0-7) or from 2 to 7h post infection (2-7). Infection levels were determined by measuring the luciferase activity in cell lysates relative to mock-treated cells (UNTR). Error bars represent 1 SEM, n=3*3.

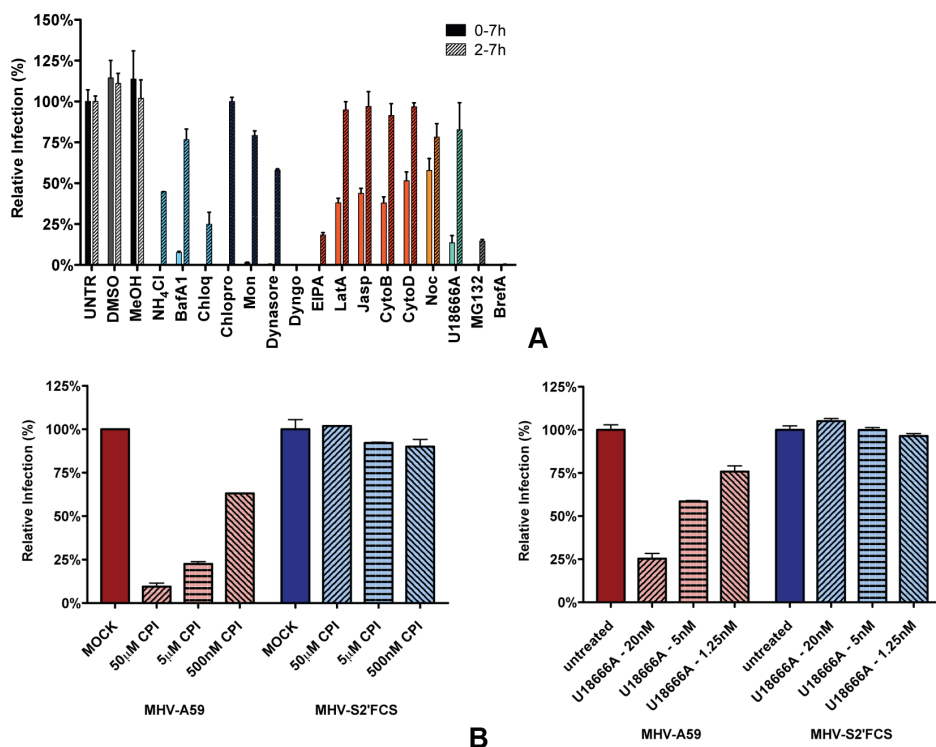
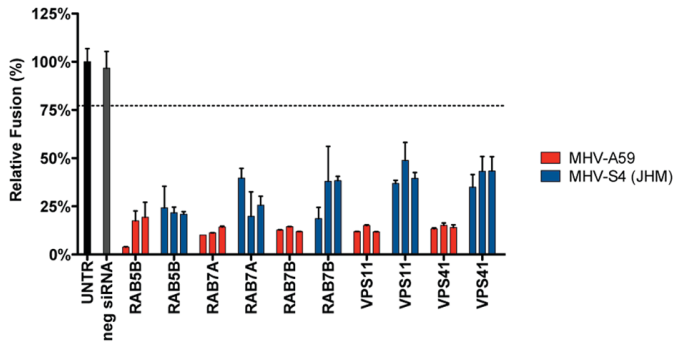
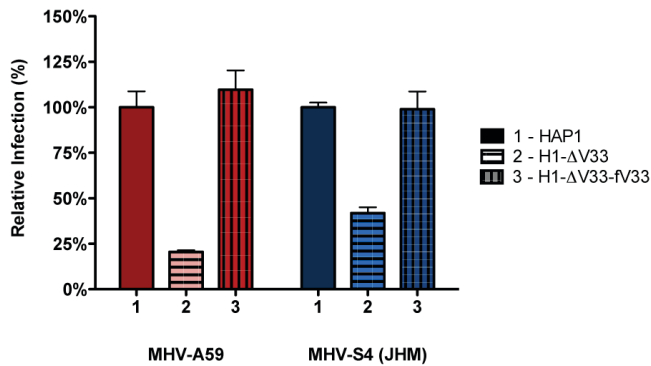


Figure S11. Entry of MHV-A59 in murine LR7 cells also requires endosomal maturation.

A Clathrin-mediated endocytosis and late endosome-to-lysosome trafficking is required for entry of MHV in murine LR7 cells. LR7 cells, inoculated with MHV-EFLM at MOI=0.2, were treated with the different inhibitors from 30 min prior to 7h post inoculation (0-7h) or from 2-7 h post inoculation (2-7h; hatched bars): ammonium chloride (NH₄Cl), Bafilomycin A1 (BafA1), Chloroquine (Chloq), Chlorpromazine (Chlopro), Monensin (Mon), Dynasore, Dyngo-4A (Dyngo), EIPA, Latrunculin A (LatA), Jasplakinolide (Jasp), Cytochalasin B (CytoB), Cytochalasin D (CytoD), Nocodazole (Noc), MG132, Brefeldin A (BrefA), as well as solvents dimethyl sulfoxide (DMSO) and methanol (MeOH). Infection levels were determined by measuring the luciferase activity in cell lysates relative to mock-treated cells (UNTR). **B** Pan-lysosomal protease inhibitor CPI blocks infection of LR7 cells with MHV-EFLM (MHV-A59) but not with MHV-S2'FCS. Cells were pretreated with increasing concentrations of CPI for 30min. Subsequently cells were inoculated with luciferase-expressing MHV-A59 or MHV-S2'FCS at MOI=0.2. Inoculum was removed at 2hpi and infection allowed to continue until 7hpi. The inhibitor was kept present at the same concentration throughout the experiment. Infection levels were determined by measuring the luciferase activity in cell lysates relative to lysates of mock-treated cells. **C** U18666A inhibits infection of LR7 cells with MHV-EFLM (MHV-A59) but not MHV-S2'FCS. Concentration dependent-inhibition of infection by U18666A was determined as described in B for CPI. **A-C**) Error bars represent SEM, n=3*3.



A



B

Figure S12. MHV-S4 (JHM) requires late endosomal factors and a functional HOPS complex for efficient infection. **A)** siRNA-mediated gene silencing was performed as described in the legend to Figure 1. At 72h post transfection, HeLa-mCC1a were inoculated with MHV-EFLM-S4 (JHM) or MHV-EFLM at MOI=0.2 and incubated until 7hpi. Infection levels were determined by measuring the luciferase activity in cell lysates relative to mock-treated cells. Dotted line shows the lower 95% confidence interval of the negative siRNA controls. **B)** Haploid HAP1 cells (HAP1), haploid cells lacking VPS33A (H1-ΔV33) or VPS33A-lacking haploid cells retransfected with FLAG-tagged VLP33A (H1-ΔV33-fV33) were infected (MOI=0.2) with MHV-EFLM (MHV-A59) or MHV-S4 (JHM) for 7h. Infection levels were determined by measuring the luciferase activity in cell lysates relative to mock-treated cells. **A, B)** Error bars represent SEM, n=3*3.

CHAPTER

FIVE

ATP1A1-mediated Src signaling inhibits coronavirus entry into host cells

Christine Burkard, Monique H Verheije, Bart L Haagmans,
Frank J van Kuppeveld, Peter J M Rottier, Berend-Jan Bosch,
Cornelis A M de Haan

Under Review

ABSTRACT

Besides by transporting ions the multi-subunit Na^+, K^+ -ATPase also functions by relaying cardiotoxic steroid-binding induced signals into cells. In this study we analyzed the role of Na^+, K^+ -ATPase and in particular of its ATP1A1 α -subunit during coronavirus (CoV) infection. Using gene silencing, the ATP1A1 protein was shown to be critical for infection of cells with murine hepatitis virus (MHV) and feline infectious peritonitis virus (FIPV), but not influenza A virus (IAV). Lack of ATP1A1 did not affect virus binding to host cells, but resulted in reduced fusion of MHV with these cells. Consistently, nanomolar concentrations of the cardiotoxic steroids ouabain or bufalin, which are known not to affect the transport function of Na^+, K^+ -ATPase, inhibited infection of cells with MHV, FIPV and MERS-CoV, but not IAV, when the compounds were present during virus inoculation. Cardiotoxic steroids were shown to inhibit entry of MHV at an early stage, resulting in accumulation of virions close to the cell surface and causing reduced fusion. Viral RNA replication was not affected when these compounds were added after virus entry. The anti-coronaviral effect of ouabain could be relieved by the addition of different Src kinase inhibitors, indicating that Src signaling mediated via ATP1A1 plays a crucial role in the inhibition of infections by CoVs.

IMPORTANCE

5

Coronaviruses (CoVs) are important pathogens of animals and humans as demonstrated by the recent emergence of new human CoVs of zoonotic origin. Antiviral drugs targeting CoV infections are lacking. In the present study we show that the ATP1A1 subunit of Na^+, K^+ -ATPase, an ion transporter and signaling transducer, supports CoV infection. Targeting ATP1A1 either by gene silencing or by low concentrations of the ATP1A1-binding cardiotoxic steroids ouabain and bufalin, resulted in inhibition of infection with murine, feline and MERS-CoVs at an early entry stage. Src signaling mediated by ATP1A1 was shown to play a crucial role in the inhibition of CoV entry by ouabain and bufalin. These results suggest that targeting the Na^+, K^+ -ATPase using cardiotoxic steroids, several of which are FDA-approved compounds, may be an attractive therapeutic approach against CoV infection.

INTRODUCTION

Despite the wide variety of vaccines already available to prevent viral infections, unexpected epidemics caused by zoonotic viruses, such as SARS-CoV in 2002/03 and the new pandemic H1N1 influenza A virus (IAV) in 2009, underscore the need for additional antiviral measures. Compound- and siRNA screening may aid the development of antiviral therapies by the discovery of lead compounds and target proteins (1-3). Elucidating the mechanisms by which such proteins act during infection and how drugs can interfere with the pathogen life cycle is of crucial importance herein.

Coronaviruses (CoVs) are enveloped, plus-strand RNA viruses of the *Coronaviridae* family in the order *Nidovirales*. These viruses generally cause respiratory and/or intestinal tract disease. CoVs are important pathogens of domestic livestock, poultry and companion animals as exemplified by porcine epidemic diarrhea virus, infectious bronchitis virus, and feline infectious peritonitis virus (FIPV), respectively. In addition, the emergence of new human CoVs of zoonotic origin has shown the potential of CoVs to cause life-threatening disease in humans as was demonstrated by the 2002/2003 SARS-CoV epidemic and by the recent emergence of MERS-CoV (4, 5). The murine hepatitis coronavirus (MHV) is often employed as a safe model to study CoV infections.

Like all other viruses, CoVs depend on the cellular machinery for efficient infection and replication in their host cells. The CoV infection cycle starts with attachment of the virus to a specific cellular receptor, mediated by the viral spike protein (S). Upon endocytic uptake, which has been demonstrated to occur via clathrin-mediated endocytosis for MHV (6), conformational changes in the S protein induce virus-cell fusion. The genomic RNA is thereby released into the cytoplasm and becomes translated, resulting in the formation of RNA replication-transcription complexes associated with rearranged cellular membranes (7). Structural proteins together with newly generated genomic RNAs assemble into progeny virions via budding through the membranes of the ER-to-Golgi intermediate compartment. Virions are subsequently released via exocytosis (8).

The Na⁺,K⁺-ATPase is perhaps one of the best studied membrane ion transporters. Discovered in 1957 and identified as an ion-activated ATPase in 1965, it is mainly known for its transport function of K⁺ and Na⁺ at a ratio of 2:3, creating an electrochemical gradient across the plasma membrane (9). The Na⁺,K⁺-ATPase consists of two functional (α and β) and one regulatory subunit (γ subunit or FXVD protein). The α -subunit is a large, catalytic membrane protein, containing 10 transmembrane domains that create five extracellular and four intracellular loops. Four different isoforms of the α -subunit exist, which are encoded by *ATP1A1-4*. The $\alpha 1$ -isoform is ubiquitously expressed in almost all tissues. The β -subunit is a type II membrane protein, responsible for the proper translocation of the α -subunit into the endoplasmic reticulum and its delivery to the cell surface and is crucial to the functioning of the pump. Little is known about the function of the regulatory subunit γ (reviewed in (10)). Specific inhibitors of the Na⁺,K⁺-ATPase, so called cardiotonic steroids (CTSs), can block the transport function of the pump and are used to treat congestive heart failure. Well-known CTSs are the foxglove plant-derived digoxin and ouabain, and the vertebrate-derived analogues bufalin and marinobufagenin (11, 12).

In addition to the classical ion-pumping function of the Na⁺,K⁺-ATPase, more recent work has shown additional roles of Na⁺,K⁺-ATPase in signal transduction. Especially the

α -subunit appears to be associated with a number of additional proteins and to carry out various signaling functions (reviewed in (13, 14)), which may differ between the different α -subunit isoforms (15). (Endogenous) CTSs can trigger the signaling functions of the Na^+, K^+ -ATPase at concentrations that do not affect the pump function or intracellular ion concentration (16-21). There are four main signaling targets of α -subunit known so far; PI3K, Src, IP3R, and PLC. Binding of nanomolar concentrations of ouabain to Na^+, K^+ -ATPase triggers a conformational change in the α -subunit, which activates the bound Src protein and results in the recruitment of other signaling factors. Activation of these targets may lead to a number of downstream signaling effects controlling apoptosis, cell-cell interaction, gene-expression, as well as other processes (16-18, 22-28).

In a high-throughput RNAi screen we previously identified ATP1A1 as a protein that supports MHV infection (unpublished results). ATP1A1 is an appealing antiviral target in view of the large number of (FDA-approved) compounds available that target this protein. Therefore, the main goal of the present study was to obtain mechanistic insight into the role of the Na^+, K^+ -ATPase in CoV infection. Targeting ATP1A1 either by gene silencing or by low concentrations of CTSs ouabain and bufalin resulted in inhibition of CoV infection at an early entry stage. Src signaling mediated by ATP1A1 was shown to play a crucial role in the inhibition of CoV entry by CTSs. These results suggest that targeting the Na^+, K^+ -ATPase using CTSs may be an attractive therapeutic approach against CoV infection.

MATERIALS AND METHODS

Cells, viruses, and plasmids.

Murine LR7 (29) (murine L-2 fibroblast cells (ATCC), stably expressing murine CEACAM1a (mCC1a), and feline FCWF cells (ATCC) were used to propagate the (recombinant) MHV and FIPV viruses, respectively. MDCK-HA and Huh7 cells were used to propagate *Renilla* luciferase expressing IAV-WSN pseudovirus (IAV-Rluc) or MERS-CoV, respectively, as described previously (30, 31). Cells were maintained as monolayers cultured in Dulbecco's modified Eagle's medium (DMEM, Lonza), supplemented with 10% fetal bovine serum (FBS). HeLa-ATCC cells stably expressing mCC1a (HeLa-mCC1a;(32)) and HeLa-fAPN cells (33) were used for infection experiments with MHV and FIPV, respectively. HeLa-mCC1a cells stably expressing the defective β -galactosidase Δ M15 (HeLa-mCC1a- Δ M15) were used in entry assays (34). Generation of recombinant viruses MHV-EFLM (35), FIPV- Δ 3abcRL (36), IAV-Rluc pseudovirus (30), MHV- α N(34), MHV-2aFLSRec (37), and MHV-S2'FCS (32) has been described previously. MHV-2aGFPSRec, which contains a GFP expression cassette between the 2a and the S gene at the position of the HE pseudogene was generated similarly as described for MHV-2aFLSRec (37). cDNAs encoding human or mouse ATP1A1 were obtained from Thermo Scientific Open biosystems. ATP1A1 cDNAs were subcloned into a pCAGGS expression vector, using conventional cloning methods, thereby generating pCAGGS-hATP1A1 and pCAGGS-mATP1A1.

Chemicals.

The MHV fusion inhibitor HR2 peptide has been described before (38) and was synthesized by GenScript. The peptide was diluted in Tris/HCl 50 mM, pH7.8, 4 μ M EGTA at 1 mM stock solution and used at 10 μ M final concentration. Stocks of 125 μ M bafilomycin A1 (BafA1, Enzo Life Sciences), 15 mM Dyngo-4a (Dyngo, Abcam), 500 μ M wortmannin (Wort, Enzo Life Sciences), 10 mM PP2 (Sigma), and 10 μ M bufalin (Buf, Enzo Life Sciences) were prepared in DMSO and diluted 1:1000 in the experiments, except when indicated otherwise. Stocks of 10 mM chlorpromazine (Chlopro, Sigma), 20 mM U18666A (Enzo Life Sciences), 50 μ M ouabain (Ou, Sigma) were prepared in H₂O and diluted 1:1000 in the experiments, except when indicated otherwise. pNaKtide peptide (39), which was kindly provided Z. Xie (Marshall University, Institute for Interdisciplinary Research), was dissolved in PBS at 2 mM and used at 2 μ M final concentration. Solvent DMSO was obtained from Sigma-Aldrich.

siRNA transfections.

In assays using luciferase-based read-outs 96-well plates were used. For other assays a 24-well plate format was used. 7,500 or 30,000 HeLa-mCC1a or HeLa-fAPN cells were seeded one day prior to transfection in each well of the 96-well or 24-well plate, respectively. Using Oligofectamine (Life Technologies) reagent three independent, non-overlapping siRNAs (Ambion) targeting ATP1A1 were individually transfected into target cells according to the manufacturer's instructions. Transfection mix for four wells (96-well format) or 1 well (24-well format) contained 2.5 μ l of 1 μ M siRNA and 0.5 μ l Oligofectamine in 50 μ l OptiMEM (Gibco). Transfection was done in 62.5 μ l or 250 μ l final volume of OptiMEM, while 4 hours post transfection 32 μ l or 125 μ l of DMEM, 30% FBS were added, depending on the plate format used. Cells were infected 72 hours post transfection.

qRT-PCR of siRNA-mediated gene knockdowns.

HeLa-mCC1a cells were subjected to siRNA-mediated gene knockdown as described above. At 72 hpi cells were harvested by trypsinization, single-cell suspension counted, and collected by centrifugation. Cellular RNA was extracted using the RNeasy Mini Kit (Qiagen). mRNA levels of genes were analyzed by qRT-PCR using a custom designed pair of specific primers to the gene resulting in an approximately 150 bp product. RNA levels were measured using the GoTaq[®] 1-Step RT-qPCR system (Promega) according to the manufacturer's instructions on a LightCycler 480 (Roche). Expression levels were corrected for cell number and viability as determined by the Wst-1 assay (Roche), which were hardly affected, if at all, however by transfection of the siRNAs.

Virus infections.

Cells were inoculated with MHV-EFLM, FIPV-RLuc, IAV-RLuc, MHV-S2'FCS, or MHV-2aFLSRec at MOI=0.1 in DMEM, 2% FBS, for 2 h at 37°C. Cells were lysed at 7 hpi (MHV and FIPV) or 16 hpi (IAV) in passive lysis buffer (Promega). Firefly luciferase expression was assessed using the firefly luciferase assay system from Promega or using a homemade system (50 mM tricine, 100 μ M EDTA, 2.5 mM MgSO₄, 10 mM DTT, 1.25 mM ATP, 12.5 μ M D-Luciferin). *Renilla* luciferase expression was assessed using the *Renilla* luciferase assay system (Promega). Light emission was measured on a Centro LB 960 luminometer. When indicated cells were transfected with siRNAs prior to inoculation as described above. Luciferase expression levels (in relative light units, RLU) were corrected for cell number and viability as determined by the Wst-1 assay (Roche). When indicated cells were treated with pharmacological inhibitors starting at 30 min prior to or 2 h post inoculation.

At 72 h after transfection, siRNA transfected cells were inoculated with MHV-2aGFP-SRec at MOI=0.5 (15-20% infected cells) in DMEM, 2% FBS, for 2 h at 37°C. The inoculum was replaced by warm DMEM, 10% FBS. At 8 hpi, cells were trypsinized and fixed in 4% formaldehyde solution in PBS. Cells were washed and taken up in FACS buffer (2% FBS, 0.05M EDTA, 0.2% NaN₃ in PBS) and GFP expression was quantified by FACS analysis on a FACS Calibur (Benson Dickson) using FlowJo software. Of each sample at least 10,000 cells were analyzed.

Vero cells were inoculated with MERS-CoV at a MOI of 0.1 in FBS-containing DMEM. 8 h post infection, cells were fixed in 4% formaldehyde in PBS. Cells were stained using rabbit anti-SARS-CoV nsp4 antibodies that are cross-reactive for MERS-CoV, according to a standard protocol using a FITC-conjugated swine-anti-rabbit antibody. Number of infected cells was determined by cell counts on a wide-field fluorescent microscope. Cells were treated with ouabain or bufalin starting at 30 min prior to or 2 h post inoculation.

Binding, internalization and fusion assays using β -galactosidase complementation.

The replication-independent binding, internalization, and fusion assays were performed as described previously (34). The assay is based on complementation of an otherwise defective β -galactosidase Δ M15 protein by a small intravirion peptide that is genetically fused to the N protein. Briefly, in the binding and internalization assay MHV- α N virus was bound to HeLa-mCC1a- Δ M15 target cells at MOI=10 for 90 min on ice. In the binding assay unbound virus was removed and cells and viruses lysed with NP-40 lysis buffer buffer

(50 mM Tris/HCl pH 8.0, 150 mM NaCl, 0.5% NP-40). Complementation was analyzed using a Centro LB 960 luminometer (Berthold technologies). 30 μ l/well Beta-Glo reagent (Promega) was added to each well, the sample was mixed and incubated for 60 min and light units were measured over 0.1 second. In the internalization assay unbound virus was removed after binding and cells shifted to 37°C for 60 min. Cells were trypsinized to remove surface-bound but not internalized virus. Cells were lysed and complementation measured as described above. Dependent on the experiment type cells were transfected with siRNA for 72h as described above or pre-treated with drugs for 30 min prior to binding or internalization experiments.

To assay fusion cells were preloaded with FDG substrate by incubation of adherent target cells with 2.5% FBS, 100 mM FDG, 50% PBS at room temperature. After 3 min incubation an excess of 5% FBS in PBS was added, supernatant removed and replaced by growth medium. When pharmacological inhibitors were used cells were (mock) treated with the different inhibitors for 30 min after a recovery period of 30 min at 37°C. MHV-aN virus was bound to cells in DMEM with 2%FCS (in the absence or presence of inhibitors) at a MOI=20 for 90 min at 4°C to synchronize infection, after which cells were shifted to 37°C for 2 h. Cells were trypsinized and transferred to Eppendorf tubes, washed and immediately analyzed by FACS. siRNA transfections were performed 72h prior to fusion assays.

Ouabain time of addition experiment

MHV-EFLM virus was bound to HeLa-mCC1a cells on ice at MOI=0.5 for 90 min. Warm medium containing 10% FBS was added and cells incubated for 7h at 37°C, 5% CO₂. At time points indicated the medium was replaced by warm medium containing 50nM ouabain. 7 hpi cells were lysed and luciferase expression analyzed as described above.

Effect of ouabain on virus entry using fluorescently labeled MHV.

DyLight 488 covalently labeled MHV virus was made as described before (32). Briefly, MHV strain A59 virus was grown in LR7 cells and purified using a sucrose cushion and gradient purification. After purification virus was labeled using DyLight NHS 488 (Thermo Scientific) according to the manufacturer's instructions. Infectivity of the labeled virus was confirmed by TCID₅₀ analysis and qRT-PCR. Fluorescently labeled virus was bound to cells, either mock treated or pre-treated with ouabain for 30 min, on ice at MOI=10 for 90 min. Unbound virus was removed and virus allowed to infect for 90 min in presence or absence of ouabain. Cells were subsequently fixed and stained with DAPI (Invitrogen) and Alexa Fluor 568 Phalloidin (Life Technologies). The samples were analyzed using a confocal laser-scanning microscope (Leica SPE-II).

RESULTS

RNAi-mediated gene silencing of ATP1A1 inhibits infection with MHV and FIPV but not IAV.

In a high-throughput RNAi screen ATP1A1 was found to be required for efficient infection of HeLa cells with MHV. To validate this finding and to see whether ATP1A1 is also required for infection with other CoVs, we performed a follow-up analysis using siRNA-mediated gene silencing with oligonucleotides from a different supplier. HeLa cells or HeLa cells carrying the receptor for MHV (HeLa-mCC1a cells) or for FIPV (HeLa-fAPN) were transfected with siRNAs for 72h. Subsequently, cells were infected with luciferase expressing MHV (MHV-EFLM, (35)), FIPV (FIPV- Δ 3abcRL; (36)), or IAV (IAV-RLuc; (30)) at a multiplicity of infection (MOI) of 0.1. At 7 hpi (MHV and FIPV) or 16 hpi (IAV), cells were lysed and firefly luciferase expression levels were determined. As negative controls, scrambled siRNAs were used. Individual transfection of each of the three siRNAs targeting ATP1A1 resulted in reduced infection of cells with MHV and FIPV. IAV infection was not affected by siRNA-mediated gene silencing of ATP1A1 (fig. 1A). To confirm the efficacies of the siRNAs at the mRNA level, quantitative RT-PCR analysis was performed. All three siRNAs reduced the ATP1A1 mRNA levels with approximately 95% (fig. 1B). From these results we conclude that ATP1A1 is required for efficient infection of cells with MHV and FIPV, but not IAV.

RNAi-mediated gene silencing of ATP1A1 inhibits fusion of MHV.

To investigate whether the siRNA-mediated silencing of ATP1A1 affected entry of MHV we made use of a recently developed, replication-independent binding, internalization, and fusion assay (34). The assay is based on minimal complementation of defective β -galactosidase (β -galactosidase Δ M15) with the short α -peptide (40) that is genetically fused to the intravirion N protein in MHV- α N. Prior to virus binding, Δ M15-expressing cells were transfected with siRNAs for 72h. After binding of virus particles to cells on ice unbound viruses were removed and cells and viruses were lysed (binding assay). In the internalization assay MHV- α N was bound to cells on ice, unbound virus was removed, and virus was subsequently allowed to internalize at 37°C for 60 min, after which cell-surface bound virus particles were removed by protease treatment prior to lysis of cells and viruses. Virus particle binding and internalization into cells were quantified by measuring the amount of luminescence generated after addition of Beta-Glo substrate to the cell lysate. As shown in figure 2, both virus binding and internalization did not appear to be affected by siRNA-mediated silencing of ATP1A1. To measure fusion, MHV- α N was bound to cells pre-loaded with fluorescein-di- β -D-galactopyranoside (FDG). After binding virus was allowed to internalize and fuse. Conversion of the non-fluorescent substrate FDG by reconstituted β -galactosidase into the green fluorophore fluorescein (FIC) in intact cells was measured by FACS. In contrast to virus binding and internalization, fusion of MHV was inhibited by the lack of ATP1A1 relative to the negative-control siRNAs (fig. 2).

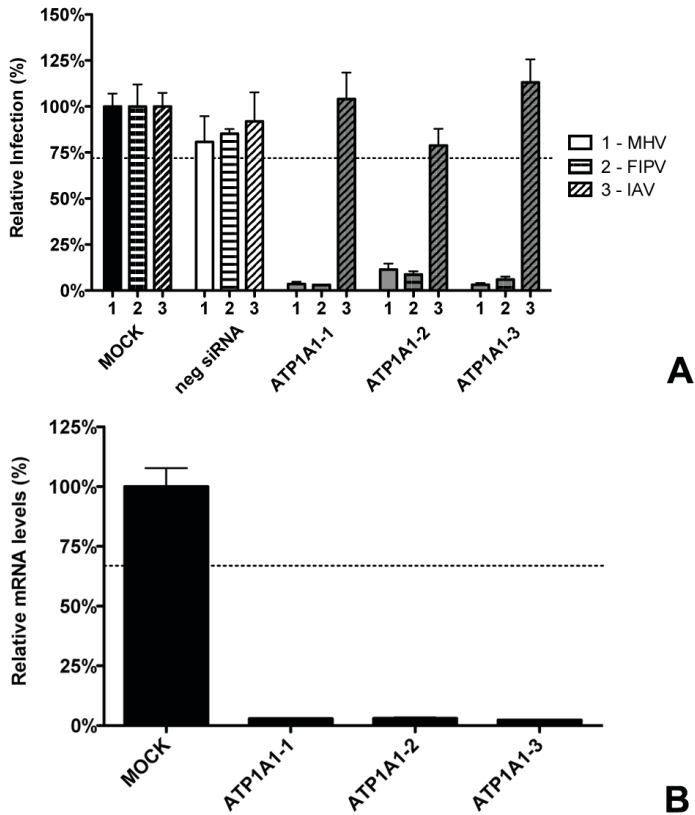


Figure 1: RNAi-mediated downregulation of ATP1A1 affects MHV and FIPV but not IAV. A) Effect of RNAi-mediated downregulation of ATP1A1 on MHV-ERLM, FIPV-RLuc, and IAV-RLuc. Gene silencing was performed using individual transfection of three different siRNAs targeting ATP1A1 (ATP1A1-1-3) in HeLa cells expressing the appropriate virus receptors. Negative siRNA (neg siRNA) was taken along as a control. Cells were infected with luciferase expressing viruses at MOI=0.1 for 7h or overnight for IAV. Infection levels were determined by assaying the luciferase activity in cell lysates relative to lysates of infected cells that had been mock treated. Infection levels were corrected for cell number and viability as determined by the Wst-1 assay. Error bars represent SEM, n=3*3. B) Confirmation of siRNA-mediated reduction in mRNA levels. mRNA levels at 72h post transfection were measured by qRT-PCR relative to mock-transfected cells. Expression levels were corrected for cell number and viability as determined by the Wst-1 assay. Error bars represent SEM, n=3*3. A,B) Dotted lines indicate the lower 95% confidence interval of negative siRNA controls or mock treatment, respectively.

RNAi-mediated gene silencing of ATP1A1 inhibits infection with MHV independent of the intracellular site of fusion or the identity of the receptor.

Trafficking of MHV and FIPV to lysosomes is a prerequisite for proteolytic activation of the S protein and for efficient virus-cell fusion to occur (32). To study whether downregulation of ATP1A1 inhibits MHV infection by negatively affecting the trafficking of MHV to lysosomes, we made use of a mutant MHV (MHV-S2^{FCS}), which is cleavage-activated by furin rather than lysosomal proteases, and which hence fuses in early endosomes (32). Thus,

HeLa-mCC1a cells were transfected with siRNAs for 72h, followed by inoculation with luciferase expressing MHV (MHV-EFLM) or MHV-S2'FCS at MOI=0.1. At 7 hpi cells were lysed and firefly luciferase expression levels were determined. As shown in figure 3A, transfection of siRNAs targeting ATP1A1 reduced luciferase expression levels to the same extent for both viruses. From these results we conclude that infection with MHV is negatively affected by downregulation of ATP1A1 regardless of the intracellular site of fusion.

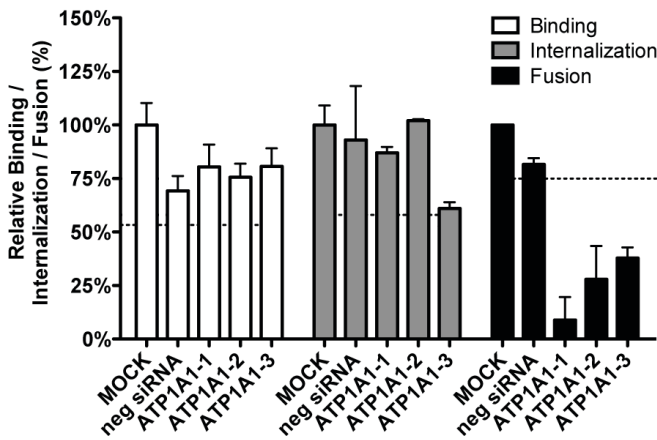


Figure 2: Knockdown of ATP1A1 affects MHV fusion. Effects of siRNA-mediated gene silencing on viral binding, internalization, and fusion using replication-independent assays. Three different siRNAs against ATP1A1 (ATP1A1-1-3) were transfected individually into HeLa-mCC1a- Δ M15. Negative siRNA (neg siRNA) was taken along as a control. At 72h post transfection MHV- α N was allowed to bind to the cells on ice at MOI=20 for 90 min. Unbound virus was washed off. For the binding assay cells and viruses were subsequently lysed and complementation of Δ M15 by α N was determined relative to mock-treated samples using Beta-Glo substrate and a luminometer. For internalization and fusion assays the cells were warmed to 37°C and virus was allowed to enter cells for 60 and 100 min, respectively. To assay internalization cell surface bound virus was removed using trypsin and cells and viruses subsequently lysed. Complementation of Δ M15 by α N was determined relative to mock-treated samples using Beta-Glo substrate and a luminometer. For the fusion assay cells were pre-loaded with FDG by hypotonic shock before inoculation. Upon infection for 100 min cells were collected and analyzed by FACS. Fusion was determined relative to the number of FIC-positive cells observed upon mock treatment of infected cells. Error bars represent SEM, n=3*3 for binding and internalization, n=3 for fusion. Dotted lines indicate the lower 95% confidence intervals of the mock treatment.

CEACAM1 has been reported to interact with ATP1A1 in porcine cells (41). Since murine CEACAM1a, the natural receptor of MHV, is a homologue thereof, we investigated whether the positive effect of ATP1A1 on MHV infection is somehow linked to MHV binding to CEACAM1a. We made use of a mutant of MHV (MHV-SRec (37)), which enters cells in a CEACAM1a-independent, but heparan sulfate-dependent manner. Transfection of HeLa or HeLa-mCC1a (expressing murine CEACAM1a) cells with three different siRNAs against ATP1A1 was followed by low MOI inoculation with GFP-expressing MHV-SRec (MHV-2aGFP-SRec) or MHV (MHV-EGFPM), respectively. After 8h of infection cells were collected and GFP expression was analyzed by fluorescence-activated cell sorting (FACS). As controls siRNA silencing GFP and negative-control siRNA were used. Infection with MHV-SRec of cells lacking the MHV receptor was reduced to the same extent as MHV infection of

receptor-expressing cells by all three siRNAs targeting ATP1A1 (fig. 3B). These results indicate that, irrespective of the entry receptor, infection with MHV depends on ATP1A1.

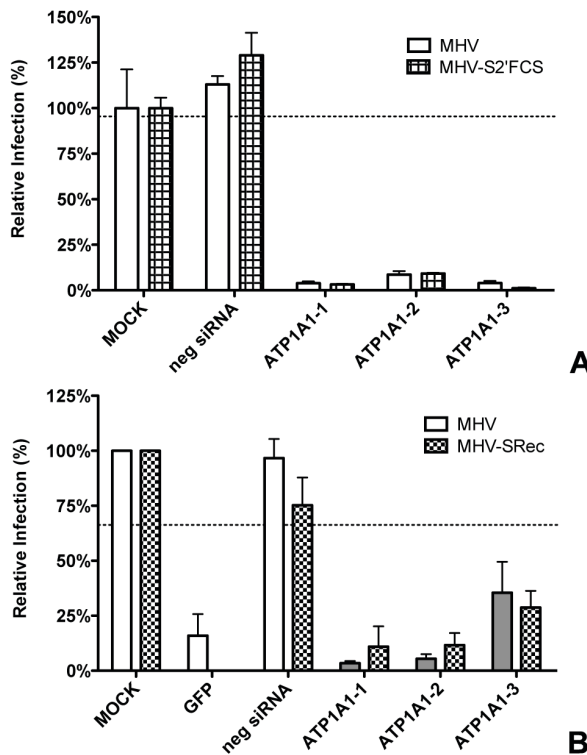


Figure 3: Knockdown of ATP1A1 inhibits infection with MHV independent of the intracellular site of fusion or the nature of the receptor used. Gene silencing was performed as described in the legend to figure 1. A) Cells were infected with luciferase expressing MHV or MHV-S2'FCS at MOI=0.1 for 7h. Infection levels were determined by assaying the luciferase activity in cell lysates relative to lysates of infected cells that had been mock treated. Infection levels were corrected for cell number and viability as determined by the Wst-1 assay. Error bars represent SEM, n=3*3. B) Cells were infected with GFP expressing MHV or MHV-SRec at MOI=0.5 for 8h. Cells were collected and virus replication and cell viability analyzed by FACS relative to mock-treated samples. Negative siRNA and siRNA targeting GFP were taken along as controls. Error bars represent SEM, n=3.

Nanomolar concentrations of CTSs inhibit infection with CoVs, but not with IAV.

High concentrations of CTSs are known to inhibit the ion-pumping function of Na⁺,K⁺-ATPase (42-44). However, recent research has revealed that CTSs, in particular ouabain and bufalin, can trigger various signal transduction pathways mediated by Na⁺,K⁺-ATPase (14, 16-21, 45, 46) at much lower concentrations. In view of the critical role of ATP1A1 on infection of MHV and FIPV, we investigated to what extent CTSs affect infection of CoVs. Therefore, HeLa cells were treated with ouabain or bufalin at high or low concentrations for 30 min and then inoculated with MHV, FIPV, MERS-CoV or IAV in the presence of the drugs, after which the CTSs were kept present until cells were lysed or fixed. CTSs were also added to cells at 2h post infection (hpi) to assess the effects of these drugs on post-entry steps. At

the indicated time points, cells were lysed or fixed and luciferase expression levels or number of virus-infected cells determined. Addition of relatively high concentrations of ouabain (250nM) or bufalin (50nM) had severe negative effects on infection with all viruses tested, both when added prior to or after inoculation (data not shown). Also translation of transfected synthetic, capped reporter mRNA was inhibited at these high concentrations (data not shown). Addition of low amounts of ouabain (50nM) or bufalin (10-15nM) inhibited infection with MHV, FIPV and MERS-CoV, but only when added prior to inoculation. Infection was not affected when the drugs were added at 2 hpi. Infection with IAV was not affected by the addition of low concentrations of ouabain or bufalin (fig. 4A and 4B). These results show that low concentrations of CTSs inhibit infection with different CoVs, but not with IAV. CTSs most likely affect CoV infection during the entry stage, as no effect was observed when they were added after inoculation.

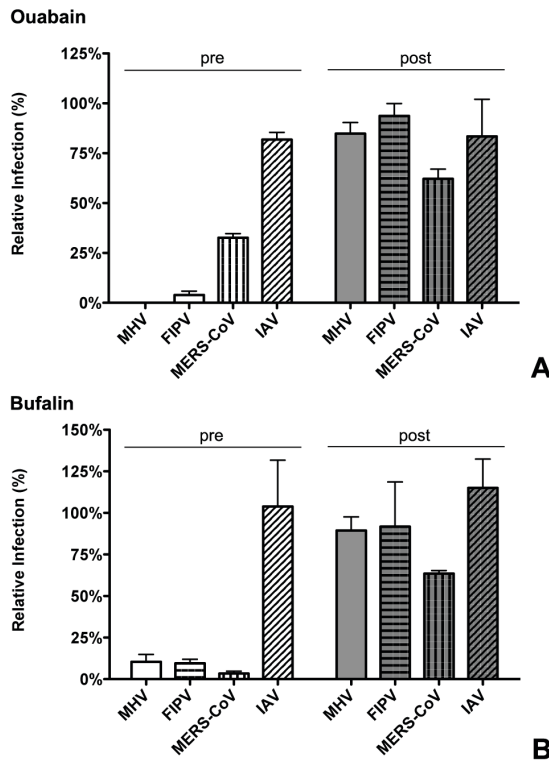


Figure 4: Low levels of ouabain and bufalin affect entry of CoVs but not of IAV. A) HeLa or Huh7 (MERS-CoV) cells were inoculated with luciferase expressing MHV, FIPV, or IAV at MOI=0.1 for 2h. Cells were treated with 50nM ouabain from 30 min prior (pre) or 2 h post (post) inoculation until 7h (MHV and FIPV), 8h (MERS-CoV) or 16h (IAV) post infection. Infection levels were determined by measuring the luciferase activity in cell lysates or by determining the number of infected cells (MERS-CoV) by immunocytochemistry relative to mock-treated cells. Error bars represent SEM, n=3*3. B) Effect of low doses of bufalin on MHV, FIPV, MERS-CoV and IAV infection. Cells were infected and treated as described in A with 10nM bufalin instead of ouabain. Error bars represent SEM, n=3*3.

Effect of ouabain on MHV is linked to ATP1A1.

To confirm that the effect of ouabain on CoV infection is indeed linked to ATP1A1 we made use of the fact that rodent ATP1A1 encoded Na⁺,K⁺-ATPase is much more resistant to ouabain due to severely decreased binding of the drug to the protein caused by two amino acid mutations in the ectodomain (47). HeLa cells were transfected with plasmids encoding either human or murine ATP1A1. Transfected cells were pre-treated with nanomolar concentrations of ouabain and subsequently inoculated with luciferase-expressing MHV or IAV in the presence of the drug. Ouabain was kept present until cells were lysed and luciferase expression levels were determined. As a control ouabain was also added to cells only from 2 hpi onwards. IAV infection was not affected by ouabain treatment, neither when human, nor when murine ATP1A1 was overexpressed (fig. 5). MHV infection of cells transfected with plasmid expressing human ATP1A1 was inhibited by ouabain. However, when the ouabain-insensitive murine ATP1A1 was overexpressed, the inhibitory effect of ouabain on infection with MHV was abolished (fig. 5). These results demonstrate that the inhibitory effect of ouabain on CoV infection is directly linked to ATP1A1.

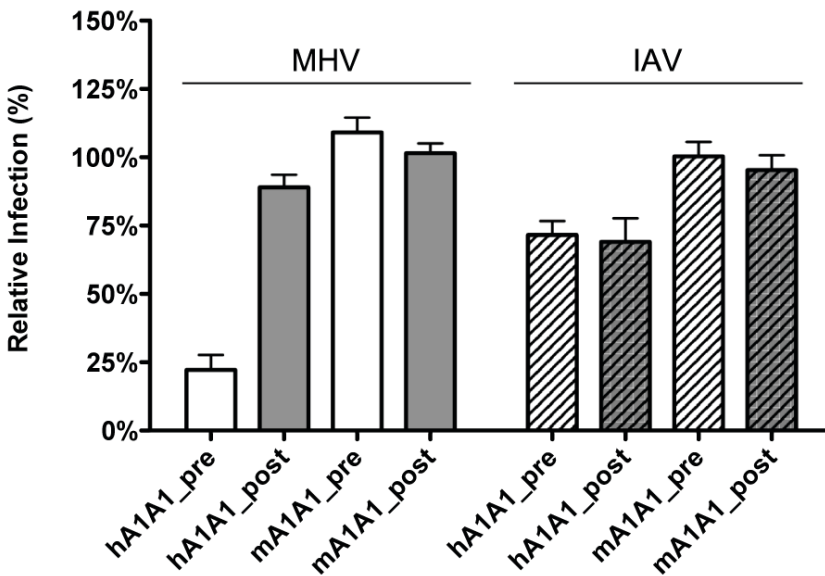


Figure 5: Effect of ouabain on MHV entry is linked to ATP1A1-encoded $\alpha 1$ -subunit. HeLa cells were transfected with plasmids expressing either human or murine derived ATP1A1 (hATP1A1 and mATP1A1, respectively). Cells were treated with 50nM ouabain from 30 min prior (pre) or from 2 h post (post) inoculation with luciferase expressing MHV or IAV at MOI=0.1 until 7h (MHV) or 16h (IAV) post infection. Infection levels were determined by measuring the luciferase activity in cell lysates relative to that in lysates of mock-treated cells. Infection levels were corrected for cell number and viability as determined by the Wst-1 assay prior to infection. Error bars represent SEM, n=3*3.

CTs inhibit fusion of MHV, independent of the receptor used or the intracellular site of fusion.

Next we investigated the inhibition of MHV infection by low levels of ouabain by performing an ouabain time-of-addition experiment (fig. 6A). Luciferase-expressing MHV was bound to HeLa-CC1a cells for 90 min on ice. Unbound virus was removed and cells were shifted to 37°C to allow infection. At the indicated time points cell culture media were replaced by warm, ouabain-containing medium. At 7 hpi cells were lysed and luciferase expression levels determined. Addition of ouabain only affected MHV infection when added during the first 2h of infection (fig. 6A), indicating that ouabain specifically inhibits MHV infection during entry.

To dissect which CoV entry step is affected by the addition of low concentrations of bufalin or ouabain we made use again of the replication-independent binding, internalization, and fusion assays. MHV- α N was bound to Δ M15-expressing cells that were pre-treated for 30 min with either ouabain or bufalin. Binding, internalization and fusion of MHV- α N were determined as described above. Binding and internalization of MHV did not appear to be affected by ouabain or bufalin treatment. However, fusion of MHV was clearly reduced (fig. 6B).

In addition, we analyzed whether the inhibition of MHV infection by ouabain is dependent on the nature of the entry receptor used or on the depth of MHV trafficking into the endo-lysosomal pathway. Therefore, HeLa-mCC1a and HeLa cells were inoculated with luciferase-expressing MHV (dependence on CEACAM1a and lysosomal trafficking), MHV-S2'FCS (fusion in early endosomes) or MHV-SRec (effect of receptor usage) in the presence of ouabain, after which the inhibitor was kept present until cell lysis. To control for any post entry effects of ouabain, the drug was also added and kept present only from 2h post inoculation onwards. As an additional control cells were treated with U18666A, which inhibits late endosome-to-lysosome trafficking (32, 48). Ouabain negatively affected infection with both MHV and MHV-S2'FCS (fig. 6C), indicating that it inhibits infection regardless of the intracellular site of fusion. In contrast, infection with MHV, but not with MHV-S2'FCS, was affected by U18666A. Also CEACAM1a-independent infection of MHV-SRec was inhibited to the same extent as MHV.

Ouabain inhibits virus entry at an early stage.

The replication-independent binding, internalization and fusion assays indicate that nanomolar levels of ouabain prevent MHV fusion but not internalization. To get more insight into the inhibition of virus entry by ouabain, we made use of the observation that MHV infection recovered during an overnight incubation upon removal of ouabain at 2 hpi. This allowed us to study whether the block induced by ouabain inhibited entry of MHV upstream or downstream of the inhibitory effects of known inhibitors of virus entry. Cells were (mock-) treated with ouabain prior to and during inoculation with luciferase-expressing MHV. After removal of the inoculum, cells were incubated for another 14 h in the absence or presence of inhibitory agents, using ouabain or other drugs known to affect MHV entry. Subsequently cells were lysed and luciferase expression levels determined. Luciferase expression levels obtained after ouabain treatment prior to and during inoculation but not thereafter were set to 100% (fig. 7; black bar). Overnight incubation in the presence of ouabain inhibited virus infection, but only when cells had been treated with ouabain during inoculation, in agreement with results described above. Overnight incubation in the presence of the MHV fusion inhibitor

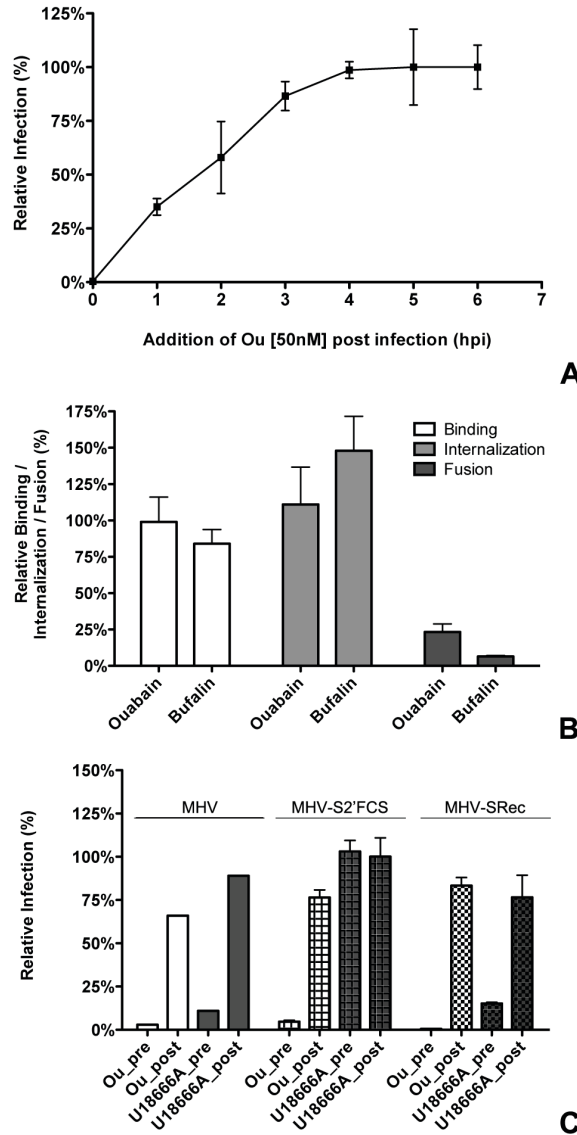


Figure 6: Low levels of ouabain and bufalin prevent MHV fusion. A) Time-of-addition experiment using 50nM ouabain. Luciferase expressing MHV was bound to HeLa-mCC1a cells at MOI=0.5 for 90 min on ice. Unbound virus was washed off and incubation continued at 37°C. At indicated time points medium was replaced by warm medium containing 50nM ouabain. Luciferase expression levels were determined relative to mock-treated cells. Error bars represent SEM, n=3. B) Binding, internalization, and fusion assays upon ouabain or bufalin treatment were performed as described in the legend to figure 2. HeLa-mCC1a-DM15 cells were pre-treated with 50nM ouabain or 10nM bufalin. Error bars represent SEM, n=3*3 for binding and internalization, n=3 for fusion. C) Effect of ouabain treatment on infection with MHV-SRec or MHV-S2'FCS. Cells were treated with ouabain as described in the legend to figure 5 and inoculated with luciferase expressing MHV, MHV-S2'FCS, or MHV-SRec at MOI=0.1. As a control cells were treated with U18666A. Infection levels were determined by measuring the luciferase expression levels in cells at 7h post infection relative to those in mock-treated cells. Error bars represent SEM, n=3*3.

peptide HR2 (49) did not inhibit MHV infection regardless of the absence or presence of ouabain during virus inoculation. However, virus infection was severely reduced when HR2 peptide was present during virus inoculation, confirming the ability of the HR2 peptide to inhibit entry. Addition of inhibitors of dynamin-2 (Dyngo-4A; Dyngo), clathrin-mediated endocytosis (chlorpromazine; Chlopro), or endosomal maturation (bafilomycin A1; BafA1) all reduced infection with MHV when added after removal of ouabain (fig. 7). The inhibitors did not affect luciferase expression levels without prior incubation with ouabain, indicating that they do not affect MHV infection at a post entry stages. These results indicate that ouabain inhibits infection with MHV upstream of the inhibitory effects of Dyngo, Chlopro and BafA1.

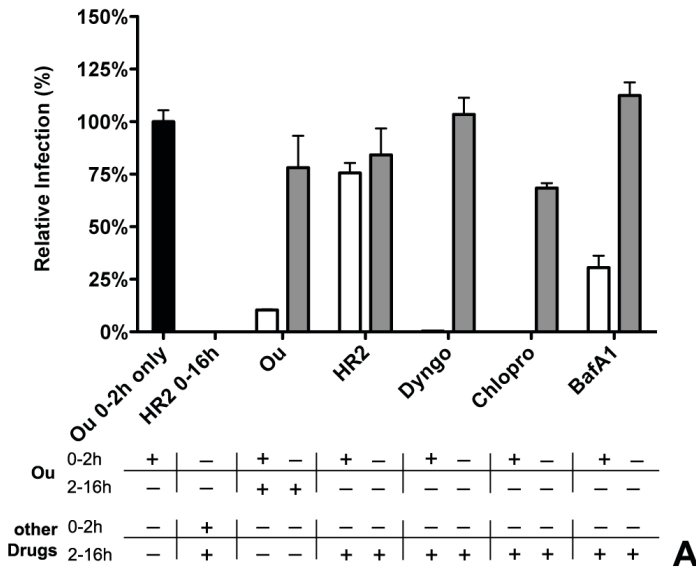


Figure 7: Ouabain inhibits virus entry at an early stage. Cells were (mock-)treated with 50nM ouabain starting at 30 min prior to and during inoculation with luciferase expressing MHV at MOI=0.1. After removal of the inoculum the medium was replaced by drug containing medium (Ou; ouabain, HR2; HR2 peptide, Dyngo; Dyngo-4A, Chlorpro; Chlorpromazine, and BafA1; Bafilomycin A1). White and grey bars correspond to cells treated with ouabain or mock-treated, respectively. As a control, cells were not treated with ouabain, but HR2 peptide was kept present prior to and throughout the infection (HR2 0-16h). After overnight infection cells were lysed and infection levels were determined by measuring the luciferase activity in cell lysates relative to control cells that were only treated with ouabain prior to and during inoculation (Ou 0-2h only, black bar). Error bars represent SEM, n=3*3.

MHV particles remain associated close to the cell surface.

To confirm and visualize the early block in infection by ouabain, MHV covalently labeled with DyLight 488 (MHV-DL488; (32)) was bound to ouabain- or mock-treated cells for 90 min at MOI=20 on ice. After removal of unbound virus particles, cells were incubated for 90 min at 37°C in the presence or absence of ouabain. Cells were then fixed and analyzed by confocal microscopy. The contours of the cells were visualized using phalloidin, which stains the actin cytoskeleton. In mock-treated cells, relatively few fluorescent virions were visible inside the cells (fig. 8). On the other hand, in ouabain-treated cells a larger number of virions were observed which appeared however to remain associated close to the cell surface (fig. 8B),

in agreement with ouabain inhibiting virus entry at an early stage.

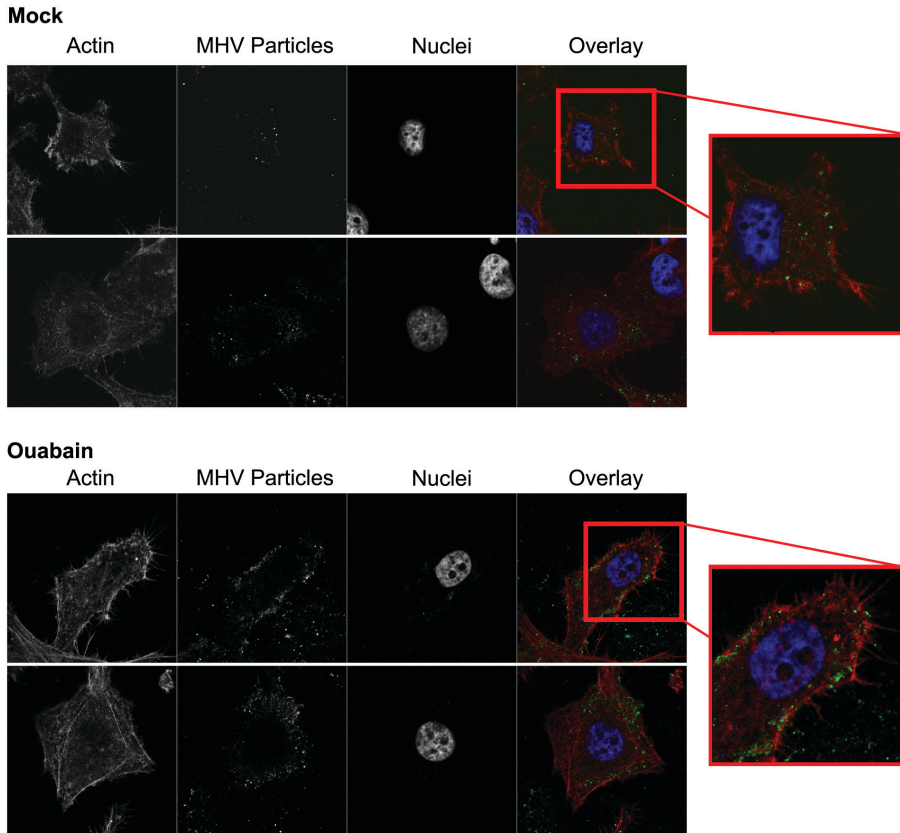


Figure 8: *MHV particles accumulate close to the cell surface.* Imaging of ouabain-treated cells inoculated with DyLight 488-labelled MHV by confocal microscopy. Cells were mock-treated (upper two rows) or treated with 50nM ouabain (lower two rows) throughout the experiment starting at 30 min prior to inoculation. MHV covalently labeled with DyLight 488 (MHV particles) was bound to cells at MOI=20 for 70 min on ice. Unbound virus was removed and cell-bound virus was allowed to infect at 37°C for 90 min. Cells were fixed, stained with DAPI (Nuclei) and Phalloidin (Actin), and analyzed by confocal microscopy.

Inhibitory effects of ouabain on CoV infection can be rescued by inhibitors of Src but not PI3K.

CoV infection is inhibited by low concentrations of CTSs known to trigger different Na^+, K^+ -ATPase-mediated signaling pathways but not to affect the ion-pump function (16-21). Two of the main signaling pathways induced by CTSs and mediated through Na^+, K^+ -ATPase involve the activation of Src or PI3K (50). In order to elucidate whether these signaling pathways are involved in the antiviral action of ouabain we (mock-)treated cells with ouabain alone or in combination with either PI3K inhibitor wortmannin (51), Src inhibitor PP2 (52), or Na^+, K^+ -ATPase-mimetic Src-inhibitor peptide (pNaKtide) (39). As a control cells were treated with the kinase inhibitors in the absence of ouabain. The cells were inoculated with luciferase-expressing MHV or FIPV in the presence of the inhibitors, after which the drugs

were kept present until cell lysis. To check for inhibitory effects after virus entry, cells were also treated with inhibitors starting at 2 hpi. At 7 hpi cells were lysed and luciferase expression levels determined. For reasons unknown, treatment of cells with wortmannin or PP2 during virus inoculation reduced MHV infection by about 75% (fig. 9A), while the pNaKtide had a smaller negative effect. Infection with FIPV was not affected by these inhibitors (fig. 9B). MHV- and FIPV-driven luciferase expression levels were severely reduced by ouabain when the drug was present during virus inoculation, yet not when added at 2 hpi only, as observed earlier. The combined treatment with ouabain and wortmannin did not positively affect MHV or FIPV infection compared to ouabain treatment alone. However, combined treatment of ouabain with PP2 or pNaKtide almost completely restored MHV and FIPV infection to the levels observed after treatment with PP2 or pNaKtide alone (fig. 9A and B). These results show that the negative effect of ouabain on the entry of MHV and FIPV can be relieved by inhibition of Src.

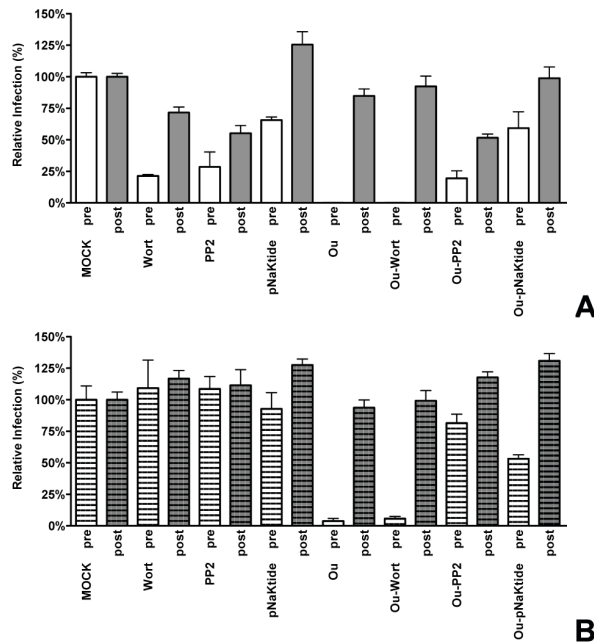


Figure 9: Inhibition of infection by ouabain is rescued by inhibition of Src. HeLa cells were inoculated with luciferase expressing MHV (A) or FIPV (B) at MOI=0.1 for 2h. Cells were (pre-)treated with 50nM ouabain (Ou), wortmannin (Wort), PP2, pNaKtide or a combination thereof as indicated from 30 min prior to (pre) or 2h post (post) until 7h post inoculation. Infection levels were determined by measuring the luciferase activity in lysates of treated relative to mock-treated cells. Error bars represent SEM, n=3*3.

DISCUSSION

This study provides an extensive analysis of the role of the *ATP1A1*-encoded $\alpha 1$ -subunit of Na^+, K^+ -ATPase in CoV infection. Using gene silencing we showed that *ATP1A1* is important for infection of cells with MHV and FIPV, but not IAV. Lack of *ATP1A1* was found not to affect MHV binding to cells or endosomal uptake but to reduce its fusion with cellular membranes. Consistently, nanomolar concentrations of CTSs inhibited infection of cells with MHV, FIPV, MERS-CoV but not IAV, when the compounds were present during virus entry. CTSs were shown to inhibit entry of MHV at an early stage, resulting in the accumulation of virions close to the cell surface and in reduced fusion. Viral RNA replication *per se* was not affected by these compounds at the concentrations used. In agreement with low concentrations of CTSs not affecting the ion transport function of Na^+, K^+ -ATPase (16-21), the anti-coronaviral effect could be relieved by the addition of inhibitors of Src kinases, indicating that Src signaling mediated via *ATP1A1* plays a crucial role in the inhibition of infection with CoVs.

Knockdown of *ATP1A1* or additions of low concentrations of CTSs inhibit CoV infection during the virus entry stage. Using our recently developed replication-independent entry assay (34) we could demonstrate that the effect was not at the level of virus binding or internalization but by inhibition of virus membrane fusion. CoV replication was not affected as revealed by adding the CTSs after inoculation. Inhibition of MHV was found to be independent of the particular virus receptor being used by the virus, despite the reported interaction between CEACAM1 and *ATP1A1* (41). This is in line with FIPV and MERS-CoV being similarly inhibited while using entirely different entry receptors (53, 54). FIPV on the one and MHV and MERS-CoV on the other hand belong to the α - and β -CoV genera, respectively, suggesting that CTSs may function as pan-CoV inhibitors.

Interpreting our combined results, we developed the model shown in figure 10. In this model, two elements are addressed. First, it recapitulates the early stage of CoV entry as we and others have described (32, 55-58): uptake of CoV in a pre-endosome that pinches off to form an early endosome. Based on our data we propose a model in which the uptake of MHV particles is arrested in pre-endosomal structures by transfection of siRNAs targeting *ATP1A1* or by the addition of CTSs. This model explains the apparent paradoxical observations that internalization of MHV particles was not affected by *ATP1A1* interference, while on the other hand, ouabain was shown to inhibit a very early step in MHV entry, upstream of the inhibitory effect of compounds affecting dynamin-2 and/or clathrin-mediated endocytosis (32). The internalization assay depends on the removal of cell surface-bound virions by proteases. The lack of internalization inhibition observed with this assay can be explained by MHV particles accumulating in pre-endosomal invaginations, which are not accessible by the membrane-impermeable protease in the presence of ouabain. Similarly, also the inability of the membrane-impermeable inhibitory HR2 peptide to prevent MHV infection after ouabain wash-out can be explained by the inability of the HR2 compound to access the pre-endosomal structures. The inhibition of MHV entry by inhibitors of clathrin-mediated endocytosis after ouabain wash-out indicates that further internalization of the pre-endosomal invaginations is sensitive to these inhibitors. In agreement with our model, interference with the Na^+, K^+ -ATPase (either by *ATP1A1* knockdown or addition of CTSs) inhibited CoV entry, regardless whether viruses fusing in early endosomes (MHV-2'FCS and MERS-CoV) or lysosomes (MHV and FIPV) were used (32). These results indicate that interference with the *ATP1A1* subunit acts prior to

the formation of early endosomes and does not result from a defect in endosome maturation. Our model is further supported by confocal microscopy analysis, which showed MHV particles to accumulate close to the cell surface in the presence of ouabain.

The second element represented in our model (fig. 10) addresses the mechanism by which interference with the ATP1A1 subunit activity blocks CoV entry. Our results indicate that CoV infection is inhibited by low concentrations of CTSs via Na^+, K^+ -ATPase-mediated Src signaling. CoV infection of HeLa cells expressing ouabain insensitive murine ATP1A1-encoded $\alpha 1$ -subunit (47) was unaffected by ouabain treatment. These results show that ouabain mediates its antiviral effect via the $\alpha 1$ -subunit and not via an off-target effect, in agreement with the literature (reviewed in (13, 14)). Ample evidence exists in the literature demonstrating that nanomolar concentrations of CTSs induce $\alpha 1$ -subunit-mediated signaling pathways, including the activation of Src. At these concentrations, ouabain binding to the $\alpha 1$ -subunit triggers a conformational change in this subunit, which results in release of Src from Na^+, K^+ -ATPase and its concomitant activation (16-18, 22-28). The alleviation of inhibition of CoV infection by ouabain with two chemically different Src inhibitors, PP2 and pNaKtide, but not by an inhibitor of PI3K, shows that the activation of Src via the $\alpha 1$ -subunit is the inhibitory mode of action of this compound on CoV infection. In agreement with the inhibitory effect of Na^+, K^+ -ATPase-mediated Src signaling on CoV infection, also gene silencing of ATP1A1 has been shown to result in activation of Src (20, 39, 59). We speculate that Src signaling induced by the lack of ATP1A1 or addition of CTSs somehow negatively affects the endocytic uptake of CoVs. Similar to MHV (32, 55-58), also MERS-CoV and FIPV appear to be taken up via clathrin-mediated endocytosis as infection with these viruses is inhibited by chlorpromazine in a dose-dependent manner ((60) and unpublished results), although FIPV has also been reported to enter monocytes via a clathrin- and caveolae-independent endocytic pathway (61). The link between the endocytic uptake of CoVs and Na^+, K^+ -ATPase-mediated Src signaling may be supported by the observed modulation of dynamin-2 phosphorylation and clathrin-coated pit formation by Src signaling (62, 63). An explanation for the lack of inhibition of IAV could be that this virus is able to enter cells via multiple fully redundant endocytic routes (64-68).

Inhibition of infection by CTSs has been reported earlier for several other viruses including Sindbis virus (70), Sendai virus (71), Semliki Forest virus (72), several herpes viruses (73), and PRRSV (74). Most of these studies, however, employed relatively high concentrations of the CTSs (micromolar range) which inhibit the Na^+, K^+ -ATPase pump function and affect intracellular ion-concentrations (75, 76). In the present study, the low levels of CTSs did not affect infection with IAV. However, at high concentrations infections by CoVs and IAVs were inhibited also when the compounds were only present after virus entry. This more general inhibitory effect at these concentrations may result from side effects of the drugs such as, for instance, inhibition of mRNA translation (data not shown). Indeed, intracellular levels of Na^+ and K^+ have been implicated previously in the regulation of cellular protein synthesis (77, 78). Interestingly, for human cytomegalovirus, low nanomolar concentrations of ouabain were shown to inhibit an early step in the infection cycle of this virus prior to DNA replication, but following binding to cellular receptors, suggesting that also for this virus entry may be impaired (73).

Ouabain and several other CTSs are FDA-approved compounds. Targeting host factors using FDA-approved compounds to combat viral infections is certainly attractive. Drugs

targeting host-, rather than viral factors may lower the probability of generating drug-resistant viral variants since mutation of the drug target is not possible. In addition, the repurposing of FDA-approved compounds may enable relatively fast clinical application. Elucidation of the action mechanism of the anti-viral compounds as exemplified here by the anti-coronaviral effect of low concentrations of CTSs may aid the development and design of new compounds with improved therapeutic efficacy and less side effects.

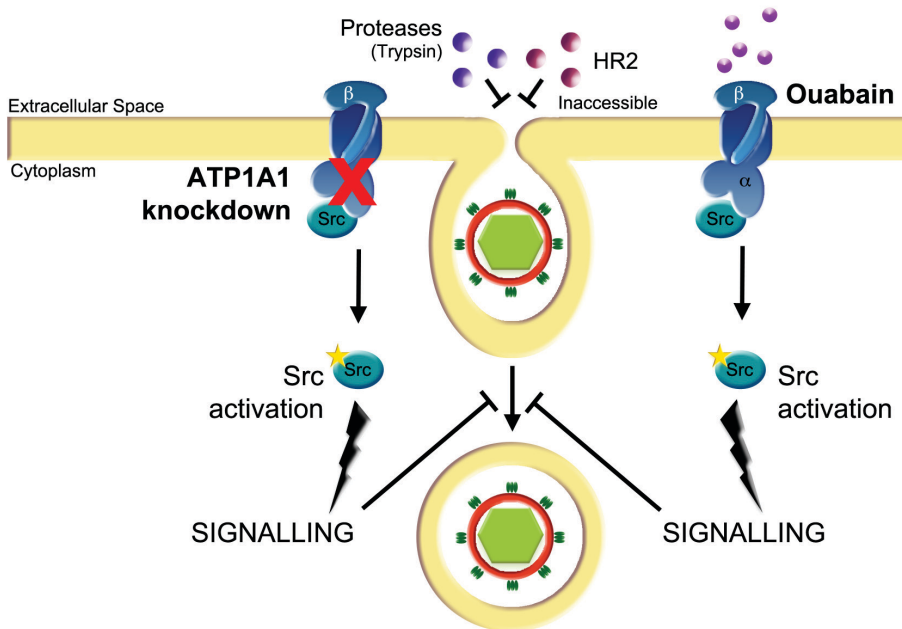


Figure 10: Model of the effect of ATP1A1 knockdown and CTSs treatment on coronavirus entry. siRNA-mediated gene silencing of *ATP1A1* encoding the α 1-subunit of the Na^+,K^+ -ATPase or treatment of cells with CTSs inhibits CoV infection at an early entry stage, resulting in reduced virus-cell fusion. In the presence of CTSs CoV particles accumulate in pre-endosomal invaginations that are not accessible for the membrane impermeable HR2 peptide or trypsin. Knockdown of ATP1A1 leads to release of an Na^+,K^+ -ATPase-bound subset of Src, Src activation, and increased Src signaling (20, 39, 59). Ouabain binding to the α 1-subunit subunit of Na^+,K^+ -ATPase triggers a conformational change in this subunit, which also results in release of Src from Na^+,K^+ -ATPase and its concomitant activation (20, 69). Activated Src induces yet unknown downstream signaling, which inhibits MHV entry at an early stage upstream of the inhibitory effects of inhibitors of clathrin-mediated endocytosis.

ACKNOWLEDGMENTS

We would like to thank Zijian Xie, Marshall University, Institute of Interdisciplinary Research, Huntington, US-VA, for providing us with pNaKtide. This work was supported by the EU 7th Framework Programme (Virus Entry, project 235649, P.J.M.R) and by a Utrecht University High potential grant to C.A.M.d.H.

REFERENCES

1. **Alvarez-Salas LM.** 2008. Nucleic acids as therapeutic agents. *Current topics in medicinal chemistry* **8**:1379-1404.
2. **Hirsch AJ.** 2010. The use of RNAi-based screens to identify host proteins involved in viral replication. *Future microbiology* **5**:303-311.
3. **Pauli I, Timmers LF, Caceres RA, Soares MB, de Azevedo WF, Jr.** 2008. In silico and in vitro: identifying new drugs. *Current drug targets* **9**:1054-1061.
4. **Peiris JS, Lai ST, Poon LL, Guan Y, Yam LY, Lim W, Nicholls J, Yee WK, Yan WW, Cheung MT, Cheng VC, Chan KH, Tsang DN, Yung RW, Ng TK, Yuen KY.** 2003. Coronavirus as a possible cause of severe acute respiratory syndrome. *Lancet* **361**:1319-1325.
5. **Zaki AM, van Boheemen S, Bestebroer TM, Osterhaus AD, Fouchier RA.** 2012. Isolation of a novel coronavirus from a man with pneumonia in Saudi Arabia. *N Engl J Med* **367**:1814-1820.
6. **Burkard C, Verheije MH, Wicht O, van Kasteren SI, van Kuppeveld FJ, Haagmans BL, Pelkmans L, Rottier PJ, Bosch BJ, de Haan CA.** 2014. Coronavirus Cell Entry Occurs through the Endo-/Lysosomal Pathway in a Proteolysis-Dependent Manner. *PLoS pathogens* **10**:e1004502.
7. **Hagemeijer MC, Rottier PJ, de Haan CA.** 2012. Biogenesis and dynamics of the coronavirus replicative structures. *Viruses* **4**:3245-3269.
8. **de Haan CA, Rottier PJ.** 2005. Molecular interactions in the assembly of coronaviruses. *Advances in virus research* **64**:165-230.
9. **Skou JC.** 2004. The identification of the sodium pump. *Bioscience reports* **24**:436-451.
10. **Kaplan JH.** 2002. Biochemistry of Na,K-ATPase. *Annual review of biochemistry* **71**:511-535.
11. **Withering W.** 1785. *An Account of the Foxglove and some of its Medical Uses With Practical Remarks on Dropsy and Other Diseases.*
12. **Schoner W, Scheiner-Bobis G.** 2007. Endogenous and exogenous cardiac glycosides and their mechanisms of action. *American journal of cardiovascular drugs : drugs, devices, and other interventions* **7**:173-189.
13. **Reinhard L, Tidow H, Clausen MJ, Nissen P.** 2013. Na(+),K (+)-ATPase as a docking station: protein-protein complexes of the Na(+),K (+)-ATPase. *Cellular and molecular life sciences : CMLS* **70**:205-222.
14. **Aperia A.** 2007. New roles for an old enzyme: Na,K-ATPase emerges as an interesting drug target. *Journal of internal medicine* **261**:44-52.
15. **Karpova LV, Bulygina ER, Boldyrev AA.** 2010. Different neuronal Na(+)/K(+)-ATPase isoforms are involved in diverse signaling pathways. *Cell biochemistry and function* **28**:135-141.
16. **Aizman O, Uhlen P, Lal M, Brismar H, Aperia A.** 2001. Ouabain, a steroid hormone that signals with slow calcium oscillations. *Proceedings of the National Academy of Sciences of the United States of America* **98**:13420-13424.
17. **Haas M, Askari A, Xie Z.** 2000. Involvement of Src and epidermal growth factor receptor in the signal-transducing function of Na+/K+-ATPase. *The Journal of biological chemistry* **275**:27832-27837.

18. **Mohammadi K, Kometiani P, Xie Z, Askari A.** 2001. Role of protein kinase C in the signal pathways that link Na⁺/K⁺-ATPase to ERK1/2. *The Journal of biological chemistry* **276**:42050-42056.
19. **Su CT, Hsu JT, Hsieh HP, Lin PH, Chen TC, Kao CL, Lee CN, Chang SY.** 2008. Anti-HSV activity of digitoxin and its possible mechanisms. *Antiviral research* **79**:62-70.
20. **Tian J, Cai T, Yuan Z, Wang H, Liu L, Haas M, Maksimova E, Huang XY, Xie ZJ.** 2006. Binding of Src to Na⁺/K⁺-ATPase forms a functional signaling complex. *Molecular biology of the cell* **17**:317-326.
21. **Tian J, Gong X, Xie Z.** 2001. Signal-transducing function of Na⁺-K⁺-ATPase is essential for ouabain's effect on [Ca²⁺]_i in rat cardiac myocytes. *American journal of physiology. Heart and circulatory physiology* **281**:H1899-1907.
22. **Barwe SP, Anilkumar G, Moon SY, Zheng Y, Whitelegge JP, Rajasekaran SA, Rajasekaran AK.** 2005. Novel role for Na,K-ATPase in phosphatidylinositol 3-kinase signaling and suppression of cell motility. *Molecular biology of the cell* **16**:1082-1094.
23. **Belusa R, Wang ZM, Matsubara T, Sahlgren B, Dulubova I, Nairn AC, Ruoslahti E, Greengard P, Aperia A.** 1997. Mutation of the protein kinase C phosphorylation site on rat alpha1 Na⁺,K⁺-ATPase alters regulation of intracellular Na⁺ and pH and influences cell shape and adhesiveness. *The Journal of biological chemistry* **272**:20179-20184.
24. **Contreras RG, Shoshani L, Flores-Maldonado C, Lazaro A, Cerejido M.** 1999. Relationship between Na(+),K(+)-ATPase and cell attachment. *Journal of cell science* **112** (Pt 23):4223-4232.
25. **Li J, Zelenin S, Aperia A, Aizman O.** 2006. Low doses of ouabain protect from serum deprivation-triggered apoptosis and stimulate kidney cell proliferation via activation of NF-kappaB. *Journal of the American Society of Nephrology : JASN* **17**:1848-1857.
26. **Kometiani P, Li J, Gnudi L, Kahn BB, Askari A, Xie Z.** 1998. Multiple signal transduction pathways link Na⁺/K⁺-ATPase to growth-related genes in cardiac myocytes. The roles of Ras and mitogen-activated protein kinases. *The Journal of biological chemistry* **273**:15249-15256.
27. **Liu J, Tian J, Haas M, Shapiro JI, Askari A, Xie Z.** 2000. Ouabain interaction with cardiac Na⁺/K⁺-ATPase initiates signal cascades independent of changes in intracellular Na⁺ and Ca²⁺ concentrations. *The Journal of biological chemistry* **275**:27838-27844.
28. **Miyakawa-Naito A, Uhlen P, Lal M, Aizman O, Mikoshiba K, Brismar H, Zelenin S, Aperia A.** 2003. Cell signaling microdomain with Na,K-ATPase and inositol 1,4,5-trisphosphate receptor generates calcium oscillations. *The Journal of biological chemistry* **278**:50355-50361.
29. **Kuo L, Godeke GJ, Raamsman MJ, Masters PS, Rottier PJ.** 2000. Retargeting of coronavirus by substitution of the spike glycoprotein ectodomain: crossing the host cell species barrier. *J Virol* **74**:1393-1406.
30. **Konig R, Stertz S, Zhou Y, Inoue A, Hoffmann HH, Bhattacharyya S, Alamares JG, Tscherne DM, Ortigoza MB, Liang Y, Gao Q, Andrews SE, Bandyopadhyay S, De Jesus P, Tu BP, Pache L, Shih C, Orth A, Bonamy G, Miraglia L, Ideker T, Garcia-Sastre A, Young JA, Palese P, Shaw ML, Chanda SK.** 2010. Human host factors required for influenza virus replication. *Nature* **463**:813-817.

-
31. **van Boheemen S, de Graaf M, Lauber C, Bestebroer TM, Raj VS, Zaki AM, Osterhaus AD, Haagmans BL, Gorbalenya AE, Snijder EJ, Fouchier RA.** 2012. Genomic characterization of a newly discovered coronavirus associated with acute respiratory distress syndrome in humans. *mBio* **3**.
 32. **Burkard C, Verheije MH, Wicht O, van Kasteren SI, van Kuppeveld FJ, Haagmans BL, Pelkmans L, Rottier PJ, Bosch BJ, de Haan CA.** 2014. Coronavirus cell entry occurs through the endo-/lysosomal pathway in a proteolysis-dependent manner. *PLoS pathogens* **Under Revision**.
 33. **Wurdinger T, Verheije MH, Raaben M, Bosch BJ, de Haan CA, van Beusechem VW, Rottier PJ, Gerritsen WR.** 2005. Targeting non-human coronaviruses to human cancer cells using a bispecific single-chain antibody. *Gene therapy* **12**:1394-1404.
 34. **Burkard C, Bloyet LM, Wicht O, van Kuppeveld FJ, Rottier PJ, de Haan CA, Bosch BJ.** 2014. Dissecting Virus Entry: Replication-Independent Analysis of Virus Binding, Internalization, and Penetration Using Minimal Complementation of beta-Galactosidase. *PloS one* **9**:e101762.
 35. **de Haan CA, van Genne L, Stoop JN, Volders H, Rottier PJ.** 2003. Coronaviruses as vectors: position dependence of foreign gene expression. *Journal of virology* **77**:11312-11323.
 36. **de Haan CA, Haijema BJ, Boss D, Heuts FW, Rottier PJ.** 2005. Coronaviruses as vectors: stability of foreign gene expression. *Journal of virology* **79**:12742-12751.
 37. **de Haan CA, Li Z, te Lintelo E, Bosch BJ, Haijema BJ, Rottier PJ.** 2005. Murine coronavirus with an extended host range uses heparan sulfate as an entry receptor. *Journal of virology* **79**:14451-14456.
 38. **Bosch BJ, van der Zee R, de Haan CA, Rottier PJ.** 2003. The coronavirus spike protein is a class I virus fusion protein: structural and functional characterization of the fusion core complex. *J Virol* **77**:8801-8811.
 39. **Li Z, Cai T, Tian J, Xie JX, Zhao X, Liu L, Shapiro JI, Xie Z.** 2009. NaKtide, a Na/K-ATPase-derived peptide Src inhibitor, antagonizes ouabain-activated signal transduction in cultured cells. *The Journal of biological chemistry* **284**:21066-21076.
 40. **Langley KE, Villarejo MR, Fowler AV, Zamenhof PJ, Zabin I.** 1975. Molecular basis of beta-galactosidase alpha-complementation. *Proceedings of the National Academy of Sciences of the United States of America* **72**:1254-1257.
 41. **Gupta S, Yan Y, Malhotra D, Liu J, Xie Z, Najjar SM, Shapiro JI.** 2012. Ouabain and insulin induce sodium pump endocytosis in renal epithelium. *Hypertension* **59**:665-672.
 42. **Blaustein MP, Juhaszova M, Golovina VA.** 1998. The cellular mechanism of action of cardiotoxic steroids: a new hypothesis. *Clinical and experimental hypertension* **20**:691-703.
 43. **Dvela M, Rosen H, Feldmann T, Neshar M, Lichtstein D.** 2007. Diverse biological responses to different cardiotoxic steroids. *Pathophysiology : the official journal of the International Society for Pathophysiology / ISP* **14**:159-166.
 44. **Wasserstrom JA, Aistrup GL.** 2005. Digitalis: new actions for an old drug. *American journal of physiology. Heart and circulatory physiology* **289**:H1781-1793.
 45. **Kurosawa M, Numazawa S, Tani Y, Yoshida T.** 2000. ERK signaling mediates the induction of inflammatory cytokines by bufalin in human monocytic cells. *American journal of physiology. Cell physiology* **278**:C500-508.
-

46. **Watabe M, Masuda Y, Nakajo S, Yoshida T, Kuroiwa Y, Nakaya K.** 1996. The cooperative interaction of two different signaling pathways in response to bufalin induces apoptosis in human leukemia U937 cells. *The Journal of biological chemistry* **271**:14067-14072.
47. **Jewell-Motz EA, Lingrel JB.** 1993. Site-directed mutagenesis of the Na,K-ATPase: consequences of substitutions of negatively-charged amino acids localized in the transmembrane domains. *Biochemistry* **32**:13523-13530.
48. **Huynh KK, Gershenson E, Grinstein S.** 2008. Cholesterol accumulation by macrophages impairs phagosome maturation. *The Journal of biological chemistry* **283**:35745-35755.
49. **Bosch BJ, van der Zee R, de Haan CA, Rottier PJ.** 2003. The coronavirus spike protein is a class I virus fusion protein: structural and functional characterization of the fusion core complex. *Journal of virology* **77**:8801-8811.
50. **Liu J, Xie ZJ.** 2010. The sodium pump and cardiotonic steroids-induced signal transduction protein kinases and calcium-signaling microdomain in regulation of transporter trafficking. *Biochimica et biophysica acta* **1802**:1237-1245.
51. **Yano H, Nakanishi S, Kimura K, Hanai N, Saitoh Y, Fukui Y, Nonomura Y, Matsuda Y.** 1993. Inhibition of histamine secretion by wortmannin through the blockade of phosphatidylinositol 3-kinase in RBL-2H3 cells. *The Journal of biological chemistry* **268**:25846-25856.
52. **Hanke JH, Gardner JP, Dow RL, Changelian PS, Brisette WH, Weringer EJ, Pollok BA, Connelly PA.** 1996. Discovery of a novel, potent, and Src family-selective tyrosine kinase inhibitor. Study of Lck- and FynT-dependent T cell activation. *The Journal of biological chemistry* **271**:695-701.
53. **Raj VS, Mou H, Smits SL, Dekkers DH, Muller MA, Dijkman R, Muth D, Demmers JA, Zaki A, Fouchier RA, Thiel V, Drosten C, Rottier PJ, Osterhaus AD, Bosch BJ, Haagmans BL.** 2013. Dipeptidyl peptidase 4 is a functional receptor for the emerging human coronavirus-EMC. *Nature* **495**:251-254.
54. **Tresnan DB, Levis R, Holmes KV.** 1996. Feline aminopeptidase N serves as a receptor for feline, canine, porcine, and human coronaviruses in serogroup I. *Journal of virology* **70**:8669-8674.
55. **Eifart P, Ludwig K, Bottcher C, de Haan CA, Rottier PJ, Korte T, Herrmann A.** 2007. Role of endocytosis and low pH in murine hepatitis virus strain A59 cell entry. *Journal of virology* **81**:10758-10768.
56. **Qiu Z, Hingley ST, Simmons G, Yu C, Das Sarma J, Bates P, Weiss SR.** 2006. Endosomal proteolysis by cathepsins is necessary for murine coronavirus mouse hepatitis virus type 2 spike-mediated entry. *Journal of virology* **80**:5768-5776.
57. **Stauber R, Pfeleiderer M, Siddell S.** 1993. Proteolytic cleavage of the murine coronavirus surface glycoprotein is not required for fusion activity. *The Journal of general virology* **74** (Pt 2):183-191.
58. **Sturman LS, Ricard CS, Holmes KV.** 1985. Proteolytic cleavage of the E2 glycoprotein of murine coronavirus: activation of cell-fusing activity of virions by trypsin and separation of two different 90K cleavage fragments. *Journal of virology* **56**:904-911.

-
59. **Cai T, Wang H, Chen Y, Liu L, Gunning WT, Quintas LE, Xie ZJ.** 2008. Regulation of caveolin-1 membrane trafficking by the Na/K-ATPase. *The Journal of cell biology* **182**:1153-1169.
 60. **de Wilde AH, Jochmans D, Posthuma CC, Zevenhoven-Dobbe JC, van Nieuwkoop S, Bestebroer TM, van den Hoogen BG, Neyts J, Snijder EJ.** 2014. Screening of an FDA-approved compound library identifies four small-molecule inhibitors of Middle East respiratory syndrome coronavirus replication in cell culture. *Antimicrobial agents and chemotherapy*.
 61. **Van Hamme E, Dewerchin HL, Cornelissen E, Verhasselt B, Nauwynck HJ.** 2008. Clathrin- and caveolae-independent entry of feline infectious peritonitis virus in monocytes depends on dynamin. *The Journal of general virology* **89**:2147-2156.
 62. **Harris TL, Xie Z.** 2012. Ouabain regulates caveolin-1 vesicle trafficking by a Src-dependent mechanism (Doctoral dissertation). Retrieved from ProQuest Dissertations and Theses Database. (AAT 3512447).
 63. **Liu J, Kesiry R, Periyasamy SM, Malhotra D, Xie Z, Shapiro JI.** 2004. Ouabain induces endocytosis of plasmalemmal Na/K-ATPase in LLC-PK1 cells by a clathrin-dependent mechanism. *Kidney international* **66**:227-241.
 64. **de Vries E, Tscherne DM, Wienholts MJ, Cobos-Jimenez V, Scholte F, Garcia-Sastre A, Rottier PJ, de Haan CA.** 2011. Dissection of the influenza A virus endocytic routes reveals macropinocytosis as an alternative entry pathway. *PLoS pathogens* **7**:e1001329.
 65. **Lakadamyali M, Rust MJ, Zhuang X.** 2004. Endocytosis of influenza viruses. *Microbes and infection / Institut Pasteur* **6**:929-936.
 66. **Matlin KS, Reggio H, Helenius A, Simons K.** 1981. Infectious entry pathway of influenza virus in a canine kidney cell line. *The Journal of cell biology* **91**:601-613.
 67. **Patterson S, Oxford JS, Dourmashkin RR.** 1979. Studies on the mechanism of influenza virus entry into cells. *The Journal of general virology* **43**:223-229.
 68. **Sieczkarski SB, Whittaker GR.** 2002. Influenza virus can enter and infect cells in the absence of clathrin-mediated endocytosis. *Journal of virology* **76**:10455-10464.
 69. **Ye J, Chen S, Maniatis T.** 2011. Cardiac glycosides are potent inhibitors of interferon-beta gene expression. *Nature chemical biology* **7**:25-33.
 70. **Mento SJ, Stollar V.** 1978. Effect of ouabain on sindbis virus replication in ouabain-sensitive and ouabain-resistant *Aedes albopictus* cells (Singh). *Virology* **87**:58-65.
 71. **Nagai Y, Maeno K, Iinuma M, Yoshida T, Matsumoto T.** 1972. Inhibition of virus growth by ouabain: effect of ouabain on the growth of HVJ in chick embryo cells. *Journal of virology* **9**:234-243.
 72. **Helenius A, Kielian M, Wellstead J, Mellman I, Rudnick G.** 1985. Effects of monovalent cations on Semliki Forest virus entry into BHK-21 cells. *The Journal of biological chemistry* **260**:5691-5697.
 73. **Kapoor A, Cai H, Forman M, He R, Shamay M, Arav-Boger R.** 2012. Human cytomegalovirus inhibition by cardiac glycosides: evidence for involvement of the HERG gene. *Antimicrobial agents and chemotherapy* **56**:4891-4899.
 74. **Karuppannan AK, Wu KX, Qiang J, Chu JJ, Kwang J.** 2012. Natural compounds inhibiting the replication of Porcine reproductive and respiratory syndrome virus. *Antiviral research* **94**:188-194.
-

75. **Beuschlein F, Boulkroun S, Osswald A, Wieland T, Nielsen HN, Lichtenauer UD, Penton D, Schack VR, Amar L, Fischer E, Walther A, Tauber P, Schwarzmayr T, Diener S, Graf E, Allolio B, Samson-Couterie B, Benecke A, Quinkler M, Fallo F, Plouin PF, Mantero F, Meitinger T, Mulatero P, Jeunemaitre X, Warth R, Vilsen B, Zennaro MC, Strom TM, Reincke M.** 2013. Somatic mutations in ATP1A1 and ATP2B3 lead to aldosterone-producing adenomas and secondary hypertension. *Nature genetics* **45**:440-444, 444e441-442.
76. **Chang JT, Lowery LA, Sive H.** 2012. Multiple roles for the Na,K-ATPase subunits, At-*p1a1* and *Fxyd1*, during brain ventricle development. *Developmental biology* **368**:312-322.
77. **Frugulhetti IC, Rebello MA.** 1989. Na⁺ and K⁺ concentration and regulation of protein synthesis in L-A9 and *Aedes albopictus* cells infected with Marituba virus (Bunyaviridae). *The Journal of general virology* **70** (Pt 12):3493-3499.
78. **Pauw PG, Kaffer CR, Petersen RJ, Semerad SA, Williams DC.** 2000. Inhibition of myogenesis by ouabain: effect on protein synthesis. *In vitro cellular & developmental biology. Animal* **36**:133-138.

CHAPTER

SIX

*Summarizing
Discussion*

Virus entry relies on the tight interplay between viral proteins and host cells in order for the virus to induce the correct entry pathway to deliver its genome into the cytoplasm. A small number of structural viral proteins, particularly the viral fusion proteins, are capable of recruiting hundreds of cellular proteins to assist with virus attachment, internalization, and penetration. These processes are complex and tightly regulated, which makes the study of viral entry challenging.

In this thesis we set out to elucidate the entry process of CoVs in great detail. Therefore we first established new assays to study the cell biological and biochemical aspects of binding, uptake, triggering, and fusion. Then we combined our novel assays with a variety of other techniques, including siRNA-mediated gene silencing, live-cell microscopy, drug treatment and established virological methods, to describe the CoV entry pathway and host factors involved in it. This allowed us to provide an explanation for several, apparently conflicting results from earlier studies with respect to the process of MHV cell entry.

In this chapter I will highlight the implications that our findings have on the understanding of CoV entry. I discuss our findings on the close interplay between host factors involved in entry and proteolytic processing of CoV S and place them in a broader perspective. At last I will try to give an outlook on putative future directions of CoV entry research.

1. Novel assays to investigate the cell-biological and biochemical aspects of virus entry

The study of virus entry is hampered by the relatively low numbers of virions entering individual cells under natural conditions, making a direct analysis of this process almost impossible. Therefore most researchers have been relying on post-entry parameters while studying virus entry, by measuring virus replication and/or viral or reporter protein expression. Techniques used previously to investigate viral entry, such as radioactive labeling of structural proteins, electron microscopy, or fluorescence microscopy, all presented limitations and drawbacks and did not appear suitable for medium or high-throughput experiments. Also novel, more specialized fusion assays, such as labeling with self-quenching dyes or the incorporation of enzymes into virions seemed unsuitable for our purposes (1-9). The dyes would only allow investigation of fusion but not of the preceding steps of binding and internalization. Integration of entire enzymes into CoV virions did not appear feasible, based on previous findings demonstrating the low stability of GFP encoding sequences in the viral genome when fused to the S protein of murine hepatitis virus (MHV) (10). In addition, also the enzymatic assays have mostly been used for investigations of fusion only and not of the preceding steps (4-9). Therefore there was a clear need for novel cell biological assays, with which to study attachment, uptake, and fusion of CoVs without having to rely on indirect post-entry parameters.

Proteolytic priming of the S fusion glycoprotein of CoVs and the biochemical nature of the cleavage product have been studied extensively. While some CoV S proteins contain a furin-like cleavage site at the S1/S2 junction there are indications for alternative positions within the S2 domain, cleavage at which could promote fusion competence. Even though alternative cleavage sites had been suggested and described for some CoVs, including severe acute respiratory syndrome coronavirus (SARS-CoV), MHV, and infectious bronchitis virus (IBV) (reviewed in (11)), the exact position of the priming cleavage within the CoV S protein remained obscure. Thus, unbiased biochemical assays were required to identify and

characterize the nature of fusion-active S proteins.

Both of our novel assays developed to study attachment, uptake or fusion of virions (Chapter 2) or cleavage of the S protein (Chapter 3) rely on expression of *E. coli* derived enzymes in target cells. The chosen strategies required only minor adjustments to the virions by integration of either a small 45-aa α -peptide or a 15-aa biotin acceptor peptide (BAP) tag. In chapter 2 we describe our cell biological assays, which are based on minimal complementation of the β -galactosidase enzyme with the α -peptide. We were able to discriminate between binding, internalization, and fusion at low numbers of infecting virus particles independent of replication. The novel entry assays provide several advantages over conventional assays. Enzymatic amplification of a readout parameter allows for strong signals without having to rely on gene amplification, which allows performing infections at physiologically relevant conditions. Drugs affecting replication in general, such as translation inhibitors, which will inadvertently affect viral gene expression, can be tested independently of virus replication for their effect on virus entry. With complementation occurring immediately after the membrane fusion event, the assay allows for more precise kinetic measurements on virus entry. Also it should become easier to dissect effects of mutations in virions on entry and/or replication. Furthermore, the enzymatic activity can be quantified by a variety of different methods, opening up opportunities for high-throughput analysis by FACS or by automated fluorescence microscopy. Unfortunately, the need to express Δ M15 in the target cells hampers the investigation of fusion in e.g. primary cells. Yet, for cells not expressing Δ M15, the assay can still be used to investigate binding and internalization by supplying Δ M15 during or after cell lysis. In chapter 2, 4 and 5 we demonstrated the entry assays can be used in combination with various methods to perturb cellular processes involved in viral entry, including the use of inhibitors, RNA interference, knock-out cells, and by expression of dominant-negative or constitutive-active proteins.

In chapter 3 we describe our biochemical fusion assay to analyze only the S proteins of particles that have fused with the host cell. This is desirable in view of the often high abundance of non-infectious particles occurring in preparations of many viruses including CoVs. For SARS-CoV, the particle to plaque forming unit (pfu) ratio was estimated to be 300-2000:1 (12-14). This makes it difficult to analyze molecular details of fusion-active spike proteins only. Research is also hampered by the absence of structural information on the full-length CoV S protein. So far no assays had been available which could determine the biochemical identity of fusion proteins immediately after fusion, particularly when isolating solely proteins that had undergone fusion. Using our conditional biotinylation assay relying on the attachment of biotin to BAP by the biotin ligase BirA we could specifically study the S proteins derived from MHV virions that had fused with the host cell. The assay allowed us to identify a proteolytically processed subunit of S. Unfortunately, as only a fraction of the virions undergo fusion, relatively high amounts of viruses were required. Moreover, not only the spike proteins forming the fusion pore will be exposed to the cytosol where biotinylation occurs but also the other spike proteins present in the fusing virion will be biotinylated.

Due to their versatility and the small tags required both methods may be adapted to other viruses, including non-enveloped viruses, to investigate viral entry. Indeed, the fusion assay was also successfully applied for vesicular stomatitis virus (VSV). Hence we expect both the cell biological binding, internalization and penetration assay, as well as the biochemical fusion protein assay to facilitate research on virus entry significantly.

2. Coronavirus entry and proteolytic processing

2.1. Proteolytic priming and triggering of coronavirus spike proteins

One of the characteristics described for class I viral fusion proteins is that they require proteolytic priming to render them fusion-competent. For most class I fusion proteins this proteolytic priming occurs during release from the producer cells, after which the cleaved products stay attached covalently linked by disulfide bonds. Prominent examples are the retrovirus human immunodeficiency virus (HIV) Env protein, which gets cleaved into gp120 and gp41, and the orthomyxovirus Influenza A virus (IAV), in which HA0 gets cleaved into HA1 and HA2. Also some coronaviruses undergo a proteolytic cleavage in the trans-Golgi network, whereby the S protein is cleaved into subunits S1 and S2 at a furin cleavage site (reviewed in (11)). However, whereas the priming cleavage of other class I fusion proteins is located immediately upstream of the putative fusion peptide (FP), the S1/S2 site is located more than 100 amino acid residues upstream of the putative FP. Cleavage at this S1/S2 site is mediated by furin-like proteases at suboptimal cleavage recognition motifs, leading to only a fraction of the spike proteins in virions being cleaved. Strikingly, MHV virions containing an optimal furin cleavage site at this position of the S protein, which would thus be expected to carry only cleaved spike proteins, seem not to be viable (unpublished results). The furin cleavage site at the S1/S2 junction of MHV S could, however, be removed without affecting virus infectivity (15), in agreement with several CoVs, including MHV-2 lacking an obvious cleavage site at this position (11, 16). For IBV, however, it has been demonstrated that proteolytic cleavage at the S1/S2 site enhances viral entry (17). While these results do not exclude cleavage at the S1/S2 junction to play a role in the priming of CoV S proteins, it indicates that there might be additional or other cleavage(s) required for making the CoV S protein fusion competent.

Several studies have used cell-cell fusion assays to study proteolytic priming of the CoV S protein. The capability of the spike protein or virions to induce syncytia was increased by the addition of proteases, indicating that proteolytic cleavage is necessary for efficient fusion (17). However, S protein cleaved at the S1/S2 interface is capable of inducing cell-cell fusion, even without addition of proteases. Yet, fusion was strongly reduced when the S1/S2 cleavage site of these proteins was removed (15, 18). The apparent discrepancy between the requirements of S protein cleavage to induce virus-cell or cell-cell fusion probably indicates that cell-cell fusion is not a good model for studying the requirements of virus-cell fusion. Still, the capability of syncytia induction of several coronaviruses may be advantageous for cell-cell spread *in vivo*.

Potential positive effects of S1/S2 cleavage could involve the removal of potential steric hindrances thereby allowing accessibility to other (more downstream) proteolytic priming sites. Over the last few years another cleavage site, marked by a crucial and highly conserved arginine residue, the so-called S2' site has been described to be located just upstream of a highly conserved FP (11, 18). Compared to other class I proteins this location seems to be reflecting the general priming location. In chapter 3 of this thesis we could show biochemically, using our novel fusion assay to label S proteins of fused viral particles only, that MHV S is indeed cleaved downstream of the S1/S2 interface. Furthermore, the kinetics of cleavage were shown to correspond with viral entry.

It is not yet clear, however, whether this cleaved S protein product (named S2*) corresponds to the protein product resulting from cleavage at S2'. The observation that the S2*

is found in a heat- and SDS-stable multimer, which shows similar properties as the six-helix bundle-containing post-fusion form of class I fusion proteins, appears to indicate that the S2* form is capable of adopting the conformational changes associated with fusion. This observation may suggest that S2* corresponds with the fusion-competent form of the S protein. It is difficult, however, to conclude based on the gel electrophoretic mobility of the S2* protein where cleavage occurs and whether S2* results from cleavage at S2'. Interestingly, the S2* protein appears as a fuzzy band, even after enzymatic removal of the N-glycans, which may indicate that this protein product results from alternative cleavages at different positions downstream of S1/S2 rather than from cleavage at S2' specifically. In agreement herewith, mutation of the conserved arginine at the S2' site did not affect the formation of S2*. The emergence of S2* could also not be inhibited by several compounds that were shown to inhibit fusion of MHV by using our novel fusion assay (chapter 4). The observation that the formation of S2* does not require transport of MHV through the endosomal system, seems to contradict with the requirement for lysosomal protease activity for fusion of MHV. This latter requirement could be lifted however by introduction of a furin cleavage site at the S2' site, resulting in furin-dependent virus. Probably, the intravirion tails of all S proteins of a virus particle will be exposed to the cytosol upon virus-cell fusion and will become biotinylated. Thus it may be that only a fraction of the biotinylated S2* proteins were actually involved in the process of the actual fusion pore formation. Based on the results of chapter 3 and 4, I would therefore like to hypothesize that the S2* protein does not result from cleavage at the S2' site, but rather corresponds to S proteins that are cleaved further upstream of S2'. Cleavages resulting in the formation of S2* may occur even at the plasma membrane and may be important for obtaining fusion competence. Progressive cleavages at the plasma membrane and during endosomal uptake might eventually result in the formation of the fusion-active form. Anyway, the data presented in chapter 4 indicate that another cleavage event is subsequently needed in the endo-lysosomal system for fusion to occur.

Although cleavage at the S1/S2 junction may occur for some CoVs in the cells in which the viruses are produced (producer cells), the proteolytic priming of CoV S resulting from cleavages downstream of S1/S2 seems to occur only in the target cells. In this respect, CoV S proteins appear to diverge from most class I fusion proteins, which are mostly proteolytically primed in the producer cells. However, a few other class I fusion protein viruses, such as the filovirus Ebola or the paramyxovirus RSV have also been shown to require proteolytic cleavage of their fusion proteins in the target cells (19, 20). Also the HA protein of influenza A viruses is not only cleaved in the producer cell or by extracellular proteases, but can also become cleaved upon binding or endocytic uptake of virus particles to/into the target cell (21).

At the start of my studies, it was not clear to what extent entry of CoVs in general and MHV in particular depended on low pH as a microenvironmental cue for viral fusion. A dependence on low pH or endosomal acidification had been shown for SARS-CoV, IBV, MHV-2 and an isolate of MHV-4 (22-26). However, for SARS-CoV the pH dependence was attributed to the pH-dependent activation of cathepsin L. For MHV-A59 two studies had shown different requirements of acidification and low pH (24, 27). Interestingly, the virions of MHV strains A59, 4 (JHM), and SRec seem to be very stable with respect to their infectivity when exposed to pH values as low as 3.5 or as high as 8.0 (unpublished data). This may be explained either by the S protein conformation being insensitive to low pH or by the S protein being able to reversibly refold upon low-pH exposure, as has been observed for the proteolytically

unprocessed fusion glycoprotein G of VSV (reviewed in (28)). Our results in chapter 4 show that entry of MHV virus requires endocytosis, but is less sensitive to perturbation of endosomal pH than the well-studied viruses VSV and IAV, which are both known to undergo fusion upon exposure to low pH as trigger (29-32). Also in haploid HOPS complex knockout cells, where acidification until the late endosome is still intact, MHV did not fuse, despite the low-pH induced IAV being able to fuse in these cells. These results strongly indicate that a low pH is not sufficient to induce MHV fusion.

Our results show that rather than low pH, cleavage at the S2' site may function as a fusion trigger. Fusion of viruses not containing a (minimal) furin cleavage site (FCS, R-X-X-R motif) immediately upstream of the FP require trafficking to the lysosome, where proteases are present capable of cleaving those CoVs. We could show this by using a pan-lysosomal protease inhibitor CPI, which combines the effects of an endosomal papain-like cysteine protease inhibitor (PLCP), an aspartyl protease inhibitor, and an asparagine endopeptidase inhibitor (AEP). The wide coverage of the inhibitor towards the three major classes of proteases present in the lysosome is necessary since many of them are redundant in their function and they may be upregulated upon inhibition of another protease (33, 34). We could show that both MHV and feline infectious peritonitis virus (FIPV) were inhibited in their fusion by CPI. However, infection by MERS-CoV, which contains a FCS at the S2' site, was not inhibited by lysosomal protease inhibitors but rather by furin inhibitors. Likewise, a mutant MHV with an engineered FCS at the position of the S2' site lost the requirement for lysosomal trafficking, but rather became dependent on furin-like proteases.

Our results (chapter 4) and those of others (24, 35) indicate that MHV-A59, in contrast to MHV-2, is not dependent on cleavage by cathepsin L. While inhibitors of cathepsin L have been shown to inhibit entry of MHV-2 and SARS-CoV (24, 36), this was not observed for MHV-A59. In agreement herewith, the S2' cleavage site of MHV-A59 (AIRGR | SA) differs from that of MHV-2 (AQTGR | SA). The requirement for a pan-lysosomal protease to inhibit virus entry indicates a redundancy in the proteases that can cleave at the S2' site of MHV-A59. The difficulty of studying the proteolytic processing of CoV S proteins is probably illustrated best by looking at SARS-CoV for which at least six proteases have been described to play a role in entry (reviewed in (11)).

Based on our results and the work of others, we conclude that cleavage at the FP proximal position is likely to be a general requirement for CoV entry and may even be the fusion trigger. With the possible exception of IBV, cleavage at this position does not appear to occur in the virion-producing cell as it is not observed in released virions, but in the target cell (33, 37-40). This suggests that receptor binding and/or other environmental cues are necessary to render the triggering cleavage site accessible for proteolysis in the intact virion. These other cues may involve cleavages that correspond with the generation of S2*, while we cannot exclude a role for low pH in this process. Also for other class I fusion protein containing viruses, such as RSV (19) and Ebola virus (20), cleavage of the fusion protein upon endocytosis may function as a fusion trigger.

2.2. Host factor dependency of CoV entry

Our results indicate that MHV requires CME for the infection of host cells. This is in agreement with previous studies, which have shown the requirement for CME for entry of MHV (24, 27, 41, 42). In our investigations we could show both in murine L2 cells and

in human HeLa cells expressing the MHV receptor murine Ceacam1a that MHV enters via CME. Strikingly, also the highly fusogenic strain MHV-JHM, which is able to induce vast syncytia formation needs to enter cells via endocytosis. Besides MHV, also MERS-CoV, FIPV and SARS-CoV appear to be taken up via clathrin-mediated endocytosis. This is supported by the fact that all three viruses are inhibited by chlorpromazine in a dose-dependent manner ((24, 27, 40-44) and unpublished results), although for FIPV and SARS-CoV clathrin- and caveolae-independent endocytic pathway have been reported as well (45, 46) For the HCoV-229E a caveolae-dependent endocytic uptake has been suggested (47). We could show that endocytosis of MHV is dependent on the clathrin-coat accessory factor Dab2 but not on Eps15. The independence on Eps15 is unusual, as it was previously thought to be an essential factor for the formation of the coated pit; Eps15-independent entry was, however, also shown for MHV-2 (48-50).

In chapter 5 we elucidate the role of another host factor, ATP1A1, critical for entry of CoVs, but not of IAV. CoV entry was inhibited, when the protein ATP1A1 was knocked down or targeted by cardiotonic steroids. Our results indicate that Src signaling induced by the lack of ATP1A1 or addition of CTSs somehow negatively affected the endocytic uptake of CoVs, possibly by disturbance of the assembly of the scission process of the clathrin-coated pit formed prior to internalization of the virus. In the presence of the CTS ouabain virus particles accumulated close to the cell surface in pre-endosomal structures, further uptake of which could be inhibited by inhibitors of CME and dynamin. The negative effect of ouabain on MHV infection could be reversed by the addition of inhibitors of Src signaling. The link between the endocytic uptake of CoVs and Na^+, K^+ -ATPase-mediated Src signaling may be supported by the observed modulation of dynamin-2 phosphorylation and clathrin-coated pit formation by Src signaling (51, 52). The lack of inhibition of infection with IAV by the knockdown of ATP1A1 or by induction of ATP1A1 signaling by cardiotonic steroids may be explained by this virus' ability to enter cells in the absence of CME via macropinocytosis (53, 54).

Many host-factors involved in the entry of MHV can clearly be associated with the endosomal maturation process. Factors, like EEA1 and RAB5, associated with the formation of early endosomes were found to be important for CoVs, regardless of their intracellular site of fusion. This confirms that both early and late fusing forms of the virus, as demonstrated nicely in chapter 4 for MHV-A59 and MHV containing a furin cleavage site at the S2' location, are relying on CME and uptake into early endosomes. Due to the presence of furin and furin-like proteases in early endosomes CoVs containing a furin-cleavage site immediately upstream of the FP could be shown to escape the endocytic vesicles already at that early stage and to no longer rely on late endosomal and lysosomal host-factors. This could be demonstrated for the MERS-CoV, which contains an R-X-X-R motif at the S2' site. Other CoVs, such as MHV A59 and FIPV, which do not contain furin cleavage sites adjacent to the FP, were shown to additionally depend on host factors involved in endosomal maturation such as RAB7 and members of the HOPS complex. The host factors are required in the maturation of early endosomes to form late endosomes and lysosomes. Viruses that required trafficking to these late endosomal compartments could be shown to rely on the activity of lysosomal proteases for virus-cell fusion. A good indicator drug to distinguish early or late fusion of CoVs seems to be U18666A, a cholesterol transport-affecting agent, which also prevents maturation of late endosomes (55). The negative effect of U18666A on MHV entry is most likely not related to the effect of this drug on cholesterol transport as cells lacking NPC1, which display a

similar cholesterol trafficking defect, could be readily infected with MHV (unpublished results). MHV virions that were shown to fuse in different intracellular compartments displayed very similar growth and reporter gene expression kinetics. This either indicates that there are no particular uncoating factors required or, if they are required, these are available at or recruited to both early endosomal and lysosomal vesicles.

It is not surprising that CoVs employ endocytosis for entry. By using the cellular endosomal entry pathways viruses are able to avoid many cellular obstacles and immune responses. Engulfment and uptake of entire viral particles does not leave traces at the plasma membrane that could be recognized by the immune system. Viruses can 'hide' in endocytic vesicles from cellular defense mechanisms until they are at the correct location for their replication and for the synthesis of their own proteins, which can then help silencing or preventing cellular defense reactions (56). And most importantly of course, through endocytic uptake viruses are able to avoid intracellular barriers posed by the cytoskeleton, get a free ride to the cytosol, and receive specific cues from the changing environment in maturing endosomes in order to recognize their point of exit (57-61). CoVs are in good company with other viruses earlier presumed to enter via direct fusion at the plasma membrane that now have been shown to enter via endocytic uptake pathways. This can be seen for instance in the case of human immunodeficiency virus and respiratory syncytial virus (19, 62). Even though there is a small number of viruses, such as Sendai virus and herpes simplex virus, still suggested to enter via direct fusion, these viruses seem to have specific properties by which they are able to interact with the cytoskeleton and to overcome this barrier (63-67).

3. Concluding remarks and future directions

In conclusion, our results shed new light on the CoV entry process. In particular we have demonstrated the tight link between CoV endocytosis and fusion and the proteolytic processing of the S protein. We have shown that the intracellular site of fusion is determined by the cleavage site immediately upstream of the FP. It may well be that this proteolytic cleavage triggers the viral fusion process. However, we cannot exclude that other environmental cues such as low pH play additional roles in the triggering of the actual coronavirus fusion process. Our results furthermore indicate that although several CoVs are capable of inducing cell-cell fusion, this is not reflected in virus particles entering cells via fusion at the plasma membrane. Conclusions drawn based on cell-cell fusion assays should therefore not be translated without caution to the virus-cell fusion process.

Proteolytic cleavage of the S protein may not only be involved in triggering viral fusion, but also in making the S protein fusion competent. These cleavages may take place at the S1/S2 junction, possibly also for viruses that are not cleaved at this position in the producer cell. In addition, cleavages downstream of S1/S2 and upstream of the S2' sites, which may result in the formation of S2*-like products may play a role in priming the S protein for fusion competence. While receptor-binding is likely required for making the S2' site accessible for proteases (68), it is not yet clear whether prior cleavage at S1/S2 or other positions in the S protein is also required.

To make the next step in understanding the mechanism of the CoV fusion process, it will probably be required to establish *in vitro* fusion assays, in which all required components (receptor, S protein and lipids) can be manipulated at will and characterized biochemically. In addition, it will be of invaluable importance to gain structural insights into the pre- and post-

fusion conformation of the CoV S protein.

Besides pursuing *in vitro*-based approaches, it will also be needed to study CoV entry in the *in vivo* context. This is of importance as the infection conditions *in vivo* and *in vitro* are obviously very different. This may particularly be the case with respect to the host cell proteases that are available for cleavage of the S protein. For the SARS-CoV at least 6 different proteases have already been identified to be able to stimulate virus entry. It will be of importance to identify the full arsenal of host proteases that may be used for the priming and triggering of CoV S proteins. It will, however, be very challenging technically to study the virus entry process *in vivo*. The use of primary cell cultures or the organoids that reflect the physiological conditions that are found in the respiratory or intestinal tract will probably be a good first step in this respect.

Our studies also resulted into new insights into the host factors required for CoV entry. Thus, we not only confirmed the importance of CME in the entry of MHV, but we also identified several other host factors to be important for this process. This is of importance as coronaviruses are highly adaptable viruses. They have shown their ability to switch hosts as evidenced by the various zoonotic forms of CoVs (MERS-CoV and SARS-CoV) that made the news recently. Such zoonotic transmission events are likely to continue occurring in the future. Therefore the targeting of commonly used host cell factors by different CoVs might be a good antiviral strategy. While targeting host factors involved in late endosome-to-lysosome trafficking may be used to inhibit some CoVs, others are not affected with this strategy. It is probably more attractive to target host proteins that are required by all CoVs. One of the candidates for an antiviral strategy against CoVs may be found in chapter 5, where we show the inhibition of all CoVs tested by the addition of cardiotonic steroids targeting ATP1A1. This may be an attractive strategy to pursue as FDA-approved cardiotonic steroids are available.

Taken together, the research described in this thesis provides new insights into the CoV entry process. Our results indicate that the CoV-cell fusion process has its peculiarities but, unlike earlier contradictory publications suggested, in the end it does not appear to deviate fundamentally from the general principles of class I fusion. Furthermore, new insights are not only provided with respect to virus-cell fusion, but also about basic cellular processes that are misused by CoVs to enter cells. These new insight may contribute to the development of new antiviral therapies.

REFERENCES

1. **Chen YD, Blumenthal R.** 1989. On the use of self-quenching fluorophores in the study of membrane fusion kinetics. The effect of slow probe redistribution. *Biophysical chemistry* **34**:283-292.
2. **Lowy RJ, Sarkar DP, Chen Y, Blumenthal R.** 1990. Observation of single influenza virus-cell fusion and measurement by fluorescence video microscopy. *Proc Natl Acad Sci U S A* **87**:1850-1854.
3. **Raviv Y, Viard M, Bess J, Jr., Blumenthal R.** 2002. Quantitative measurement of fusion of HIV-1 and SIV with cultured cells using photosensitized labeling. *Virology* **293**:243-251.
4. **Cavrois M, De Noronha C, Greene WC.** 2002. A sensitive and specific enzyme-based assay detecting HIV-1 virion fusion in primary T lymphocytes. *Nature biotechnology* **20**:1151-1154.
5. **Kolokoltsov AA, Davey RA.** 2004. Rapid and sensitive detection of retrovirus entry by using a novel luciferase-based content-mixing assay. *J Virol* **78**:5124-5132.
6. **Saeed MF, Kolokoltsov AA, Davey RA.** 2006. Novel, rapid assay for measuring entry of diverse enveloped viruses, including HIV and rabies. *J Virol Methods* **135**:143-150.
7. **Wolf MC, Wang Y, Freiberg AN, Aguilar HC, Holbrook MR, Lee B.** 2009. A catalytically and genetically optimized beta-lactamase-matrix based assay for sensitive, specific, and higher throughput analysis of native henipavirus entry characteristics. *Virology journal* **6**:119.
8. **Tscherne DM, Manicassamy B, Garcia-Sastre A.** 2010. An enzymatic virus-like particle assay for sensitive detection of virus entry. *J Virol Methods* **163**:336-343.
9. **Laliberte JP, Weisberg AS, Moss B.** 2011. The membrane fusion step of vaccinia virus entry is cooperatively mediated by multiple viral proteins and host cell components. *PLoS pathogens* **7**:e1002446.
10. **Bosch BJ, de Haan CA, Rottier PJ.** 2004. Coronavirus spike glycoprotein, extended at the carboxy terminus with green fluorescent protein, is assembly competent. *Journal of virology* **78**:7369-7378.
11. **Belouza S, Millet JK, Licitra BN, Whittaker GR.** 2012. Mechanisms of coronavirus cell entry mediated by the viral spike protein. *Viruses* **4**:1011-1033.
12. **Keyaerts E, Vijgen L, Maes P, Neyts J, Van Ranst M.** 2005. Growth kinetics of SARS-coronavirus in Vero E6 cells. *Biochemical and biophysical research communications* **329**:1147-1151.
13. **Sampath R, Hofstadler SA, Blyn LB, Eshoo MW, Hall TA, Massire C, Levene HM, Hannis JC, Harrell PM, Neuman B, Buchmeier MJ, Jiang Y, Ranken R, Drader JJ, Samant V, Griffey RH, McNeil JA, Croke ST, Ecker DJ.** 2005. Rapid identification of emerging pathogens: coronavirus. *Emerging infectious diseases* **11**:373-379.
14. **Vicenzi E, Canducci F, Pinna D, Mancini N, Carletti S, Lazzarin A, Bordignon C, Poli G, Clementi M.** 2004. Coronaviridae and SARS-associated coronavirus strain HSR1. *Emerging infectious diseases* **10**:413-418.
15. **de Haan CA, Stadler K, Godeke GJ, Bosch BJ, Rottier PJ.** 2004. Cleavage inhibition of the murine coronavirus spike protein by a furin-like enzyme affects cell-cell but not virus-cell fusion. *Journal of virology* **78**:6048-6054.

16. **Yamada YK, Takimoto K, Yabe M, Taguchi F.** 1998. Requirement of proteolytic cleavage of the murine coronavirus MHV-2 spike protein for fusion activity. *Advances in experimental medicine and biology* **440**:89-93.
17. **Otsuki K, Tsubokura M.** 1981. Plaque formation by avian infectious bronchitis virus in primary chick embryo fibroblast cells in the presence of trypsin. *Archives of virology* **70**:315-320.
18. **Yamada Y, Liu DX.** 2009. Proteolytic activation of the spike protein at a novel RRRR/S motif is implicated in furin-dependent entry, syncytium formation, and infectivity of coronavirus infectious bronchitis virus in cultured cells. *Journal of virology* **83**:8744-8758.
19. **Krzyzaniak MA, Zumstein MT, Gerez JA, Picotti P, Helenius A.** 2013. Host cell entry of respiratory syncytial virus involves macropinocytosis followed by proteolytic activation of the F protein. *PLoS pathogens* **9**:e1003309.
20. **Chandran K, Sullivan NJ, Felbor U, Whelan SP, Cunningham JM.** 2005. Endosomal proteolysis of the Ebola virus glycoprotein is necessary for infection. *Science* **308**:1643-1645.
21. **Bottcher E, Matrosovich T, Beyerle M, Klenk HD, Garten W, Matrosovich M.** 2006. Proteolytic activation of influenza viruses by serine proteases TMPRSS2 and HAT from human airway epithelium. *Journal of virology* **80**:9896-9898.
22. **Chu VC, McElroy LJ, Chu V, Bauman BE, Whittaker GR.** 2006. The avian coronavirus infectious bronchitis virus undergoes direct low-pH-dependent fusion activation during entry into host cells. *Journal of virology* **80**:3180-3188.
23. **Gallagher TM, Escarmis C, Buchmeier MJ.** 1991. Alteration of the pH dependence of coronavirus-induced cell fusion: effect of mutations in the spike glycoprotein. *Journal of virology* **65**:1916-1928.
24. **Qiu Z, Hingley ST, Simmons G, Yu C, Das Sarma J, Bates P, Weiss SR.** 2006. Endosomal proteolysis by cathepsins is necessary for murine coronavirus mouse hepatitis virus type 2 spike-mediated entry. *Journal of virology* **80**:5768-5776.
25. **Regan AD, Shraybman R, Cohen RD, Whittaker GR.** 2008. Differential role for low pH and cathepsin-mediated cleavage of the viral spike protein during entry of serotype II feline coronaviruses. *Veterinary microbiology* **132**:235-248.
26. **Simmons G, Gosalia DN, Rennekamp AJ, Reeves JD, Diamond SL, Bates P.** 2005. Inhibitors of cathepsin L prevent severe acute respiratory syndrome coronavirus entry. *Proceedings of the National Academy of Sciences of the United States of America* **102**:11876-11881.
27. **Eifart P, Ludwig K, Bottcher C, de Haan CA, Rottier PJ, Korte T, Herrmann A.** 2007. Role of endocytosis and low pH in murine hepatitis virus strain A59 cell entry. *Journal of virology* **81**:10758-10768.
28. **Albertini AA, Baquero E, Ferlin A, Gaudin Y.** 2012. Molecular and cellular aspects of rhabdovirus entry. *Viruses* **4**:117-139.
29. **Sieczkarski SB, Whittaker GR.** 2003. Differential requirements of Rab5 and Rab7 for endocytosis of influenza and other enveloped viruses. *Traffic* **4**:333-343.

30. **Skehel JJ, Bayley PM, Brown EB, Martin SR, Waterfield MD, White JM, Wilson IA, Wiley DC.** 1982. Changes in the conformation of influenza virus hemagglutinin at the pH optimum of virus-mediated membrane fusion. *Proceedings of the National Academy of Sciences of the United States of America* **79**:968-972.
31. **Carneiro FA, Ferradosa AS, Da Poian AT.** 2001. Low pH-induced conformational changes in vesicular stomatitis virus glycoprotein involve dramatic structure reorganization. *The Journal of biological chemistry* **276**:62-67.
32. **White J, Matlin K, Helenius A.** 1981. Cell fusion by Semliki Forest, influenza, and vesicular stomatitis viruses. *The Journal of cell biology* **89**:674-679.
33. **Matthews SP, Werber I, Deussing J, Peters C, Reinheckel T, Watts C.** 2010. Distinct protease requirements for antigen presentation in vitro and in vivo. *Journal of immunology* **184**:2423-2431.
34. **van Kasteren SI, Berlin I, Colbert JD, Keane D, Ovaa H, Watts C.** 2011. A multifunctional protease inhibitor to regulate endolysosomal function. *ACS chemical biology* **6**:1198-1204.
35. **Matsuyama S, Taguchi F.** 2009. Two-step conformational changes in a coronavirus envelope glycoprotein mediated by receptor binding and proteolysis. *Journal of virology* **83**:11133-11141.
36. **Huang IC, Bosch BJ, Li F, Li W, Lee KH, Ghiran S, Vasilieva N, Dermody TS, Harrison SC, Dormitzer PR, Farzan M, Rottier PJ, Choe H.** 2006. SARS coronavirus, but not human coronavirus NL63, utilizes cathepsin L to infect ACE2-expressing cells. *The Journal of biological chemistry* **281**:3198-3203.
37. **Kam YW, Okumura Y, Kido H, Ng LF, Bruzzone R, Altmeyer R.** 2009. Cleavage of the SARS coronavirus spike glycoprotein by airway proteases enhances virus entry into human bronchial epithelial cells in vitro. *PloS one* **4**:e7870.
38. **Watanabe R, Matsuyama S, Shirato K, Maejima M, Fukushi S, Morikawa S, Taguchi F.** 2008. Entry from the cell surface of severe acute respiratory syndrome coronavirus with cleaved S protein as revealed by pseudotype virus bearing cleaved S protein. *Journal of virology* **82**:11985-11991.
39. **Belouzard S, Chu VC, Whittaker GR.** 2009. Activation of the SARS coronavirus spike protein via sequential proteolytic cleavage at two distinct sites. *Proceedings of the National Academy of Sciences of the United States of America* **106**:5871-5876.
40. **Burkard C, Verheije MH, Wicht O, van Kasteren SI, van Kuppeveld FJ, Haagmans BL, Pelkmans L, Rottier PJ, Bosch BJ, de Haan CA.** 2014. Coronavirus Cell Entry Occurs through the Endo-/Lysosomal Pathway in a Proteolysis-Dependent Manner. *PLoS pathogens* **10**:e1004502.
41. **Stauber R, Pfeleiderera M, Siddell S.** 1993. Proteolytic cleavage of the murine coronavirus surface glycoprotein is not required for fusion activity. *The Journal of general virology* **74** (Pt 2):183-191.
42. **Sturman LS, Ricard CS, Holmes KV.** 1985. Proteolytic cleavage of the E2 glycoprotein of murine coronavirus: activation of cell-fusing activity of virions by trypsin and separation of two different 90K cleavage fragments. *Journal of virology* **56**:904-911.

43. **de Wilde AH, Jochmans D, Posthuma CC, Zevenhoven-Dobbe JC, van Nieuwkoop S, Bestebroer TM, van den Hoogen BG, Neyts J, Snijder EJ.** 2014. Screening of an FDA-approved compound library identifies four small-molecule inhibitors of Middle East respiratory syndrome coronavirus replication in cell culture. *Antimicrobial agents and chemotherapy*.
44. **Inoue Y, Tanaka N, Tanaka Y, Inoue S, Morita K, Zhuang M, Hattori T, Sugamura K.** 2007. Clathrin-dependent entry of severe acute respiratory syndrome coronavirus into target cells expressing ACE2 with the cytoplasmic tail deleted. *Journal of virology* **81**:8722-8729.
45. **Van Hamme E, Dewerchin HL, Cornelissen E, Verhasselt B, Nauwynck HJ.** 2008. Clathrin- and caveolae-independent entry of feline infectious peritonitis virus in monocytes depends on dynamin. *The Journal of general virology* **89**:2147-2156.
46. **Wang H, Yang P, Liu K, Guo F, Zhang Y, Zhang G, Jiang C.** 2008. SARS coronavirus entry into host cells through a novel clathrin- and caveolae-independent endocytic pathway. *Cell research* **18**:290-301.
47. **Nomura R, Kiyota A, Suzuki E, Kataoka K, Ohe Y, Miyamoto K, Senda T, Fujimoto T.** 2004. Human coronavirus 229E binds to CD13 in rafts and enters the cell through caveolae. *Journal of virology* **78**:8701-8708.
48. **de Melker AA, van der Horst G, Borst J.** 2004. Ubiquitin ligase activity of c-Cbl guides the epidermal growth factor receptor into clathrin-coated pits by two distinct modes of Eps15 recruitment. *The Journal of biological chemistry* **279**:55465-55473.
49. **Pu Y, Zhang X.** 2008. Mouse hepatitis virus type 2 enters cells through a clathrin-mediated endocytic pathway independent of Eps15. *Journal of virology* **82**:8112-8123.
50. **Schmid SL.** 1997. Clathrin-coated vesicle formation and protein sorting: an integrated process. *Annual review of biochemistry* **66**:511-548.
51. **Harris TL, Xie Z.** 2012. Ouabain regulates caveolin-1 vesicle trafficking by a Src-dependent mechanism (Doctoral dissertation). Retrieved from ProQuest Dissertations and Theses Database. (AAT 3512447).
52. **Liu J, Kesiry R, Periyasamy SM, Malhotra D, Xie Z, Shapiro JI.** 2004. Ouabain induces endocytosis of plasmalemmal Na/K-ATPase in LLC-PK1 cells by a clathrin-dependent mechanism. *Kidney international* **66**:227-241.
53. **Sieczkarski SB, Whittaker GR.** 2002. Influenza virus can enter and infect cells in the absence of clathrin-mediated endocytosis. *Journal of virology* **76**:10455-10464.
54. **Rossman JS, Leser GP, Lamb RA.** 2012. Filamentous influenza virus enters cells via macropinocytosis. *Journal of virology* **86**:10950-10960.
55. **Huynh KK, Gershenson E, Grinstein S.** 2008. Cholesterol accumulation by macrophages impairs phagosome maturation. *The Journal of biological chemistry* **283**:35745-35755.
56. **Hewitt EW.** 2003. The MHC class I antigen presentation pathway: strategies for viral immune evasion. *Immunology* **110**:163-169.
57. **Marsh M, Bron R.** 1997. SFV infection in CHO cells: cell-type specific restrictions to productive virus entry at the cell surface. *Journal of cell science* **110 (Pt 1)**:95-103.
58. **Radtke K, Dohner K, Sodeik B.** 2006. Viral interactions with the cytoskeleton: a hitchhiker's guide to the cell. *Cellular microbiology* **8**:387-400.

-
59. **Authier F, Posner BI, Bergeron JJ.** 1996. Endosomal proteolysis of internalized proteins. *FEBS letters* **389**:55-60.
 60. **Huotari J, Helenius A.** 2011. Endosome maturation. *The EMBO journal* **30**:3481-3500.
 61. **Plempner RK.** 2011. Cell entry of enveloped viruses. *Current opinion in virology* **1**:92-100.
 62. **Permanyer M, Ballana E, Este JA.** 2010. Endocytosis of HIV: anything goes. *Trends in microbiology* **18**:543-551.
 63. **Lyman MG, Enquist LW.** 2009. Herpesvirus interactions with the host cytoskeleton. *Journal of virology* **83**:2058-2066.
 64. **Fuller AO, Spear PG.** 1987. Anti-glycoprotein D antibodies that permit adsorption but block infection by herpes simplex virus 1 prevent virion-cell fusion at the cell surface. *Proceedings of the National Academy of Sciences of the United States of America* **84**:5454-5458.
 65. **Sodeik B, Ebersold MW, Helenius A.** 1997. Microtubule-mediated transport of incoming herpes simplex virus 1 capsids to the nucleus. *The Journal of cell biology* **136**:1007-1021.
 66. **Okada Y.** 1969. Factors in fusion of cells by HVJ. *Current topics in microbiology and immunology* **48**:102-128.
 67. **Stein BS, Gowda SD, Lifson JD, Penhallow RC, Bensch KG, Engleman EG.** 1987. pH-independent HIV entry into CD4-positive T cells via virus envelope fusion to the plasma membrane. *Cell* **49**:659-668.
 68. **Gomez I, Sanchez J, Miranda R, Bravo A, Soberon M.** 2002. Cadherin-like receptor binding facilitates proteolytic cleavage of helix alpha-1 in domain I and oligomer prepore formation of *Bacillus thuringiensis* Cry1Ab toxin. *FEBS letters* **513**:242-246.

SUMMARY

English

In 1977 a combined effort of disease surveillance and worldwide, coordinated vaccination managed to eradicate smallpox, one of the most devastating virus-caused diseases of all times. Following this victory over smallpox people thought that viral infections would soon be a thing of the past. However, today we know better. Viruses are small particles containing genetic information and in some cases are able to cause illnesses in their hosts. Viral illnesses are one of the major health problems of our time, including measles epidemics, flu, AIDS, and many more. Not only humans get affected by these diseases, in fact almost every living thing can be infected by viruses. Yet viruses are no living organisms but merely an assembly of genetic information wrapped by proteins and sometimes lipids. They are skillfully assembled entities with the sole purpose of gaining access into host organisms and -cells to make them multiply the virus particles, named virions, and thereby their genetic information. A hosts defense system can be prepared to recognize viruses and destroy them quicker by getting vaccinated. For many viruses vaccines are however not always readily available. Therefore we need to think of other strategies of how to prevent viral spread and disease. One strategy is to study how their host helps them to multiply and to prevent this support from occurring without doing damage to the host organism.

The present dissertation deals with a family of viruses, the coronaviruses (CoVs), whose members cause a wide variety of illness in humans and animals. The human variants cause roughly 30-50% of the common cold cases. Other members of the family can cause array of infections affecting mainly the respiratory and intestinal system in various animals, including livestock. However, in recent years coronaviruses that usually infect animals have managed to infect humans when they had close contact with these animals, causing what are known as zoonotic infections. Incidents like this caused epidemics of the severe lung and breathing illnesses spreading in Asia and Canada in 2002/2003 and in the Middle East in 2012. The cause of these illnesses were the severe acute respiratory syndrome coronavirus (SARS-CoV), presumably transmitted from bats, and the Middle East respiratory syndrome coronavirus (MERS-CoV), presumably transmitted from camels, respectively. The thesis on hand made primarily use of the mouse hepatitis virus (MHV). This coronavirus, which usually causes very mild respiratory and intestinal infections, serves as a model for other coronavirus family members. Additionally, results obtained with MHV were confirmed using the previously mentioned MERS-CoV and feline infectious peritonitis coronavirus (FIPV),

CoV particles contain a single-stranded genome made of ribonucleic acids (RNA). This genome is wrapped up and packaged by the nucleocapsid (N) protein, making up the so-called ribonucleocapsid core. A lipid casing, the so-called envelope, surrounds this core. Additional proteins are anchored in the envelope to tether the core and envelope together and fulfill certain other functions; these are the membrane (M) and envelope (E) protein. Though, the most important protein in the virus for the purpose of this thesis is the spike (S) protein. The S protein has multiple functions in the entry of the virus into the host cell.

Virus entry is the first step of viral infection. During this step the virus has to overcome various obstacles provided by the cell, such as passing the outer barrier of the cell, the so-called plasma membrane, and get transported through the very dense contents of the inside of the cell, the so-called cytoplasm, to the point where ideal surroundings are present to allow replication. In the case of CoVs they need to reach the area close to the cell nucleus. The S protein is fulfilling multiple functions during the entry process. Amongst others, initially S coordinates binding to the outer cell surface but later it mediates the fusion process between

the viral membrane envelope and the cellular membranes to release the core, containing the genome, into the cytosol.

To avoid the barriers and get access to host cells viruses have developed sophisticated mechanisms to hijack cellular pathways and get a “free” ride into the cells. These uptake mechanisms, so-called endocytosis, are usually meant for transporting nutrients and extracellular signals into the cell. During uptake, the viral particle gets engulfed by the plasma membrane, which then pinches off towards the cytoplasm creating a lipid membrane surrounded bubble containing the virus, a so-called endosome. During endosome transport, the endosomes mature and ultimately form lysosomes. These lysosomes contain a very destructive and harsh environment which functions in the breakdown of nutrients and other components in order to be able to reuse them. To avoid destruction themselves viruses need to escape this harsh environment in time and release their core in the cytosol for replication. Usually the virus surface proteins get modified by the changing intra-endosomal environment to induce membrane fusion and make an escape possible.

In the case of CoVs it was first thought that the virus binds and fuses at the plasma membrane since the S protein is able to induce fusion between cells and thus does not appear to require additional endosomal environmental triggers. However, recent studies indicated that also CoVs use endocytosis to enter host cells. CoVs seem to be relatively insensitive to the usual cues causing membrane fusion in endosomes, such as increased acidity. In addition, for MHV, also a specific activation of S by cleavage of protein cleaving enzymes, so-called proteases, could not be found. In this dissertation I aimed to get a better understanding of CoV entry processes in general and that of MHV in particular. Thus, I aimed to get more insight into cleavage requirements of the CoV S proteins, the CoV uptake mechanism and the role of host factors in CoV entry.

It is usually technically difficult to look at entry of virus particles directly. It is easier to look at infections in cells once replication has occurred. In chapter two and three of this thesis I describe the development new techniques, which allow us to analyze the CoV entry of only a few viral particles per cell. In chapter two, we devised a sensitive entry assay, in which entry of virus particles into cells can be detected independent of virus replication by an ingenious amplification strategy. To this end, a small part of an enzyme was attached to the N or S protein of the virus. Upon entry, this small tag is paired with an inactive part of the enzyme expressed in the cytosol. This reconstitutes an active enzyme, which then can convert lots of substrates into detectable products, thereby amplifying the “entry” signal. This method allowed us to dissect and detect binding, internalization, and fusion of viruses during host cell entry. In chapter three we showed an assay allowing us to specifically mark S proteins of viruses, which had undergone the escape from the lipid bubble (endosome). This allowed us to investigate biochemical properties of the fused S proteins. Thereby we could show that these S proteins of MHV need to be cleaved by proteases in order for fusion to occur.

By combining our newly developed assay for observing fusion with several other cell-biological techniques we could investigate the cellular process involved in MHV entry in details. Whereas others had already found that MHV can trigger a specific kind of endocytosis, so-called clathrin-mediated endocytosis, we could confirm this and furthermore elucidate several additional host factors involved in this process in chapter four. We could further show that MHVs are staying in the endosomes until the latest stage of their maturation, the lysosome, before they can fuse and escape. We could show that CoVs seem to need the harsh and

destructive environment of the lysosome, in particular certain proteases to cleave and activate the S protein for fusion. By comparison with other CoVs, including FIPV and MERS-CoV, we could show that a certain sequence in the S proteins amino acid code is responsible for determining the point of escape in the endosomal pathway for CoVs.

In chapter five, we zoomed in on one critical cellular component in the CoV entry process and elucidated the importance of a specific subunit of the Na⁺,K⁺-ATPase. By using gene silencing as well as by applying cardiotonic drugs that bind to this subunit, we could show that a specific signaling pathway, so-called Src signaling, mediated via this subunit plays a crucial role in the inhibition of CoV infections. Cardiotonic steroids could be shown to inhibit entry of MHV at an early stage resulting in the accumulation of virus particles close to the cell surface.

Finally, chapter six of this thesis provides a summarizing discussion in which our findings on CoV entry are placed in the broader context of the available literature with the aim to integrate the different aspects of CoV entry – including endocytic uptake, proteolytic cleavage of S and the intracellular site of fusion – into a general picture.



SAMENVATTING

Nederlands

In 1977 werd het pokkenvirus uitgeroeid door een gecombineerde, wereldwijde aanpak van surveillance en vaccinatie. De overwinning op dit virus en de verschrikkelijke ziekte die het veroorzaakte gaf mensen het idee dat virussen snel iets uit het verleden zouden zijn. Tegenwoordig weten we echter beter. Virussen zijn kleine partikels die erfelijke informatie bevatten en vaak in staat zijn om ziekte te veroorzaken in hun gastheer. Virusziektes zoals mazelen, griep, AIDS en vele anderen behoren tot de grote gezondheidsproblemen van onze tijd. Niet alleen mensen worden getroffen door deze ziektes, eigenlijk kunnen alle levende wezens door virussen geïnfecteerd worden. Zelf zijn virussen geen levende wezens en bestaan ze alleen maar uit erfelijke informatie verpakt in eiwitten en soms lipiden. Virussen lijken virtuoos in elkaar gezet met als enig doel om een gastheer(cel) te infecteren en zich te vermenigvuldigen, leidend tot de vorming van nieuwe viruspartikels. Het afweersysteem van een gastheer kan door middel van vaccinatie voorbereid worden, waardoor het virussen sneller kan herkennen en vernietigen. Voor veel virussen zijn er echter geen vaccins. Daarom moeten we ook aan andere strategieën denken om verspreiding van een ziekte veroorzaakt door virussen tegen te gaan. Eén mogelijkheid is om te bestuderen hoe virussen gebruik maken van hun gastheer om zich te vermenigvuldigen. Deze kennis kan vervolgens toegepast worden om deze gastheerhulp te voorkomen, zonder overigens de gastheer zelf ziek te maken.

Deze dissertatie gaat over coronavirussen. Leden van deze virusfamilie veroorzaken ziekte in mens en dier. De humane coronavirussen veroorzaken ongeveer 30-50% van de verkoudheden. De andere leden van deze familie kunnen verschillende infecties veroorzaken van voornamelijk het respiratoire of het intestinale systeem in verschillende soorten dieren, waaronder de veestapel. Echter, de laatste jaren zijn coronavirussen die normaal gesproken dieren infecteren in staat gebleken om mensen, die in nauw contact met dieren waren geweest, te infecteren. Dit worden zoönotische infecties genoemd. Deze gevallen hebben geleid tot epidemieën van ernstige long- en ademhalingsziektes in Azië en Canada in 2002/2003 and het Midden Oosten in 2012. De veroorzakers van deze epidemieën waren het severe acute respiratory syndrome coronavirus (SARS-CoV) en het Middle East respiratory syndrome coronavirus (MERS-CoV), die respectievelijk waarschijnlijk werden overgedragen vanuit vlermuizen en kamelen. In dit proefschrift werd voornamelijk gebruik gemaakt van het zogenaamde muizen hepatitis virus (MHV). Dit coronavirus, dat milde respiratoire en intestinale infecties in muizen veroorzaakt, doet dienst als model voor andere coronavirussen. Daarnaast werden resultaten behaald met MHV bevestigd met het eerder genoemde MERS-CoV en het feline infectieus peritonitis virus (FIPV), een coronavirus van de kat.

CoV partikels bevatten een genoom dat bestaat uit een enkele ribonucleïnezuur (RNA) streng. Dit genoom wordt ingepakt door het nucleocapside (N) eiwit, waarbij het zogenaamde ribonucleocapside gevormd wordt. Het ribonucleocapside wordt omgeven door een lipide mantel, die ook wel envelop wordt genoemd. Verschillende eiwitten zijn verankerd in de envelop. De eiwitten M en E verbinden het ribonucleocapside met de envelop en vervullen daarnaast ook andere functies. Het belangrijkste eiwit in de envelop, tenminste met betrekking tot dit proefschrift, is het S eiwit. Het S eiwit heeft verschillende functies in de binnenkomst van het virus in de gastheercel.

De binnenkomst van het virus in een gastheercel is de eerste stap in een virusinfectie. Gedurende deze stap moet het virus verschillende obstakels zien te overwinnen, zoals het passeren van de buitenste barrière van de cel, de zogenaamde plasmamembraan. Vervolgens moet het virus getransporteerd worden door het dichte binnenste van de cel, het cytoplasma,

naar dat punt waar de optimale omstandigheden zijn voor virusreproductie. In het geval van CoVs is dat de omgeving dicht bij de celkern. In eerste instantie is het S eiwit verantwoordelijk voor binding van het virus aan het oppervlak van de cel. Vervolgens induceert S de fusie van de virale membraan envelop met cellulaire membranen waardoor het ribonucleocapside vrijkomt in het cytoplasma.

Om de barrières te omzeilen en toegang te krijgen tot de gastheercel hebben virussen geraffineerde mechanismes ontwikkeld om bestaande gastheerroutes om de cel binnen te komen te misbruiken. Deze opname mechanismes, ook wel endocytose genoemd, worden normaal gesproken gebruikt om voedingsstoffen en signalen van buiten de cel in te brengen. Gedurende de opname wordt het viruspartikel omgeven door het plasmamembraan dat vervolgens afsnoert in het cytoplasma waardoor er een virus-bevattend membraan-belletje wordt gevormd, het endosoom. Gedurende het transport van endosomen in de cel, rijpen ze en vormen uiteindelijk lysosomen. Deze lysosomen bevatten een erg destructief milieu dat een rol speelt in de afbraak van voedingsstoffen en andere componenten met als doel om ze opnieuw te kunnen gebruiken. Virussen moeten zien te ontsnappen aan vernietiging door het destructieve milieu van de lysosomen en hun ribonucleocapside laten vrijkomen in het cytoplasma voor reproductie. Gewoonlijk worden de oppervlakte-eiwitten van het virus gemodificeerd door het veranderde milieu in de endosomen waardoor fusie tussen membranen wordt geïnduceerd en ontsnapping mogelijk is.

Voor CoVs werd in eerste instantie gedacht dat het virus bindt en vervolgens fuseert aan het plasmamembraan omdat het S eiwit in staat is om fusie tussen cellen te induceren en dus ogenschijnlijk geen modificatie en activatie door het endosomale milieu nodig heeft. Echter, recente studies hebben laten zien dat ook CoVs endocytose gebruiken om een cel binnen te komen. CoVs lijken relatief ongevoelig voor de gewoontelijke triggers van membraanfusie in endosomen zoals een verhoogde zuurgraad. Verder kon voor MHV ook geen activatie van het S eiwit gevonden worden door klieving door zogenaamde protease eiwitten. In het onderzoek beschreven in dit proefschrift beoogde ik een beter begrip te krijgen van de binnenkomst in cellen van CoVs in het algemeen en MHV in het bijzonder. Ik beoogde dus meer inzicht te krijgen in het belang van klieving van CoV S eiwitten, de opname van CoV partikels en de rol van gastheerfactoren in de binnenkomst van CoVs in cellen.

Over het algemeen is het technisch moeilijk om de binnenkomst van virussen direct te bestuderen. Het is gemakkelijker om infectie van cellen te detecteren nadat er reproductie heeft plaatsgevonden. In hoofdstuk 2 en 3 van dit proefschrift beschrijf ik de ontwikkeling van nieuwe technieken waarmee we de binnenkomst van enkele CoV partikels per cel kunnen analyseren. In hoofdstuk 2 ontwikkelden we een gevoelige proefopzet (assay) waarin de binnenkomst van viruspartikels in een cel gedetecteerd kan worden zonder dat er virus reproductie nodig is door gebruik te maken van een ingenieuze amplificatie strategie. Hiertoe werd een klein gedeelte van een enzym geplakt aan het N of S eiwit van het virus. Na binnenkomst kan dit aanhangsel interacteren met een anderszins inactief enzym. Door deze interactie wordt er een actief enzym gevormd dat heel veel substraten kan omzetten in meetbare producten, waardoor het signaal geamplificeerd wordt. Deze methode maakte het voor ons mogelijk om binding, opname en fusie van virussen gedurende de binnenkomst in gastheercellen te onderscheiden en te detecteren. In hoofdstuk 3 beschrijven we een assay dat het mogelijk maakt om specifiek naar die S eiwitten te kijken die daadwerkelijk betrokken zijn bij het ontsnappen van het virus uit het lipide belletje (endosoom). Dit maakte het mogelijk om de biochemische

eigenschappen te onderzoeken van de S eiwitten betrokken bij fusie. Daardoor konden we laten zien dat de S eiwitten van MHV door proteases gekliefd moeten worden om fusie mogelijk te maken.

Door ons nieuwe fusie-assay uit hoofdstuk 2 te combineren met verschillende andere celbiologische technieken konden we het cellulaire proces dat betrokken is bij de binnenkomst van MHV in detail onderzoeken. Terwijl anderen eerder hadden laten zien dat MHV opgenomen wordt via de zogenaamde clathrine-gemedieerde route, konden wij dit bevestigen en vervolgens verschillende andere gastheerfactoren ophelderen die betrokken zijn in dit proces (hoofdstuk 4). We toonden aan dat MHV partikels verblijven in endosomen totdat deze veranderd zijn in lysosomen voordat de partikels kunnen fuseren en ontsnappen. We konden ook laten zien dat CoVs het destructieve milieu van de lysosomen nodig hebben, in het bijzonder bepaalde proteases om het S eiwit te klieven en te activeren voor fusie. Vergelijking met andere CoVs, zoals FIPV en MERS-CoV, liet zien dat een bepaalde sequentie in de aminozuurvolgorde van het S eiwit verantwoordelijk is voor het bepalen van het ontsnappingspunt van CoVs in the endosomale route.

In hoofdstuk 5 hebben we ingezoomd op één cellulaire factor die betrokken is bij de binnenkomst van CoV en hebben het belang van een specifiek onderdeel van Na^+, K^+ -ATPase opgehelderd. Door gebruik te maken van “gene silencing” als ook door gebruik te maken van cardiotonische drugs die binden aan dit onderdeel konden we laten zien dat een specifieke signaal-route, de zogenaamde Src signalering, die via dit onderdeel gemedieerd wordt een belangrijke rol speelt in het remmen van CoVs infecties. Cardiotonische drugs konden de binnenkomst van MHV in een vroeg stadium remmen, wat resulteerde in een accumulatie van viruspartikels dicht bij het oppervlakte van de cel.

Uiteindelijk bevat hoofdstuk 6 een samenvattende discussie, waarin onze bevindingen over de binnenkomst van CoVs in de bredere context van de beschikbare literatuur worden geplaatst met als doel om de verschillende aspecten van de binnenkomst van CoVs, waaronder opname via endocytose, klieving van S door proteases and the intracellulaire plek van fusie, te integreren in een algemeen beeld.



ACKNOWLEDGMENTS

Like most things in life this PhD thesis would not have been possible to achieve without the support and help of other people. Therefore it is not only my pleasure but my honor to use this space to say thanks.

First I would like to thank my promotor, Peter Rottier, not only for trusting me to do my PhD work in his lab but also to give me the freedom to design and execute my own ideas and to perform science in a constant dialogue. Peter, you are an inspiring person, aspiring to do good science for many years and still doing it with the same enthusiasm and interest after all this time. Also, you bring a great attitude and warm hearted personality to work every single day. Equally, if not almost even more to thank are my two co-promotors Berend Jan Bosch and Xander de Haan. Berend, you helped me find my first steps in the lab and in my PhD and therefore I am very grateful. We developed interesting new methods together and despite taking more time for your family and therefore handing day-to-day supervision over to Xander, you were still always there with help and advice. Xander, despite not being my actual co-supervisor from the beginning you were always there with ideas, support and knowledge. Once you became my supervisor we were able to achieve and expand many of my and your ideas and generate interesting results. Your enthusiasm was never lacking and thereby pushing me to achieve more and new things. You also were a great support with finalizing my thesis, which, admittedly, was not always easy with me already buried in work on my new PostDoc project. I am sure it also required a lot of patience from you to deal and bear with me during that period, so here once again a BIG thank you for that.

Of course work in the lab would not have been possible and not have been half as fun without many of my colleagues. All of you were a great support and a lending helping hand whenever I needed it. Special thanks go to our helping angels in the lab, Arno and Nancy. Without you the lab would not only run out of supplies and drop into complete chaos, but also it would lose the heart and soul of its social core. Willem, you were a great person to have in the lab at the start. Your relentless organization of social activities made not only the start in a new lab but also the start in a new country much easier. Next to lab movie nights and Friday afternoon drinks I particularly remember a very special first carnival trip that immediately made me feel at home, also due to Martijn, Mattijn, Marne, Marleen, and Jildou. Of course not to forget are my wonderful office mates. Despite some of you moving on to new ventures during my PhD you all left a mark not only in my scientific work but also in my personal life. Thank you Qiushi for bringing your friendly personality to our office but also offer your help and opinion whenever needed. Marne, you became not only a lab colleague but also a very good friend. You were my dinner neighbour on many occasions and I do miss our long discussions. Luckily we still stay in contact with help and advice whenever needed on our transatlantic skype calls, despite them not being as often as we both would hope for. Ole, there is no short way to say what I would like to say thanks to you. First and foremost for a great friendship. Both you and Anna were and are very welcoming to have me over for dinner or come over to me and your home had and has always an open door. We managed to have plenty of arguments and discussion about science only pushing each other to new heights. Your professional criticism and questioning has advanced my research greatly. With you being my paranimf I could not think of a better person having my back in my defense. Thank you. But of course the list goes on. Many other people in the lab are to thank for; Martijn and Shofie, thanks for being good

friends and great colleagues. Never will I forget the culinary adventures you took me on at your lovely home or the hospitality at your wedding. So many more thanks to say all the inspiring scientists and great colleagues I had the pleasure to meet over the time, in particular, Raoul de Groot, Jos Dortmans, Matthijn de Boer, Mark Bakkers, Iryna Monastyrska, Esther Wissink, Inge Marie Stub, Lucian Albulescu, and Cristina Dorobantu.

My work at the department would not have been half as inspiring without the many students I had the pleasure to teach but also to learn from: Louis-Marie Bloyet, Nick Distasio, Miranda Overbeek, Philip V'kosvski, and Olga Patijn. Many of you have moved on to start your own scientific career and all the best of luck with your own PhDs Louis-Marie and Philip, the great continuation of your academic adventure in Europe Nick, and with your new jobs and aspirations Miranda and Olga. Also a big thanks to all the other students that made lab life more varied and interesting. In particular Shofie, Willemijn, Anniek, Mike, and Remi.

As part of a large EU FP7 network this allowed me to interact and meet many great minds in the field and make new friends within that network. Many of the PhD students and PostDocs in the network did become good friends. Thanks to Kimmo Rantalainen, allowing us to crash in your livingroom and extending our experience of Stockholm prior to our meeting. You are a great creative mind and have inspired us all to think beyond the pure science. Your drawings and pictures not only supported us to give better talks but also had us looking forward to yet another interpretation of what we were doing. Andrea Gramatica, Caroline Mair, Sarah Stauffer, and Stefanie Hetzenecker, Matthias Quandte, and Doron Gollnast, you formed the heart and core of our network and every meeting it was a great pleasure to see you again. Doron and Matze, being based in Utrecht our relationship went beyond science and the network and ended in good friendships. Matze, thanks for giving me a great welcome in Utrecht. From the start you were a good friend and allowed me in your home and your group of friends. It made my life much more colourful and made me feel at home to be invited to your home and many of the crazy parties. Thanks as well to first and foremost Eelco, you are a wonderful person and a great friend, but also Evert-Jan, Erwin, Iris, Nicky, René, Ryan, and Sandra.

Of course all of this would not have been possible without the help and inspiration by many of my teachers and former colleagues. You gave me the basis to having a creative and critical scientific mind, to understand and question what I am doing, and to be there for me when I had questions and needed advice. A great thanks goes here to Ari Helenius and Jason Mercer. You shape my scientific thinking and attitude like no others and were still there for help, collaboration, and advice during my PhD. Many thanks also to other great minds in the Helenius group. Mario Schelhaas, Arnold Hayer, Hrefna Johannsdottir, Sabrina Engel, Thomas Heger, and Friederike Thor. Many thanks also to Sabrina, Thomas and Friederike for not only being great teachers, advisors, and minds but also for being good friends over many years, despite our paths going different ways and not being able to see each other as often as, certainly I, would like.

A big thanks also goes out to the people I had the pleasure meeting along my way of living in the Netherlands. My initial flatmates Paul, Judith, and Maarten, despite my staying

with you only being of a short period you helped me feeling at home in the large seven people flat. And mostly, you stayed friends even after I had moved into a new home. And of course Sabine Gremme, you were a great flatmate I could come home to and complain about work when things were not that great but also share the joys of it. It is great to still be friends with you and keep track of where your life progresses in consulting in Germany.

One of the biggest supports I had during my entire PhD time was that I had a “home away from home” in the South of the Netherlands. Whenever I wanted to get some time away from work or had a wee stroke of home sickness and needed to hear some Swiss German, I was welcome in the home of Marloes van Tilburg or her parents Yvonne and Chris. Yvonne and Chris, you always made me feel welcome in your home and with your family. It must be ten or eleven years ago now that I had the privilege of going on my first vacation to the Netherlands with you. And since then I always had a place with you and was welcome at many events with the entire rest of the family. This means and meant so much to me and you are incredibly kind to welcome me like that time and time again. Thank you! Marloes, what can I say, you are my best friend since high school. Despite our paths separating when I moved to Zurich for studies and you moved back to the Netherlands we never lost track of each other. Even when we do not get the chance to speak for a while whenever we meet or talk it is like no time had passed. Thankfully you agreed to be my paranimf for my defense and it will be my great honor and pleasure to have you having my back at my defense.

None of this would have ever been possible without the help and constant support of my parents and my family.

Liebes Mami, lieber Papi, ohne euch hätte ich wohl kaum die Ziele erreicht in meinem Leben, die ich bis hierzu erreicht habe. Ihr habt mich immer unterstützt das zu tun was ich machen wollte. Das Studium an der ETH Zürich wäre kaum möglich gewesen ohne eure Unterstützung, sowohl mental als auch finanziell. Obwohl ihr erst nicht gerade glücklich wart, dass ich mein Doktorat in den Niederlanden machen wollte habt ihr mir immer einen grossen Rückhalt und alle eure Unterstützung gegeben. Sei es mit dem Umzug von jenen Boxen und einer langen Autofahrt durch Deutschland oder wann immer es gerade mal nicht so gut lief. Euer unerwarteter Besuch und meinem ersten Geburtstag in den Niederlanden war beispielsweise auch ein wunderbares Symbol eurer Unterstützung. Liebe Sabine, Eveline und Sibylle, obwohl ihr wohl ab und zu gedacht habt was zum Henker ich eigentlich mache, habt ihr mich immer unterstützt. Sabine, deine vielen Besuche und unsere Erkundungstouren durch die Niederlande waren immer eine tolle Abwechslung und Aufmunterung.

Many of my friends from university and high school were always good for a chat and for a meet up at Christmas or whenever I went back home to Switzerland. Thus here a special thanks to Nadja Elmiger and Heidi Lischer. Ever since high school you have been great friends and despite our lives going in slightly different directions we always have plenty to talk about when we meet up again. Sabine Schütz, Philipp Stiefel, Antonia Müller, Pascal Schläpfer, Joelle Schläpfer-Sasse, Laurent Morax, Cristina Manatschal, Anna Menet, Michael Welti, and Yves Meur, and everyone I forgot from the Spaghettata crew, it's always great to meet up with you guys again and see where life has directed you to. And on top of that you were and you are great supportive minds and let us talk about “old” times at ETH.

Dear Ewan, it seemed like one of my daftest ideas to start a long distance relationship right in the middle of my PhD. However, it seems to be one of the best ideas I have been persuaded of for a long time. You are making my life better every single day with your love and care for me. We have enjoyed our life together in Edinburgh for many months now. You have been a constant support to me in finishing my PhD whilst working on a new project. You made sure I took a break once in a while but also pushed me to write when I had a tendency to procrastinate. Also your family has been very warm and welcoming to me and made me feel at home in a new country. Thus a big thanks as well to Violet, Alistir, Lynsey, and Libby.

Last but not least I want to thank someone who is unfortunately no longer with us. Dear Alan, I am sure you will be able to read this despite no longer being with us. All too soon you passed away this year on the 20th of April 2014. You were a great friend to me during my entire PhD at the Virology department. Starting to work on the same day as me it was initially a bit of a getting to know period of the loud, opinionated, big Amsterdammer. However, soon enough you became one of the best friends one could ever wish for. During plenty of visits to the museum we had discovery tours through times and your Amsterdam. When strolling around in the Oosterpark you took me back to the 70ies, your mum pushing you in a stroller in the park, and your memories of later years. When walking around the Jewish quarters you told me stories about the history, about your grand dad, and other anecdotes. We had many Asian movie nights, a love we both shared. Together with you and your friends we celebrated many birthdays with great food, wine, and pindasoep (peanut soup) at your home. With your parents and family we had a great time celebrating your and many of your friends 40th birthday and to enjoy your birthday present we went to the opera together with your dad. All those memories will stay in our hearts for ever and we miss you in our lives. The sheep on the front page of your thesis is looking at me every single morning I enter the Roslin Institute lobby and every single time I have to think of you. I am sure you're still looking over my shoulder. We had a great last meal together eating Japanese in Utrecht and skype calls to follow. And since you will always be in our hearts I will put your recipe for pindasoep on the next page, so we and our friends can meet with some good wine and pindasoep time and time again in your memory.

Goodbye beloved friend!

Christine Burkard, December 2014

ALAN'S SURINAM STYLE PINDASOEP

Peanut soup á la Alan Rigter

500g	Boneless chicken thighs or breast
3 tbsp	Teriyaki marinade or soy sauce
1 tbsp	Thai fish sauce or oyster sauce
2 tbsp	Lemon juice
2	Medium red onions
2	Medium-sized leeks
4	Garlic cloves
2-3	Peppers
500g	Finely chopped Chinese cabbage or Endive
2-2.5lt	Chicken or beef stock
150g	Bean sprouts
400ml	Creamy coconut milk
1 bloc	Santen (condensed coconut cream) Grated coconut (to taste)
600g	Peanut butter (Hot; 2pots Faja Lobi, Spicy; 1pot Faja Lobi, 1 pot regular peanut butter, Mild; 2 pots regular peanut butter)
1 bag	Yellow thai curry paste Dried herbs; Cumin, Ginger, Coriander, Lemongrass (alternatively Chinese 5-spice mix)

PREPARATION

- Cut the chicken breast/thighs into strips and (at least) marinate at least one hour in teriyaki marinade, lemon juice, thai fish sauce, and garlic.
- Fry the chicken strips in the margarine until brown. (Add the chicken as dry as possible to prevent splattering and to allow browning.) Add the remaining marinade to the broth!
- Roughly chop the onion, peppers and leek.
- Add the onion, bell peppers and leek to the meat & fry until the onions start sweating (glassy). Add dried spices to taste and stir-fry for a couple of minutes.
- Bring the broth to a boil and “dissolve” the peanut butter in the broth. Stir well to prevent clumps
- Add canned coconut milk & block of santen, stir until dissolved.
- Add the yellow curry mix.
- Add the chicken and vegetables and bring gently to the boil.
- Taste and add more fish sauce for saltiness if necessary.
- Add grated coconut until desired soup thickness. (Relatively viscous).
- Let simmer at least 2 hours (flavor is best when soup is made 1 day in advance and warmed up again)
- For a bit of crunch, add some beansprouts (wash first!) to each bowl & pour the soup on top.

Enjoy!

CURRICULUM VITAE

Christine Burkard was born April 4th 1986 in Sursee LU, Switzerland.

EDUCATION

- 1998-2004 Secondary School, Biology and Chemistry Direction
Kantonsschule Sursee, Sursee LU, Switzerland
- 2004-2007 BSc ETH Biology, Chemical Orientation
Swiss Federal Institute of Technology (ETH) Zurich, Zurich, Switzerland
- 2007-2009 MSc ETH Biology, Major Biochemistry
Swiss Federal Institute of Technology (ETH) Zurich, Zurich, Switzerland
Masters thesis: *The Necessity of Cullin and Cullin Associated Proteins
in Vaccinia Virus Entry*
Prof. A. Helenius, Institute of Biochemistry
- 2010-2014 PhD in Virology
Virology Division, Dep. Infectious Diseases and Immunology,
Faculty of Veterinary Sciences, Utrecht University , Utrecht, The Netherlands
Marie Curie Initial Training Network, EU Virus Entry
Thesis: *Host Factors Involved in the Entry of Coronaviruses into
Mammalian Cells*
Promotor: Prof. Dr. Peter Rottier
Co-Promoters: Dr. Xander de Haan
 Dr. ing. Berend Jan Bosch
- 2014-today Research Fellow
Division of Genetics and Genomics, The Roslin Institute, R(D)SVS,
University of Edinburgh, Edinburgh, United Kingdom

POSTERS AND PRESENTATIONS

POSTERS

Burkard C., Rottier P.J.M., Bosch B.J., (September 2010), Replication Independent Virus Entry Assay Based on Enzyme Complementation. Current Opinion in Cell Biology Conference, "Cellular Host--Pathogen Interactions", Amsterdam, The Netherlands

Burkard C., Bloyet L.M., Rottier P.J.M., Bosch B.J., (May 2012), Dissecting Virus Entry – Replication-- Independent Analysis of Virus Binding, Internalization, and Fusion Using Minimal Complementation of β -- Galactosidase. 7th International Virus Assembly Symposium, Menorca, Spain

Burkard C., Bloyet L.M., Wicht O., de Haan C.A.M., Rottier P.J.M., Bosch B.J., (June 2013), Dissecting Virus Entry – Replication--Independent Analysis of Virus Binding, Internalization, and Fusion Using Minimal Complementation of β --Galactosidase. 32nd Annual Meeting, American Society for Virology, State College PA, United States of America

PRESENTATIONS

Burkard C., Rottier P.J.M., Bosch B.J., (June 2010), Investigating the Entry Pathways of Coronaviruses. ITN Network Virus Entry, 1st annual meeting, Berlin, Germany

Burkard C., Rottier P.J.M., Bosch B.J., (June 2011), Entry Pathways of Coronaviruses – Replication Independent Entry Assay Based on Enzyme Complementation. ITN Network Virus Entry, 2nd annual meeting, Stockholm, Sweden

Burkard C., Bloyet L.M., Rottier P.J.M., Bosch B.J., (November 2011), Tracking Virus Entry – Replication-- Independent Analysis of Virus Binding, Internalization, and Fusion Using Minimal Complementation of β -- Galactosidase. CHemistry As Innovative Science (CHAINS). NWO / KNCV Meeting, Maarssen, The Netherlands

Burkard C., Bloyet L.M., Rottier P.J.M., Bosch B.J., (May 2012), Dissecting Virus Entry – Replication-- Independent Analysis of Virus Binding, Internalization, and Fusion Using Minimal Complementation of β -- Galactosidase. ITN Network Virus Entry, 3rd annual meeting, Menorca, Spain

Burkard C., Bloyet L.M., Wicht O., de Haan C.A.M., Rottier P.J.M., Bosch B.J., (June 2013), MHV--A59 Entry and Fusion – The pH--Insensitive Murine Hepatitis Coronavirus is Late--Penetrating and Requires a Functional HOPS Complex for Fusion. 32nd Annual Meeting, American Society for Virology, State College PA, United States of America

LIST OF PUBLICATIONS

Burkard C, Verheije MH, Haagmans BL, van Kuppeveld FJ, Rottier PJM, Bosch BJ, de Haan CAM. 2013. The role of cardiac glycoside and the ATP1A1 gene in MHV entry and replication. Under Review.

Burkard C, Verheije MH, Wicht O, van Kasteren SI, van Kuppeveld FJ, Haagmans BL, Pelkmans L, Rottier PJ, Bosch BJ, de Haan CA. 2014. Coronavirus Cell Entry Occurs through the Endo-/Lysosomal Pathway in a Proteolysis-Dependent Manner. *PLoS pathogens* **10**:e1004502.

Burkard C, Bloyet LM, Wicht O, van Kuppeveld FJ, Rottier PJ, de Haan CA, Bosch BJ. 2014. Dissecting virus entry: replication-independent analysis of virus binding, internalization, and penetration using minimal complementation of beta-galactosidase. *PloS one* **9**:e101762.

Wicht O, Burkard C, de Haan CA, van Kuppeveld FJ, Rottier PJ, Bosch BJ. 2014. Identification and characterization of a proteolytically primed form of the murine coronavirus spike proteins after fusion with the target cell. *Journal of virology* **88**:4943-4952.

Mercer J, Snijder B, Sacher R, Burkard C, Bleck CK, Stahlberg H, Pelkmans L, Helenius A. 2012. RNAi screening reveals proteasome- and Cullin3-dependent stages in vaccinia virus infection. *Cell Rep* **2**:1036-1047.

Mercer J, Knebel S, Schmidt FI, Crouse J, Burkard C, Helenius A. 2010. Vaccinia virus strains use distinct forms of macropinocytosis for host-cell entry. *Proc Natl Acad Sci U S A* **107**:9346-9351.

